ABSTRACT

Title of Dissertation:	MOLECULAR RECOGNITION PROPERTIES OF MOLECULAR CONTAINERS IN AQUEOUS SOLUTIONS
	David William King, Doctor of Philosophy, 2023
Dissertation directed by:	Professor Lyle Isaacs, Department of Chemistry and Biochemistry

Supramolecular containers take advantage of non-covalent interactions to do a variety of tasks with high affinity. In particular, water-soluble containers are able to bind biologically relevant molecules to perform useful and interesting tasks.

Chapter 1 introduces the field of supramolecular chemistry is introduced and establishes the ability of cucurbit[n]urils (CB[*n*]) to bind guests with high affinity. It also establishes the uses of water-soluble supramolecular containers, including new-generation pilar[*n*]arene sulfate (P[*n*]AS) hosts, in biologically relevant systems.

Chapter 2 expands on previous attempts at finding high-affinity host-guest pairings by showing that triamantane amines and triamantane diamines are able to bind CB[8] with femtomolar dissociation constants. It also shows that these ultratight binding complexes can be found in competition measurements with slightly weaker ternary complexes, thus reducing the number of measurements needed and the error of those measurements.

Chapter 3 shows the discriminatory power of P6AS towards various amino acids and amino acid amides, as well as their methylated derivatives. This discriminatory power is further explored by showing P6AS shows discriminatory power towards histone 3 peptide sequences that are methylation on either the lysine or arginine. This system was also modeled computationally to investigate the role of water in binding affinity.

Chapter 4 expands on the use of P[*n*]AS in biologically relevant systems by measuring the binding constants and an assay to detect and differentiate various World Anti-Doping Agency (WADA) banned compounds in PBS. The same assay was then used to create a calibration curve in simulated urine for two compounds. In total the proof-of-concept assay is able to detect **Pseudo** down to 31.8 μM concentrations.

MOLECULAR RECOGNITION PROPERTIES OF MOLECULAR CONTAINERS IN AQUEOUS SOLUTIONS

by

David William King

Dissertation submitted to the Faculty of the Graduate School of the
University of Maryland, College Park, in partial fulfillment
of the requirements for the degree of
Doctor of Philosophy
2023

Advisory Committee:
Professor Lyle Isaacs, Chair
Professor Jeffery Davis
Professor Daniel Falvey
Professor Pratyush Tiwary
Professor Matthew Roesch, Dean's Representative

Dedication

To my parents, Donna King and Stephen King, my brother Kevin King, and sister-in-law, Catie Kennedy. Thank you for all your help getting me to where I am, and for keeping me *mostly* sane along the way.

In memory of Karen Shollenberger and Ryan King.

Acknowledgements

First, I would like to thank my advisor, Professor Lyle Isaacs, for allowing me to work in his lab and for the many lessons he's taught me over the last six years.

I would like to thank Professor Katherine Hunt at Michigan State University for her mentorship when I was an undergraduate, teaching me how to conduct research, and for suggesting that I take a class in Python and machine learning that helped put me on the path I am on now. Additionally, I would like to thank Ms. Kimball and Ms. Buxbaum for helping spark a love of chemistry and science in general.

I would like to thank the senior Isaacs group members - Dr. Kimberly Brady, Dr. Steven Murkli, Dr. Sandra Zebaze, Dr. Wei-jian Xue, Dr. Ming Cheng, Dr. Chun-lin Deng, Dr. Alok Shaurya, and Dr. Canjia Zhai for being patient with me, teaching me how to do organic reactions, helping troubleshoot experiments, and for their advice on matters beyond chemistry. I would also like to thank – Delaney Patterson, Suvenika Perera, Ayona Goswami, Manny Bazan-Bergamino, Collin Vincent, Brona O'Dowd, Chris Akakpo, Noor Singh, Noah Hornstein, and Anton Doan – for their support and asking me questions that made me thank about science in new ways to answer them.

I would like to thank our collaborators on the projects discussed in this thesis - Professor Pratyush Tiwary, Lukas Herron, Shams Medhi, Professor Fraser Hof, Chelsea Wilson, Professor Marina Šekutor, Professor Peter R. Schreiner, and Tatjana Šumanovac - for their contributions to these projects. I would also like to thank our collaborators on projects I was able to contribute to that are not listed here - Professor Matthew Roesch, Professor Volker Briken, Adam Brockett, Michael Shuster, Shivangi Rastogi, and Peter Zavalij – for allowing me to contribute to a wider range of projects.

The instrumentation facilities at UMD have been crucial to my work and I thank Dr. Fu Chen, Dr. Daoning Zhang, and Dr. Bin Chen for their invaluable help.

Thank you to my friends and classmates I met both before and during grad school for cheering me on and listening to my ramblings. Most of all my family – Mom, Dad, Kevin and Catie - thank you for always being there for me and helping me become who I am today.

Table of Contents

List of Tables

Chapter 2

Chapter 3

Chapter 4

List of Figures

Chapter 1

Chapter 2

Figure II-2. Illustration of the changes in the solvation of the host and the guest that occur during the formation of CB[*n*]-guest complexes. Aqua spheres, bulk water; Blue spheres, intracavity ‘‘high energy’’ water.

Figure II-3. Structures of cationic guests **G1**-**G4**, competators **C1**-**C3**, and comparison compounds **C4**-**C10** used in this study.

Figure II-4. ^{1}H NMR spectra recorded (600 MHz, D_2O) for (a) a mixture of **G4** (2 mM) and CB[8] (1 mM), (b) a mixture of **G4** (1 mM) and CB[8] (1 mM), (c) **G4** (1 mM), (d) a mixture of **G4** (1 mM) and CB[7] (1 mM), and (e) a mixture of **G4** (2 mM) and CB[7] (1 mM). Resonances marked with primes (‘) arise from the host-**G4** complex.

Figure II-5. Side and top views of the energy-minimized geometries of (a) CB[7]-**G4** and (b) CB[8]-**G4**. Color codes: C, gray; H, white; O, red; and N, blue.

Figure II-6. (a) ITC thermogram recorded during the titration of CB[7] (145 mM) in the cell with guest **G1** in the syringe, (b) Fitting of the data to a 1 : 1 binding model with $K_a = (1.6 \pm 0.1) \times 10^5$ M^{-1} and $\Delta H = -10.4 \pm 0.076$ kcal mol^{-1}.

Figure. II-7. (a) Schematic representation of binding models implemented in Affinimeter^{TM} to determine the K_a values for the formation of CB[8]·**C3** and CB[8]·**C3**$_2$ in the direct titration of CB[8] with **C3** and the competitive binding model used to determine the K_a value for CB[8]·**G3**

during the titration of a mixture of CB[8] and **C3** with **G3**. (b) Thermogram from the direct titration of CB[8] (5 mM) with **C3** (40 mM) in the syringe. Three successive titrations were concatenated. (c) Plot of ΔH *versus* molar ratio. The solid line represents the best fit of the data to the stepwise binding model performed using Affinimeter™. (d) Thermogram from the competitive ITC titration of a solution of CB[8] (30 mM) and **C3** (175 mM) in the cell with a solution of **G3** (100 mM) in the syringe. (e) Plot of ΔH *versus* molar ratio. The solid line represents the best fit of the data to the stepwise binding model performed using Affinimeter™.

Chapter 3

Figure III-1. Chemical Structures of CB[*n*] and pillararenes receptors.

Figure III-2. Chemical Structures of: (a) lysine derivatives, (b) arginine derivatives, and (c) other amino acids used in this study.

Figure III-3. (a) ITC thermogram recorded during the titration of P6MQ (100 μM) in the cell with **H–K(Me$_3$)–OH** (1.0 mM) in the syringe. (b) Fitting of the data to a 1 : 1 binding model with $K_a = (3.39 \pm 0.15) \times 10^6\ M^{-1}$. Conditions: phosphate buffered saline, pH 7.4, 298.0 K.

Figure III-4 (a) Cartoon of the interaction of P[*n*]MQ with lysine, lysine amide, and N-Acetyl-lysine amide. The green and red double headed arrows spot- light favorable and unfavorable electrostatic interactions, respectively. (b) Illustration of the proposed geometries of the P6MQ·**H–K(Me$_3$)–OH** and P6MQ·**Asym-H–R(Me$_2$)–OH** complexes.

Figure III-5. ^{1}H NMR spectra recorded (600 MHz, RT, 20 mM phosphate buffered D_2O, pH 7.4) for: (a) **H–K(Me$_3$)–OH** (1.0 mM), (b) a mixture of **H–K(Me$_3$)–OH** (1.0 mM) and P6MQ (0.5 mM), (c) a mixture of **H–K(Me$_3$)–OH** (1.0 mM) and P6MQ (1.0 mM), (d) a mixture of **H–K(Me$_3$)–OH** (1.0 mM) and P6MQ (2.0 mM), (e) **Asym-H–R(Me$_2$)–OH** (1 mM), (f) a mixture of **Asym-H–R(Me$_2$)–OH** (1 mM) and P6MQ (0.5 mM), (g) a mixture of **Asym-H–R(Me$_2$)–OH** (1.0 mM) and P6MQ (1.0 mM), and (h) a mixture of **Asym-H–R(Me$_2$)–OH** (1.0 mM) and P6MQ (2.0 mM).

Figure III-6. Structure of the histone **H3K4** peptides used in this study.

Figure III-7 (a) Direct fluorescence titration of a solution of **DAPI** (100 nM) with a solution of P6MQ in phosphate buffered saline at pH 7.4. (b) Competitive fluorescence titration of a solution of P6MQ (125 nM) and **DAPI** (100 nM) with a solution of **H3K4Me$_2$** in phosphate buffered saline at pH 7.4. Reported dissociation constants are the average of six measurements, curves and R^2 of exemplary triplicate data (see ESI†).

Figure III-8. Characterizing H-bonding in and around P6MQ and complexes. (a) Plot of the free energy (see ESI for definition†) of the system *versus* average number of hydrogen bonds a water molecule participates in. (b and c) The coordination of water molecules by sodium ions in uncomplexed P6MQ, with front side of P6MQ not shown for clarity in panel. Red lines correspond to H-bonds and water molecules are depicted in blue. (c and d) An example of the hydrogen bonding network in bulk water. We calculate the hydrogen bonds (red lines) formed within a region of the simulation box defined by r = 6 Å, including hydrogen bonds across the

surface of the region; solid blue molecules are located within the region and transparent ones are outside. (e) Cyclic H-bonded water network observed in the absence of Na^+.

Figure III-9. Characterizing the radial location of waters from the center of mass of the OSO_3^- groups. (a) The local density of waters less than 7 Angstroms from P6MQ sulfate oxygens, where the dashes line indicates the local density of bulk water. The local density is averaged over all oxygens. Note that the density of water is largely independent of the bound ligand. (b) The leftmost peak of (a) is explained by water mole- cules (depicted in blue) that are hydrogen bonded (depicted as red lines) to P6MQ. (c) The broader peak around 5 Å includes water molecules which are not hydrogen bonded to P6A which are typically coordinated by Na^+ ions (not pictured, see **Figure III-8** and ESI†).

Figure III-10. MD simulation structures. (a) P6MQ·**H–K(Me$_3$)–OH**. P6MQ·**H–K (Me$_3$)–OH** has only one bound conformation; **H–K(Me$_3$)–OH** is bound at an angle within P6MQ with Me_3N^+ in the center of the cavity. P6MQ flexes to accommodate the ligand. (b) P6MQ·**H3K4Me$_3$** (KMe_3 bound). P6MQ·**H3K4Me$_3$** (KMe_3 bound) has a distinct conformation in which the backbone and non-bound sidechains of **H3K4Me$_3$** form H-bonds with P6MQ. The H-bonds formed between OSO_3^- and arginine stabilizes arginine within π stacking distance of the P6MQ aromatic walls. In both panels water molecules are depicted in blue, H-bonds as red lines, and the ligand in magenta.

Chapter 4

Figure IV-1. Structures of guests used in this study

Figure IV-2. (a) ITC thermogram recorded during the titration of P6AS (25.0 μM) in the cell with **2HeptNH3** (250 μM) in the syringe. (b) Plot of the integrated heats of each titration *vs.* the molar ratio with the solid line representing the best fit of the data to a 1 : 1 binding model with $K_a = (5.59 \pm 0.32) \times 10^6\ M^{-1}$, $\Delta H = -6.38 \pm 0.03$ kcal mol^{-1}. Conditions: PBS, pH 7.4, 298.0 K.

Figure IV-4. ^{1}H NMR spectra recorded for (600 MHz, RT, phosphate buffered saline D2O, pD 7.4) for: a) P5AS (1.0 mM), b) a mixture of **2HeptNH3** (1.0 mM) and P5AS (2.0 mM), c) an equimolar mixture of **2HeptNH3** and P5AS (1.0 mM), and d) a mixture of **2HeptNH3** (1.0 mM) and P5AS (0.5 mM), e) **2HeptNH3** (1.0 mM), f) a mixture of **2HeptNH3** (1.0 mM) and P6AS (0.5 mM), g) an equimolar mixture of **2HeptNH3** and P6AS (1.0 mM), and h) a mixture of **2HeptNH3** (1.0 mM) and P6AS (2.0 mM), i) P6AS (1.0 mM).

Figure IV-5. Cross sections of the three-dimensional Linear Discriminant Analysis (LDA) plot for the discrimination of 13 WADA-banned compounds at 50 μM of guest. The predictive accuracy was determined to be 92.3 ± 6.9 % as determined via stratified K-fold (K = 15) cross-validation.

Figure IV-6. Calibration plots for ten concentrations with were measured with fifteen repetitions each between a) 0-2500 μM for **Pseudo** and b) 0-100 μM for **Epi** in simulated urine. The calibrations were able to achieve LOD of 85.4 μM and LOQ of 146.8 μM for **Pseudo**, and LOD of 5.7 μM and LOQ of 19.1 μM for **Epi**. The red lines represent the standard deviation of the predicted concentrations. The solid black line represents a perfect correlation between

predicted and actual concentrations. Two test concentrations (grey) used for each compound with one above and one below the WADA-LOQ.

List of Abbreviations

^{1}H NMR	proton nuclear magnetic resonance
^{13}C NMR	carbon-13 nuclear magnetic resonance
Å	angstrom
ANOVA	Analysis of Variance
Br	broad
C	carbon
CB[*n*]	cucurbit[*n*]uril
CD	cyclodextrin
CV	cross validation
CX[*n*]	calix[*n*]arene
d	doublet
D_2O	deuterium oxide
DMSO	dimethylsulfoxide
DAPI	4’,6-diamino-2-phenylindiole
ESI-MS	electrospray ionization-mass spectrometry
EtOH	ethanol
g	gram
H	hydrogen
h	hour
HCl	hydrochloric acid
Hz	hertz
IDA	indicator displacement assay

IR	infrared
ITC	isothermal titration calorimetry
J	coupling constant
K	kelvin
K_a	binding affinity
kg	kilogram
$KMnO_4$	potassium permanganate
LD	linear discriminant
LDA	linear discriminant analysis
LOD	limit of detection
LOQ	limit of quantification
M	molar
m	multiplet
M.p.	melting point
m/z	mass to charge ratio
M+	molecular ion
MeOH	methanol
mg	milligram
MHz	megahertz
min	minute
mL	milliliter
mM	millimolar
MW	molecular weight

N	binding stoichiometry
$NaAuCl_4$	sodium tertrachloroaurate
NaH_2PO_4	sodium monophosphate
NaO_2CCD_3	deuterated sodium acetate
NaOH	sodium hydroxide
o	ortho
p	pentuplet
p	para
P[*n*]AS	Pillar[*n*]arene sulfate
P[*n*]MQ	Pillar[*n*]arene sulfate
pK_a	negative logarithm of acid dissociation constant
ppm	parts per million
rSVM	regression support vector machine
RT	room temperature
s	singlet
σ	standard deviation
t	triplet
T	temperature
t-BuOK	potassium tert-butoxide
TFA	trifluoroacetic acid
TMSP	2,2,3,3-d(4)-3-(trimethylsilyl)propanoic acid sodium salt
UV/Vis	Ultra violet/visible
Δδ	change in chemical shift

ΔH	change in enthalpy
ΔS	change in entropy
μ	micro
π	pi
χ	mole fraction

Chapter 1: Introduction to Molecular Containers and Their Uses in Biological Applications

1.1 Introduction and evolution of Supramolecular Containers

Interactions between atoms such as covalent bonds, ionic bonds, metallic bonds, Van Der Waal forces, ion-dipole, dipole-dipole are the foundation of chemistry. In particular, non-covalent bonds are responsible for many interactions in nature,[1,2] and while weaker than covalent bonds, they can still be strong enough to be useful. In the 1960's work performed by Cram,[3] Lehn,[4] and Petersen[5] on the discovery and application of compounds that could selectively bind small molecules through non-covalent interactions such as spherands, cryptands and crown ethers won them an eventual Nobel prize in chemistry.[6]

Despite the discovery of cucurbit[*n*]urils (CB[*n*]) in 1905 by Behrend[7] through a condensation of glycoluril and formaldehyde, it wasn't until 1981 that Mock elucidated the structure of CB[6].[8] While earlier compounds were able to bind small molecules and ions, CB[n] are able to bind larger molecules, and bind them more selectively than earlier compounds. This is because CB[n] molecules differ from their predecessor in that they have much larger and well-defined cavities.[9] This cavity can trap water molecules in an energetically unfavorable state by cutting them off from the hydrogen bonding network that exists outside of the host in "bulk" water.[10,11] When a guest is able to enter the cavity of the CB, these high-energy water molecules are released leading to very tight binding complexes.[9,12,13]

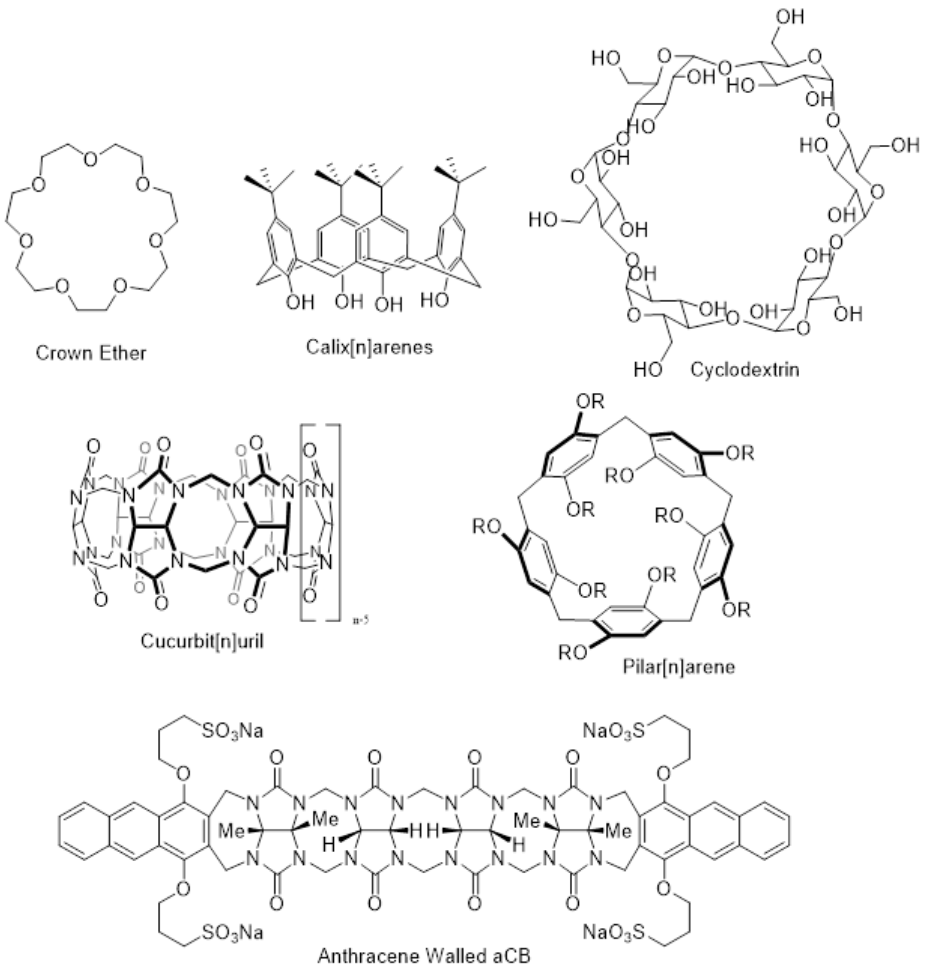

Figure I-1 Structures of various supramolecular containers.

While supramolecular containers typically have a type of guest they are best-able to encapsulate, they can also be tuned to be more or less selective towards certain types of guests. This has allowed these host molecules to be used in a variety of applications. For instance, cationic P[*n*]A hosts have been used for the prevention of biofilm formation,[14] while neutral P[n]A hosts have been shown to bind affectively to cationic guests with large non-polar hydrophobic regions.[15]

Each supramolecular host has its strengths and weaknesses. For instance, β-cyclodextrins (β-CD) are very water soluble and are easily functionalized, but they have relatively low binding affinities and are very water soluble. Conversely, CB[*n*] can form incredibly tight host-guest complexes and have a rigid well-defined cavity, but they are very hard to functionalize, not very water soluble, and their rigid shape may not allow them to accommodate larger guest molecules in the same way that P[*n*]A or CX[*n*] can.

1.2 Ultratight Binding Host-Guest Complexes

One of the greatest strengths of supramolecular containers is their selectivity and ability to bind guests very strongly. Biedermann and coworkers have shown that the "high energy" water molecules inside the cavity is part of what leads to such high binding constants in aqueous systems. When a guest is bound inside the cavity, it can push out the water molecules inside leading to an entropically favorable state.[11] When this is combined with large hydrophobic guests that can enter the hydrophobic cavity of a supramolecular host like CB[*n*] it can lead to extremely tight complexes. Notably work by Kim, Inoue, Kaifer, Isaacs, and Gilson have shown that CB[7] and CB[8] can form host•guest complexes as tight as 7.2×10^{17} M^{-1} in pure water.[13,16–23]

1.2.1 Binding Measurements of Supramolecular Containers

These association constants can be determined a variety of different ways.[24,25] Most commonly either direct or competitive titrations are carried out and monitored by either ^{1}H NMR, fluorescence or UV/Vis,[26] or isothermal calorimetry (ITC). In each instance, typically one molecule is monitored and is maintained at a constant concentration throughout the titration. This

is not always the case, as the data can still be accurately fit when the molecule being measured does not remain constant.[26] Each method can give more information that just the binding constants. For instance, ^{i}H NMR can give us information about the binding geometry by looking at which resonances have a large chemical shift. Due to this, it is very common to use multiple methods to investigate the same host•guest interaction. Typically, in direct titrations, the most accurate data is obtained when working at concentrations close to the dissociation constant ($K_d = K_a^{-1}$).[24,25]

Additionally, compounds that are not able to be easily detected by a certain method (*e.g.*, an optically silent guest measured via fluorescence) can be still be determined through competitive titrations. In competitive titrations, a guest with a known K_a with a given host is titrated with the host and a compound with an unknown K_a. While it does not matter if the known guest binds more or less strongly than the unknown guests, the weaker of the two is typically initially put in solution with the host, while the stronger guest is titrated into this solution. When one compound is silent in the given method, but the other can be monitored, it is known as indicator displacement. When used for many unknown guests in a high-throughput manor (typically involving a multiwell plate), it is known as indicator displacement assays (IDA) and is discussed in further detail below.

Of the methods listed, ITC is unique in that it can give complete thermodynamic information about the binding interaction. As the name suggests, the temperature of the cell where the binding interaction(s) occur upon titration is held at a constant temperature. Typically, the host or protein is located in the cell and guest is titrated into it (**Figure I-2a**). Upon complexation, the change heat of reaction is measured by monitoring the amount of energy

required to keep the cell at a constant temperature relative to a reference cell that contains only water. The change in heat is monitored as the guest is slowly titrated into the cell in discrete amounts. A plot of the integrated heats for each titration *vs.* the molar ratio of host to guest allows for the determination of many thermodynamic parameters of the complexation. As shown in **Figure I-2b**, the K_d can be found by taking the slope of the line integrated heats graph at the inflection point, the enthalpy (ΔH) of complexation is the difference between the initial heat of binding and the equilibrium heat, and the stoichiometry of binding (N) can be found by determining the X value of the inflection point of the sigmoidal curve (**Figure I-2b**). These values can then be used to find the Gibbs free energy (ΔG) and entropy (ΔS).

1.3 Water-soluble Molecular Containers and uses in Biological Systems

While earlier supramolecular containers were able to achieve high-affinity binding, many of them were insoluble, or only sparingly soluble in water.[27] Recently, water-soluble containers that retain high binding affinities have been developed such as sulfonated calix[*n*]arenes (CX[*n*]),[28] sulfonated acyclic cucurbit[*n*]urils (aCB),[29] and pillar[*n*]arene sulfate (P[*n*]AS).[30] In each case, the sulfonation increases water solubility, and in some cases, also increases binding affinity.

One use of water-soluble supramolecular containers such as β-cyclodextrin (β-CD) is to solubilize insoluble drugs. Supramolecular containers are very well suited for this task as they typically have hydrophobic cavities to interact and bind favorably with the hydrophobic drug molecules, as well as hydrophilic portals that help solubilize the entire complex.

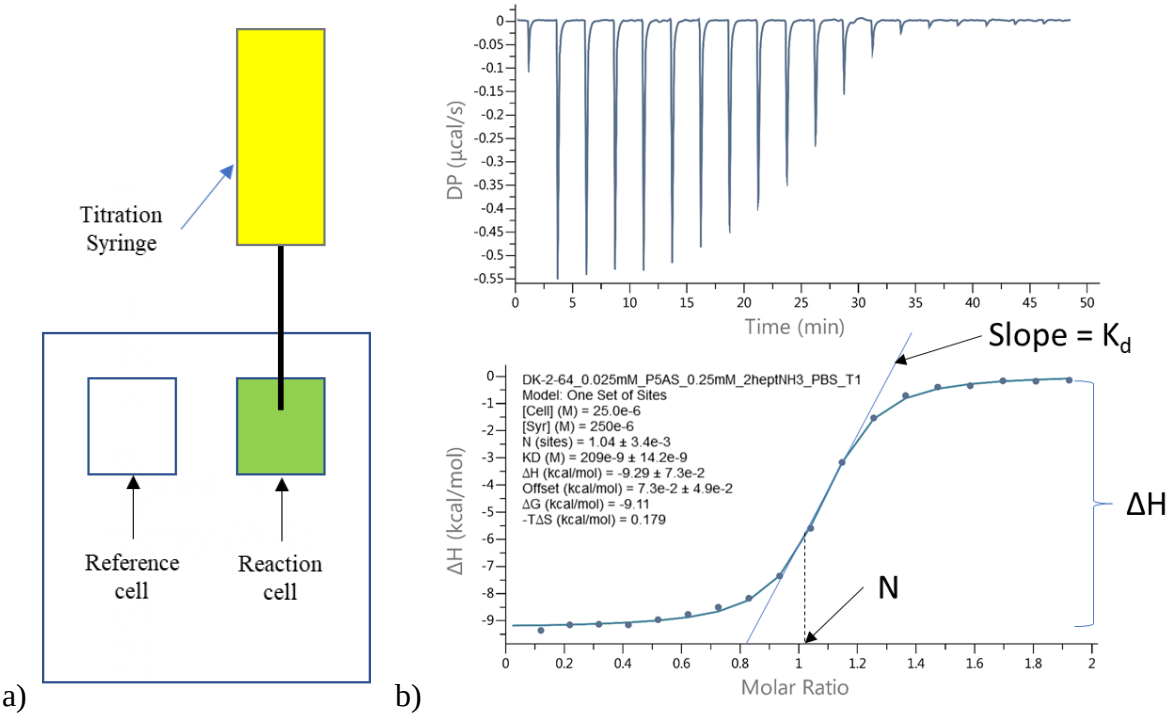

Figure I-2 a) Simplified diagram of an ITC machine b) Isothermal Titration Calorimetry (ITC) curve obtained through direct binding titration studies. A solution of P5AS (0.025 mM) in the cell was titrated with **2HeptNH3** (0.25 mM) in the syringe at 298.0 K in 10 mM sodium phosphate buffered saline at pH 7.4. The solid line represents the best non-linear fit of the data to a 1:1 binding model. (K_a = (5.59 ± 0.32) × 10^6 M^{-1}; ΔH = (–9.17 ± 0.06) kcal mol^{-1}). Annotated to show how the dissociation constant (k_d), enthalpy of complexation (ΔH) and stoichiometry of binding (N) are determined. Figure also shown without annotations in **Figure SIV-2**.

While solubilizing insoluble drugs, the binding affinity needs to be high enough that the host can bind the desired drug molecule, but low enough that it can release the drug once it gets to its desired location in the body. However, if the affinity is high enough, supramolecular containers can act in reverse by sequestering harmful molecules from the body. Due to the high

solubility and high binding affinity of supramolecular containers towards drugs of abuse, the Isaacs group has investigated the ability of supramolecular containers to sequester drug molecules from the body.[30–34]

1.4 Supramolecular Sensors

Due to the selectivity and high binding affinities of supramolecular containers, they are widely used in supramolecular sensing arrays.[35,36] There are two types of sensing arrays: lock-and-key sensors and cross-reactive sensors (**Figure I-3**). In lock-and-key sensing arrays, each sensor is only able to interact or bind with one analyte. While this means it has great selectivity, it also means that you need as many sensors as analytes you want to measure, and that you need to create a new sensor every time you want to detect a new analyte. Cross-reactive sensing arrays on the other hand, can use sensors that have some response to all the analytes measured. If these sensors are chosen carefully such that their response to each analyte differs from each other, it creates a sort of fingerprint for each analyte. This fingerprint can then be recognized by various machine learning algorithms. While this does increase noise and reduce selectivity, it also allows less selective sensors to be used. Additionally, through this method, you can use less sensors and you do not have to make a new sensor for each analyte; the array just has to be trained on the new analyte.

Typically, supramolecular containers are used as part of an indicator displacement assay (IDA). In an IDA, the host molecule is bound to a dye molecule. Through this binding interaction, the optical properties such as fluorescence are either enhanced or quenched. Upon being put into a solution with another molecule the container can bind to, some of the dye

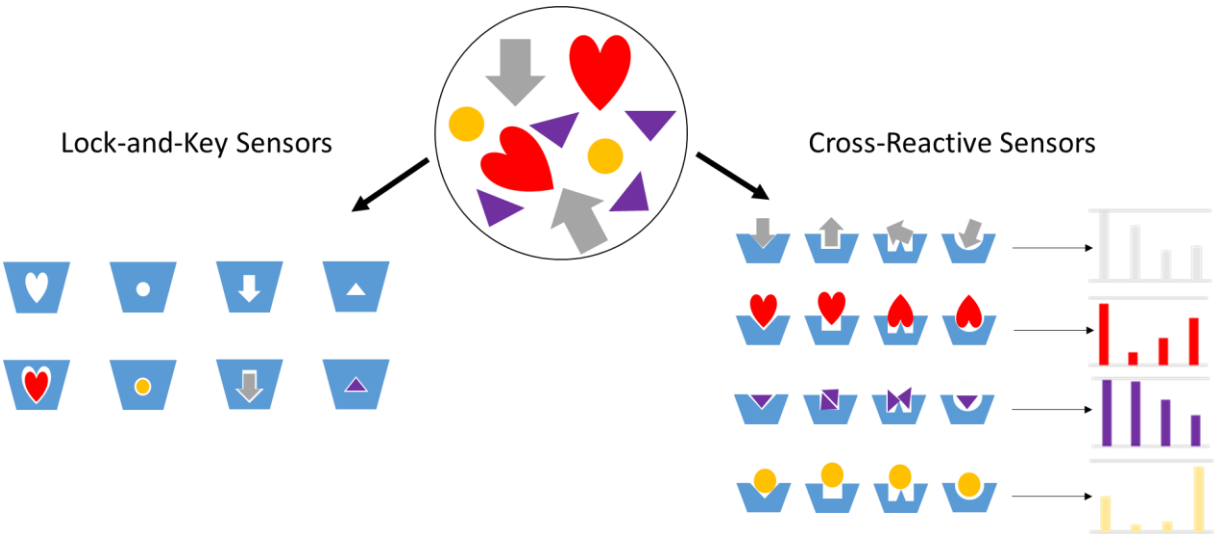

Figure I-3 A mixture of analytes being detected via a lock-and-key sensing array (left) or via a cross-reactive sensing array (right).

molecule is displaced causing a change in fluorescence. If the displacement of the dye upon addition of the guest quenches the signal, it is called a turn-off sensor. Conversely, if the analyte binding the host enhances the signal, it is called a turn-on sensor (**Figure I-4**). This change can be monitored, and if done correctly, can allow for the identification and calibration of various analyte molecules. To increase the accuracy, multiple host•guest pairings can be used such that each paring will react to each analyte differently. The resulting signals can then be put through a variety of statistical models and machine learning algorithms to properly identify and quantify each analyte.

In addition to IDA, naturally fluorescent or colorimetric hosts that react to the bound analyte have been used as molecular sensors. Hof and coworkers were able to synthesize modified CX[n] molecules that formed binary complexes with each other which they dubbed

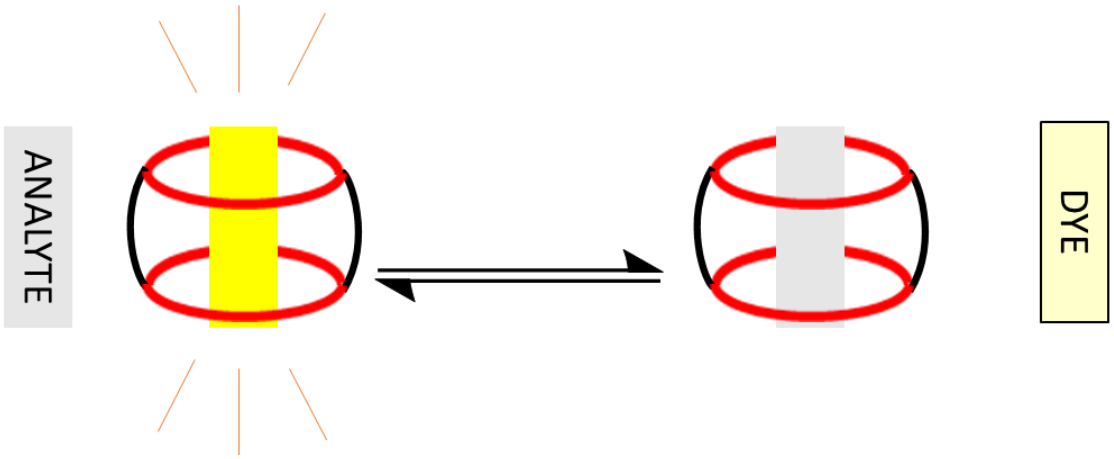

Figure I-4 Cartoon of a turn-off sensor where the dye signal is enhanced when bound to the host (left) but quenched once the analyte binds and displaces the dye (right).

Dimer Dyes.[37] While these hosts were naturally fluorescent, that fluorescence was quenched when they formed the dimer complex. When a guest molecule bound to one of the host molecules the complex was broken and the increase in fluorescence could be measured and used similarly to IDA creating a turn-on sensor. The Hof group leveraged this effect to detect methamphetamine and other drugs in saliva.[38]

Additionally the Isaacs and Anzenbacher groups have used naturally fluorescent aCB containers with a mixture of biphenyl naphthalene, and naphthalene based walls or naphthalene modified CB[6] to create sensing assays to allow for the detection of potentially harmful molecules such as over the counter drugs[39] and opioids.[40] The Isaacs group has also used an anthracene walled aCB alone to differentiate between 23 cationic molecules (**Figure I-5**).[41] This assay was also able to group the responses of each analyte into grouping according to the number of ammonium groups on each guest as well as their substitution.

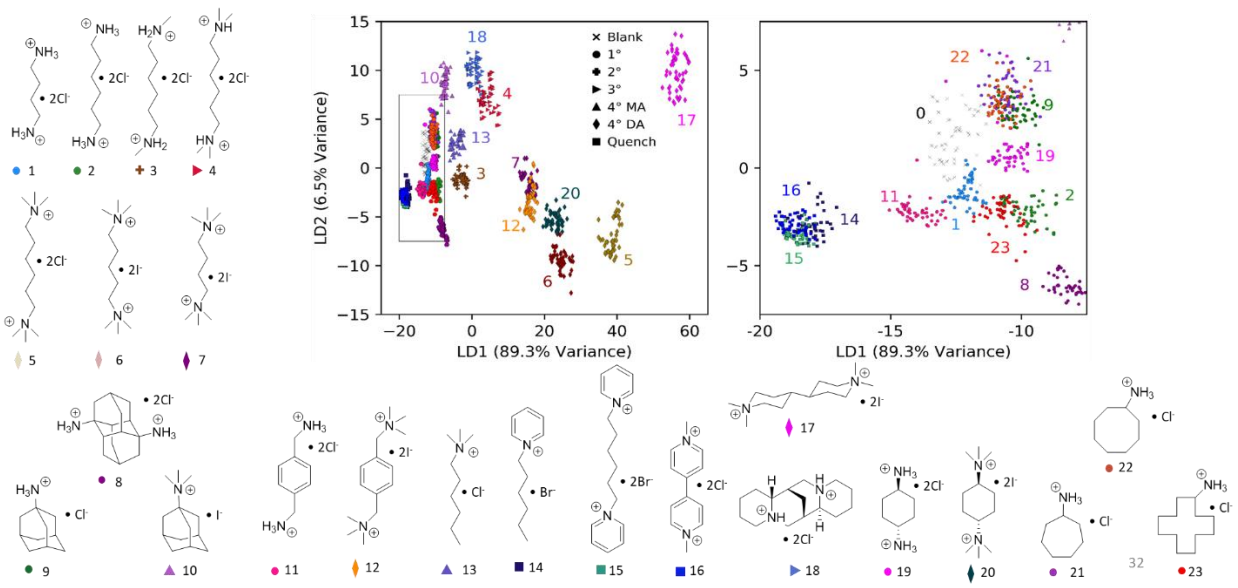

Figure I-5 Left panel) LDA plot of the first two linear discriminants (95.8 % of overall variance) showing the separation and classification of analytes 1–20, 23, 24. Right panel) Expanded region from the grey boxed area of the left panel Three different concentrations of M3. (2.0 μm, 5.0 μm, and 10.0 μm) were mixed with 5 μm analyte in separate wells of a 96-well plate and analyzed for changes in fluorescence across each spectrum (415 nm–460 nm) at intervals of every 5 nm. Analytes were predicted with 91±2 % accuracy.[41]

In each case, the high binding affinity of supramolecular containers and the quenching effects of the host-dye complexes were leveraged to create a sensor that was capable of visually distinguishing between multiple analytes. The most remarkable part is that this differentiation can be done with relatively simple and cheap light-based instruments. This should allow for the detection of even more complex systems relatively easily without the need for large expensive instrumentation. The advancements and miniaturization in optics and the availability of high-

powered computers, has started to lead to a wider range of usage and increased usage of sensing assays outside of a lab setting.

Chapter 2: Cucurbit[8]uril Forms Tight Inclusion Complexes with Cationic Triamantanes

Reproduced from King, D.; Šumanovac, T.; Murkli, S.; Schreiner, P. R.; Šekutor, M.; Isaacs, L. Cucurbit[8]uril Forms Tight Complexes with Cationic Triamantanes *New J. Chem.* **2023**. *47*, 5338-5346 with permission from the Centre National de la Recherche Scientifique (CNRS) and the Royal Society of Chemistry. Synthesis and characterization of triamantane guests were synthesized by Tatjana Šumanovac and Dr. Marina Šekutor with assistance from Dr. Peter R. Schreiner. Molecular Modeling was performed by Dr. Marina Šekutor. ITC studies and ^{1}H NMR studies were performed by David King and Dr. Steven Murkli with assistance from Dr. Lyle Isaacs.

2.1 Introduction

The synthesis and molecular recognition properties of the cucurbit[*n*]uril (CB[*n*]) family of molecular container compounds has undergone rapid development since the turn of the millennium.[13,42–44] **Figure II-1** shows the molecular structure of CB[*n*] which is composed of *n* glycoluril units connected by 2*n* methylene bridges that form a barrel shaped macrocycle with two electron rich ureidyl carbonyl fringed portals and a central hydrophobic cavity. Accordingly, CB[*n*] hosts bind strongly to guests that feature a central hydrophobic moiety that is flanked by two cationic groups. For example, Mock and co-workers showed that CB[6] binds strongly to alkanediammonium ions in aqueous formic acid solution with selectivity for pentane- and hexanediammonium ions (**1** and **2**);[45] the CB[6]-spermine (**3**) complex achieved $K_a = 1.3 \times 10^7$ M^{-1} (K_d = 76 nM). Later studies by Kim, Inoue, and co-workers demonstrated that even higher

binding affinity could be achieved by working in the less competitive environment of pure water.[46]

Clues from CB[*n*] derived self-sorting systems[21] led us to measure the binding constants of CB[*n*] (*n* = 6, 7, 8) toward a panel of ammonium ions in pH 4.74 acetate buffered water and discover the ultratight binding affinity of the CB[7] adamantane ammonium (**4**) ion ($K_a = 4.2 \times 10^{12}$ M^{-1}) using ^{1}H NMR competitive experiments.[22] The hydrophobic adamantane skeleton contains ten carbon atoms. Contemporaneously, Kim, Inoue, and Kaifer published the binding affinity of the CB[7] trimethylaminomethyl ferrocene (**5**; hydrophobic core: ten C-atoms + Fe) complex ($K_a = 4 \times 10^{12}$ M^{-1}) in pure water.[23] In the follow up work, the Kim, Kaifer, Isaacs, Gilson and Inoue group collaboratively explored the CB[7]·(bis)trimethylaminomethyl ferrocene (**6**) complex and determined $K_a = 2.9 \times 10^{15}$ M^{-1} in pure water by competitive ITC titrations.[17] The potential of [2.2.2]bicyclooctane as a hydrophobic core (eight C-atoms) (*e.g.*, **7**) to construct ultratight binding complexes was subsequently reported by the Kim, Inoue, and Gilson team.[16] The high affinity of CB[*n*] ·guest complexes has been traced, in part, to the presence of intracavity ‘‘high energy’’ water molecules that lack a full complement of H-bonds and that are released upon complexation as shown by DeSimone, Scherman, and Nau.[10,47–49] The K_a values for CB[*n*] ·guest complexes have been featured prominently in a series of blinded challenges (SAMPL and Hydrophobe) that aim to improve computational approaches to free energy computations in water.[50–52] As illustrated in **Figure II-2**, the changes in aqueous solvation of both the CB[*n*] host and the hydrophobic guest contribute to the thermodynamics of complexation.[10]

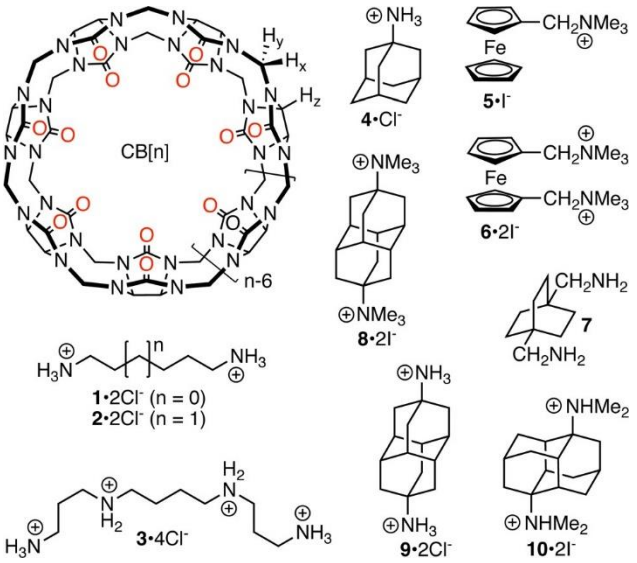

Figure II-1. Structure of ultratight binding hosts CB[*n*] (*n* = 6,7,8) and selected guests.

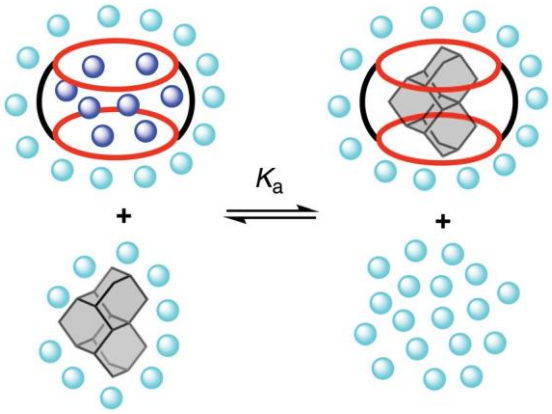

Figure II-2. Illustration of the changes in the solvation of the host and the guest that occur during the formation of CB[*n*]-guest complexes. Aqua spheres, bulk water; Blue spheres, intracavity ‘‘high energy’’ water.

More recently, in collaboration with Glaser and Mlinaric´-Majerski, we have explored various cationic guests featuring diamantane (14 C-atoms) as the hydrophobic core and

demonstrated the attomolar binding affinity of the CB[7]·diamantane-bis(trimethylammonium) ion (**8**) in pure water ($K_a = 7.2 \times 10^{17}$ M^{-1}).[53] The 10,000-fold weaker binding affinity of the CB[7]·**9** complex illustrates that the nature of the ammonium (1° versus 4°) can be a very important factor in some but not all situations.[53,54] In the CB[8] series, using the CB[8]·**10** complex $K_a = 5.7 \times 10^{14}$ M^{-1} was achieved in 50 mM acetate buffered water (pH = 4.74).[20] CB[*n*]·guest complexes have also been shown to be highly responsive to suitable stimuli (e.g., photochemical, electrochemical, chemical, and pH).[55–59] These high affinity, highly selective, and stimuli responsive binding events render CB[*n*]·guest complexes useful as a supramolecular latching and switching element in a variety of complex systems. Accordingly, macrocyclic CB[*n*] have found numerous uses including as a component of (bio)sensing and imaging ensembles,[40,60,61] for drug formulation, delivery and sequestration,[62–64] creating supramolecular organic frameworks,[65] and performing supramolecular catalysis.[49] In this paper, we further investigate into cationic CB[*n*]·diamondoid complexation events by progressing from C14 diamantane to the larger and more hydrophobic C18 triamantane skeleton. Very recently, Biedermann and co-workers have studied the binding of CB[*n*] toward diamondoid (adamantane, diamantane, and triamantane) alcohols using a combination of calorimetry and chemical computations.[66] Among other results, Biedermann and coworkers found that CB[8] binds with 3,9-dihydroxytriamantane with $\log K_a = 7.0$ in deionized water which represents the first example of triamantane complexation with CB[*n*]. Overall, Biedermann's work showed that peculiar host solvation – rather than London dispersion interactions, electronic energies, or entropic factors – is largely responsible for the ultratight binding exhibited by CB[*n*] hosts.

2.2 Results and Discussion

This results and discussion section is organized as follows. First, we describe the selection, synthesis, and characterization of guests **G1**–**G4**. Next, we investigate the complexation of **G1**–**G4** by complexation induced changes in ^{1}H NMR chemical shifts along with molecular modelling to glean information about the geometry of the CB[*n*]·**G** complexes. Subsequently, we measure the binding constants for the CB[*n*]·**G** complexes by direct isothermal titration calorimetry (ITC), ^{1}H NMR competitive experiments, and competitive ITC titrations as appropriate. Finally, we discuss the data and provide conclusions.

2.2.1 Selection, Synthesis and Characterization of G1-G4

As described above, the Isaacs group has a longstanding interest in the design and discovery of tight binding host–guest complexes with an emphasis on CB[*n*]·cationic diamondoid systems. Previous investigations focused on (di)cationic adamantane (C10) and diamantane (C14) derived guests and showed that both ion–dipole (C=O···ammonium) interactions and the hydrophobicity of the diamondoid skeleton play significant roles in determining host–guest binding affinity.[18,20,22,67,68] As the next logical step toward the creation of even tighter binding guests for CB[*n*], we decided to investigate cationic derivatives of triamantane (C18) which is the next larger diamondoid homologue. Accordingly, we synthesized hydrochloride salts **G2** and **G4** (**Figure II-3**) from triamantane by three step procedures (hydroxylation, modified Ritter reaction with chloroacetonitrile, and cleavage of the formed chloroacetamide to the corresponding amine) described in the literature.[69,70] The separate permethylation reactions of **G2** and **G4** with an excess of MeI (15 equiv.) and $NaHCO_3$ (10 equiv.) were conducted in hot (60 °C) MeOH for 48 h

which delivered quaternary ammonium salts **G1** and **G3** in 47 and 62% yields, respectively. High resolution mass spectrometry showed ions for **G1** at 298.2536 (calc. for $C_{21}H_{32}N$: 298.2535) and **G3** at 379.3100 (calc. for $C_{24}H_{40}N_2Na$: 379.8089) which are in accord with the depicted molecular formulas. Please note that **G1** and **G3** are prepared and used as iodide salts whereas **G2** and **G4** are hydrochlorides; we do not consider the influence of counterions in this paper. C_s-symmetric guests **G1** and **G2** feature a single mirror plane whereas guests **G3** and **G4** possess two mirror planes and are therefore C_2v-symmetric. In accord with symmetry considerations, the ^{13}C NMR spectrum of **G1** and **G3** recorded in $CDCl_3/CD_3OD$ consist of 14 and 9 resonances, respectively (ESI,† **Figure SII-2** and **SII-4**). While the ^{1}H NMR spectrum of **G1** suffers from spectral overlap, the spectrum for C_s-symmetric **G3** (ESI,† **Figure SII-3**) is more diagnostic and displays seven resonances in an 18 : 4 : 4 : 4 : 6 : 2 : 2 ratio; the resonance at 1.79 pm with an integral of six is caused by the accidental overlap of two resonances (4H and 2H).

2.2.2 Investigation of the host-guest complexation by ^{1}H NMR spectroscopy

After having synthesized and fully characterized guests **G1**–**G4**, we decided to perform a qualitative investigation of the host–guest binding of CB[7] and CB[8] toward guests **G1**–**G4** by ^{1}H NMR spectroscopy (ESI,† **Figure SII-5 – SII-16**). For example, **Figure II-4c** shows the ^{1}H NMR spectra recorded for **G4** along with the assignments of the resonances. Because H_b and H_c are diastereotopic they appear as a pair of coupled doublets. The resonances for H_a, H_b, and H_c

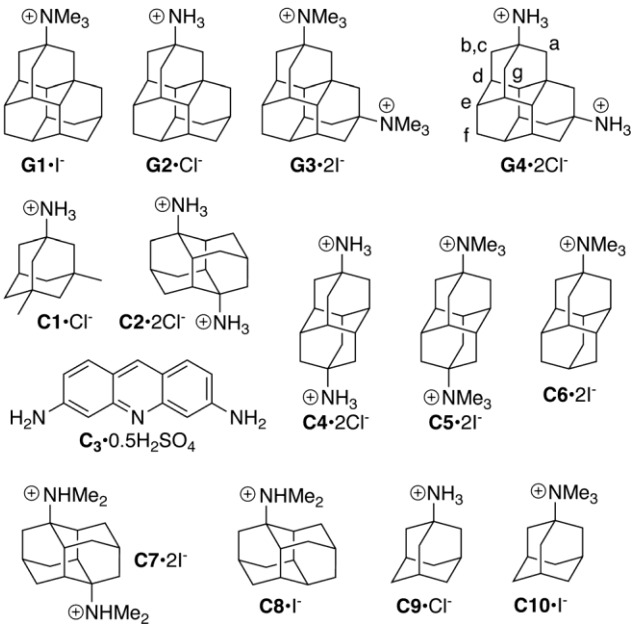

Figure II-3. Structures of cationic guests **G1**-**G4**, competitors **C1**-**C3**, and comparison compounds **C4**-**C10** used in this study.

appear downfield of the other resonances due to the electron withdrawing effect of the adjacent NH_3^+ group. The ^{1}H NMR spectra separately recorded for 1 : 1 mixtures of **G4** with CB[8] and CB[7] are shown in **Figure II-4b** and **d**, respectively. As expected, all of the resonances for guest **G4** shift upfield upon formation of CB[7]·**G4** and CB[8]·**G4** complexes indicating that guest G4 is bound within the magnetically shielding environment of the CB[*n*] cavity.[42,45] At 1 : 2 CB[*n*] : **G4** ratio (**Figure II-4a** and **e**), we observe separate resonances for free G4 and the CB[*n*]·**G4** complex which evidences the slow kinetics of guest exchange on the ^{1}H NMR timescale which is typical for ultratight CB[*n*] guest complexes.[22] The ^{1}H NMR spectrum of D_{nh}-symmetric CB[*n*] hosts shows one set of diastereotopic resonances (H_x and H_y) for the methylene bridges. In the CB[*n*]·**G4** complex we still observe one set of doublets for H_x and H_y which

indicates that its time averaged geometry has a mirror plane passing through the equator of the complex. The magnitude of the complexation induced changes in the chemical shift is presented in **Figure II-4b** and **d**. Protons H_a, H_d, and H_g undergo substantial upfield shifts ($\Delta\delta$ from 0.68 to 0.86 ppm) whereas H_b, H_c, and H_e undergo smaller shifts ($\Delta\delta$ from 0.16 to 0.51 ppm) which reflects their position with respect to the magnetically shielding CB[*n*] cavity (vide infra). To the best of our knowledge, the inclusion of the 18 carbon triamantane skeleton inside the CB[7] cavity is the largest number of heavy (non-hydrogen) atoms incorporated to date. Recently, Biedermann et al. studied the binding of CB[7] toward 3,9-dihydroxytriamantane and 9,15-dihydroxytriamantane and concluded that ‘‘the experimental evidence ruled out the positioning of the guest in the hosts’ cavity’’.[66] Accordingly, we conclude that the presence of the cationic groups on **G4** provides sufficient ion–dipole interactions to drive the formation of the otherwise unfavorable inclusion of the triamantane framework inside CB[7]. Similar ^{1}H NMR measurements were performed for CB[7]·**G1**, CB[8]·**G1**, CB[7]·**G2**, CB[8]·**G2**, and CB[8]·**G3** complexes which indicate the inclusion of the triamantane skeleton in the CB[*n*] cavity (ESI,† **Figure SII-5 – SII-12**). In contrast, the ^{1}H NMR spectra recorded for mixtures of CB[7] and **G3** show small upfield shifts for the NMe_3^+, H_b, and H_c resonances (ESI,† **Figure SII-9 – SII-10**) which suggests that CB[7]·**G3** forms an exclusion complex where only one NMe_3^+ group enters the CB[7] cavity and the other NMe_3^+ group is outside the cavity (ESI,† **Figure SII-57**). Such exclusion complexes are typically weak. In contrast, ^{1}H NMR results for CB[7]·**G1**, CB[8]·**G1**, CB[7]·**G2**, CB[8]·**G2**, and CB[8]·**G3** (ESI,† **Figure SII-5** – **SII-12**) show that the resonances for the triamantane frameworks of **G1**, **G2**, and **G3** undergo complexation induced upfield changes in the chemical shift which is indicative of cavity binding. In addition, separate ^{1}H NMR

resonances for free and complexed guests are present at 1 : 2 CB[*n*]·guest stoichiometry for CB[7]·**G1**, CB[8]·**G1**, CB[7]·**G2**, CB[8]·**G2**, and CB[8]·**G3** which indicates that the kinetics of guest exchange are slow on the chemical shift timescale. For the C_s-symmetric guest **G1** we observe a slight downfield shift of the NMe_3^+ resonance which indicates that the NMe_3^+ group is located in the deshielding region just outside the C=O portals.[42,45] In addition, upon formation of the CB[7]·**G1**, CB[7]·**G2**, and CB[8]·**G2** complexes we observe two sets of resonances for the diastereotopic methylenes of CB[*n*] (H_x, H_y) which is due to the top-bottom C=O portal dissymmetry induced by the C_s-symmetric guests.

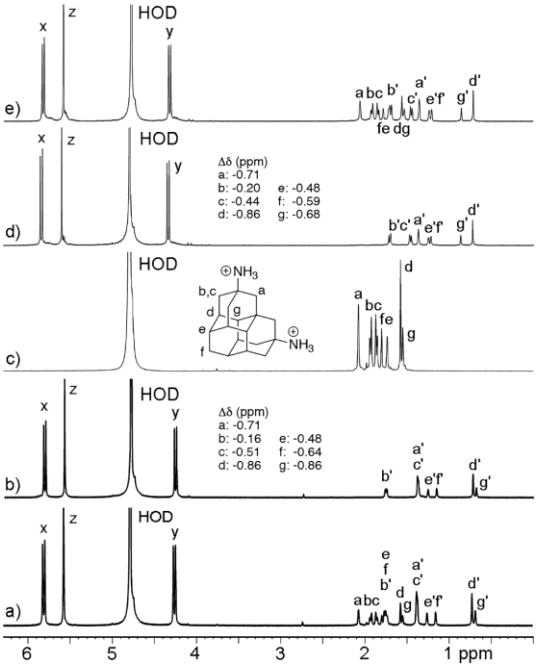

Figure II-4. ^{1}H NMR spectra recorded (600 MHz, D_2O) for (a) a mixture of **G4** (2 mM) and CB[8] (1 mM), (b) a mixture of **G4** (1 mM) and CB[8] (1 mM), (c) **G4** (1 mM), (d) a mixture of **G4** (1 mM) and CB[7] (1 mM), and (e) a mixture of **G4** (2 mM) and CB[7] (1 mM). Resonances marked with primes (‘) arise from the host-**G4** complex.

2.2.3 Molecular Modeling

To gain further insight into the geometry characteristics of the CB[*n*]·**G4** complexes we performed molecular modelling. The search for favorable complex geometries was done using the Conformer–Rotamer Ensemble Sampling Tool (CREST) based on the GFN methods[71,72] by applying iterative meta-dynamic sampling for non-covalently bound complexes, clusters or aggregates (NCIiMTD mode). The analytical linearized Poisson–Boltzmann (ALPB) solvation model was used to account for the implicit influence of water in xTB computations. **Figure II-5** shows the top and side of the found geometries of the CB[7]·**G4** and CB[8]·**G4** complexes. Minimized molecular models of the CB[7]·**G1** – CB[7]·**G3** and CB[8]·**G1** – CB[8]·**G3** complexes are shown in the ESI† (**Figure SII-55** – **SII-57**). In accordance with the analysis of the complexation induced changes in chemical shifts described above, the molecular models show the encapsulation of the hydrophobic triamantane skeleton in the center of the CB[*n*] cavity. The average distances of cage H-atoms from the mean equatorial plane defined by the glycoluril methine C-atoms are as follows for CB[7]·**G4**: H_a, 1.26; H_b, 3.37; H_c, 2.55; H_d, 1.26; H_e, 2.13; H_f, 0.07; H_g 0.19 Å and for CB[8]·**G4**: H_a, 1.20; H_b, 3.25; H_c, 2.41; H_d, 1.22; H_e, 2.05; H_f, 0.50; H_g, 0.61 Å. As shown in **Figure II-4b** and **d** for CB[7]·**G4** and CB[8]·**G4**, H_a, H_d, H_f, and H_g, which undergo substantial upfield shifts in the NMR spectrum, reside closer to the equatorial plane running through the center of the CB[*n*] cavity. In contrast, the diastereotopic methylene resonance for H_b – which shows the smallest upfield shift for both CB[7]·**G4** and CB[8]·**G4** – is the farthest from the equator. The average distance between the O-atoms on a single glycoluril ranges from 5.95 to 6.20 Å for CB[7]·**G4** and from 5.77 to 5.95 Å for

CB[8]·**G4** with averages of 6.05 and 5.87 Å, respectively. This is consistent with the expected buttressing effect of the sterically demanding **G3** guest against the C=O portals more significantly for CB[7] than CB[8]. Each NH_3^+ group in CB[7]·**G4** forms two H-bonds to the ureidyl C=O groups of CB[7] with the following NH···O=C distances (2.00 Å; 1.90 Å), N···O=C distances (2.89 Å; 2.76 Å) and NH···O=C angles (157.91; 127.71). The guests' N-atoms reside slightly outside the cavity (0.68 Å) in CB[7]·**G4** as defined by the distance to the mean plane of the ureidyl O-atoms. The H-bonding metrics for CB[8]·**G4** are NH···O=C distances (1.77 and 1.80 Å; 1.98 and 2.02 Å), N···O=C distances (2.80 and 2.83 Å; 2.87 and 2.91 Å) and NH···O=C angles (168.31 and 168.41; 143.41 and 142.41). The guests' N-atoms reside slightly outside the cavity (0.48 Å; 0.76 Å) in CB[8]·**G4** as defined by the distance to the mean plane of the ureidyl O-atoms. The distance of CB[7]·**G4** (CB[8]·**G4**) from the centroid of the equatorial methine C-atoms to those methine C-atoms averages 5.84 Å (6.58 Å) whereas the distance from the centroid of the ureidyl O-atoms back to the ureidyl O-atoms averages 4.22 Å (4.80 Å) which defines the width of the cavity and portals, respectively. Note that our modelling results also point towards the preferential formation of the CB[7]·**G3** exclusion complex since the geometry where only one NMe_3^+ group is inside the host cavity (ESI,† **Figure SII-25**) is energetically much more favorable than the hypothetical structure where full inclusion is realized (ESI,† **Table SII-1**).

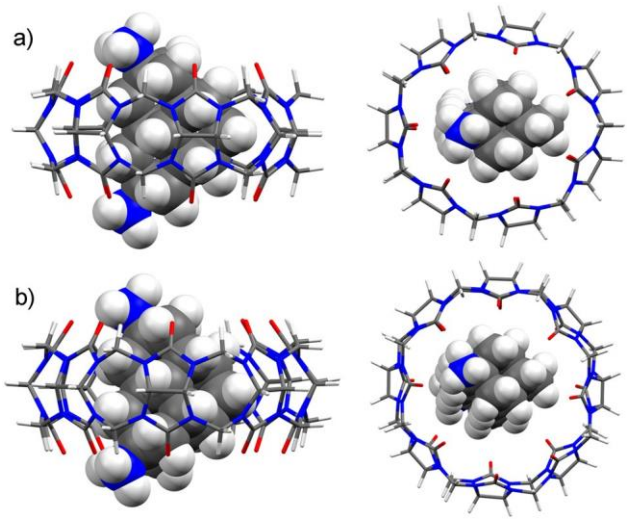

Figure II-5. Side and top views of the energy-minimized geometries of (a) CB[7]-**G4** and (b) CB[8]-**G4**. Color codes: C, gray; H, white; O, red; and N, blue.

2.2.4 Measurement and Discussion of the Thermodynamic Parameters of Complex Formation

The measurement of all binding constants in this paper was performed in 50 mM NaOAc buffered water at pH = 4.74 to allow comparison with binding constants for cationic adamantane and diamantane derivatives measured previously.[18,20,22,73] Given the bulkiness of guests **G1**–**G4** which feature the C18 triamantane skeleton and the fast kinetics of guest exchange observed for CB[7]·**G3** we suspected that the CB[7] complexes with these guests would be weak. Accordingly, we performed direct isothermal calorimetric titrations for CB[7]·**G1**, CB[7]·**G2**, and CB[7]·**G4** (ESI,† **Figure SII-17** – **SII-19**). **Figure 6a** shows the thermogram recorded when a solution of CB[7] (145 mM) in the cell was titrated with a solution of **G1** in the syringe. The direct titration data were processed and analyzed using the PEAQ ITC data analysis software. **Figure II-6b** shows a plot of the integrated heat versus CB[7] : **G1** molar ratio fitted to a 1 : 1

binding model that was used to determine the K_a = (1.6 ± 0.1) × 10^5 M^{-1} and ΔH = –10.4 ± 0.076 kcal mol^{-1} values (**Table II-1**). The K_a and ΔH values of CB[7]·**G2** and CB[7]·**G4** were determined similarly and are presented in **Table II-1** along with data for selected comparison compounds **C4**–**C10** drawn from the literature.[18,20,22] We performed ^{1}H NMR competitive experiments using the protocols described previously[18–20,22,67] to measure the K_a value for CB[7]·**G3** (K_a = (3.0 ± 0.5) × 10^5 M^{-1}) using **C1** (K_a = (2.5 ± 0.4) × 10^4 M^{-1}) as a competitor of known affinity (ESI,† **Figure SII-21**).[22]

We expected the binding constants of the cationic triamantanes toward CB[8] to far exceed the range that can be measured by direct titrations, so we elected to perform competitive titrations

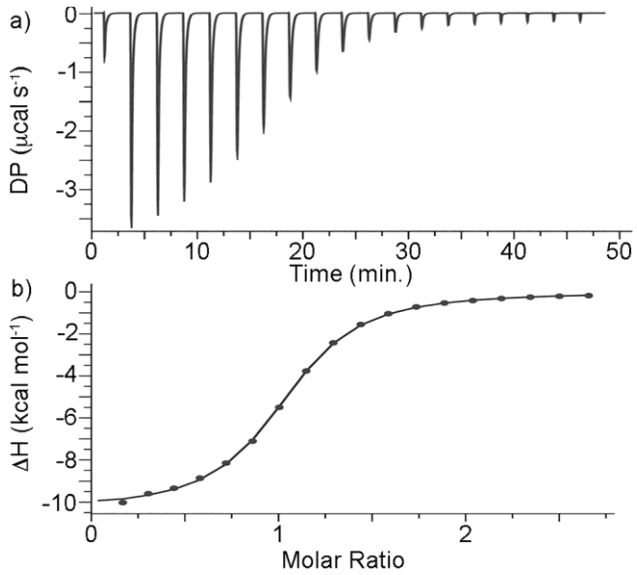

Figure II-6. (a) ITC thermogram recorded during the titration of CB[7] (145 mM) in the cell with guest **G1** in the syringe, (b) Fitting of the data to a 1 : 1 binding model with K_a = (1.6 ± 0.1) × 10^5 M^{-1} and ΔH = –10.4 ± 0.076 kcal mol^{-1}.

Table II-1 Binding constants (K_a, M^{-1}) and binding enthalpies (ΔH, kcal mol^{-1}) measured for the complexes between hosts CB[7] or CB[8] with guests **G1**–**G4** and **C1**–**C9**. Conditions: 50 mM NaOAc buffered H_2O or D_2O, 298 K, pH 4.74)

G	CB[7]	CB[8]
G1	$(1.6 \pm 0.1) \times 10^5$ [a]	$(2.1 \pm 0.1) \times 10^{14}$ [c]
G2	$(7.5 \pm 0.2) \times 10^4$ [a] -10.4 ± 0.076 -4.98 ± 0.034	n.d. [d]
G3	$(3.0 \pm 0.5) \times 10^5$ [c]	$(1.15 \pm 0.17) \times 10^{13}$ [f]
G4	$(6.73 \pm 1.41) \times 10^5$ [a] -3.79 ± 0.10	-10.1 ± 0.0 $(1.1 \pm 0.3) \times 10^{14}$ [e] $(1.14 \pm 0.21) \times 10^{14}$ [f]
C1	$(2.5 \pm 0.4) \times 10^4$ [b]	-11.5 ± 0.1 $(4.3 \pm 1.1) \times 10^{11}$ [b]
C2	2030 [b]	$(3.3 \pm 0.8) \times 10^{13}$ [b]
C3	—	$(2.67 \pm 0.32) \times 10^7$ (1 : 1) -9.23 ± 0.04 $(7.47 \pm 1.75) \times 10^6$ (1 : 2)
C4	$(1.3 \pm 0.3) \times 10^{11}$ [b]	-8.28 ± 0.06 $(8.3 \pm 2.3) \times 10^{11}$ [b]
C5	$(1.9 \pm 0.4) \times 10^{15}$ [b]	$(2.0 \pm 0.6) \times 10^{12}$ [b]
C6	$(8.0 \pm 1.9) \times 10^{11}$ [b]	$(2.7 \pm 0.7) \times 10^{12}$ [b]
C7	686 [b]	$(5.7 \pm 1.5) \times 10^{14}$ [b]
C8	643 [b]	$(7.8 \pm 0.8) \times 10^{13}$ [b]
C9	$(4.2 \pm 1.0) \times 10^{12}$ [b]	$(8.2 \pm 1.8) \times 10^8$ [b]

[a] Measured by direct ITC titration. [b] Literature values. [c] Measured by ^{1}H NMR competitive experiments with **C1** as a competitor. [d] CB[8]-**G2** complex is insoluble at room temperature. [e] Measured by ^{1}H NMR competitive experiments with **C2** as a competitor. [f] Measured by ITC competitive experiments using **C3** as a competitor.

monitored by ^{1}H NMR or ITC. The literature K_a values of CB[8]-**C1** and CB[8]-**C2** are given in **Table II-1**. Initially, we performed ^{1}H NMR competitive studies for CB[8]·**G1** using **C1** (K_a = 4.3×10^{11} M^{-1}) as a competitor. Experimentally, we prepared a solution of CB[8] (0.100 mM)

and **C1** (16.5 mM) and then added **G1** (0.110 mM) and monitored the equilibration process by ^{1}H NMR spectroscopy (ESI,† **Figure SII-20**). Specifically, we monitor the two separate Hz resonances for CB[8]·**C1** and CB[8]·**G1** at ≈ 5.5 ppm until equilibrium is reached. Integration of the resonances by spectral deconvolution, followed by application of the equilibrium and mass balance equations as described previously[18–20,22,67] allowed the calculation of $K_a = (2.12 \pm 0.1) \times 10^{14}$ M^{-1} for CB[8]·**G1**. Separate experiments that approached equilibrium from the other direction (e.g., starting with CB[8]·**G1** and adding **C1**) gave identical results. The binding constant for CB[8]·**G4** (($K_a = (1.1 \pm 0.3) \times 10^{14}$ M^{-1}), ESI,† **Figure SII-22**) was similarly measured by competitive ^{1}H NMR assays using **C2** as a competitor. Unfortunately, we were not able to measure the binding constant for CB[8]·**G3** by ^{1}H NMR competitive assays because equilibration was extraordinarily slow and complicated by extraneous resonances due to unknown guest decomposition products.

Given the difficulties in measuring K_a for CB[8]·**G3** by ^{1}H NMR competitive assays, we turned to ITC competitive experiments.[74–76] Biedermann *et al.* have previously suggested a cationic cyclophane as a tight binding competitor for CB[8],[77] but because this compound was not commercially available we were unable to test this approach. To avoid problems of slow kinetics which plagued ^{1}H NMR competitive assays, after much experimentation, we selected the tight binding CB[8]·**C3$_2$** ternary complex as the competitive complex.[78] **Figure II-7a** depicts the equilibrium binding model governing this system. Initially, we performed a concatenated series of three direct ITC titrations of a solution of CB[8] (5 mM) in the cell with a solution of **C3** (40 mM) from the syringe (**Figure II-7b**). **Figure II-7c** shows a plot of the integrated heat data versus molar ratio fitted to the stepwise binding model shown (**Figure II-7a**) using the

Affinimeter™ software package to deliver the thermodynamic parameters for the formation of the CB[8]·**C3** and CB[8]·**C3**$_2$ complexes. Affinimeter™ was used because the PEAQ ITC data analysis software cannot implement the model shown in **Figure II-7a**. Subsequently, we performed the competitive ITC titration of a solution of CB[8] (30 mM) and **C3** (175 mM) in the cell with a solution of **G3** (100 mM) from the syringe (**Figure II-7d**). The DP *versus* time data were exported to Affinimeter™ and then integrated to create the plot of ΔH versus molar ratio shown in **Figure II-7e**. The solid line represents the best global fit of the data to the binding model given in **Figure II-7a** to calculate the K_a value for CB[8]·**G3** ($K_a = (1.15 \pm 0.17) \times 10^{13}$ M^{-1}). The complete Affinimeter™ reports are given in the ESI† (**Figure SII-23** – **SII-54**). Given that this strategy of using a tight CB[8]·**C3**$_2$ ternary complex as a competitor is new and uses a new analysis package (Affinimeter™) we decided to further validate our results by performing related competitive titration of CB[8]·**C3**$_2$ with **G4** which was measured above by ^{1}H NMR competitive experiments. Gratifyingly, the K_a value measured for CB[8]·**G4** by competitive ITC titration ($K_a = (1.1 \pm 0.3) \times 10^{14}$ M^{-1}) is the same as that measured by ^{1}H NMR competitive experiments ($K_a = (1.14 \pm 0.21) \times 10^{14}$ M^{-1}).

With a complete dataset of CB[*n*]·**G** thermodynamic parameters in hand, some discussion of the trends in the data is warranted. The magnitude of the binding constants of **G1**–**G4** toward CB[7] (7.5×10^4 to 6.7×10^5 M^{-1}) is dramatically different than that toward CB[8] (1.15×10^{13} to 2.1×10^{14} M^{-1}). Related effects were seen previously in the binding constants of **C1**, **C7**, and **C8**) toward CB[7] and CB[8] which differ dramatically (**C1** : 10^7 , **C7** : 10^{12}, **C8** : 10^{11}).[22] We attribute this effect to the fact that the triamantane skeleton (254 Å^3, PM3 calculation) is too

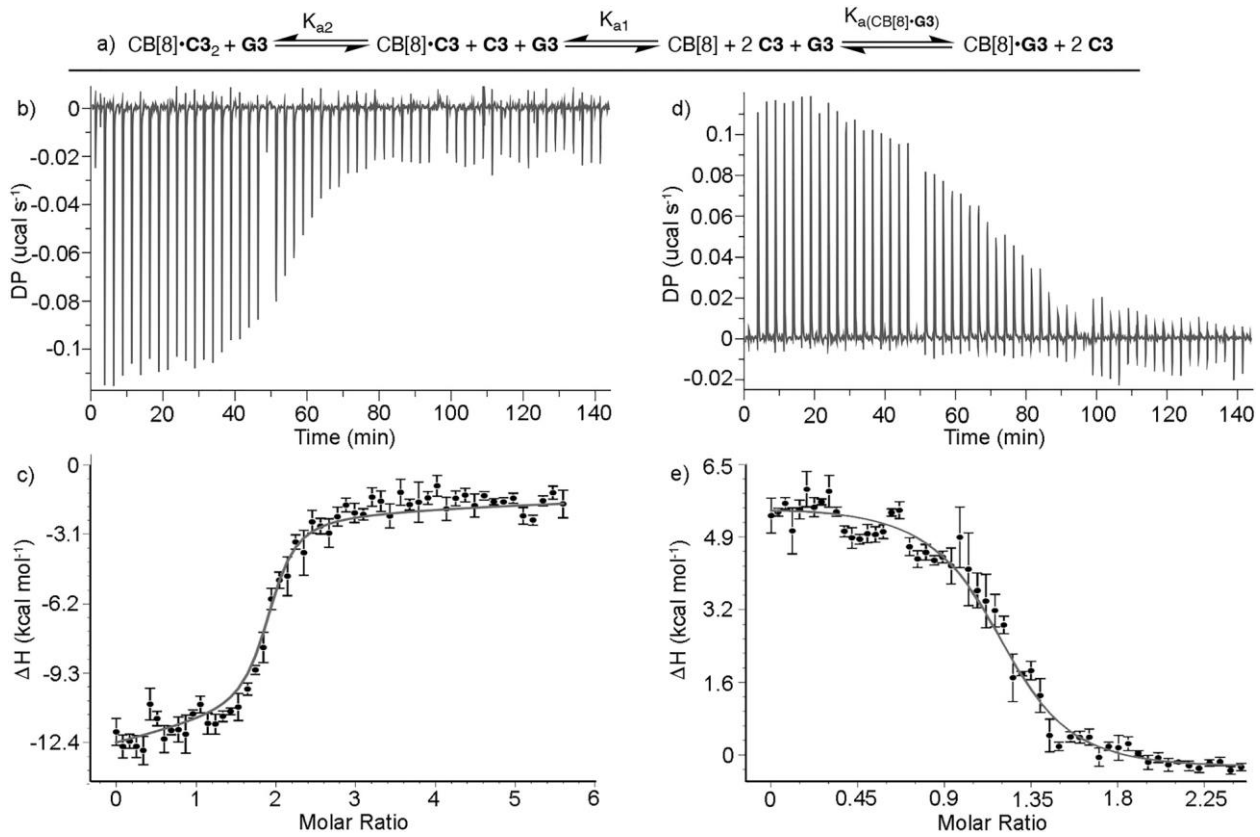

Figure II-7. (a) Schematic representation of binding models implemented in Affinimeter™ to determine the K_a values for the formation of CB[8]·**C3** and CB[8]·**C3**$_2$ in the direct titration of CB[8] with **C3** and the competitive binding model used to determine the K_a value for CB[8]·**G3** during the titration of a mixture of CB[8] and **C3** with **G3**. (b) Thermogram from the direct titration of CB[8] (5 mM) with **C3** (40 mM) in the syringe. Three successive titrations were concatenated. (c) Plot of ΔH *versus* molar ratio. The solid line represents the best fit of the data to the stepwise binding model performed using Affinimeter™. (d) Thermogram from the competitive ITC titration of a solution of CB[8] (30 mM) and **C3** (175 mM) in the cell with a solution of **G3** (100 mM) in the syringe. (e) Plot of ΔH *versus* molar ratio. The solid line represents the best fit of the data to the stepwise binding model performed using Affinimeter™.

voluminous to be comfortably encapsulated inside CB[7] (volumes: expanded, 272; inner, 242; truncated 158 Å^3)[47] with a packing coefficient over 100% of the inner cavity whereas triamantane can be easily encapsulated inside CB[8] (volumes: expanded, 479; inner, 367; truncated 263 Å^3) with a packing coefficient of 69% which is in line with other tight binding CB[*n*]·diamondoid complexes.[66] For comparison, the calculated volume of diamantane is 206 Å^3 (PM3) which is known to display high affinity toward both CB[7] (packing coefficient 85%) and CB[8].[18,20,66] The observation of inclusion complexes for CB[7]·**G1**, CB[7]·**G2**, and CB[7]·**G4** demonstrates that the binding free energies of **G1**, **G2**, and **G4** are sufficiently large to pay the energetic cost to overstuff the cavity of CB[7]. This, coupled with the observation that CB[7]·**G3** forms an exclusion complex explains the overall modest binding affinities of CB[7] toward **G1**–**G4**. In the CB[7] complexes there is little difference in the binding affinity of the primary ammonium **G2** relative to the quaternary ammonium **G1**. Somewhat surprisingly, amongst the CB[8] complexes, the quaternary ammonium guest **G1** binds 18-fold stronger than the quaternary diammonium guest **G3** and two-fold more strongly than the primary diammonium guest **G4**. Unfortunately, the strongest binding achieved among **G1**–**G4** toward CB[8] was for CB[8]·**G1** ($K_a = 2.21 \times 10^{14}$ M^{-1}) which is lower than the diamantane diammonium compounds (*e.g.*, **C7**) measured previously. Informative comparisons can also be made across homologous series of guests and comparators (*e.g.*, adamantane vs. diamantane vs. triamantane) to tease out the effect of enlarging the hydrophobic framework. For example, the binding of mono trimethylammonium ions **C10**, **C6**, and **G1** toward CB[7] decrease in magnitude as the size of the hydrophobic skeleton increases due to the overstuffing of the CB[7] cavity as described

above. Conversely, the binding constants of **C10**, **C6**, and **G1** toward CB[8] increase by three orders of magnitude as the hydrophobic skeleton is increased from 10 to 14 to 18 C-atoms, which reflects the enhanced hydrophobic effect associated with desolvation of the larger hydrophobic residue. In a similar way, CB[8] prefers to bind to the primary diammonium triamantane **G4** over the diamantane **C4** by a factor of 137-fold which once again reflects the influence of the larger hydrophobic residue. Conversely, CB[7] prefers **C4** over **G4** by over five orders of magnitude because the packing coefficient of the triamantane derivative **G4** is too high for CB[7]. Related trends are seen when comparing the binding constants for quaternary triamantane and diamantane diammonium ions **G3** and **C5** toward CB[*n*]. CB[7] prefers the smaller diamantane **C5** by nearly ten orders of magnitude whereas the larger CB[8] binds six-fold more strongly to the larger triamantane derivative **G3**.

2.3 Conclusions

We report the preparation and characterization of cationic triamantane derivatives **G1**–**G4** which differ in overall charge (mono- and dication) and in the degree of nitrogen substitution (primary and quaternary). The binding behavior of **G1**–**G4** toward CB[7] and CB[8] was studied by a combination of ^{1}H NMR spectroscopy, analysis of complexation induced changes in chemical shift, and molecular modelling. Remarkably, CB[7] forms inclusion complexes with triamantanes **G1**, **G2**, and **G4** which exhibit slow kinetics of exchange on the ^{1}H NMR timescale. To the best of our knowledge, the encapsulation of 18 heavy (nonhydrogen) atoms inside CB[7] is the highest number observed to date. The binding constants of CB[7] and CB[8] toward triamantane guests **G1**–**G4** were determined by ^{1}H NMR competitive experiments, direct

ITC titrations, and competitive ITC titrations as appropriate based on the magnitude of the binding constants and the kinetics of guest exchange. The use of an ultratight binding ternary complex (CB[8]·**C3**$_2$) with fast kinetics of guest exchange represents a new method to measure ultratight CB[8] · guest complexes. This new method capitalized on the ability of Affinimeter^{TM} to implement this complex binding model and perform global fits of the binding data. Comparisons of the binding data of the homologous series of guests (e.g., adamantane to diamantane to triamantane) showed that the larger C-18 triamantane skeleton delivered enhanced binding affinity toward CB[8] whereas the smaller CB[7] cavity could not accommodate the triamantane framework without incurring substantial energetic penalties due to over-packing. Overall, this work extends our knowledge of the importance of the hydrophobic residue on the binding affinity of cationic diamondoids toward CB[*n*] and delivers a new competitive ITC method via an ultratight but fast exchanging ternary complex CB[8]·**C3**$_2$ to measure ultratight CB[8]·guest complex affinity.

2.4 Experimental

2.4.1 General Experimental

^{1}H and ^{13}C NMR spectra were recorded with Bruker AV-300, AV-400 or AV-600 NMR spectrometers and the NMR spectra were referenced to tetramethylsilane as an internal standard. The spectral reference for spectra recorded in D_2O was one drop of dioxane-d_8 added after recording the original spectrum. IR spectra were recorded with an FT-IR ABB Bomem MB 102 or FT IR-ATR PerkinElmer UATR Two spectrometer. MALDI-TOF MS spectra were obtained in reflectron mode with an Applied Biosystems Voyager DE STR instrument (Foster City, CA).

GCMS analyses were performed using an Agilent 7890B/5977B GC/MSD instrument equipped with an HP-5ms column. Melting points were obtained by using Original Kofler Mikroheitztisch apparatus (Reichert, Wien). All solvents were obtained from commercial sources and used without further purification. Aminotriamantanes **G2** and **G4** were prepared according to the previously published procedures[69,70] and their permethylation afforded salts **G1·I**$^{-}$ and **G3·2I**$^{-}$, respectively.

2.4.2 General Procedure for the Permethylation Reactions

A mixture of the respective amine (1 equivalent), excess methyl iodide (15 equivalents) and $NaHCO_3$ (10 equivalents) in methanol (10 mL) was heated in a sealed tube for 48 h at 60 ˚C.[53] The mixture was cooled, the solvent was evaporated, and the crude product was washed with a suitable solvent mixture to afford the corresponding permethylated salt.

2.4.3 *N,N,N*-Trimethyltriamantane-9-aminium iodide (G1·I^{-})

Permethylation of 9-aminotriamantane hydrochloride (**G2**·Cl^{-}) (146 mg, 0.5 mmol) afforded a solid that was washed with CH_2Cl_2 (20 mL). Evaporation of CH_2Cl_2 gave the crude product which was dissolved in a minimal amount of MeOH and then an excess of Et_2O (20 mL) was added. The solvent was decanted and the washing was repeated two more times, finally yielding the quaternary ammonium salt **G1**·I^{-} as a white solid (100 mg, 47%). M.p. 296–297 ˚C. IR (KBr, cm^{-1}): 3473 (br), 3006 (w), 2905 (s), 2874 (s), 2854 (s), 1635 (w), 1480 (m), 1441 (m), 1418 (m), 1341 (w), 1233 (w), 1136 (w), 945 (w), 847 (m). ^{1}H NMR ($CDCl_3$ + few drops of CD_3OD, 400 MHz): 1.47 (br. s, 2H), 1.52 (br. s, 2H), 1.64 (s, 2H), 1.67–1.83 (m, 10H), 1.90 (br. s, 1H), 1.99-2.05 (m, 2H), 2.06–2.14 (m, 4H), 3.04 (s, 9H, Me). ^{13}C NMR ($CDCl_3$ + few drops of CD_3OD,

100 MHz): 26.3 (CH, 1C), 32.2 (CH, 1C), 33.5 (CH, 1C), 34.2 (CH_2, 2C), 34.8 (C, 1C), 35.8 (CH_2, 1C), 36.1 (CH, 2C), 36.5 (CH_2, 2C), 38.8 (CH, 2C), 40.9 (CH_2, 1C), 43.7 (CH_2, 1C), 43.8 (CH, 2C), 47.0 (CH_3, 3C, Me), 71.8 (C, 1C, C-N). HR-MS: calcd for $[C_{21}H_{32}N]^+$ 298.2535; found 298.2536.

2.4.4 *N,N,N,N',N',N'*-Hexamethyltriamantane-9,15-diaminium diiodide (G3·2I$^-$)

Permethylation of 9,15-diaminotriamantane dihydrochloride (**G4**·2Cl$^-$) (137 mg, 0.40 mmol) afforded a solid that was washed with CH_2Cl_2 (20 mL). Evaporation of CH_2Cl_2 gave the crude product which was washed with a MeOH/CH_2Cl_2/ether (0.1 : 1.9 : 8 v : v : v ratio, 100 mL) mixture, yielding the quaternary ammonium salt **G3**·2I$^-$ as a white solid (152 mg, 62%). M.p. >350 ˚C. IR (neat, cm^{-1}): 3421 (br), 3210 (m), 1621 (m), 1604 (s), 1045 (w), 560 (w). ^{1}H NMR (600 MHz, D_2O): 1.55 (s, 2H), 1.73 (s, 2H), 1.79 (s, 6H), 2.02-2.07 (m, 4H), 2.10–2.16 (m, 4H), 2.21 (s, 4H), 3.03 (s, Me, 18H) ppm. ^{13}C NMR (75 MHz, CD_3OD), d: 33.5 (CH, 2C), 35.8 (CH_2, 4C), 36.2 (CH_2, 1C), 39.5 (C, 1C), 39.6 (CH, 4C), 42.0 (CH_2, 2C), 43.4 (CH, 2C), 49.4 (CH_3, Me, 6C), 73.3 (C-N, 2C) ppm. HR-MS: calcd for $[C24H_{40}N_2 + Na]^+$ 379.3089; found 379.3100.

Chapter 3: Molecular Recognition of Methylated Amino Acids and Peptides by Pillar[6]MaxQ

Reproduced from King, D.; Wilson, C. R.; Herron, L.; Deng, C.; Mehdi, S.; Tiwary, P.; Hof, F.; Isaacs, L. Molecular recognition of methylated amino acids and peptides by Pillar[6]MaxQ *Org. Biomol. Chem.* **2022**, *20*, 7429-7438 with permission from the Royal Society of Chemistry. Molecular dynamics simulations were performed by Lukas Herron with assistance from Shams Medhi and Dr. Pratyush Tiwary and initial conformations provided by David King. Indicator displacement assays were performed by Chelsea R. Wilson, with assistance from Dr. Fraser Hof. Synthesis of P[*n*]AS was performed by Dr. Chun-Lin Deng with assistance from Dr. Lyle Isaacs. All ITC and ^{1}H NMR experiments were performed by David King with assistance from Dr. Lyle Isaacs. In this chapter Pillar[*n*]arene (P[*n*]AS) is referred to as Pillar[*n*]MaxQ (P[*n*]MQ) to maintain consistency with the published source material.

3.1 Introduction

The design and realization of advanced supramolecular systems for a variety of biological (e.g. drug delivery, in vivo imaging, sequestration) and chemical (sensing, purifications, catalysis) applications is accelerated by the ready availability of a diverse set of building blocks. Molecular containers – cyclodextrins, calix[*n*]arenes, crown ethers, cyclophanes, coordination cages, molecular clips and tweezers, cucurbit[*n*]urils (CB[*n*]), H-bonded capsules, pillararenes, and others – are among the most commonly employed building blocks.[28,43,79–93] When considering biosupramolecular applications, good water solubility, excellent biocompatibility, and high binding affinity in salty water are particularly important.[94] Over the past decade, the

synthesis,[95–111] molecular recognition properties, and applications (*e.g.* drug delivery, fluorescent materials, chemical sensing, supramolecular antidotes, supramolecular catalysis, and porous materials) of organic and water soluble pillar[*n*]arenes has developed rapidly and been thoroughly reviewed. WP*n* (**Figure III-1**) which feature CH_2CO_2Na solubilizing groups, good biocompatibility and good host·guest binding affinity are particularly popular and have been used to recognize lysine and arginine.[112–115] Recently, we reported that Pillar[*n*]MaxQ (P[*n*]MQ) which feature OSO_3Na groups displayed greatly enhanced binding affinity compared to WP*n*, especially toward tertiary and quaternary ammonium ions.[30]

As a new host the biosupramolecular applications of P[*n*]MQ have not been explored. One important application of cation receptors like P[*n*]MQ is the binding and detection of biomarkers. Post-translational modifications (PTMs) play an important role in the regulation of protein function.[116,117] The N-methylation of lysine and arginine on the tail of histone 3 (**H3**) is an important class of PTMs. These methylation signatures have the potential to act as biomarkers in various diseases.[118,119] For example, high levels of **H3K4** trimethylation (**H3K4Me$_3$**) have been associated with a poor patient outcome in hepatocellular carcinoma.[120] These methylations

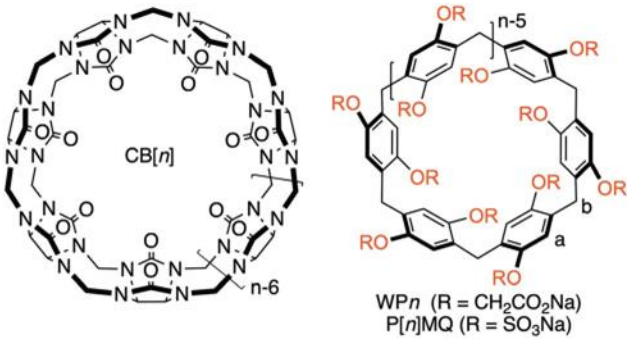

Figure III-1. Chemical Structures of CB[*n*] and pillararenes receptors.

commonly occur inside the nucleus where methyl transferase and demethylase enzymes orchestrate the degree of methylation resulting in distinct chromatin structure, function, and ultimately biological outcome.[121–123] To study the methylated states of lysine and arginine, chemical tools are needed that can selectively recognize the methylated over non-methylated residue. Accordingly, the molecular recognition of post-translationally methylated amino acid residues has been investigated using a variety of supramolecular hosts as a route toward new diagnostics and therapeutics.[124–136] Given our collective interest in using molecular containers in biosupramolecular applications[31,44] and the observed high selectivity of P6MQ for tertiary and quaternary ammonium ions,[30] we decided to explore the molecular recognition properties of P[*n*]MQ toward methylated *vs.* nonmethylated amino acids, amino acid amides, and the methylated peptide fragments of the histone 3 tail.

3.2 Results and Discussion

This results and discussion section is organized as follows. First, we present the measurement of the binding affinity of P5MQ and P6MQ toward a series of (methylated) amino acids and amino acid amides by isothermal titration calorimetry and discuss trends in the data. Subsequently, we present investigations of the geometry of the stronger host·guest complexes by ^{1}H NMR spectroscopy. Given the high binding affinity of P6MQ toward methylated amino acids, we next used indicator displacement assays to measure the binding of P6MQ toward a series of post-translationally modified peptides derived from the tail of histone 3. Finally, we

present the results of all-atom explicit water[137] molecular dynamics (MD) simulations to gain insight into the geometrical features and the driving forces for the P6MQ complexation events.

3.2.1 Selection of amino acids and amino acid amides

As described above, we have previously studied the binding of P[*n*]MQ toward a series of cationic and dicationic guests that also differ in the degree of alkylation of the cationic N-atoms.[30] We observed that P[*n*]MQ preferentially binds to quaternary over primary diammonium ions and that monocations bind more weakly than dications.[30] Accordingly, we selected a series of amino acids, amino acid amides, and N-acetyl amino acid amides (**Figure III-2**) that allow us to assess the importance of: (1) ion–ion interactions (*e.g.* **H–K–OH** *vs.* **H–K–NH$_2$** *vs.* **Ac–K–NH$_2$**), (2) the degree of methylation of the cationic side chains on lysine and arginine, and (3) the nature of the hydrophobic residue on the complexation strength.

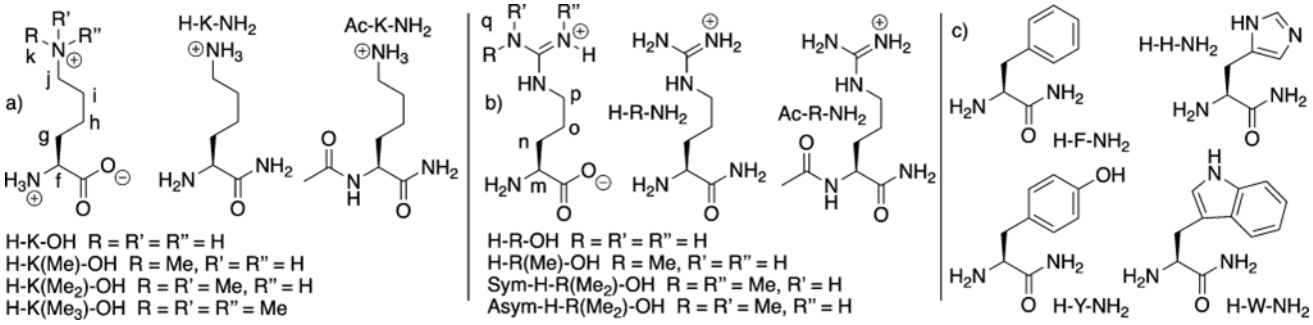

Figure III-2. Chemical Structures of: (a) lysine derivatives, (b) arginine derivatives, and (c) other amino acids used in this study.

3.2.2 Measurement of thermodynamic parameters by isothermal titration calorimetry (ITC)

We first decided to measure the thermodynamic parameters of complexation for P[*n*]MQ with the panel of amino acid derivatives shown in **Figure III-2**. Given the known ultratight binding of P[*n*]MQ toward cationic guests,[30] we expected that the strength of some of the P[*n*]MQ·amino acid complexes would exceed the range that is measured accurately by ^{1}H NMR titrations ($K_a > 10^4$ M^{-1}).[24] Accordingly, we elected to use ITC as the main analytical technique. **Figure III-3a** shows the thermogram recorded when a solution of P6MQ (0.1 mM) in the cell was titrated with a solution of **H–K(Me$_3$)–OH** (1.0 mM) from the syringe. Integration of the data in **Figure III-3a** allows the construction of a plot of ΔH versus molar ratio (**Figure III-3b**) which was fitted to a standard 1 : 1 binding isotherm using the PEAQ data analysis software to extract $K_a = (3.39 \pm 0.15) \times 10^6$ M^{-1} and $\Delta H = -5.94 \pm 0.02$ kcal mol^{-1}. The results of related direct titrations of P5MQ and P6MQ with the panel of amino acid derivatives (**Figure III-2**) were performed similarly and the results are collected in **Table III-1**. For the weaker complexes (*e.g.* $K_a < 10^4$ M^{-1}), the working concentrations of host and the guest were increased in order sample a larger portion of the binding isotherm (*e.g.* more appropriate ITC c-value).[74–76] The binding constants for the P5MQ·guest complexes span from 926 M^{-1} to 5.42×10^5 M^{-1} whereas those of P6MQ·guest span from 1740 M^{-1} to 3.20×10^6 M^{-1}. All of the complexes are driven by favorable changes in enthalpy (ΔH) upon complexation. This thermodynamic signature is well known for macrocyclic hosts (*e.g.* cyclodextrins, cyclophanes, CB[*n*], pillararenes) where it is known as the non-classical hydrophobic effect which is due to the release of water molecules from the cavity of uncomplexed host upon host·guest complexation.[11,138–142]

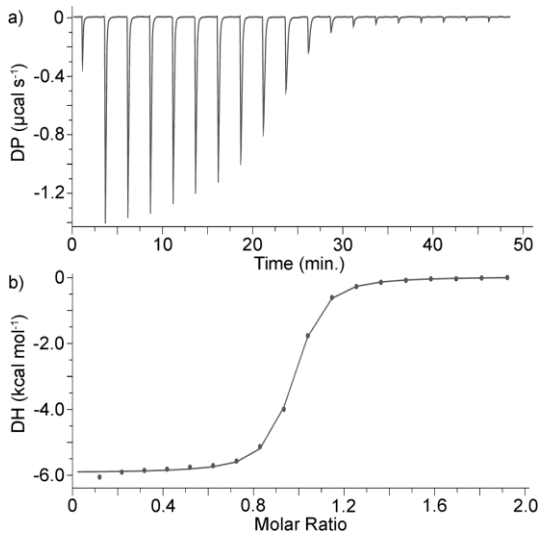

Figure III-3. (a) ITC thermogram recorded during the titration of P6MQ (100 μM) in the cell with **H–K(Me$_3$)–OH** (1.0 mM) in the syringe. (b) Fitting of the data to a 1 : 1 binding model with $K_a = (3.39 \pm 0.15) \times 10^6\ M^{-1}$. Conditions: phosphate buffered saline, pH 7.4, 298.0 K.

Table III-1 Thermodynamic parameters (K_a [M^{-1}], ΔH° [kcal mol^{-1}]) determined for the P5MQ·**guest** and P6MQ·**guest** complexes by ITC. Conditions: 298K, PBS buffered H_2O, pH 7.4

	P5MQ		P6MQ	
Guest	K_a (M^{-1})	ΔH (kcal mol^{-1})	K_a (M^{-1})	ΔH (kcal mol^{-1})
H–R–OH	$(3.77 \pm 0.24) \times 10^3$	−6.57 ± 0.18	$(5.85 \pm 0.13) \times 10^3$	−6.65 ± 0.06
H–R(Me)–OH	$(5.87 \pm 0.17) \times 10^3$	−5.50 ± 0.19	$(1.15 \pm 0.04) \times 10^4$	−5.42 ± 0.05
Sym-H–R(Me$_2$)–OH	$(5.35 \pm 0.16) \times 10^3$	−4.84 ± 0.05	$(6.45 \pm 0.36) \times 10^4$	−4.78 ± 0.10
Asym-H–R(Me$_2$)–OH	$(3.25 \pm 0.34) \times 10^3$	−3.36 ± 0.16	$(1.71 \pm 0.06) \times 10^5$	−6.64 ± 0.12
H–R–NH$_2$	$(2.12 \pm 0.06) \times 10^5$	−8.01 ± 0.13	$(1.16 \pm 0.03) \times 10^6$	−11.2 ± 0.0
Ac–R–NH$_2$	$(3.27 \pm 0.29) \times 10^4$	−4.94 ± 0.30	$(4.51 \pm 0.17) \times 10^4$	−8.49 ± 0.11
H–K–OH	$(9.26 \pm 2.67) \times 10^2$	−1.70 ± 0.38	$(1.74 \pm 0.09) \times 10^3$	−4.84 ± 0.14
H–K(Me)–OH	$(1.24 \pm 0.23) \times 10^3$	−4.79 ± 0.61	$(9.19 \pm 0.18) \times 10^3$	−5.13 ± 0.03
H–K(Me$_2$)–OH	$(6.13 \pm 0.18) \times 10^3$	−7.31 ± 0.20	$(2.52 \pm 0.05) \times 10^5$	−8.10 ± 0.04
H–K(Me$_3$)–OH	$(1.76 \pm 0.07) \times 10^4$	−10.8 ± 0.3	$(2.89 \pm 0.13) \times 10^6$	−6.44 ± 0.02
H–K–NH$_2$	$(5.42 \pm 0.10) \times 10^5$	−9.67 ± 0.11	$(3.20 \pm 0.19) \times 10^6$	−10.5 ± 0.0
Ac-K–NH$_2$	$(7.19 \pm 0.28) \times 10^4$	−7.99 ± 0.20	$(9.29 \pm 0.46) \times 10^4$	−9.37 ± 0.11
H–H–NH$_2$	n.b.	n.b.	$(9.01 \pm 2.49) \times 10^3$	−6.09 ± 0.04
H–F–NH$_2$	n.b.	n.b.	$(4.43 \pm 0.25) \times 10^4$	−9.54 ± 0.03
Ac–F–NH$_2$	—	—	$(5.99 \pm 1.89) \times 10^4$	−2.39 ± 0.03
H–Y–NH$_2$	n.b.	n.b.	$(2.66 \pm 0.30) \times 10^4$	−12.0 ± 0.2
H–W–NH$_2$	n.b.	n.b.	$(8.20 \pm 1.28) \times 10^3$	−7.62 ± 0.02

n.b = no heat detected. - = not measured.

3.2.3 Influence of ion–ion interactions on the molecular recognition of P[n]MQ toward amino acids and amino acid amides

The data in **Table III-1** allows us to discern the influence of ion– ion interactions on the binding of the poly-anionic P5MQ and P6MQ hosts toward ionic guests. For example, lysine (**H–K–OH**) and arginine (**H–R–OH**) are expected to be overall cationic at neutral pH although they contain two cationic and one anionic group. **Figure III-4a** shows a cartoons of the proposed geometry P[*n*]MQ·**H–K–OH** derivative complexes and highlights the attractive $NH_3^+\cdots{}^-O_3SO$ and repulsive $CO_2^-\cdots{}^-O_3SO$ ionion interactions. In contrast, lysine amide (**H–K–NH$_2$**) and arginine amide (**H–R–NH$_2$**) are dicationic at neutral pH and do not suffer the unfavorable $CO_2^-\cdots{}^-O_3SO$ interactions. Conversely N-acetyl-lysine amide (**Ac–K–NH$_2$**) and N-Acetyl-arginine amide (**Ac–R–NH$_2$**) are mono-cationic at neutral pH and should benefit from favorable $NH_3^+\cdots{}^-O_3SO$ interactions. **Figure III-4a** shows the differences in binding free energy of the P[*n*]MQ·**H– K–OH** *versus* the P[*n*]MQ·**H–K–NH$_2$** complexes and the P[*n*]MQ·**H–K–NH$_2$** *versus* P[*n*]MQ·**Ac–K–NH$_2$** complexes. The elimination of the unfavorable $CO_2^-\cdots{}^-O_3SO$ interactions results in complexes that are substantially more stable (P5MQ: $\Delta\Delta G = -3.78$ kcal mol^{-1}; P6MQ: $\Delta\Delta G = -4.45$ kcal mol^{-1}) whereas the elimination of favorable $NH_3^+\cdots{}^-O_3SO$ interactions is energetically costly (P5MQ: $\Delta\Delta G = +1.20$ kcal mol^{-1}; P6MQ: $\Delta\Delta G = +2.10$ kcal mol^{-1}). Values for the P[*n*]MQ·**H–R–OH** to P[*n*]MQ·**H–R–NH$_2$** (P5MQ: $\Delta\Delta G = -2.38$ kcal mol^{-1}; P6MQ: $\Delta\Delta G = -3.13$ kcal mol^{-1}) and P[*n*]MQ·**H–R–NH$_2$** to P[*n*]MQ·**Ac–R–NH$_2$** (P5MQ: $\Delta\Delta G = +1.46$ kcal mol^{-1}; P6MQ: $\Delta\Delta G = +1.92$ kcal mol^{-1}) complexes show similar trends for similar pairwise comparisons. We conclude that favorable electrostatic interactions (cation⋯anion) provide an important driving force for P[*n*]MQ·amino acid derivative

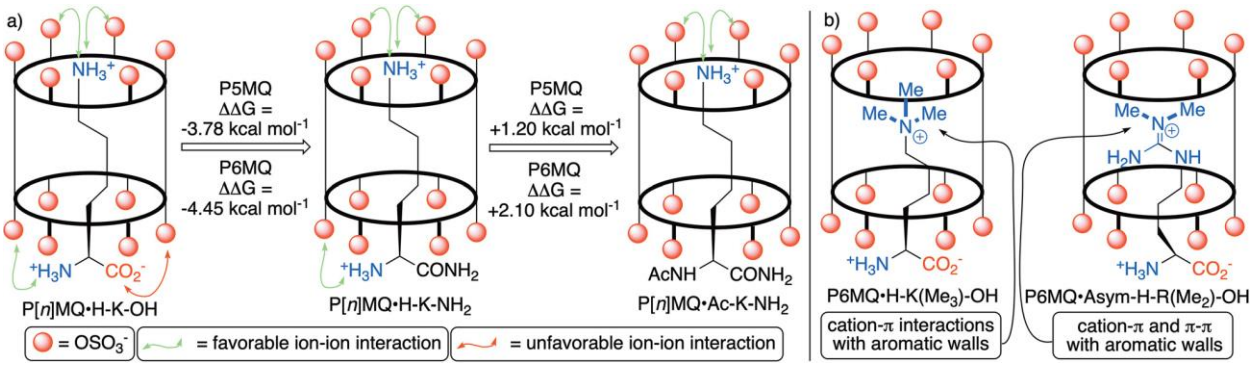

Figure III-4 (a) Cartoon of the interaction of P[*n*]MQ with lysine, lysine amide, and N-Acetyl-lysine amide. The green and red double headed arrows spot- light favorable and unfavorable electrostatic interactions, respectively. (b) Illustration of the proposed geometries of the P6MQ·**H–K(Me$_3$)–OH** and P6MQ·**Asym-H–R(Me$_2$)–OH** complexes.

complexation and that unfavorable (anion···anion) electrostatic interactions can result in large free energy penalties.

3.2.4 Influence of the degree of methylation on the molecular recognition of P[*n*]MQ toward amino acids and amino acid amides

The panel of amino acid derivatives contains a series of lysine (**H–K-OH**, **H–K(Me)–OH**, **H–K(Me$_2$)–OH**, **H–K(Me$_3$)–OH**) and arginine (**H–R–OH**, **H–R(Me)–OH**, **Sym-H–R(Me$_2$)–OH**, **AsymH–R(Me$_2$)–OH**) derivatives that differ in the degree and pattern of methylation. As the degree of methylation increases across the series of lysine derivatives, we observe that K_a values toward P5MQ and P6MQ increases 19-fold and 166-fold, respectively (**Table III-1**). Similarly, along the series of methylated arginine derivatives, we observe a 29-

fold increase in binding affinity for P6MQ·**Asym-H–R(Me$_2$)–OH** compared to P6MQ·**H–R–OH**. The increased affinity of P6MQ toward the more highly methylated amino acid derivatives is consistent with the previously reported binding of P[*n*]MQ toward alkane diammonium ions,[30] and also with other macrocyclic host systems. We believe that the more hydrophobic NMe_3^+ group enhances both the hydrophobic effect and the cation-π components of binding which allows the P6MQ·**H–K(Me$_3$)–OH** complex to assume the geometry shown in **Figure III-4**, and which in turn reduces the unfavorable electrostatic interactions ($CO_2^-\cdots{}^-O_3SO$) upon binding.

3.2.5 Influence of the Nature of the Hydrophobic Residue on Binding

The P6MQ host features two equivalent hexa-anionic portals separated by a hydrophobic cavity which explains the tight binding exhibited toward derivatives of lysine and arginine which feature hydrophobic and cationic sidechains. To gain insight into the importance of the nature of the hydrophobic side chain, we determined the binding between P[*n*]MQ and the four aromatic amino acid amides (**H–H–NH$_2$**, **H–F–NH$_2$**, **H–Y–NH$_2$**, **H–W–NH$_2$**) which feature imidazole, phenyl, hydroxyphenyl, and indole rings (**Table III-1**). We find that all four P6MQ·aromatic amino acid amide K_a values cluster in the range of 8200–44,300 M^{-1}. In contrast, no heat was detected during the titration of P5MQ (100 μM) with the four amino acid amides which is indicative of weak binding ($K_a < 10^4\ M^{-1}$). This weak binding of these aromatic amino acid derivatives arise due to the narrower cavity of P5MQ which recognized linear alkyl chains preferentially over aromatic rings. Related ITC titrations of P6MQ and methionine amide, leucine amide, or glutamine amide did not show any heat evolved indicating even weaker binding for these amino acid amides. Taken together, these results suggest that the presence of an

aromatic side chain promotes complexation by π–π interactions with the walls of P6MQ, but that the presence of a cationic and preferably methylated sidechain (e.g. lysine or arginine) is needed to achieve submicromolar binding in PBS buffered water.

3.2.6 Qualitative ^{1}H NMR Host·Guest Recognition Study

Having determined the thermodynamic parameters of binding, we proceeded to glean information on the geometry of the tighter host guest complexes (P6MQ·**Asym-H–R(Me$_2$)–OH** and P6MQ·**H–K(Me$_3$)–OH**) by ^{1}H NMR spectroscopy. **Figure III-5a** shows the ^{1}H NMR recorded for **H–K(Me$_3$)–OH** in PBS using the labelling scheme given in **Figure III-1** and **III-2**. **Figure III-5c** shows the ^{1}H NMR spectrum of an equimolar mixture of P6MQ and **H–K(Me$_3$)–OH**. We observe that the methonium group (H_k; $\Delta\delta = -1.9$ ppm) and the methylene groups alpha (H_j; $\Delta\delta = -2.0$ ppm) and beta (H_i; $\Delta\delta = -1.4$ ppm) to NMe_3^+ undergo substantial upfield shifts upon formation of P6MQ·**H–K(Me$_3$)–OH** whereas the protons closer to the carboxylate substituent (*e.g.* H_f, H_g, H_h) undergo small to no change in chemical shift upon binding. This pattern of changes in chemical shift establishes that the $Me_3NCH_2CH_2$ group is located within the anisotropic magnetic shielding environment of the P6MQ cavity whereas the carboxylate terminus is located outside the cavity. The resonances for H_a and H_b of P6MQ do not undergo significant ($\Delta\delta \leq 0.1$ ppm) changes in chemical shift upon complexation. The proposed geometry of P6MQ·**H–K(Me$_3$)–OH** is presented in **Figure III-4b**. This geometry allows for maximization of the cation-π and CH–π interactions between the electrostatically positive Me_3N^+ CH_2 group and the electron rich aromatic walls of the cavity. **Figure III-5b** shows the ^{1}H NMR spectrum of a 1 : 2 mixture of P6MQ and **H–K(Me3)–OH**; the presence of a single set of resonances for **H–**

K(Me3)–OH at chemical shifts in between those of uncomplexed **H–K(Me3)–OH** and P6MQ·**H–K(Me3)–OH** establishes fast kinetics of exchange on the chemical shift timescale. **Figure III-5e–h** shows a similar set of ^{1}H NMR spectra recorded for **Asym-H–R(Me2)–OH**. Formation of the P6MQ·**Asym-H–R(Me$_2$)–OH** complex results in substantial upfield shifts for methylated guanidinium group (H_q, $\Delta\delta = -1.7$ ppm; H_p, $\Delta\delta = -1.0$ ppm) and only small shifts for the protons closer to the carboxylate group (H_m, $\Delta\delta = +0.1$ ppm; H_n, $\Delta\delta \leq 0.1$ ppm; H_o, $\Delta\delta = -0.15$ ppm). The direction and magnitude of the changes in chemical shift upon formation of the P6MQ·**Asym-H–R(Me$_2$)–OH** complex indicated that the dimethyl arginine unit is bound within the magnetic shielding environment of the P6MQ cavity where it benefits from cationπ and π–π interactions with the walls of the P6MQ host as illustrated in **Figure III-4b**.

3.2.7 Molecular Recognition of H3K4 Peptides by P6MQ Monitored by Fluorescence Titrations

The high binding affinities of P6MQ toward **H-R-NH2**, **H–K(Me$_3$)–OH**, **Asym-H–R(Me$_2$)–OH** and **Sym-H–R(Me=)–OH** prompted us to study the interaction of P6MQ towards a peptide fragment of the histone 3 (which will be referred to as **H3K4**) and the various N-methylated states of arginine at position 2 (**R2**) or lysine at position 4 (**K4**) (**Figure III-6**). Given the high binding constants observed (*vide infra*) and the small quantities of the peptides available, we decided to use direct and competitive fluorescence titrations to measure the binding constants for the P6MQ·peptide complexes. Through the screening of various host : dye complexes we found 4′,6-diamidino-2-phenylindole (**DAPI**) was a suitable fluorescent guest for indicator displacement assay. **DAPI** is well known to bind to AT-rich regions of DNA and undergo an

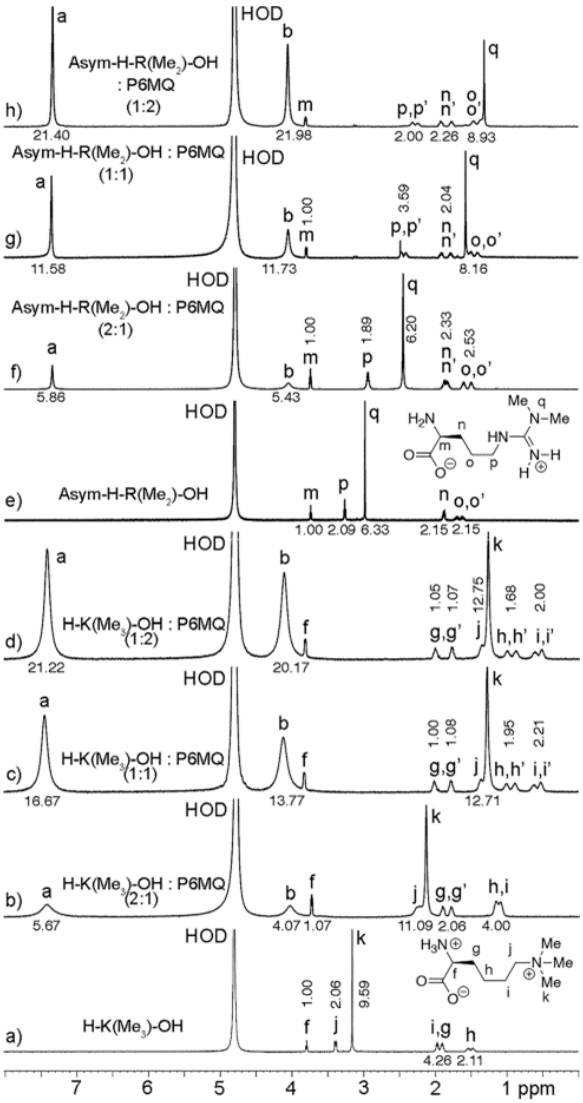

Figure III-5. ^{1}H NMR spectra recorded (600 MHz, RT, 20 mM phosphate buffered D_2O, pH 7.4) for: (a) **H–K(Me$_3$)–OH** (1.0 mM), (b) a mixture of **H–K(Me$_3$)–OH** (1.0 mM) and P6MQ (0.5 mM), (c) a mixture of **H–K(Me$_3$)–OH** (1.0 mM) and P6MQ (1.0 mM), (d) a mixture of **H–K(Me$_3$)–OH** (1.0 mM) and P6MQ (2.0 mM), (e) **Asym-H–R(Me$_2$)–OH** (1 mM), (f) a mixture of **Asym-H–R(Me$_2$)–OH** (1 mM) and P6MQ (0.5 mM), (g) a mixture of **Asym-H–R(Me$_2$)–OH** (1.0 mM) and P6MQ (1.0 mM), and (h) a mixture of **Asym-H–R(Me$_2$)–OH** (1.0 mM) and P6MQ (2.0 mM).

≈20-fold enhancement of fluorescence;[143] **DAPI** also binds to other macrocyclic cation receptors (e.g. CB[7]).[144] First, we performed a direct titration of a solution of **DAPI** (100nM) with a solution of P6MQ (0–2 μM) and monitored the emission at 450 nm after excitation at 360 nm. **Figure III-7a** shows a plot of fluorescence (RFU) versus concentration fitted to a standard 1 : 1 host:guest binding model (ESI†) which allowed the determination of K_d = 15 ± 4 nM for P6MQ·**DAPI** in PBS. Subsequently, we implemented an indicator displacement assay[35] using **DAPI** as a fluorescent indicator to determine the binding of P6MQ toward the **H3** peptides. For this purpose, we titrated a solution of P6MQ (125 nM) and **DAPI** (100 nM) with a solution of **H3** peptide and monitored the fluorescence emission at 450 nm. **Figure III-7b** shows a plot of change in fluorescence versus [**H3K4Me$_2$**] fitted to a competitive binding model which allows for the determination of K_d = 230 ± 40 nM for the P6MQ·**H3K4Me$_2$** complex. The binding constants for the remaining P6MQ·**H3** peptide complexes were measured analogously and the results are presented in **Table III-2**. Interestingly, we find that **H3K4**, **H3K4Me**, and **H3K4Me$_2$** bind with submicromolar affinity to P6MQ by factors of >1000, >300, and 17-fold stronger than the corresponding amino acids **H–K–OH**, **H–K(Me)–OH**, and **H–K(Me$_2$)–OH**, respectively. This enhancement of affinity can be rationalized by the removal of the unfavorable anion-anion interactions ($CO_2^- \cdots {}^-O_3SO$, **Figure III-4**) and by the additional cationic residues on the guest (N-terminus and side chain residue). The **H3K4Me$_3$** peptide is the strongest binder in the series (P6MQ·**H3K4Me$_3$**, K_d = 16 nM) and binds 14-fold stronger than the unmodified peptide as expected based on the preference of P6MQ for quaternary ammoniums.[30] The nanomolar affinity of P6MQ towards the known biomarker **H3K4Me$_3$** in a salty media (137 mM NaCl) indicates

the potential of P6MQ to be used in biological systems. To our knowledge P6MQ has the strongest reported affinity to **H3K4Me$_3$** of any supramolecular host. Additionally, the **H3R2Me$_2$a** and **H3R2Me$_2$s** peptides also bind P6MQ with K_d values of 50 nM and 70 nM, respectively. These binding constants are 117-fold and 221-fold stronger than for the analogous amino acid complexes P6MQ·**Asym-H-R(Me)$_2$-OH** and P6MQ·**Sym-H-R(Me)$_2$-OH** which again shows the loss of unfavorable $CO_2^- \cdots {}^-O_3SO$ interactions. Encouraged by the high levels of binding affinity and good selectivity for the methylated **H3** peptides, we decided to delve into the complexation geometries and driving forces computationally.

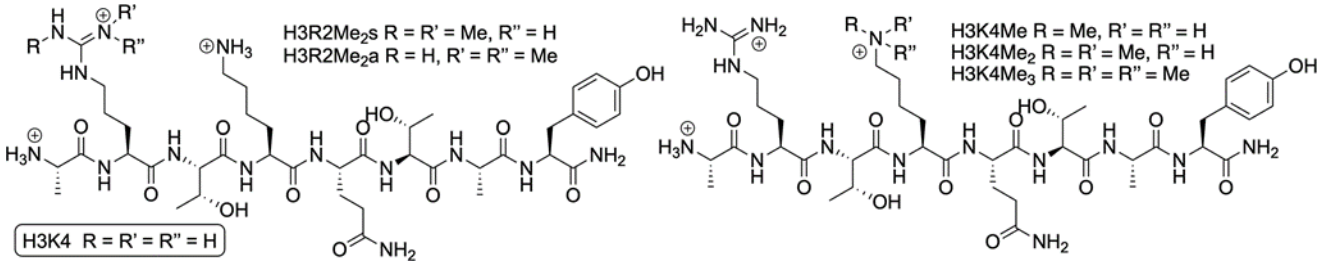

Figure III-6. Structure of the histone **H3K4** peptides used in this study.

Table III-2 P6MQ·**peptide** dissociation constants (K_d, nM) measured by fluorescence detected indicator displacement assays. Conditions: 10 mM PBS buffered H_2O, pH 7.4

Guest	K_d (nM)
H–K(Me$_3$)–OH	430 ± 70
H3K4	540 ± 70
H3K4Me	340 ± 50
H3K4Me$_2$	230 ± 40
H3K4Me$_3$	16 ± 3
H3R2Me$_2$a	50 ± 6
H3R2Me$_2$s	70 ± 10

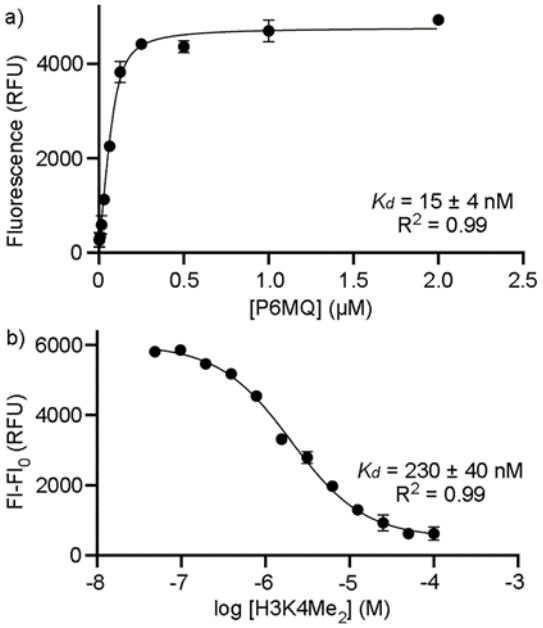

Figure III-7 (a) Direct fluorescence titration of a solution of **DAPI** (100 nM) with a solution of P6MQ in phosphate buffered saline at pH 7.4. (b) Competitive fluorescence titration of a solution of P6MQ (125 nM) and **DAPI** (100 nM) with a solution of **H3K4Me2** in phosphate buffered saline at pH 7.4. Reported dissociation constants are the average of six measurements, curves and R^2 of exemplary triplicate data (see ESI†).

3.2.8 Investigation of the Binding Processes of P6MQ Toward Amino Acids, Amino Acid Amides, and H3 Peptides by Molecular Dynamics Simulations

The high binding affinities of P6MQ toward **H–R–NH2**, **H–K(Me3)–OH** and especially the **H3** peptides prompted us to perform molecular dynamics simulations to better understand the geometry and the molecular determinants behind the complexation driving forces. A total of eight systems were studied: uncomplexed P6MQ, P6MQ·**H–K–OH**, P6MQ·**H–K–NH2**,

P6MQ·**H–K(Me$_3$)–OH**, P6MQ·**H3K4** (lysine bound), P6MQ·**H3K4** (arginine bound), P6MQ·**H3K4Me$_3$** (KMe3 bound), and P6MQ·**H3K4Me$_3$** (arginine bound). All the systems were initialized in a physically reasonable configuration, using Spartan for the **H3** complexes.[145] The complexes were parameterized using the AMBER GAFF2 force field and each system was neutralized with Na^+ and Cl^- counter-ions at a concentration of 0.15 M to reflect the nature of the PBS buffer used experimentally.[146] The equilibration and production simulations used the Nose–Hoover thermostat[147] and the Parrinello–Rahman barostat[148] held at 298 K and 1 bar, placing the simulation under the constant number, pressure, and temperature (NPT) ensemble. In all cases the GROMACS[149] simulation engine was used to perform the equilibration and production simulations, and calculations were performed using PLUMED.[150] Below, we separately report our observations derived from these MD simulations separately for uncomplexed P6MQ, P6MQ·amino acid (amide), and P6MQ·**H3** peptide complexes.

3.2.4.1 Uncomplexed P6MQ

The (in)ability of water to solvate the hydrophobic cavity of uncomplexed macrocyclic hosts has been shown to provide an important enthalpic driving force for high affinity hosts.[11,138–142] Accordingly, we performed MD simulation of uncomplexed P6MQ to explore its aqueous solvation. We analyzed the number of hydrogen bonds (nHB) that each water molecule participates in within a distance r of the center of mass of P6MQ using eqn (III-1) where the function Hbonds(X, Y) counts the number of hydrogen bonds formed between the groups X and Y. In eqn (III-1) P6MQ and LIG represent the hydrogen bond acceptors and donors atoms of the host and bound ligand which accept and donate hydrogen bonds (N, O, H), and H_2O_{int} and H_2O_{ext}

respectively refer to water molecules within and outside of the region of interest defined by r. For uncomplexed P6MQ, no ligand is considered (vide infra for liganded systems).

$$n_{HB}(r) = 2 \times \mathrm{Hbonds}(\mathrm{H_2O_{int}}, \mathrm{H_2O_{int}}) + \mathrm{Hbonds}(\mathrm{H_2O_{int}}, \mathrm{H_2O_{ext}}) + \mathrm{Hbonds}(\mathrm{H_2O_{int}}, \mathrm{P[6]AS}) + \mathrm{Hbonds}(\mathrm{H_2O_{int}}, \mathrm{LIG}) \quad \text{(III-1)}$$

Figure III-8a shows a free energy plot of the number of hydrogen bonds formed within 6 Å of the P6MQ center of mass for bulk water, P6MQ, and various P6MQ·ligand complexes. We find that the number of hydrogen bonds formed per water within 6 Å of the center of mass of uncomplexed P6MQ (1.93) is substantially smaller than the number formed per water in bulk water (3.5). The H-bond deficiency of waters encapsulated inside other hosts have been tabulated previously Biedermann, Nau, and Schneider and range from 1.00 for Klaerner's tweezer to 3.06 for CB[8].[11] What disrupts the H-bonding network for P6MQ? We find that waters between 4 Å and 6 Å from the center of mass of P6MQ (e.g. near the portals) tend to form H-bonds to the sulfate groups of P6MQ, orienting the O–H bonds outward and pointing the O-atoms inwards with a deficiency of H-Bonds. In contrast, for H_2O molecules in the core of the P6MQ cavity (r < 4 Å), we find two distinct populations of water depending on whether a Na^+ ion is present in the core of the P6MQ cavity. In the presence of Na^+ ions (**Figure III-8b** and **c**), water molecules orient themselves such that the O-atoms coordinate to the Na^+ ion at the center of the P6MQ cavity resulting in large deficiency of H-bonds. In the relatively rare event that an Na+ ion is not present inside P6MQ, 2.15 H-bonds are formed on average between H_2O molecules and different H-bond topologies arise due to the confinement inside P6MQ. For example, a cyclic H-bonding

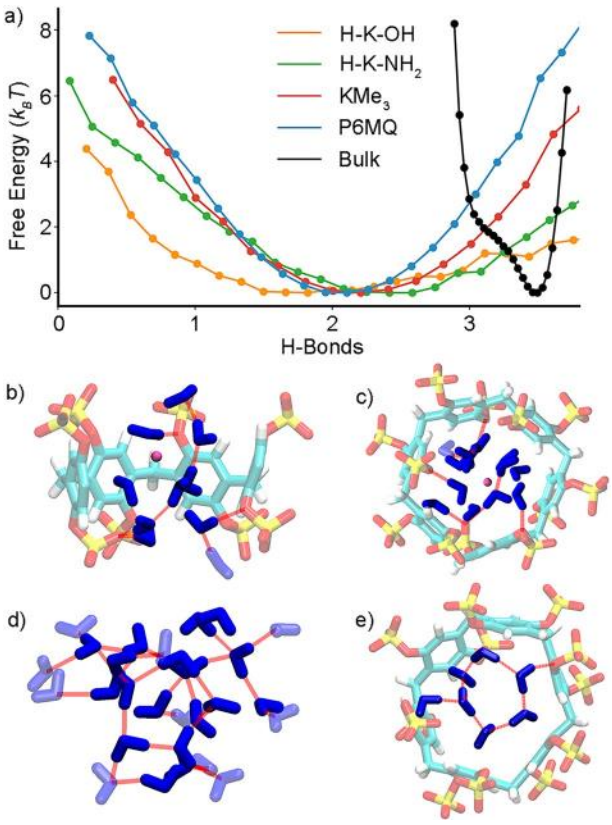

Figure III-8. Characterizing H-bonding in and around P6MQ and complexes. (a) Plot of the free energy (see ESI for definition†) of the system *versus* average number of hydrogen bonds a water molecule participates in. (b and c) The coordination of water molecules by sodium ions in uncomplexed P6MQ, with front side of P6MQ not shown for clarity in panel. Red lines correspond to H-bonds and water molecules are depicted in blue. (c and d) An example of the hydrogen bonding network in bulk water. We calculate the hydrogen bonds (red lines) formed within a region of the simulation box defined by r = 6 Å, including hydrogen bonds across the surface of the region; solid blue molecules are located within the region and transparent ones are outside. (e) Cyclic H-bonded water network observed in the absence of Na^+.

network comprising five or six water molecules is observed in the MD simulation as shown in **Figure III-8e**.

We also computed local density plots derived from radial distribution functions which aim to quantify the structure of water around the cavity. Since the radial distribution function g(r) is related to the local density ρ(r) through $\rho(r) = \rho_{bulk}\, g(r)$, we may directly interpret g(r) as the local density ρ(r).[151] We examined local densities around the P6AS sulfate oxygen atoms (4 Å ≤ r ≤ 7 Å), as presented in **Figure III-9**, and near the P6MQ center of mass (r ≤ 4 Å, see ESI†). The local density of water molecules for uncomplexed P6MQ shows a broad peak for 2.78 Å < r < 3 Å (considering r ≤ 4 Å waters; O–O distance) (data in ESI†) whereas the local density of waters with 4 Å ≤ r ≤ 6 Å shows a sharper peak at 2.80 Å. In contrast, bulk water shows a sharp peak at 2.78 Å. The broad peak seen for P6MQ (r ≤ 4 Å) is consistent with the fact that fewer hydrogen bonds are formed in the core of P6MQ as established in **Figure III-8c** and **d**. When Na^+ is present in the P6MQ cavity, water molecules are oriented such that hydrogen bonding is less likely, resulting in a broader distribution of O–O distances.

From the regions of high local density in **Figure III-9a** we identify two populations of water molecules. There are two regions of high local density in **Figure III-9a**. The leftmost peak in local density corresponds to water molecules which are hydrogen bonded to OSO_3^-; the integral of this peak suggests that most sulfate oxygens are H-bonded to a water molecule (*e.g.* **Figure III-9b**). A single water molecule can form either one or two hydrogen bonds to OSO_3^-, and the inter-oxygen distance between water and sulfate corresponds to the leftmost (2.78 Å) peak. The integral of the first peak indicates each OSO_3^- group forms 3.51 H-bonds with water

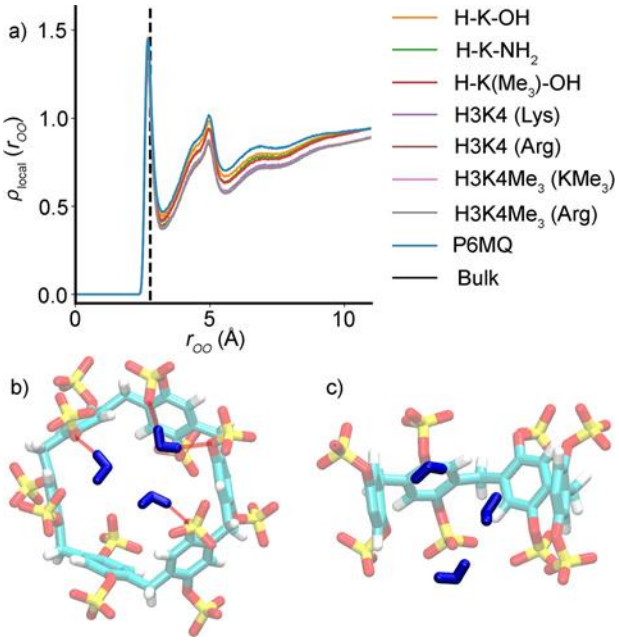

Figure III-9. Characterizing the radial location of waters from the center of mass of the OSO_3^- groups. (a) The local density of waters less than 7 Angstroms from P6MQ sulfate oxygens, where the dashes line indicates the local density of bulk water. The local density is averaged over all oxygens. Note that the density of water is largely independent of the bound ligand. (b) The leftmost peak of (a) is explained by water mole- cules (depicted in blue) that are hydrogen bonded (depicted as red lines) to P6MQ. (c) The broader peak around 5 Å includes water molecules which are not hydrogen bonded to P6AS which are typically coordinated by Na^+ ions (not pictured, see **Figure III-8** and ESI†).

molecules on average, suggesting that water molecules sacrifice H-bonds with one another to preferentially form H-bonds with P6MQ.

The results of the local density and hydrogen bonding analysis suggest that the presence of sodium in the core of the binding cavity of P6MQ causes water molecules to reorient such that

they are not able to form hydrogen bonds with one another as effectively as in bulk. Similarly, the intense negative charge of the portals of P6MQ causes water molecules to preferentially form hydrogen bonds with OSO_3^- over other waters. Our findings unequivocally show that water structure plays an important role in the high affinity binding of P6MQ.

3.2.4.2 P6MQ·Amino Acid (Amide) Complexes

Snapshots of a representative geometry of P6MQ·**H–HK(Me$_3$)–OH** is shown in **Figure III-10a** and snapshots of P6MQ·**H–K–OH** and P6MQ·**H–K–NH$_2$** are given in the ESI.† We computed the depth of binding (d_{bound}) for these amino acid (amides) by considering the position of the center of mass of each amino acid (amide) relative to P6MQ as described in the ESI.† We find that the P6MQ·**H–K–OH** and P6MQ·**H–K–NH$_2$** complexes show d_{bound} values in the −0.2 to +0.6 Å range which indicates that the α-carbon mainly protrudes (positive d_{bound}) from the P6MQ portal; the ε-carbon sometime protrudes further (negative d_{bound}). The amino acid (amide) NH_3^+ groups form ion-ion/H-bonds to the sulfate groups on P6MQ. In contrast, d_{bound} for P6MQ·**H–K(Me$_3$)–OH** is +0.4 Å reflecting that the Me_3N^+ group is bound in the center of the P6MQ cavity and the alpha-carbon protrudes from the sulfated portal. These results are in accord with the complexation induced changes in ^{1}H NMR chemical shift discussed above and the geometries depicted in **Figure III-4b** and **III-10a**. In all three cases, the MD simulations show that complex formation results in exclusion of water from the central cavity of P6MQ which constitutes an important driving force for complexation (**Figure III-8a**).

3.2.4.3 P6MQ·H3 Peptide Complexes

We did not find any differences in the dbound values for P6MQ·**H3K4** versus P6MQ·**H3K4Me$_3$** when a common residue is bound (e.g. arginine at position 2 or lysine residue

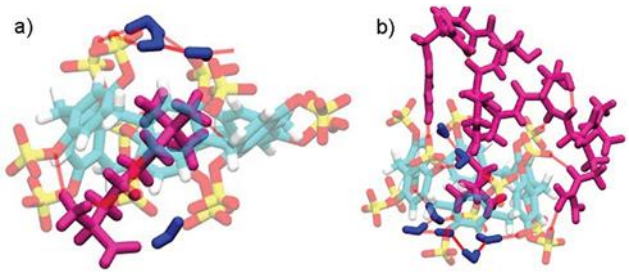

Figure III-10. MD simulation structures. (a) P6MQ·**H–K(Me$_3$)–OH**. P6MQ·**H–K (Me$_3$)–OH** has only one bound conformation; **H–K(Me$_3$)–OH** is bound at an angle within P6MQ with Me_3N^+ in the center of the cavity. P6MQ flexes to accommodate the ligand. (b) P6MQ·**H3K4Me$_3$** (KMe_3 bound). P6MQ·**H3K4Me$_3$** (KMe_3 bound) has a distinct conformation in which the backbone and non-bound sidechains of **H3K4Me$_3$** form H-bonds with P6MQ. The H-bonds formed between OSO_3^- and arginine stabilizes arginine within π stacking distance of the P6MQ aromatic walls. In both panels water molecules are depicted in blue, H-bonds as red lines, and the ligand in magenta.

at position 4). It appears that secondary interactions between P6MQ and **H3** peptide play significant roles in complex geometry. For example, when K or KMe_3 at position 4 is bound by P6MQ, we find: (1) that the N-terminus NH_3^+ undergoes backfolding to the sulfate portal to engage in ion-ion/H-bonds, (2) that the arginine at position 2 sometimes engages in π–π stacking interactions (**Figure III-10b** and ESI†) with the aromatic wall of P6MQ, and (3) the peptide backbone amide N–H groups form H-bonds to the sulfate groups (**Figure III-10b**). Related H-bonding of peptide N–H groups back to portal C=O groups has been seen with CB[8].[152] These additional modes of interaction that are not available to the amino acids (amides) are likely

responsible for the enhanced binding affinities determined for the **H3** peptides. And yet the solution-phase preference for binding methylated peptides shown in the ITC data establishes that the engagement of methylated side chains is an important part of recognition in the context of whole peptides.

3.3 Conclusions

In summary, we have measured the thermodynamics of binding of P6MQ toward a series of methylated derivatives of the amino acids lysine and arginine by ITC in PBS. We also measure the K_a values for nine amino acid amides to quantify the energetic benefits (costs) of favorable (unfavorable) electrostatic interactions upon complexation. We find a 4.45 kcal mol^{-1} energetic penalty for $CO_2^-\cdots{}^-O_3SO$ interactions and a 2.1 kcal mol^{-1} benefit for $NH_3^+\cdots{}^-O_3SO$ interactions for P6MQ. The geometry of the complexes were established on the basis of ^{1}H NMR complexation induced changes in chemical shift and by MD simulations. The P6MQ·**H–K(Me_3)–OH** and P6MQ·**Asym-H–R(Me_2)–OH** complexes feature the NMe_3^+ and NMe_2^+ groups located in the center of the P6MQ cavity. Fluorescence competition assays demonstrated that P6MQ recognizes **H3K3Me_3**, **H3R2Me_2a**, and **H3R2Me_2s** with K_d values below 70 nM which is attributed to the presence of secondary ion–ion, π–π, and H-bond interactions of the remainder of the peptide with the portals and outer surface of P6MQ. The MD simulations show that the structure of water in the core cavity of P6MQ and near the sulfated portals are unusual in that a deficiency of H-bonds is observed, in part due to the presence of sodium in the binding cavity. In addition, we find that water molecules preferentially form H-bonds with P6MQ rather than other waters due to the intensely negative charges of the sulfated portals. Overall, the work

established P6MQ as a promising new host for the recognition of post-translational modifications in salty media with potential future application as reagents for enzyme assays, analyte detection, and proteomics enrichment strategies.

3.4 Experimental

3.4.1 General Experimental

Chemicals were purchased from commercial suppliers and used without further purification or were prepared by literature procedures.[30,135] NMR spectra were measured on commercial instruments operating at 600 MHz for ^{1}H using D_2O as solvent. Chemical shifts (δ) are referenced relative to the residual resonances for HOD (4.80 ppm). ITC data were collected on a Malvern Microcal PEAQ-ITC instrument and analyzed using the software provided by the vendor. The fluorescence titrations were performed using a BioTek Cytation5 multimode plate reader.

Chapter 4: Detection of WADA Banned Substances in Simulated Urine Using a Pillar[*n*]MaxQ Based Assay

4.1 Introduction

Sports are enjoyed in various forms by people all over the world. Due to this widespread admiration, there is a large amount of money involved both at the player level, and team ownership level. Due to this large incentive to perform at the highest level no matter the cost, it is imperative that safety measures are in place to help make sure that the athletes are competing fairly and not taking drugs that could harm them or give them an unfair advantage.[153] To put it mildly, this has proven to be difficult[154–157] with scandals across many sports from steroid use in Major League Baseball in the early 2000's that lead to Congressional hearings,[158] to the state-sponsored doping of Russian athletes.[159] Most recently, in 2021 the International Olympic Committee announced that weightlifting was removed from the list of events for the 2028 Olympics with the press release naming the "historical incidence of doping" as a contributing factor.[160]

While the most accurate and precise drug testing is currently performed using techniques such as gas-chromatography,[156,161] and ultra high-performance liquid chromatography[155,161] among other methods, they are expensive and are not very mobile. Advancements in light-based sensors[162] and sensing assays such as enzyme-linked immunoassays allow for the relatively quick detection of prohibited substances.[155,156] In addition to enzyme-linked immunoassays, indicator displacement assays (IDA)[35,38,77] with supramolecular hosts have been effective at the

detection and differentiation of compounds such as opiods,[40] and amphetamines[38] in biologically relevant mediums.

We have previously studied the binding interactions of Pillar[*n*]MaxQ (P[*n*]AS) towards a variety of cationic and dicationic guests, including some biologically relevant molecules such as amino acids,[163] neuromuscular blocking agents,[30] and drugs of abuse such as methamphetamine and fentanyl.[32] To investigate further the selectivity of P[*n*]AS towards cationic and biologically relevant targets, we identified compounds listed on the World Anti-Doping Agency (WADA) Prohibited List[164] as possibly useful targets.

We report here the successful implementation of a sensing assay based on host·guest interactions with P[*n*]AS that is able to detect and differentiate 13 compounds that are either on the 2023 WADA Prohibited List,[164] or are structurally similar to those on the list.

4.2 Results and Discussion

The information in this section is organized as follows. First, we present and discuss the binding affinity of P[*n*]AS towards a panel of WADA-banned drugs as measured via isothermal titration calorimetry (ITC) and indicator displacement. Then, we use ^{1}H NMR spectroscopy to probe deeper into the structural relationships in the host-guest binding interactions for the more structurally similar guests. Having established the selectivity of P[*n*]AS we leverage this selectivity to create a sensing assay in phosphate-buffered saline (PBS) to accurately identify each target at micromolar concentrations. Finally, we use the same conditions used to assay to quantify two targets in simulated urine to obtain a limit of quantification (LOQ) for each substance below the threshold required for drug testing.

4.2.1 Selection of World Anti-Doping Agency (WADA) Banned Substances

As P[*n*]AS has been previously found to bind cationic guests more strongly than neutral or anionic guests, we have selected mostly cationic stimulants as we believe they will be most readily bound. We observed that P[*n*]AS is able to effectively bind cationic guests with P5AS in particular preferring linear aliphatic cations over cyclic cations.[32,165] To further probe this selectivity, we chose the compounds shown in **Figure IV-1.** In particular we wanted to include branched and linear monocationic stimulants to determine how much of an effect the length, and branching location, play in determining the association constant. Conversely, P6AS shows a preference for larger guests that can more completely fill the cavity.[30,32] With this in mind, we chose a selection of larger cationic stimulants and several neutral steroidal compounds to determine if the selectivity remains even for non-cationic compounds. Additionally, we added beta-blocker to determine if our sensing assay can differentiate compounds based on their role in the body. Finally, two compounds that are not explicitly stated as WADA-banned substances were included (**1HeptNH3** and **HCort**) to show that the assay can differentiate structurally similar substances that are not banned to reduce the chance of a type 1 error (false positive).

4.2.2 Measurement of Binding Constant for the Panel with P[*n*]AS

4.2.2.1 Determination of thermodynamic parameters by isothermal titration calorimetry (ITC)

First, we decided to measure the thermodynamic variables of binding for the panel of WADA-banned compounds with P[*n*]AS (n = 5,6). Given the relatively tight binding shown previously

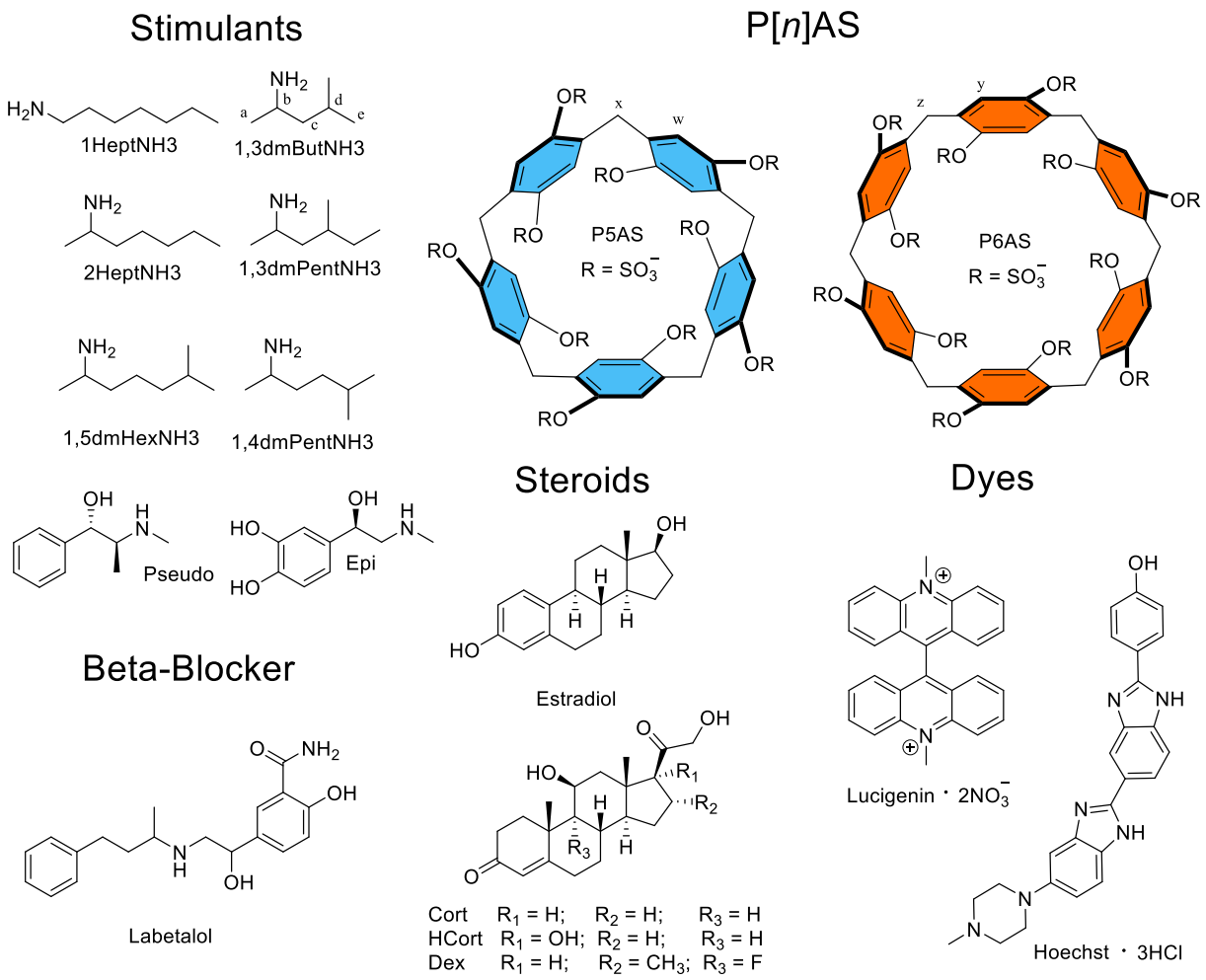

Figure IV-1. Chemical structures of compounds used in this study.

for P[*n*]AS with linear amines,[30,165] we felt comfortable that the binding interactions would be strong enough to probe via ITC. **Figure IV-2a** shows the thermogram recorded when a solution of **2HeptNH3** (250 μM) in PBS buffer (pH 7.4) was titrated into a similarly buffered solution of P5AS (25.0 μM). For each guest the concentrations of hosts and guests were chosen to sample a

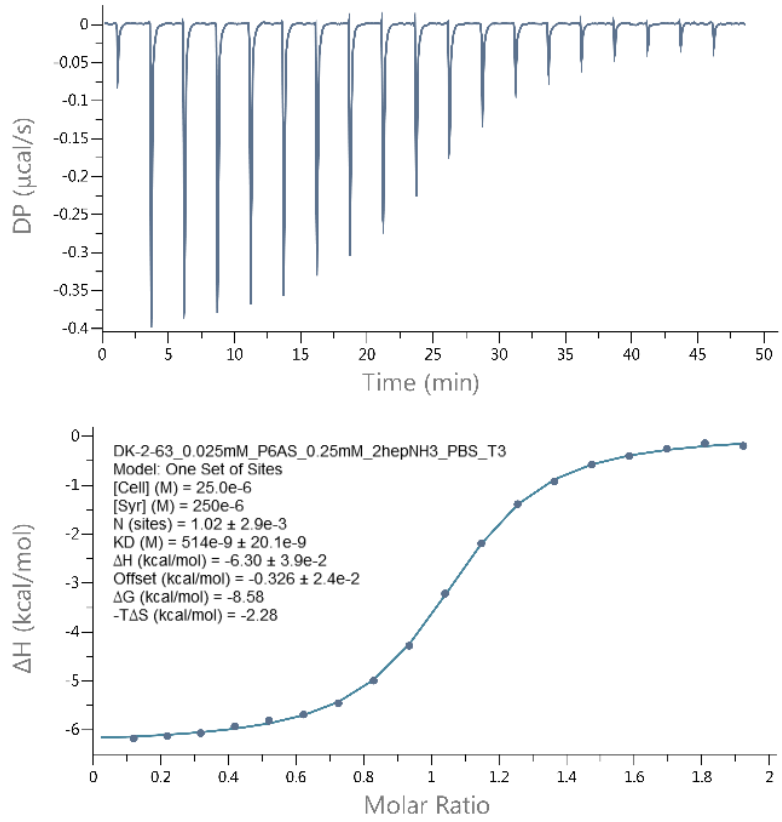

Figure IV-2. (a) ITC thermogram recorded during the titration of P6AS (25.0 µM) in the cell with **2HeptNH3** (250 µM) in the syringe. (b) Plot of the integrated heats of each titration *vs.* the molar ratio with the solid line representing the best fit of the data to a 1:1 binding model with K_a = (5.59 ± 0.32) × 10^6 M^{-1}, ΔH = -6.38 ± 0.03 kcal mol^{-1}. Conditions: PBS, pH 7.4, 298.0 K.

large portion of the binding isotherm (*e.g.,* more appropriate Wiseman c-value).[74–76] By integrating the raw heat data, a plot of ΔH *vs.* molar ratio (**Figure IV-2b**) can be created. Fitting this plot to a standard 1:1 binding isotherm using PEAQ data analysis software allows the K_a and ΔH values to be directly obtained. These measurements were done in triplicate resulting in a K_a = (5.59 ± 0.32) × 10^6 M^{-1} and ΔH = -9.17 ± 0.06 kcal mol^{-1} after error propagation[166] for the

Table IV-1. Thermodynamic parameters (K_a [M^{-1}], ΔH° [kcal mol^{-1}]) determined for the P5AS·Guest and P6AS·Guest complexes in PBS buffered H_2O, pH 7.4, 298 K.

	P5AS		P6AS	
Guest	K_a (M^{-1})	ΔH° (kcal/mol)	K_a (M^{-1})	ΔH° (kcal/mol)
1HeptNH3 %	$(1.12 \pm 0.06) \times 10^7$	-6.84 ± 0.03	$(3.65 \pm 0.22) \times 10^6$	-7.68 ± 0.07
2HeptNH3	$(5.59 \pm 0.32) \times 10^6$	-9.17 ± 0.06	$(1.82 \pm 0.06) \times 10^6$	-6.38 ± 0.03
1,3dmButNH3	$(4.64 \pm 0.34) \times 10^4$	-5.29 ± 0.13	$(7.89 \pm 0.17) \times 10^5$	-6.43 ± 0.02
1,3dmPentNH3	$(2.95 \pm 0.15) \times 10^4$	-5.70 ± 0.13	$(1.89 \pm 0.05) \times 10^6$	-7.11 ± 0.02
1,4dmPentNH3	$(9.90 \pm 0.28) \times 10^3$	-5.08 ± 0.23	$(3.55 \pm 0.13) \times 10^6$	-8.01 ± 0.04
1,5dmHexNH3	$(1.53 \pm 0.08) \times 10^6$	-9.87 ± 0.08	$(6.37 \pm 0.43) \times 10^6$	-7.88 ± 0.05
Epi	n.b.	n.b.	$(4.39 \pm 0.17) \times 10^4$	-9.44 ± 0.14
Pseudo	n.b.	n.b.	$(3.76 \pm 0.05) \times 10^5$	-7.94 ± 0.02
Labetalol	$(9.65 \pm 0.27) \times 10^3$	-10.6 ± 0.1	$(9.26 \pm 0.13) \times 10^5$	-11.0 ± 0.0
Hcort	n.b.	n.b.	$(2.78 \pm 0.18) \times 10^4$	-12.7 ± 0.4
Cort %	n.b.	n.b.	$(1.84 \pm 0.09) \times 10^5$	-14.1 ± 0.2
Hoechst 33258	-	-	$(3.49 \pm 1.88) \times 10^8$ (1:1) [H:G] $(1.18 \pm 0.33) \times 10^6$ (2:1) [b]	-
Lucigenin	$(2.83 \pm 0.14) \times 10^6$ [a]	-	-	-

a) Measured via change in fluorescence of **Lucigenin** fitted to a 1:1 binding model; b) Measured via change in fluorescence of **Hoechst 33258** fitted to a sequential 2:1 (H:G) model; n.b.) No heat detected via ITC; %) Not explicitly a WADA-Banned Substance; - Not measured

P5AS·**2HeptNH3** binding interaction. Similar direct titrations were completed for most of the remaining guests with both P5AS and P6AS and the results are shown in **Table IV-1**.

4.2.2.2 Determination of Binding via Fluorescence Based Measurements

The binding constant of the two dyes eventually used in the IDA, **Lucigenin** and **Hoechst 33258**, were measured directly with P5AS and P6AS respectively by monitoring the fluorescence of each dye with varying concentrations of host. The data from three replications for each host concentration was then fitted to a binding model using Scientist.™ While

Lucigenin fit a 1:1 biding model, **Hoechst 33258** was fit using a sequential 2:1 binding model. Interestingly the fluorescence intensity for P6AS·**Hoechst 33258** increased roughly 80-fold at 1:1 (H:G) ratio before decreasing slowly until it was roughly 50-fold more intense than the uncomplexed dye. The sequential 2:1 binding interaction with **Hoechst 33258** has previously been reported with CB[7][167] and CB[8][168] by Barooah and coworkers.

4.2.3 Influence of Length and Branching of Aliphatic Stimulants on P[*n*]AS Binding

We knew from previous studies[30] that P5AS preferentially bound linear alkane molecules. This can be seen once again here as the tightest binding complex of all of the WADA-banned substances measured is that of P5AS·**1HeptNH3**. With this in mind, let us first focus on the set of branched constitutional isomers (**1HeptNH3**, **2HeptNH3**, **1,3dmPentNH3**, and **1,4dmPentNH3**) to examine the effect the number of branches and branching location has on binding affinity towards P5AS. We can see that generally, the more linear the molecule, the higher the association constant. This can be seen as **1HeptNH3** binds two-fold stronger than **2HeptNH3**, 380-fold stronger than **1,3dmPentHN3**, and over 1100-fold stronger than **1,4dmPentNH3**. We can also see that when the linear portion between the ammonium group and the branched methyl group is lengthened by one carbon (**1,3dmPentNH3** *vs.* **1,4dmPentNH3**) the binding affinity becomes roughly three-fold weaker.

Moving our attention to the other alkyl stimulants measured, we can see that when the additional methyl spacer lengthens the molecule, (**1,5dmHexNH3** *vs.* **1,4dmPentNH3**) the binding affinity actually increases by over 150-fold. When the additional methyl spacer is added after the branched methyl group (**1,3dmPentNH3** *vs.* **1,3dmButNH3**) the binding affinity

towards P5AS decreases slightly but largely remains the same. These results, taken with our previous findings that alkyl diammonium guest have a positive correlation between P5AS binding affinity and chain length (from 3-6 carbon chains),[30] suggest that the location of the branched methyl group may affect how much of the guest is able to enter the binding cavity, thus reducing the effect of the increase in chain length. These results are in agreement with the ^{1}H NMR spectra of selected guests as explained below.

These trends largely exist for P6AS but the binding strength remains relatively agnostic of chain length and branching location for the guests measured. While the difference between the weakest and strongest binding of guests mentioned above is over a 1,000-fold difference, it is only about an 8-fold difference for P6AS. Conversely, for P6AS, lengthening the alkyl chain results in an enhancement in binding affinity regardless of if it is before or after the branched methyl group. This suggests that total chain length is the most important factor for P6AS binding strength. This is most likely because P6AS is able to accommodate the entirety of the bulkier branched methyl group throughout the entirety of its binding cavity. This is also in agreement with the ^{1}H NMR data as explained below.

4.2.3 Selectivity of Aliphatic vs. Aromatic Stimulants and Effect of Hydroxide Groups on Binding Affinity of Stimulants

Two aromatic stimulants, namely **Epi** and **Pseudo**, were measured in this study. In both cases, P5AS was not found to have noticeable binding towards either stimulant which, is similar to what has been previously reported with a similar stimulant, methamphetamine.[32] This is consistent with the idea that P5AS is not able to effectively encapsulate these larger guests.

However, P6AS was able to bind both guests, but at lower affinities compared to the other stimulants. This is most likely due to the hydrophilic hydroxyl groups close to the cationic ammonium group present in each molecules. When comparing the K_a for P6AS·**Pseudo** (K_a = (3.76 ± 0.05) × 10^5 M^{-1}) to P6AS·methamphetamine (K_a = (9.90 ± 0.39) × 10^6 M^{-1}),[32] it is clear that the presence of the hydrophilic hydroxyl group is the driving factor for the relatively low affinity of **Epi** and **Pseudo**. Similarly, when comparing **Epi** to **Pseudo**, it is not surprising that **Epi**, which has two additional hydroxyl groups at the meta and para positions of the ring relative to the alkyl chain, binds almost an order of magnitude weaker than **Pseudo** despite the added steric bulk near the ammonium group of **Pseudo**.

4.2.4 Influence of Functional Group on P[*n*]AS Binding Naturally Occurring Steroids.

Previously the Isaacs group has investigated the binding affinity of P[*n*]AS with modified cationic steroids and found that both P5AS and P6AS were able to bind the various cationic steroid analogues with affinities ranging from 10^5-10^6 M^{-1} for P5AS and 10^5-10^{12} M^{-1} for P6AS in 20 mM phosphate buffer.[30] Nau and coworkers have similarly investigated the binding of naturally occurring steroids with CB[7] and CB[8] in various biologically relevant solutions.[12] Both of these studies suggest that the larger P6AS may be able bind naturally occurring steroids. While P5AS was not found to have noticeable binding towards any of the steroids tested, P6AS was able to bind each of them and showed some selectivity. When looking at **Hcort**, we can see it binds roughly 6.6 times than **Cort**. The only difference between these compounds is the hydroxyl group on carbon 17 of the steroid backbone for **Hcort** versus just hydrogen for **Cort**.

4.2.6 Qualitative ^{1}H NMR Host·Guest Recognition Study

With the association strengths now established, we conducted qualitative investigations with selected guests to further investigate the binding geometry for P[*n*]AS and selected ammonium compounds, via ^{1}H NMR spectroscopy. In particular, we were interested in the penetration of each branched chain into the cavity of P[*n*]AS. To this end, we measured the spectra of P5AS·**2HeptNH3**, P5AS·**1,3dmButNH3**, P5AS·**1,3dmPentNH3**, P5AS·**1,4dmPentNH3**, P6AS·**2HeptNH3**, P6AS·**1,3dmButNH3**, and P6AS·**1,3dmPentNH3** each in 1:2, 1:1, and 2:1 (H:G) ratios. **Figure IV-3** shows **1,3dmButNH3** with varying concentrations of either P5AS or P6AS.

Most notably, we can see the large upfield shift in the signal for the proton located on the alpha carbon to the amine group (H_b $\Delta\delta$ = -1.2 ppm) for P6AS·**1,3dmButNH3**. Conversely, the signal for same proton for the P5AS·**1,3dmButNH3** complex shows almost no change in chemical shift (H_b $\Delta\delta$ = < -0.1 ppm). The signal for the adjacent methyl shows a similar effect for P6AS·**1,3dmButNH3** (H_a $\Delta\delta$ = -1.1 ppm) *vs.* P5AS·**1,3dmButNH3** (H_a $\Delta\delta$ = < +0.1 ppm). Taken together, this establishes that the cationic head of the amine is not able to enter the cavity of P5AS, but it is able to enter the cavity of P6AS. If we then turn our attention to the resonances of the methyl H_e protons at the tail, we can see that there is a large upfield shift for both P6AS (H_e $\Delta\delta$ = -1.7, $H_{e'}$ $\Delta\delta$ = -1.9) and P5AS (H_e $\Delta\delta$ = -1.3, $H_{e'}$ $\Delta\delta$ = -1.8). Additionally, the hydrogens become chemically non-equivalent upon complexation. The large upfield shift establishes that the dimethyl 'tail' of both amines is able to enter into the cavity while the disparity between the $\Delta\delta$ for P5AS suggests that while one methyl group is firmly inside the host, the other may be

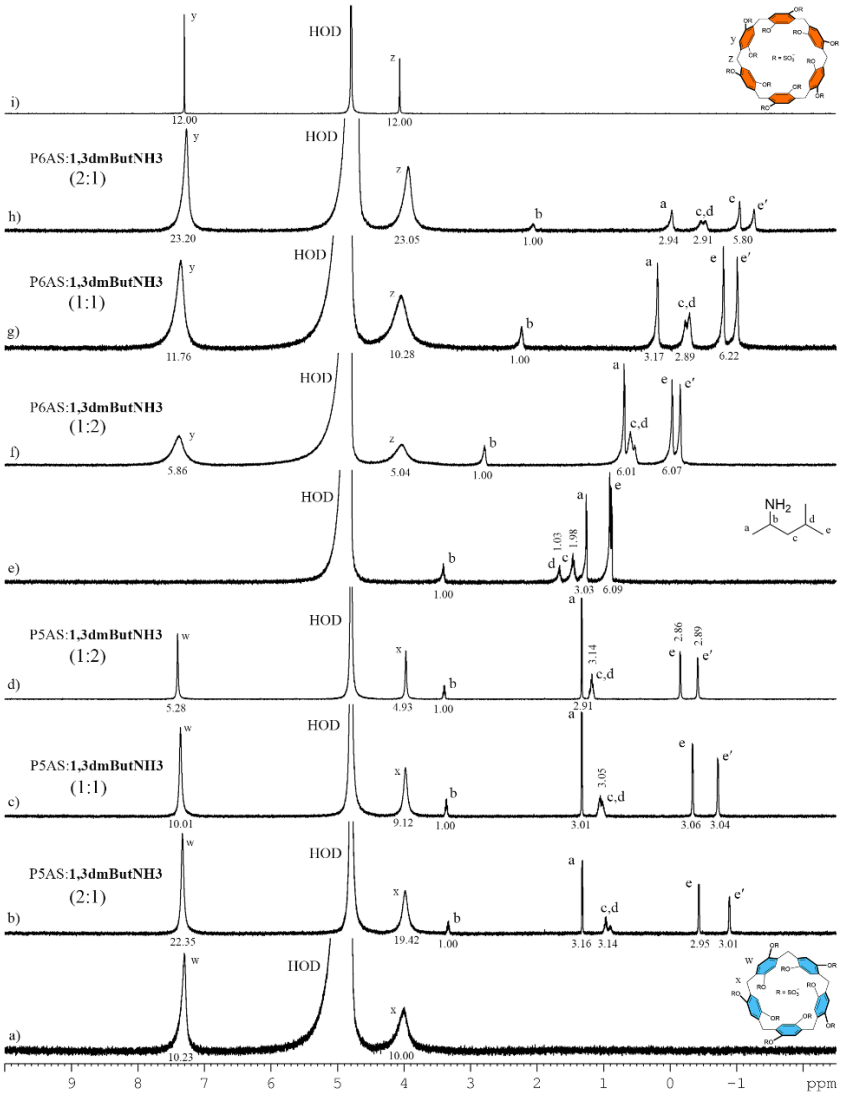

Figure IV-3. ^{1}H NMR spectra recorded for (600 MHz, RT, PBS buffered D_2O, pD 7.4) for: a) P5AS (1.0 mM), b) a mixture of **1,3dmButNH3** (0.5 mM) and P5AS (1.0 mM), c) an equimolar mixture of **1,3dmButNH3** and P5AS (1.0 mM), and d) a mixture of **1,3dmButNH3** (2.0 mM) and P5AS (1.0 mM), e) **1,3dmButNH3** (1.0 mM), f) a mixture of **1,3dmButNH3** (2.0 mM) and P6AS (1.0 mM), g) an equimolar mixture of **1,3dmButNH3** and P6AS (1.0 mM), and h) a mixture of **1,3dmButNH3** (0.5 mM) and P6AS (1.0 mM), i) P6AS (1.0 mM).

pointed outside of the cavity. This pattern can be seen for all of the branched aliphatic amines (**Figures SIV-21** – **SIV-25**).

4.2.7 Detection of WADA Banned Substances in PBS Buffer

4.2.7.1 Determination of the Conditions for Assay

Initially a series of host·dye complexes were tested against a panel of the tighter binding and structurally similar stimulants (Blank, **2HeptNH3**, **1HeptNH3**, **1,3dmButNH3, 1,3dmPentNH3, 1,4dmPentNH3, 1,5dmHexNH3**) at a concentration of 2 μM to determine which host·dye complex would yield the greatest change in signal for the indicator displacement assay (IDA). This should in turn tell us which conditions would result in the largest separation between molecules in the final assay. Previously, we have used 4′,6-diamidino-2-phenylindole (DAPI) with P6AS effectively as a way of measuring the binding constant of modified peptides.[165] In addition to DAPI, we tested thioflavin T, proflavine, rhodamine 6G, **Lucigenin**, and **Hoechst 33258** individually in equimolar mixtures of either P5AS or P6AS. Since Leucigenin and Hoechst 33258, when bound to P5AS and P6AS respectively, had the largest signal changes allowing us to separate the compounds the most effectively. We also found that at the concentrations we were testing mixtures of P5AS·**Lucigenin**, and P6AS·**Hoechst**, each at concentrations of 2 μM and 5 μM were the best conditions. No further optimization was carried out when the guest concentration was increased for the sensing assay because we still wanted to maintain as much differentiation at low concentrations as possible.

4.2.7.2 Implementation of Linear Discriminant Analysis (LDA) to Detect and Differentiate WADA Banned Substances in PBS Buffer

Once we had settled on the dyes and concentrations, the next step was to determine the best emission wavelengths to monitor. Two conditions involving P5AS·**Lucigenin** (equimolar at 2 μM and 5 μM), and two conditions involving P6AS·**Hoechst 33258** (equimolar at 2 μM and 5 μM) were used. The emission spectra of each condition were measured every 5 nm from 435-470 nm and 335-435 nm respectively. Typically, in order to increase the predictive accuracy as much as possible similar differential sensing assays have been conducted in pure water,[12,41] and at relatively high concentrations of guest.[38] These strategies increase the predictive accuracy as much as possible by increasing the total amount of dye displaced, thus maximizing the change in spectroscopic signal. To show a more representative view of the predictive power of the P[*n*]AS-based assay as a method for drug testing, we decided to use a more competitive and biologically relevant PBS buffer (pH 7.4) as our medium. We then chose the lowest concentration of guest that yielded over a 90% accuracy (50 μM) with 15 separate measurements of each analyte.

To prevent overfitting, thereby increasing the generalizability of the resulting model, the number of dimensions (wavelengths used) was reduced. First, unhelpful and extraneous wavelengths were removed. To determine the best wavelengths, we used analysis of variance (ANOVA) on the data to help select the 15 best wavelengths. To do this, for each wavelength measured, the variance in signal within each compound was compared to the overall variance at that wavelength. An additional 3 wavelengths that were best able distinguish guests like the aromatic amines and steroids were added resulting in a total of 18 variables. Then new variables which explain the data more efficiently, called features or linear discriminants (LD), were found

using the feature extraction algorithm linear discriminant analysis (LDA).[169,170] LDA is a supervised learning technique that finds new variables that are a linear combination of the original variables that both reduce the variance within each class (compound) while maximizing the variance between each class. To do this, LDA Through this technique, LD1-LD3 were able to include 98.5% of the total variance, or information, contained in the 18 variables remaining after feature extraction. These LDs not only more efficiently explain the data, but they are also carefully chosen to reduce the spread within of each group while maximizing the separation between groups. These new variables also theoretically describe underlying principles that differentiate each compound's spectra. The cross-plots of the first three LD are shown in **Figure IV-4**.

LDA can also be used as a predictive tool. To find the predictive power of the assay, stratified K-fold cross validation (CV) with K=15 was used.[169] To do this the data for 12 different guests at 50 μM were separated into 15 different groups such that a single measurement of each compound was randomly assigned to each group. One of the 15 groups were held-out as the remaining data were used to train a LDA model. After the LDA was trained on the 14 groups, the held-out group was then used to test the accuracy of the model. This was repeated for each of the 15 groups, with a new model trained each time (for a total of 15 models). Using this method, in total, the models were able to predict the held-out data with 92.3 ± 6.9 % accuracy. By making a chart of the predicted identity for each compound on on axis, and the actual identity on the other axis, you can create a confusion matrix (**Figure SIV-30**) which allows us to easily see what compounds were the easiest and hardest to accurately predict as well as what the model consistently confuses; this gives us an idea of what the model determines to be the most similar.

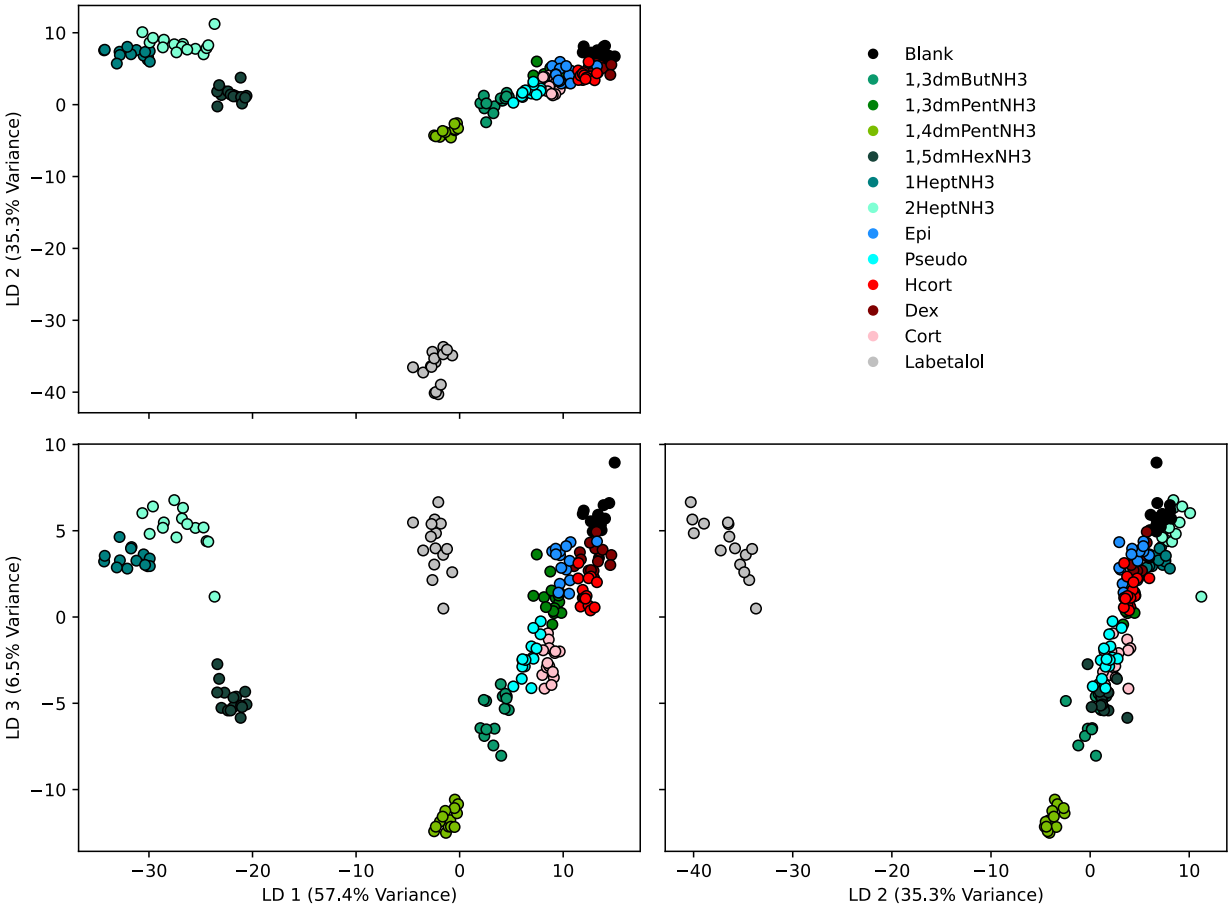

Figure IV-4. Cross sections of the three-dimensional Linear Discriminant Analysis (LDA) plot for the discrimination of 12 WADA-banned analytes at 50 μM of each guest. The predictive accuracy was determined to be 92.3 ± 6.9 % as determined via stratified K-fold (K = 15) cross-validation.

If the model perfectly predicts every compound, the diagonal would show 15/15 in this case, while every other place in the table would show 0/15. Looking at the confusion matrix, we find that compounds with similar binding constants are most often confused for each other. Most

notably we see that **Epi** was predicted with the lowest accuracy (10/15) and was most often confused for **Cort**. Both of these analytes do not bind strongly to P5AS and have similar association constant with P6AS. In order to further improve the model and the accuracy score for this proof-of-concept assay, the following things can be done: 1) increase the concentrations of guest, 2) use a less competitive buffer to get a larger signal changes, 3) use more data points so that the model can pick out the pattern more easily, or 4) add more conditions, particularly one that is adept at differentiating between the compounds that are currently the hardest to differentiate between (steroids in this instance). As a note, condition that fulfills criteria 4 would be helpful even if it cannot differentiate any of the other guests from each other.

An interesting feature that we recognized was that the plot separated chemicals of different pharmacological classes from each other. The steroids were separated from the stimulants along a boundary that extends from the blank towards **1,4dmPentNH3**, which can be seen readily in the LD1 *vs.* LD3 plot (**Figure IV-4c**). The LDA function appears to plot all of the stimulant and steroid data points along the same plane, with only the beta-blocker, labetalol, located in another plane. This should mean that if a new unknown analyte were to be introduced and detected, the assay should be able to suggest which to which pharmacological subgroup the analyte belongs. To test this theory **Estradiol**, new steroid that was not used in creating the classifier, was measured using the same protocol. When the classifier was then asked to predict what the compound was, the LDA classifier predicted it was a steroid 80% of the time (**Dex** – 8, **Hcort** – 4) and it was twice confused for the blank. Since pharmacologically similar compounds are able to be grouped together, this assay offers useful information even when analyzing novel analytes.

Since each LD theoretically represents some underlying variable, it is worthwhile to take a moment to attempt to determine what those underlying variables (LD1 and LD2) might be since they should be able to tell us more about the nature of each binding interaction. It is natural to think that LD1 and LD2 might correspond to the binding constants of each guest with P6AS and P5AS. This can be easily checked by plotting each LD vs the binding constants and looking for a trend (**Figure SIV-31 – SIV-34**). The log of the K_a values for P5AS and P6AS show a parabolic correlation towards LD1; as LD1 becomes more positive, the K_a for both P6AS and P5AS increasingly approaches 0. This increase is sharper for P6AS than for P5AS. Interestingly, LD2 appears to contain information regarding the entropy for the binding interaction of the linear stimulants with P5AS as there is a slight positive correlation between the two values. This would help to explain why the value for labetalol in LD2 is so different compared to every other host since labetalol is the only guest to have a positive $-T\Delta S^o$ value. Unfortunately, since the binding interactions are too weak to probe via ITC effectively, accurate entropy values could not be obtained for all guests to see if this correlation holds for all guests.

4.2.8 Quantitative Detection of Epinephrine and Pseudoephedrine in Simulated Urine.

With the conditions now optimized for the separation of each compound, the ability of the assay to determine concentration in simulated urine was determined. We chose simulated urine for two reasons: 1) of the 241,430 samples tested and entered into the Anti-Doping Administration & Management System (ADAMS) in 2021, over 90% were conducted on urine samples,[171] 2) we wanted to remove the use of a biohazard. To do this, simulated urine was

spiked with various concentrations of either **Epi** or **Pseudo**. The aim was to be able to accurately detect **Epi** and **Pseudo** below the threshold limits for competitions defined by WADA, 0.27 μM and 908 μM respectively.[172,173] The calibration measurements for concentrations from 0-2500 μM of **Pseudo** and 0-100 μM of **Epi** were collected using the same conditions and wavelengths as above without further optimization.

This data was then run through a new LDA algorithm for each analyte to prevent overfitting. The first discriminant was then fitted to a regression support vector machine (rSVM).[169] rSVM works similarly to traditional linear regression curves with a few notable exceptions. In this instance the main advantage is that, instead of fitting a line with infinitely small thickness, it fits a line with a tunable width, ε, on either side of the central line. Any point inside this width is essentially assumed to lie along the line and no penalty is applied to these data points when fitting allowing the fitting curve to be influenced less by outliers. After looking at the data, it was clear that the concentrations of **Pseudo** were non-linear with respect to LD1, so the data was transformed into a plot of LD1 *vs.* the natural log of the concentrations. After the line was fit, the concentrations were transformed back to the original space by taking the exponent of the calibrated y values (**Figure SIV-31**). After calibration, two previously unmeasured concentrations were chosen to test the accuracy of the assay. For **Pseudo** one of these two concentrations was between the limit of LOD of our model and the WADA-defined threshold limit, and the other was above the WADA threshold limit. For **Epi** it quickly became apparent that the current assay would not be able to measure **Epi** at concentrations close to the WADA-threshold. The results of the calibration and prediction can be seen in **Figure IV-5**. The

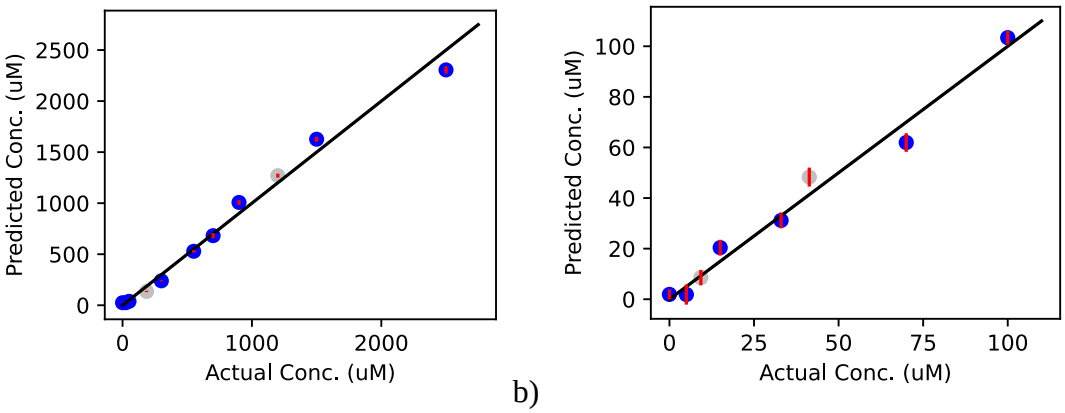

a) b)

Figure IV-5. Calibration plots for a) 0-2500 µM for **Pseudo** and b) 0-100 µM for **Epi** in simulated urine. Each concentration was measured 10 times and K-fold CV (K-10) was used to minimize the error of the training concentrations. The calibrations were able to achieve LOD of 28.6 µM and LOQ of 31.8 µM for **Pseudo**, and LOD of 5.7 µM and LOQ of 19.1 µM for **Epi**. The red lines represent the standard deviation of the predicted concentrations. The solid black line represents a perfect correlation between predicted and actual concentrations. Two test concentrations (grey) used for each compound with one above and one below the WADA threshold limit.

LOD and LOQ for each model were defined according to previously defined values[170] of $3\sigma_b$ and $10\sigma_b$ respectively plus the predicted blank concentration, where σ_b represents the standard deviation of the predicted blank concentration.

The calibration plots yielded an LOD of 28.6 µM and LOQ of 31.8 µM for **Pseudo**. For the **Epi** calibration plots, the LOD was 5.7 µM, and the LOQ was 19.1 µM. For **Epi** concentrations of 9.3 µM, 41.3 µM were tested, and the predicted concentrations were 8.6 ± 3.2 µM, and 48.3 ± 4.0 µM respectively. For **Pseudo**, concentrations of 186 µM and 1200 µM were

tested, and the predicted concentrations were 135.2 ± 7.0 μM, and 1270 ± 21 μM respectively. As stated previously, the assay is not sensitive enough at the moment to detect concentrations of **Epi** near the WADA-threshold. However, the assay is able to fairly accurately predict the concentrations of **Pseudo** not only around the WADA-threshold, but it has a remarkable range as it has a LOQ 30-fold lower than the WADA threshold while still being able to predict concentrations above millimolar concentrations with less than 6% error. Taken together, this suggests that this proof-of-concept assay, with further optimization, could be useful as a quick and cheap way to screen athletes for banned stimulants.

4.3 Conclusions

In summary we have measured the thermodynamics of the binding of P[*n*]AS toward a panel of stimulants,908 steroids, and a beta-blocker by ITC in PBS buffer. We also use those measurements to make conclusions about the favorability of various small structural changes to the guest molecule such as alkyl chain length and branching location. The geometry of various complexes were established through the use of ^{1}H NMR analysis to study the changes in chemical shift induced by the formation of a host·**guest** complex. Namely, the smaller P5AS is not able to fully encapsulate the cationic head of the branched alkyl ammonium groups while P6AS is large enough to encapsulate the entire molecule into its cavity. Additionally, we were able to show that an indicator displacement assay made from P5AS·**Lucigenin** and P6AS·**Hoechst 33258** complexes is able to differentiate structurally similar compounds at 50 μM concentrations of guest with over 90 % accuracy in PBS. This was then taken one step further and we were able to show that using the same conditions, the assay is able to accurately calibrate

Pseudo in simulated urine with a LOQ well below the WADA threshold level for drug testing. Overall we have established P[*n*]AS as a promising container family for use in an IDA and provided a proof-of-concept drug testing assay for the detection and differentiation of structurally similar compounds.

4.4 Experimental

4.4.1 General Experimental

Chemicals were purchased from commercial suppliers and used without further purification or were prepared by literature procedures. Simulated urine was purchased from Flinn Scientific ("Artificial Urine, Normal" Lot#294189). PBS buffer was made by dissolving MP Biomedicals brand tablets (Lot#S7091) in HPLC grade H_2O and using minimal NaOH or HCl to adjust the pH as needed. ^{1}H NMR spectra were measured on commercial instruments operating at 600 MHz for using sodium phosphate buffered D_2O saline (pD 7.4) as the solvent. Chemical shifts (δ) are referenced relative to the residual resonances for HOD (4.79 ppm). ITC data were collected on a Malvern Microcal PEAQ-ITC instrument and analyzed using the software provided by the vendor. All fluorescence measurements were performed using in a Greiner Bio-One black, flat-bottomed, polystyrene 96 well plate and measured with a SpectraMax 5^e multimode plate reader. Data analysis and machine learning algorithms were implemented in Python using pandas,[174] numPy,[175] and scikit-learn[176] libraries. All data analysis files and csv files for the calibration curves and LDA plot can be found on GitHub: https://github.com/daking11/WADA_sensor.git

Appendix 1

Cucurbit[8]uril Forms Tight Inclusion Complexes with Cationic Triamantanes

By David King,[a] Tatjana Šumanovac,[b] Steven Murkli,[a] Peter R. Schreiner,[c] Marina Šekutor,[b,] and Lyle Isaacs[a,*]*

[a] Department of Chemistry and Biochemistry, University of Maryland, College Park, Maryland 20742, United States; [b] Department of Organic Chemistry and Biochemistry, Ruđer Bošković Institute, Bijenička cesta 54, 10000, Zagreb, Croatia; [c] Institute of Organic Chemistry, Justus Liebig University, Heinrich-Buff-Ring 17, 35392 Giessen, Germany

*To whom correspondence should be addressed. Prof. Lyle Isaacs, Email: LIsaacs@umd.edu; Dr. Marina Šekutor, Email: msekutor@irb.hr

^{1}H and ^{13}C NMR spectra recorded for new compounds (G1 and G3)

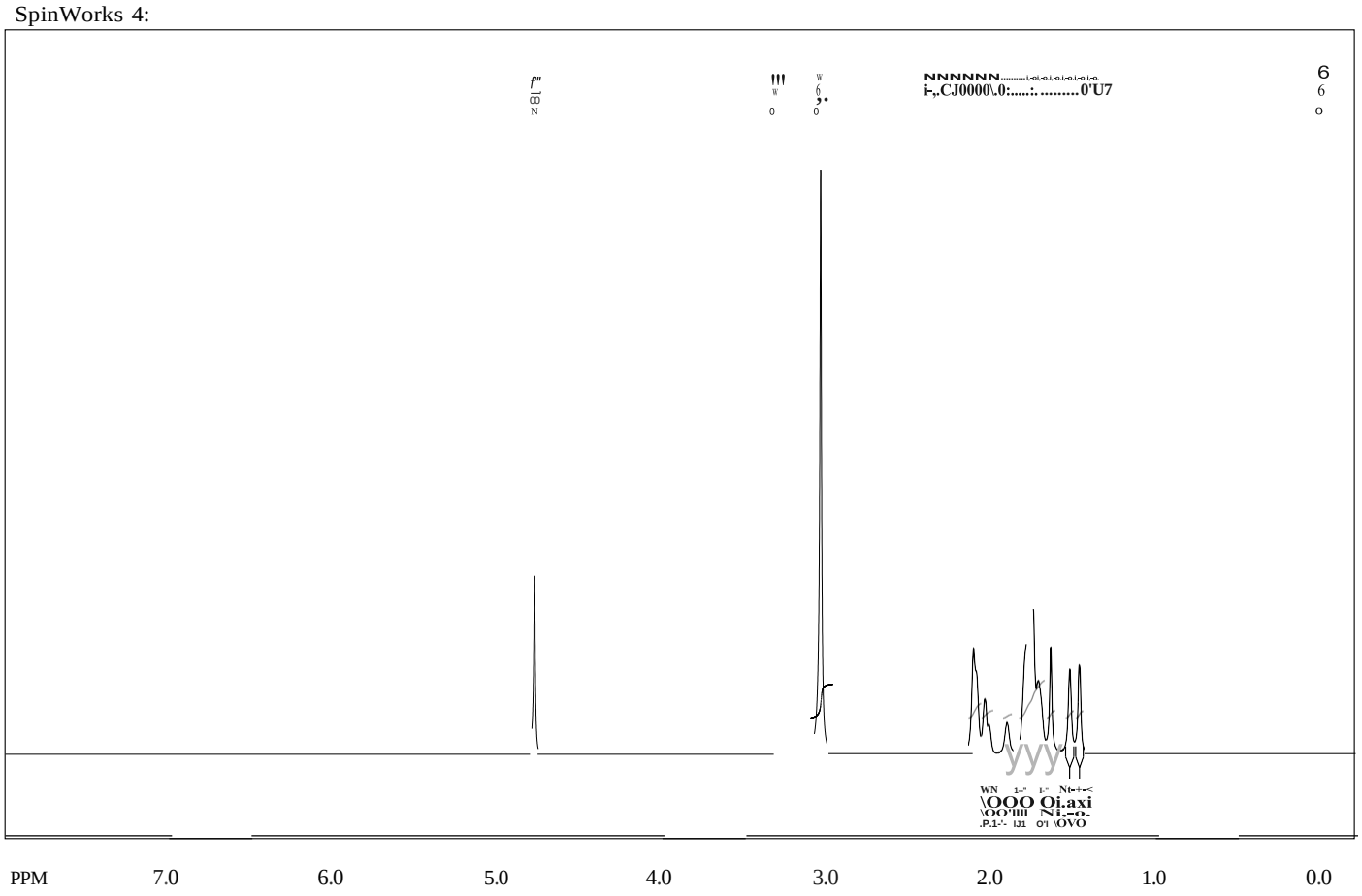

Figure SII-1. ^{1}H NMR (400 MHz, $CDCl_3$ + few drops of CD_3OD) recorded for *N*,*N*,*N*-trimethyltriamantane-9-aminium iodide (**G1**•I^-).

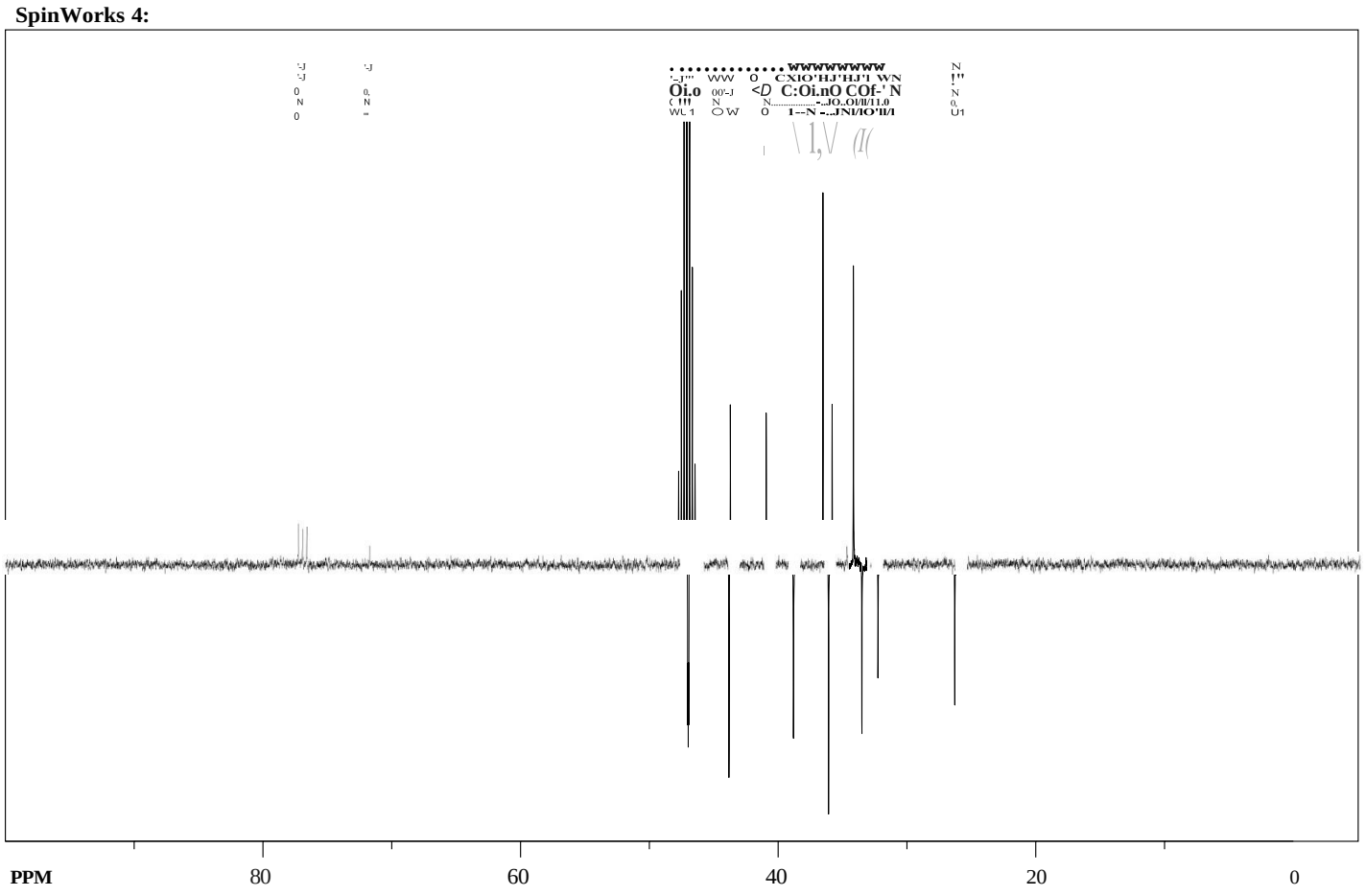

Figure SII-2. ^{13}C NMR (100 MHz, $CDCl_3$ + few drops of CD_3OD) of *N*,*N*,*N*-trimethyltriamantane-9-aminium iodide (**G1**•I^-)

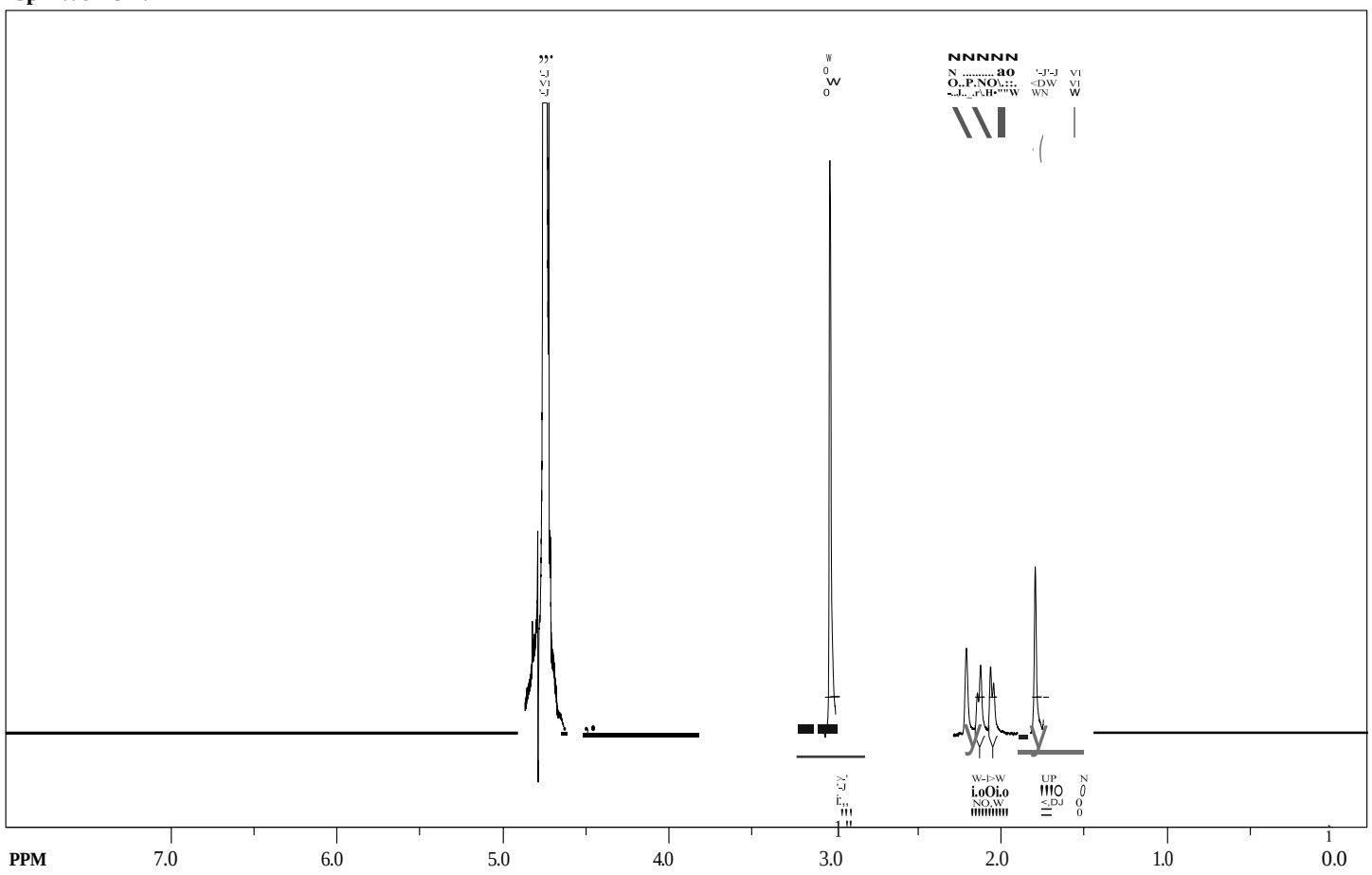

Figure SII-3. ^{1}H NMR (600 MHz, D_2O) recorded for *N*,*N*,*N*,*N*',*N*',*N*'-hexamethyltriamantane-9,15-diaminium diiodide (**G3**•2I^{-}).

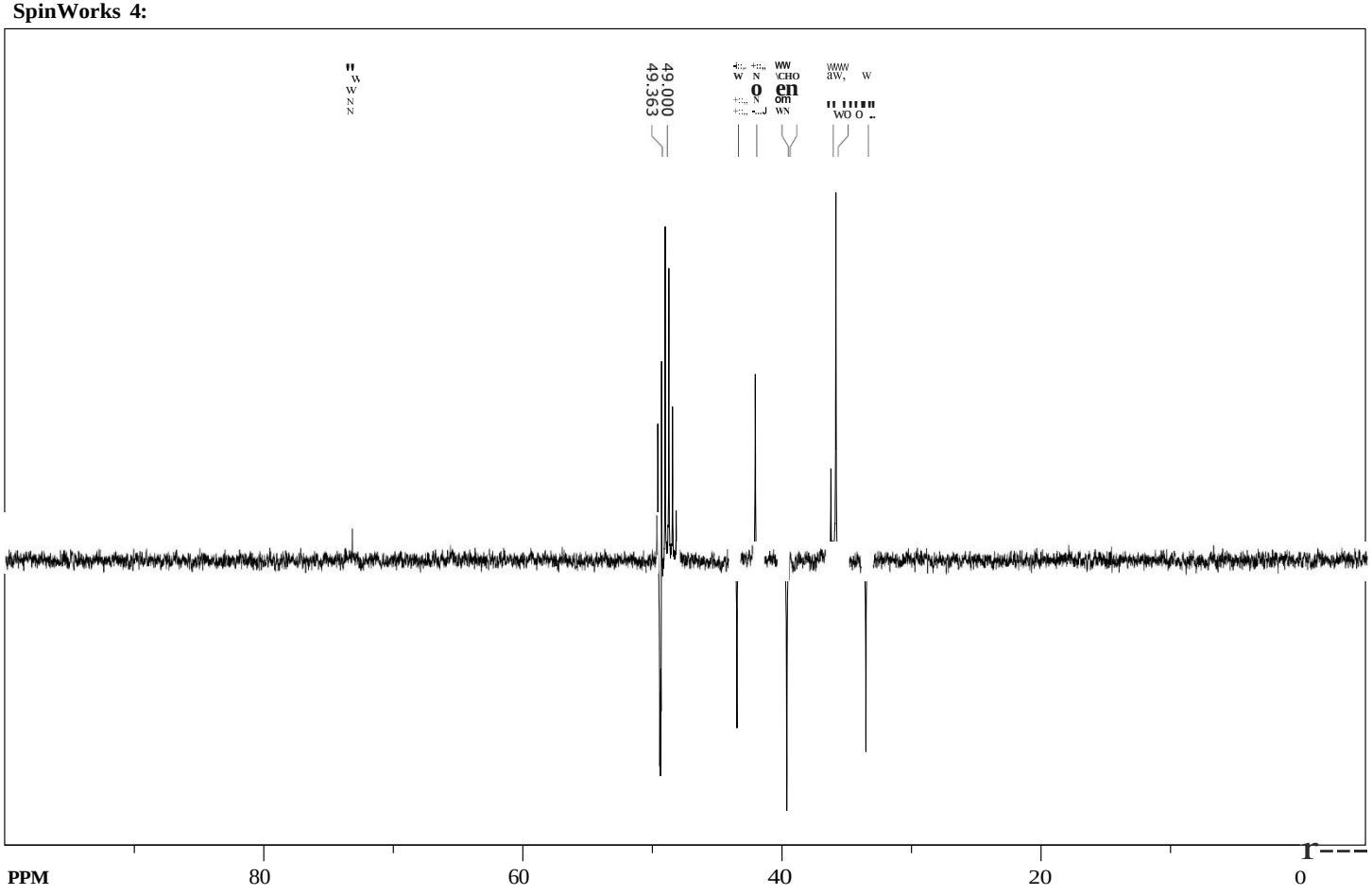

Figure SII-4. ^{13}C NMR (75 MHz, CD_3OD) recorded for *N*,*N*,*N*,*N*',*N*',*N*'-hexamethyltriamantane-9,15-diaminium diiodide (**G3**•2I$^-$).

^{1}H NMR binding studies for CB[7] and CB[8] toward triamantanes G1 – G4

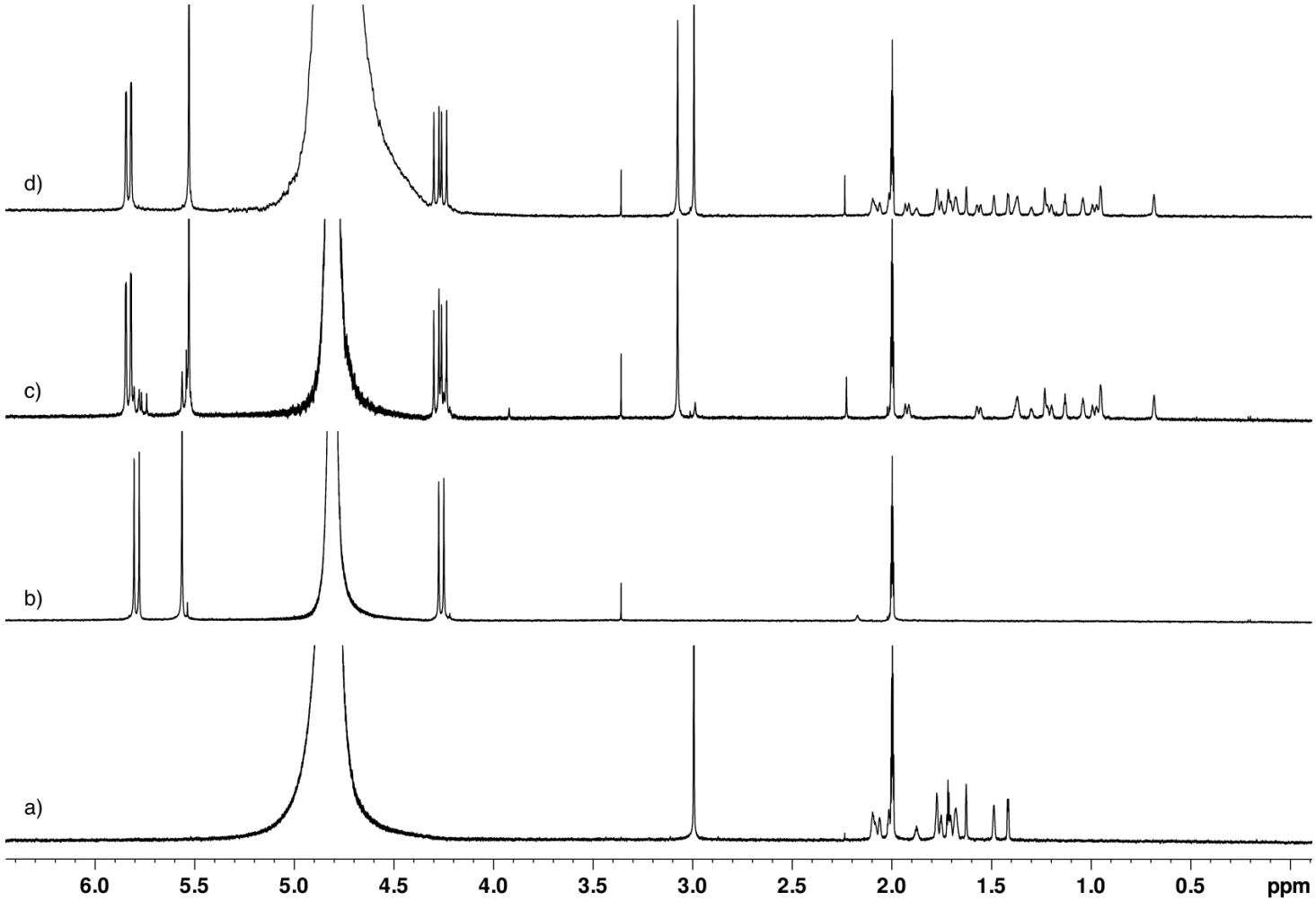

Figure SII-5. ^{1}H NMR spectra recorded (600 MHz, RT, 50 mM NaO_2CCD_3, pD 4.74) for: a) **G1** (0.5 mM), b) CB[7] (0.2 mM), c) an equimolar mixture of **G1** and CB[7] (0.2 mM), and d) a mixture of **G1** (0.4 mM) and CB[7] (0.2 mM).

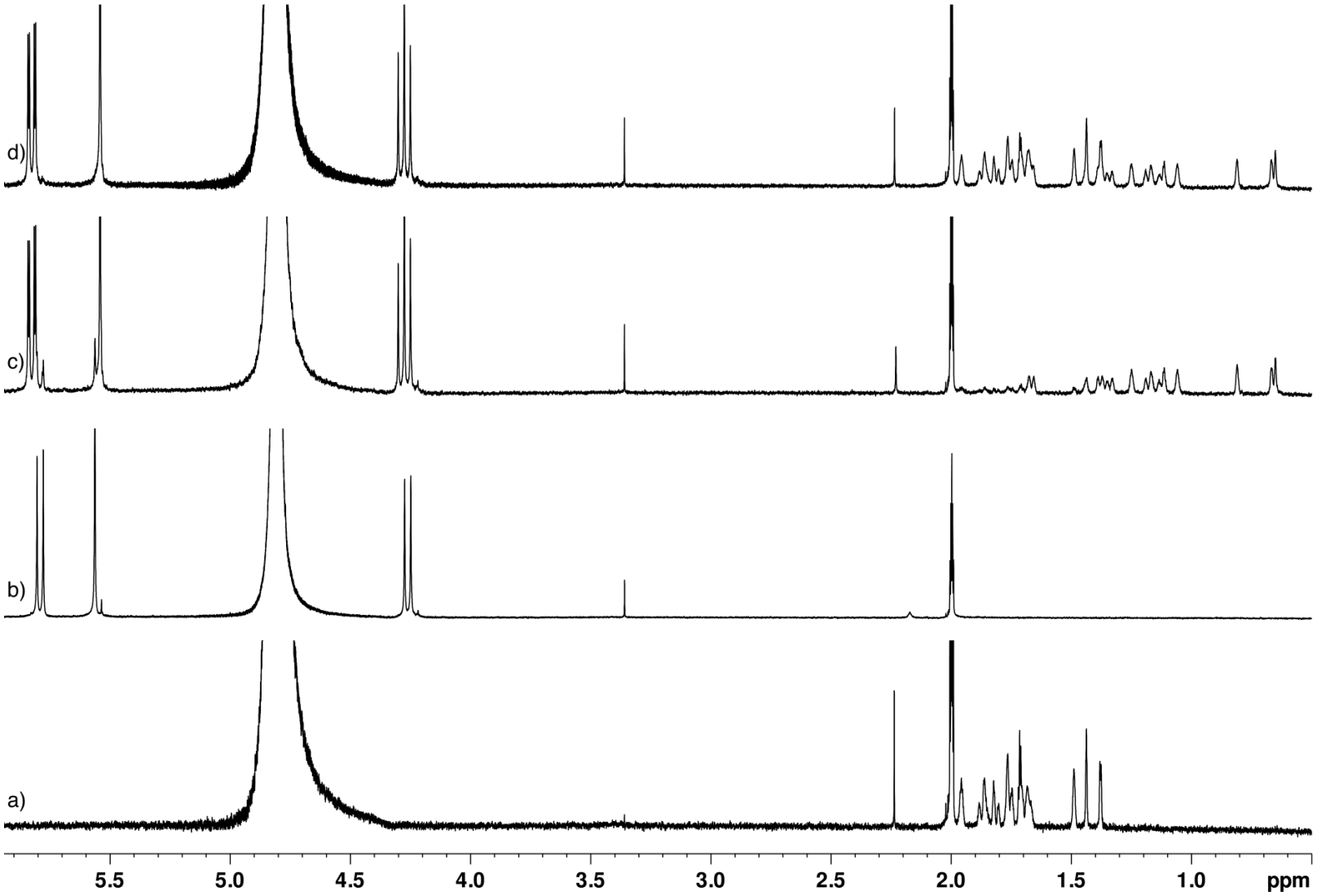

Figure SII-6. ^{1}H NMR spectra recorded (600 MHz, RT, 50 mM NaO_2CCD_3, pD 4.74) for: a) **G2** (0.5 mM), b) CB[7] (0.2 mM), c) an equimolar mixture **G2** and CB[7] (0.2 mM), and d) a mixture of **G2** (0.4 mM) and CB[7] (0.2 mM).

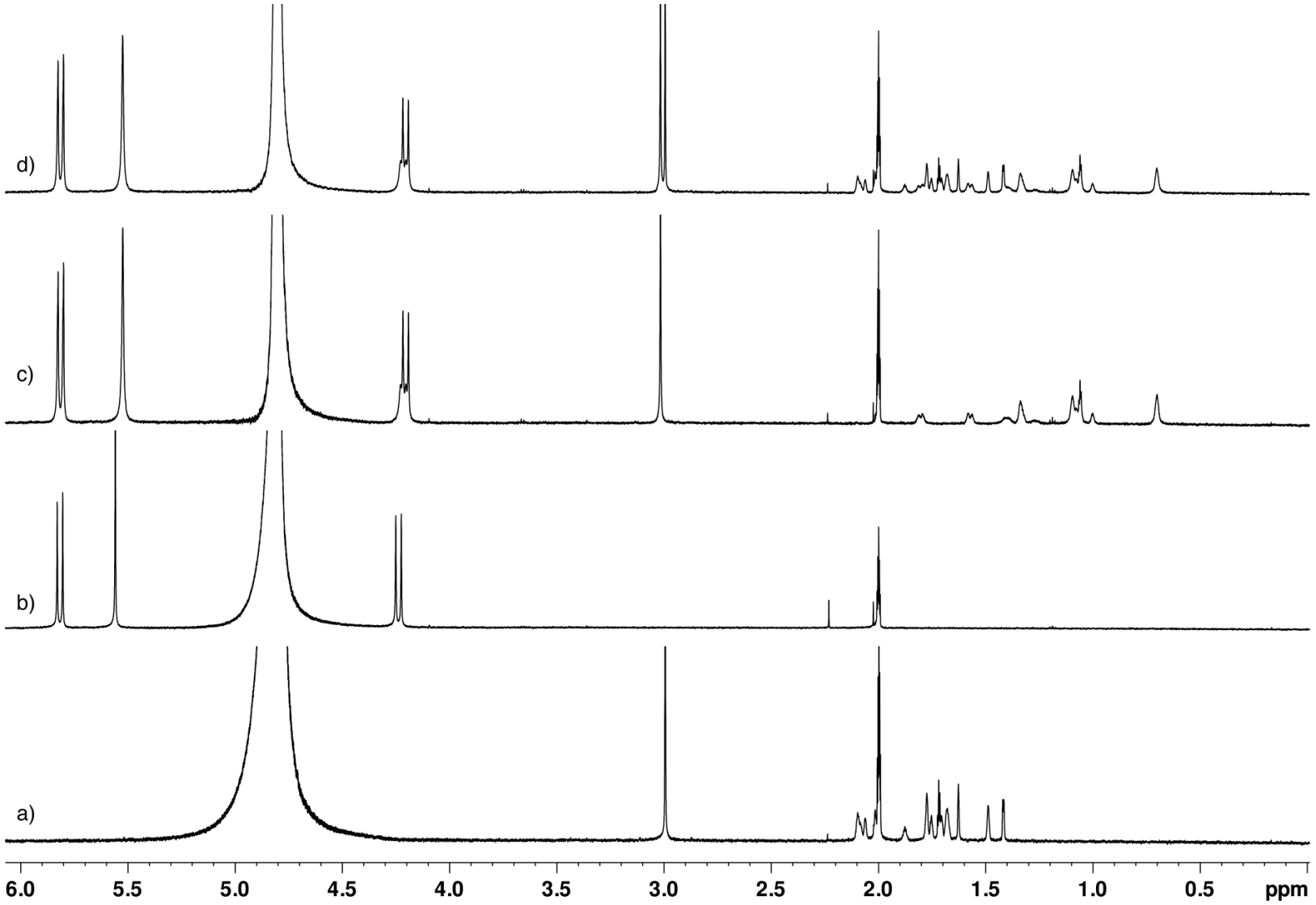

Figure SII-7. ^{1}H NMR spectra recorded (600 MHz, RT, 50 mM NaO_2CCD_3, pD 4.74) for: a) **G1** (0.5 mM), b) CB[8] (0.2 mM), c) an equimolar mixture of **G1** and CB[8] (0.2 mM), and d) a mixture of **G1** (0.4 mM) and CB[8] (0.2 mM).

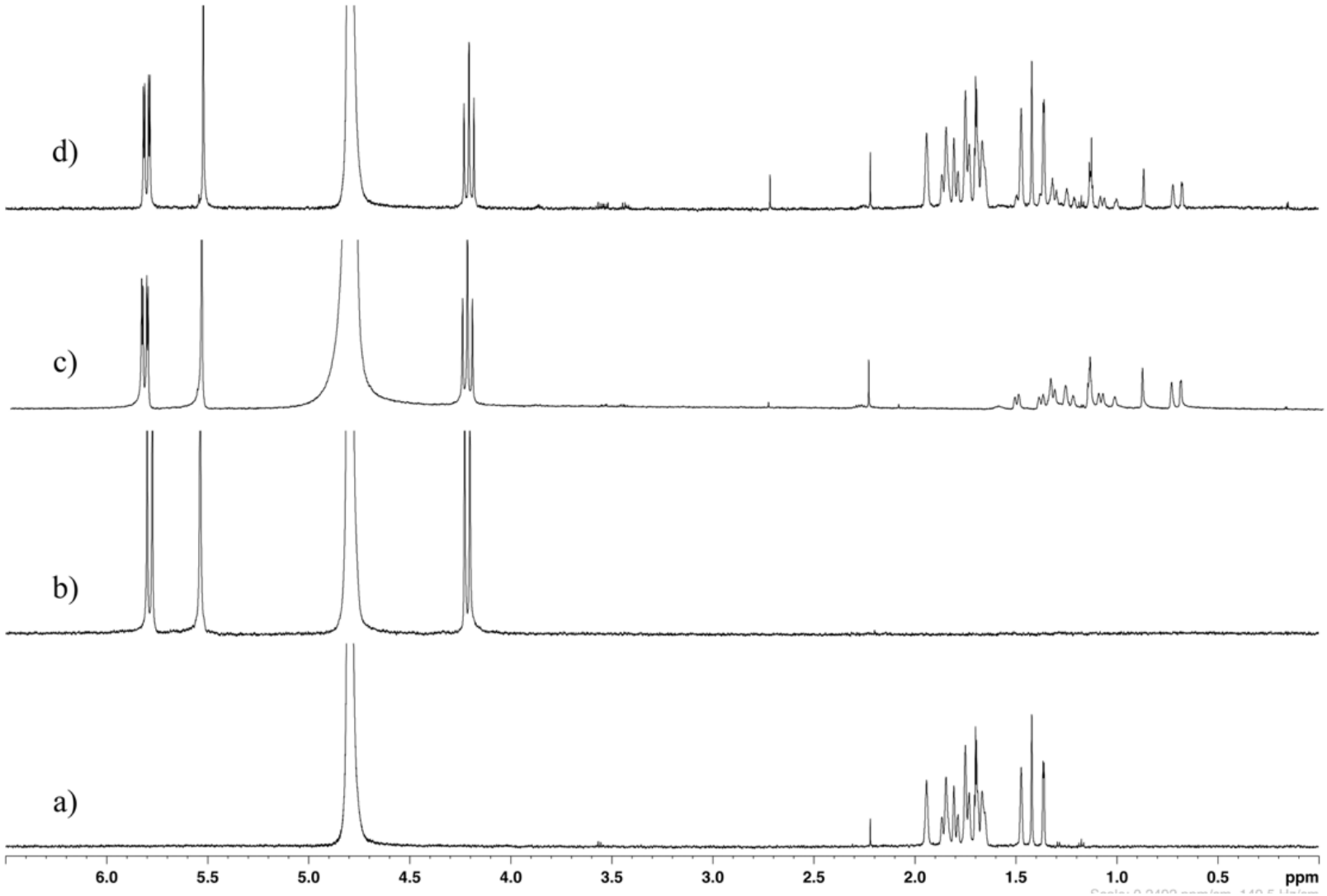

Figure SII-8. ^{1}H NMR spectra recorded (600 MHz, RT, D_2O) for: a) **G2** (0.5 mM), b) CB[8] (0.2 mM), c) an equimolar mixture of **G2** and CB[8] (0.2 mM), and d) a mixture of **G2** (0.4 mM) and CB[8] (0.2 mM). The CB[8]•**G2** complex precipitates from solution but can be made temporarily soluble by heating to obtain the NMR spectra given above.

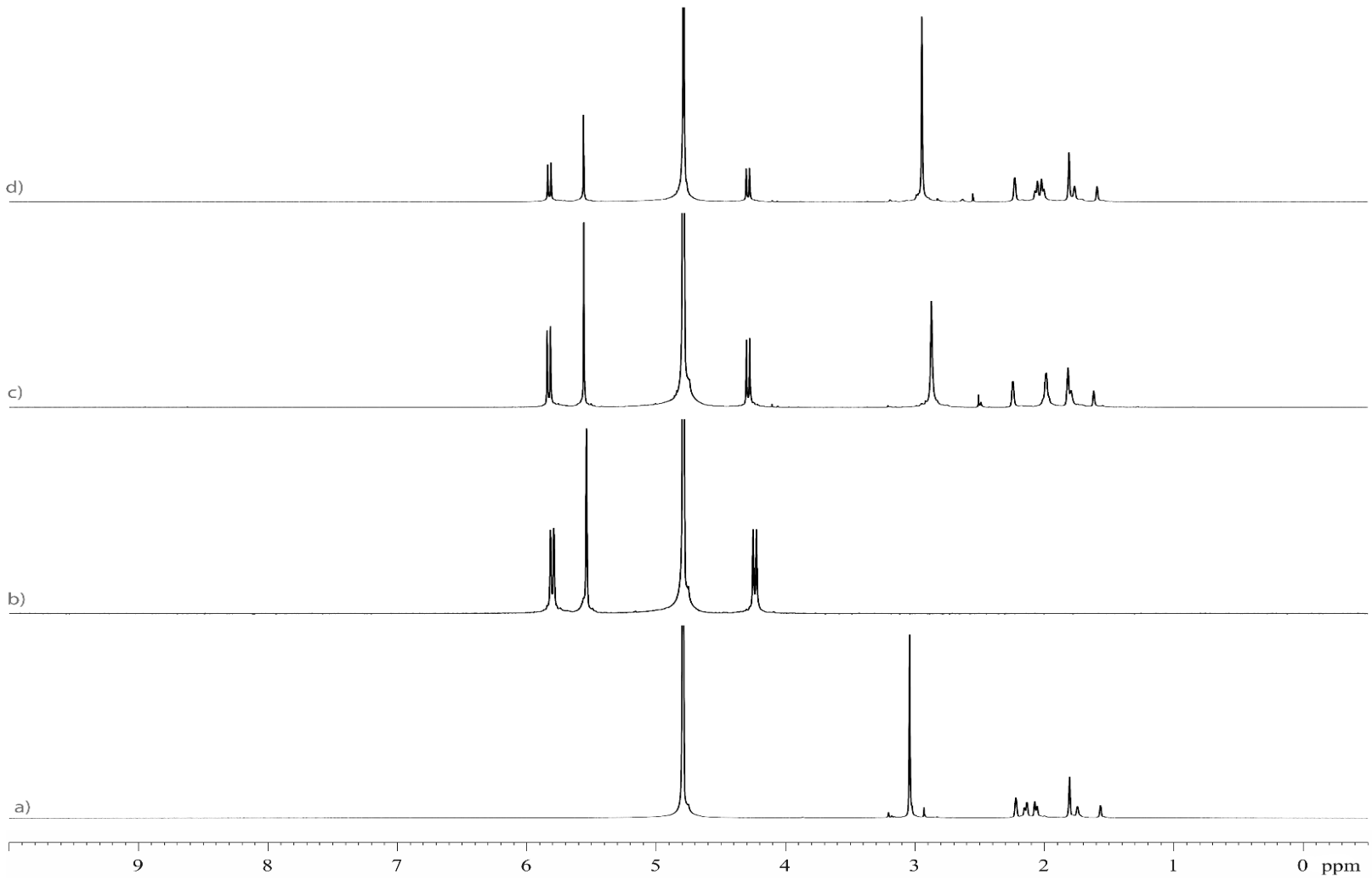

Figure SII-9. ^{1}H NMR spectra recorded for (600 MHz, RT, D_2O) for: a) **G3** (1.0 mM), b) CB[7] (1.0 mM), c) an equimolar mixture of **G3** and CB[7] (1.0 mM), and d) a mixture of **G3** (2.0 mM) and CB[7] (1.0 mM).

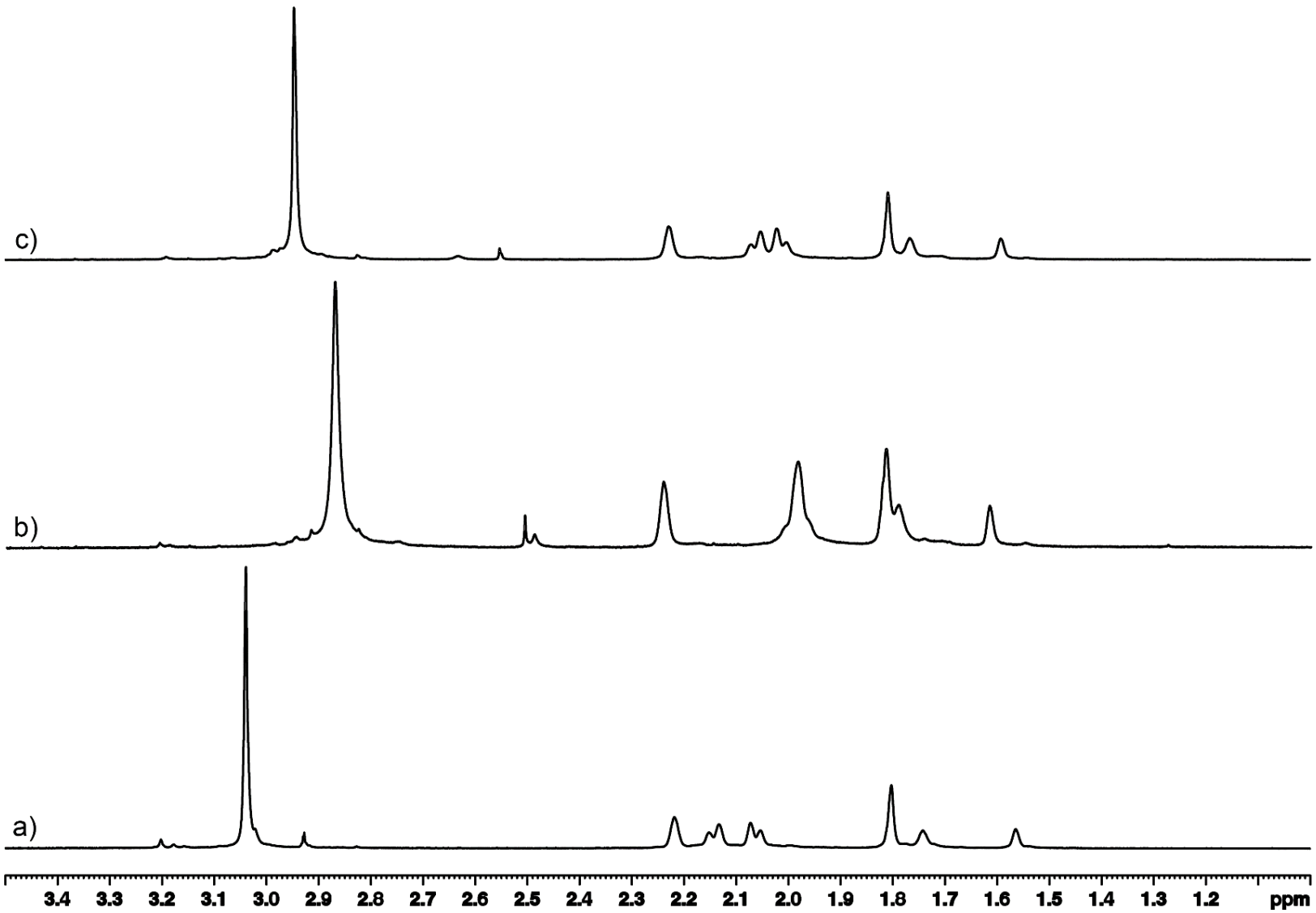

Figure SII-10. The expanded guest region for ^{1}H NMR spectra recorded for (600 MHz, RT, D_2O) for: a) **G3** (1.0 mM), b) an equimolar mixture of **G3** and CB[7] (1.0 mM), and c) a mixture of **G3** (2.0 mM) and CB[7] (1.0 mM).

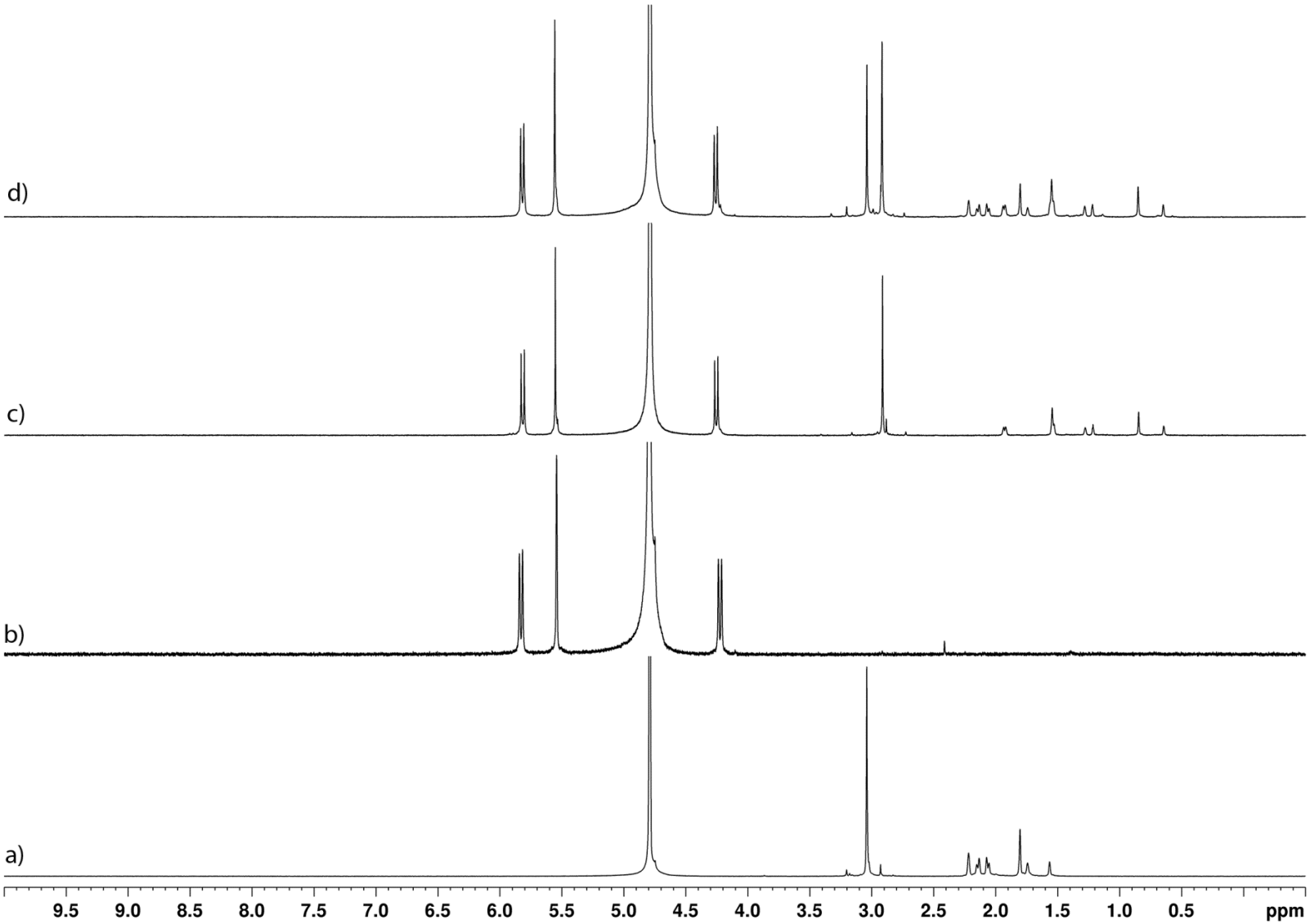

Figure SII-11. ^{1}H NMR spectra recorded for (600 MHz, RT, D_2O) for: a) **G3** (1.0 mM), b) CB[8] (0.5 mM), c) an equimolar mixture of **G3** and CB[8] (0.5 mM), and d) a mixture of **G3** (1.0 mM) and CB[8] (0.5 mM).

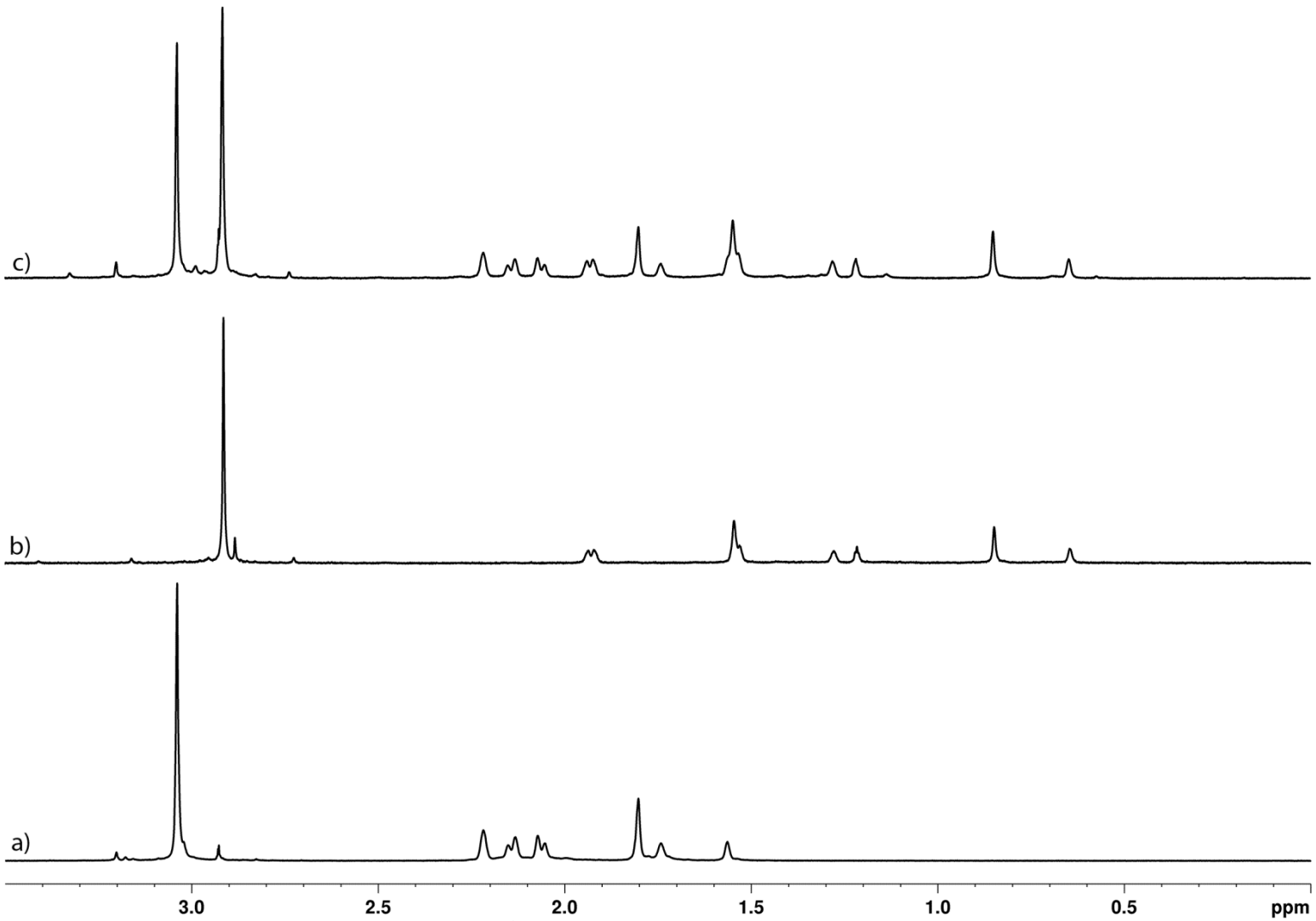

Figure SII-12. The expanded guest region for ^{1}H NMR spectra recorded for (600 MHz, RT, D_2O) for: a) **G3** (1.0 mM), b) an equimolar mixture of **G3** and CB[8] (0.5 mM), and c) a mixture of **G3** (1.0 mM) and CB[8] (0.5 mM).

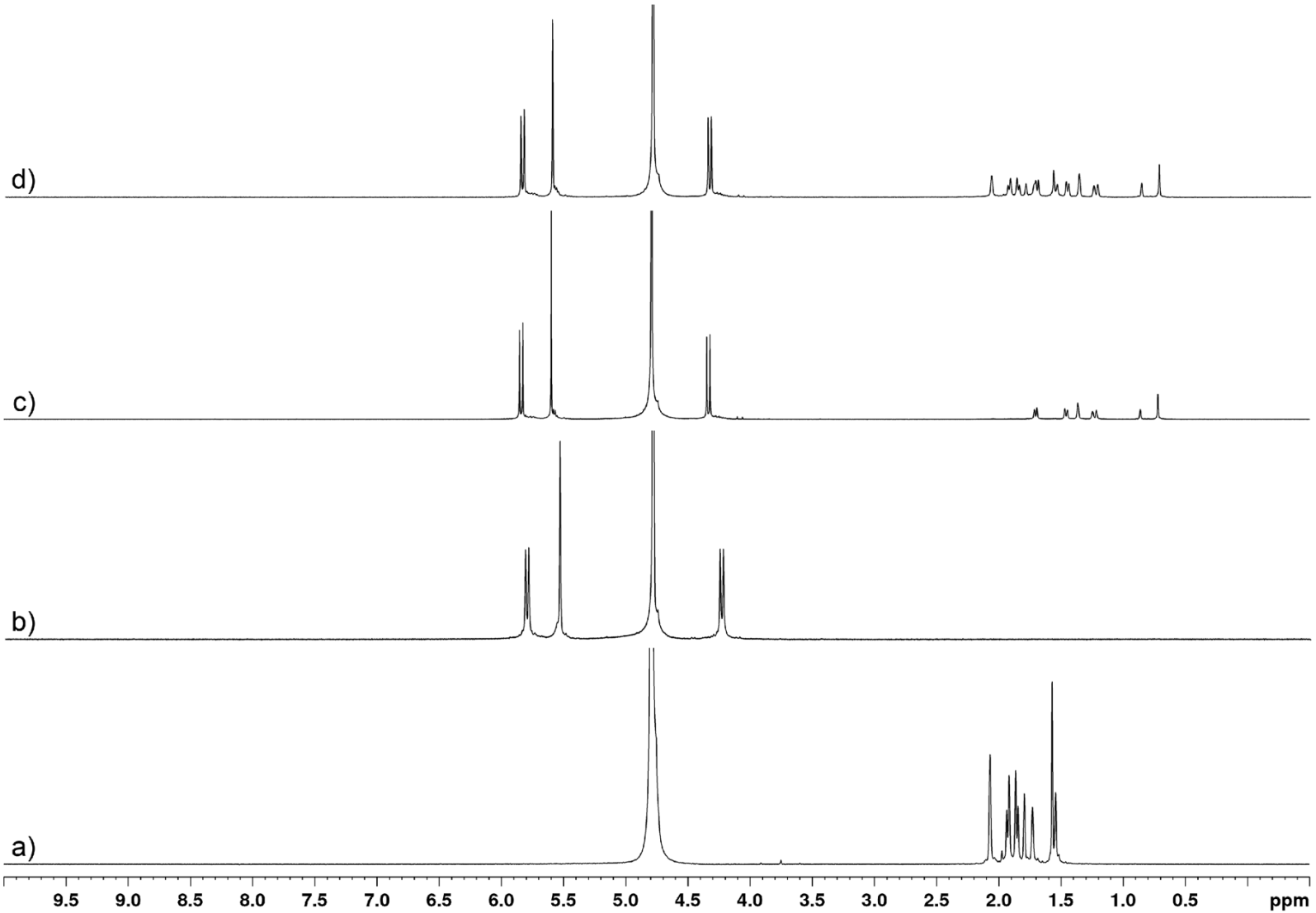

Figure SII-13. ^{1}H NMR spectra recorded for (600 MHz, RT, D_2O) for: a) **G4** (1.0 mM), b) CB[7] (1.0 mM), c) an equimolar mixture of **G4** and CB[7] (1.0 mM), and d) a mixture of **G4** (2.0 mM) and CB[7] (1.0 mM).

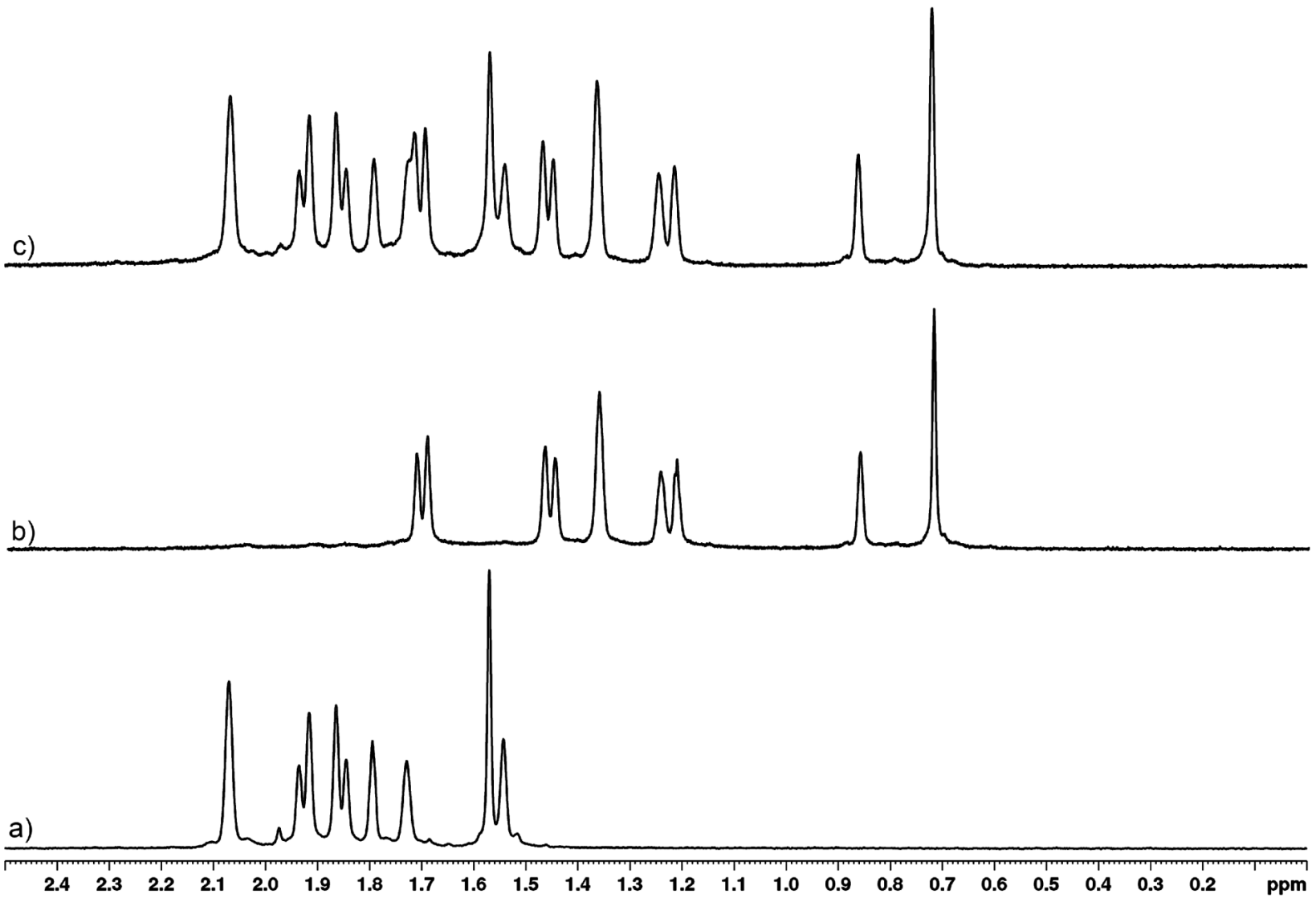

Figure SII-14. The expanded guest region for ^{1}H NMR spectra recorded for (600 MHz, RT, D_2O) for: a) **G4** (1.0 mM), b) an equimolar mixture of **G4** and CB[7] (1.0 mM), and c) a mixture of **G4** (2.0 mM) and CB[7] (1.0 mM).

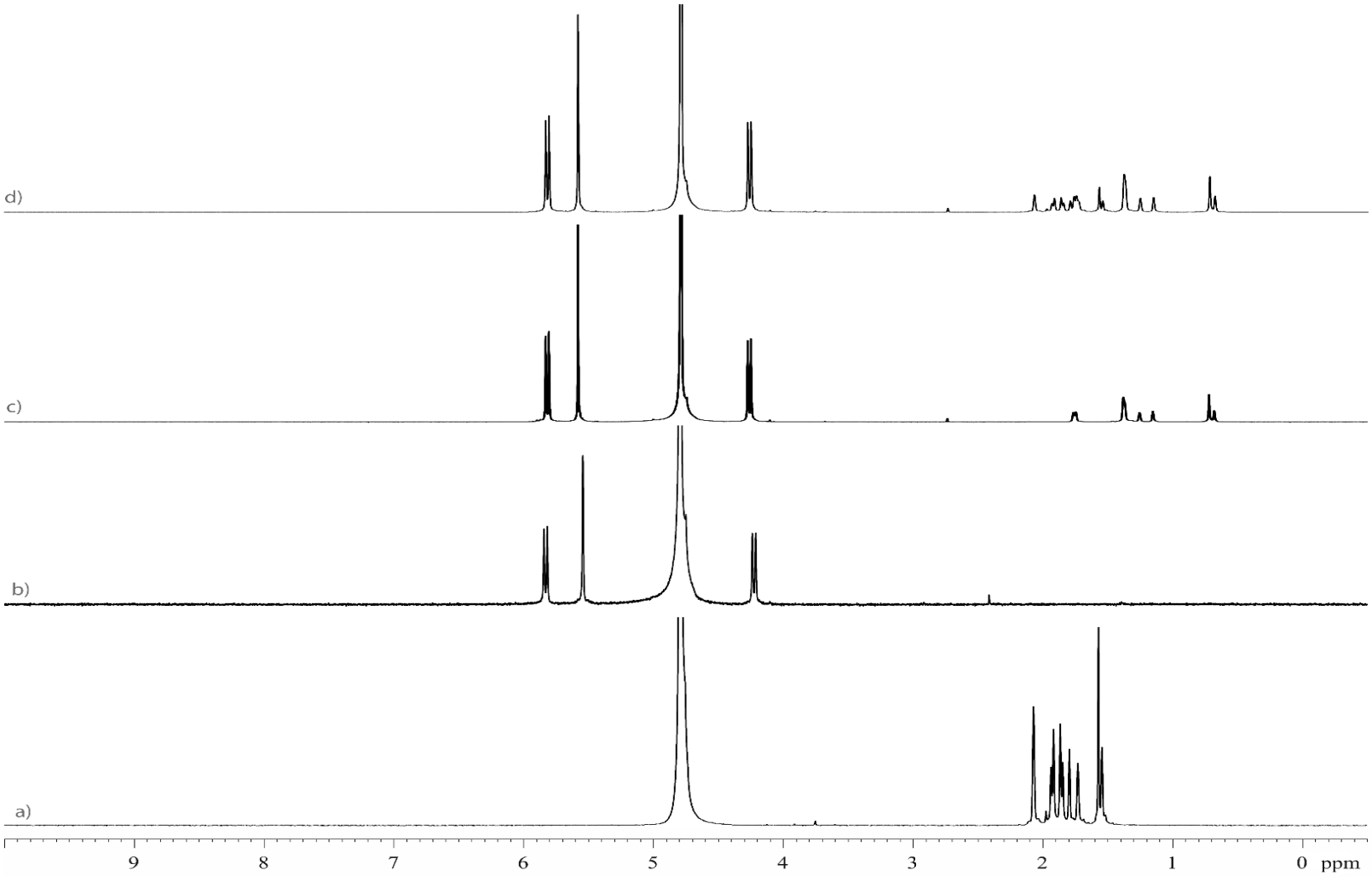

Figure SII-15. ^{1}H NMR spectra recorded for (600 MHz, RT, D_2O) for: a) **G4** (1.0 mM), b) CB[8] (0.5 mM), c) an equimolar mixture of **G4** and CB[8] (1.0 mM), and d) a mixture of **G4** (2.0 mM) and CB[8] (1.0 mM).

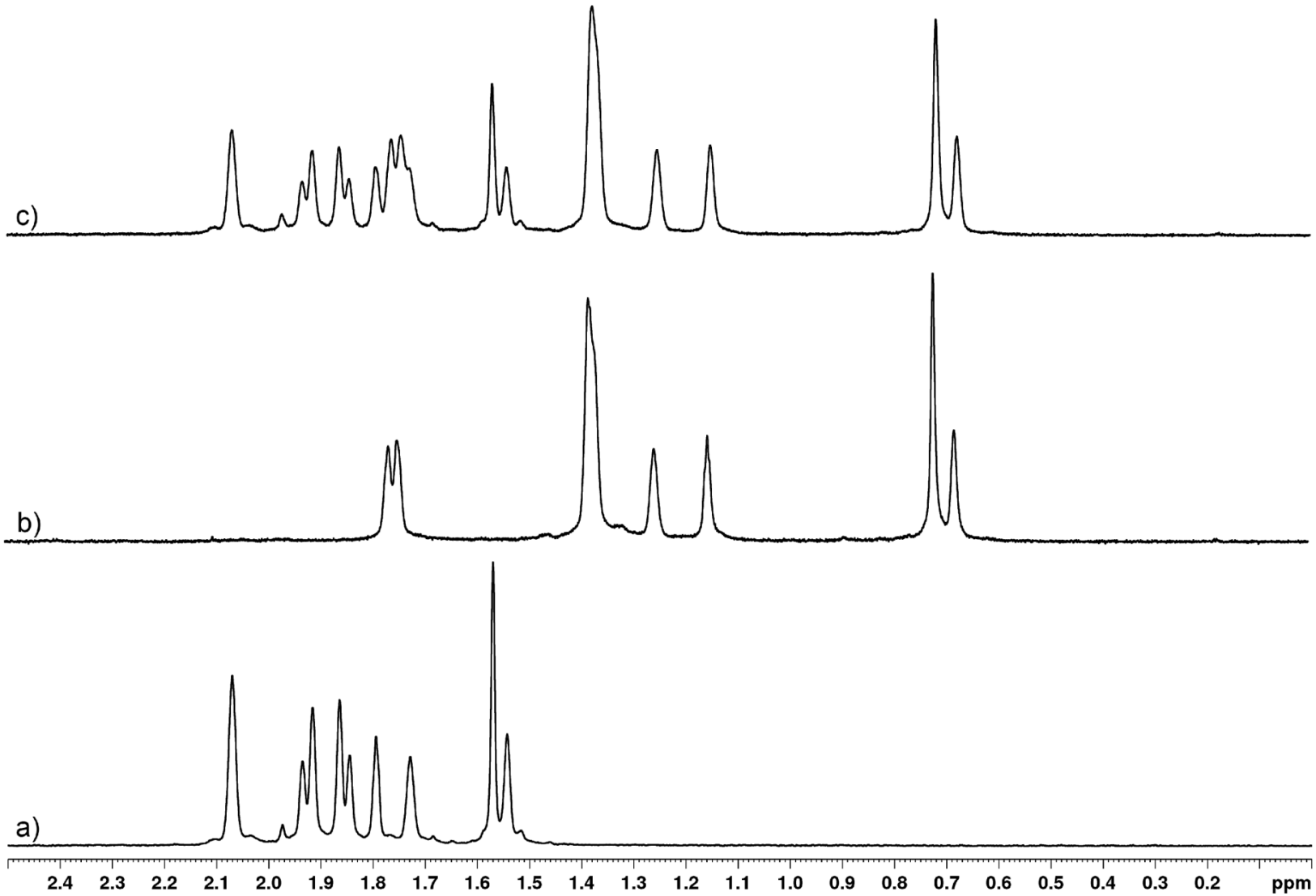

Figure SII-16. The expanded guest region for ^{1}H NMR spectra recorded for (600 MHz, RT, D_2O) for: a) **G4** (1.0 mM), b) an equimolar mixture of **G4** and CB[8] (1.0 mM), and c) a mixture of **G4** (2.0 mM) and CB[8] (1.0 mM).

Determination of K_a of Cucurbit[7]uril towards G1, G2 and G4 using Isothermal Titration Calorimetry (ITC).

The binding data was fitted using the single set of sites binding model in MicroCal PEAQ-ITC analysis software.

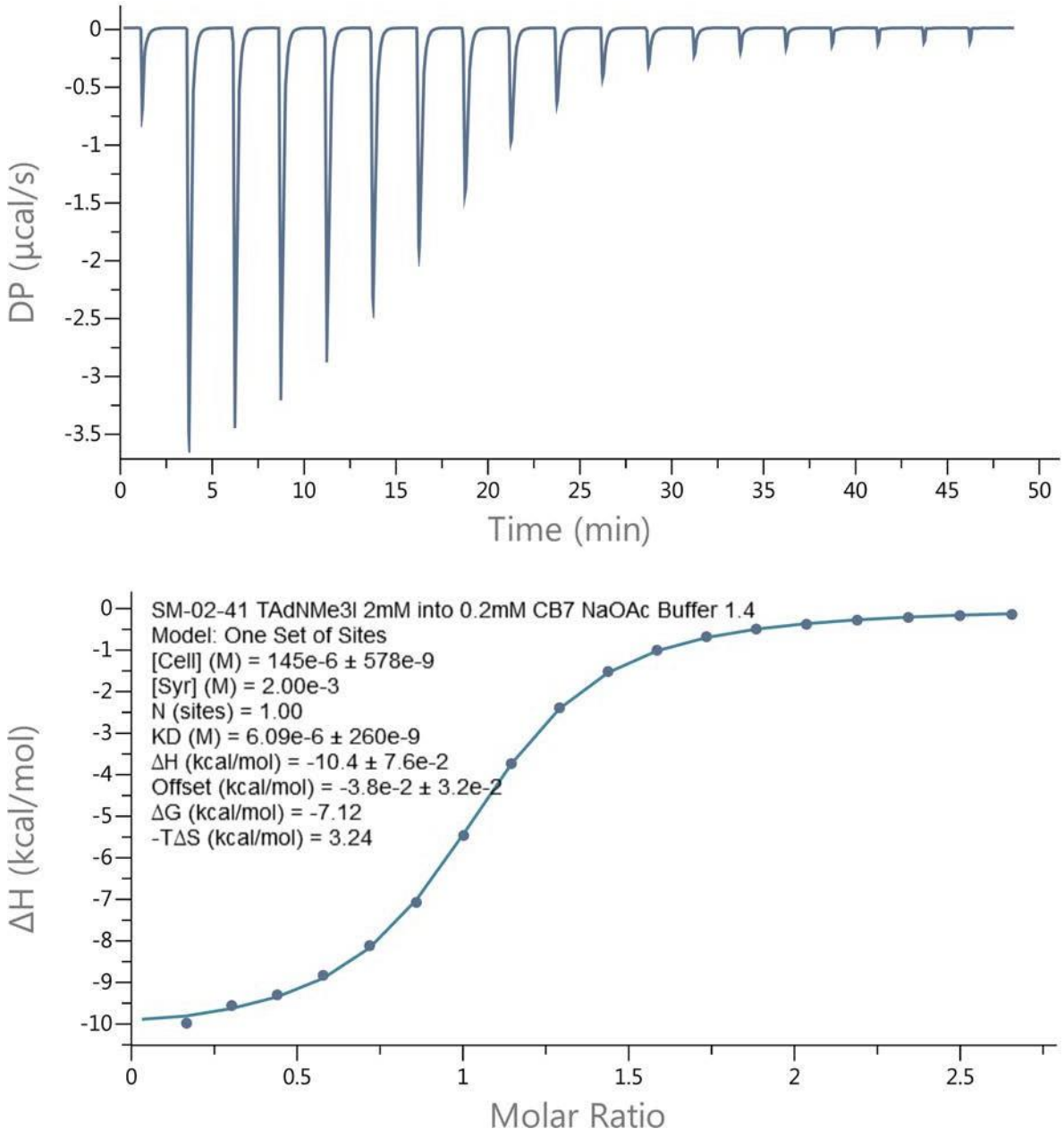

Figure SII-17. a) Plot of change in DP vs time from the titration of CB[7] (0.145 mM) with **G1** (0-0.362 mM) in 50 mM NaOAc buffered H2O, pH = 4.74. b) Plot of the ΔH as a function of molar ratio of CB[7]:**G1**. The solid line represents the best non-linear fit of the data to a 1:1 binding model (Ka = (1.6 ± 0.1) × 10^5 M^{-1}; ΔH = (–10.4 ± 0.076) kcal mol^{-1}).

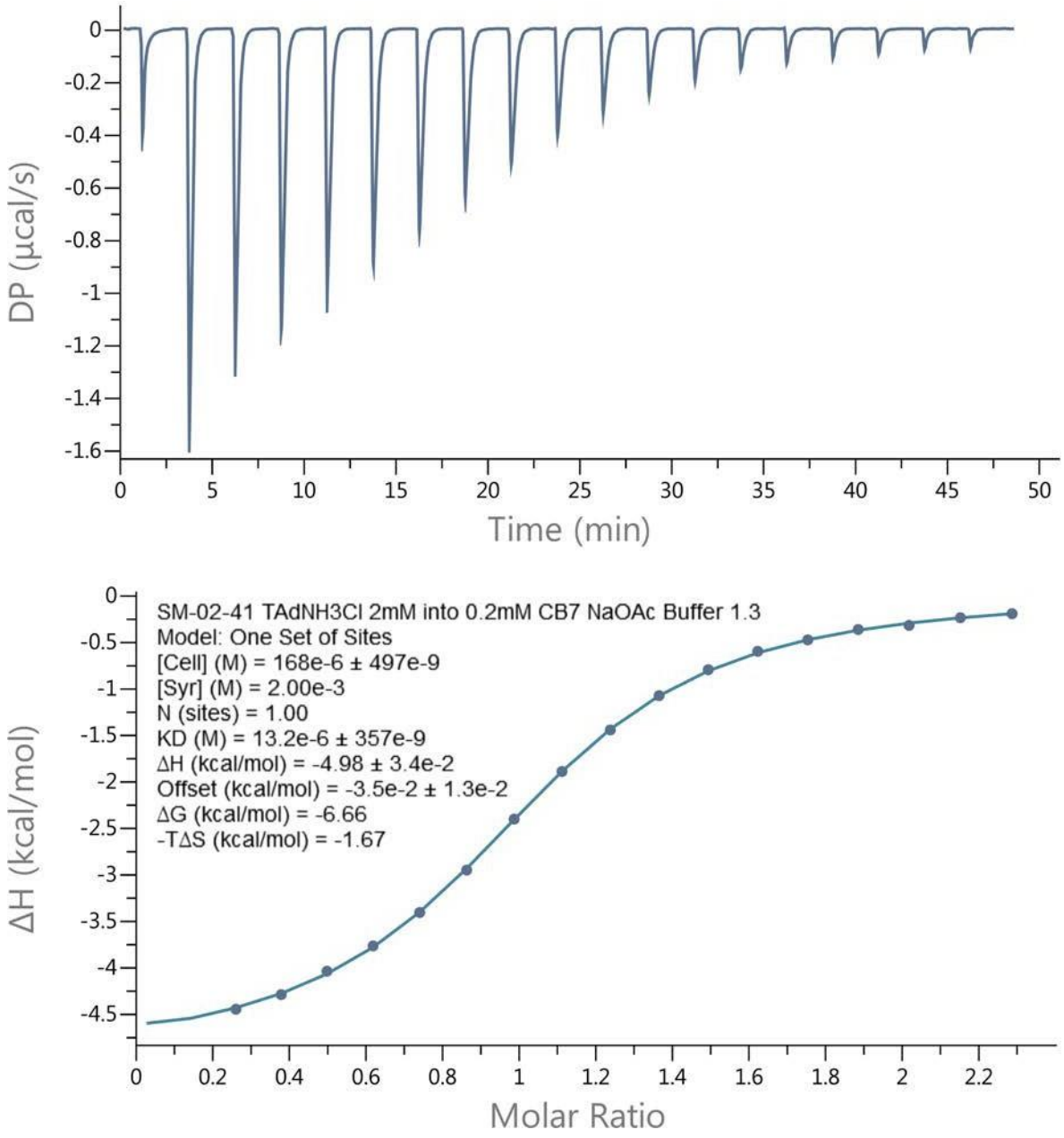

Figure SII-18. a) Plot of change in DP vs time from the titration of CB[7] (0.168 mM) and with **G2** (0 – 0.375 mM) in 50 mM NaOAc buffered H_2O, pH = 4.74. b) Plot of the ΔH as a function of molar ratio of CB[7]•**G2**. The solid line represents the best non-linear fit of the data to a 1:1 binding model (K_a = (7.5 ± 0.2) × 10^4 M^{-1}; ΔH = (–4.98 ± 0.034) kcal mol^{-1}).

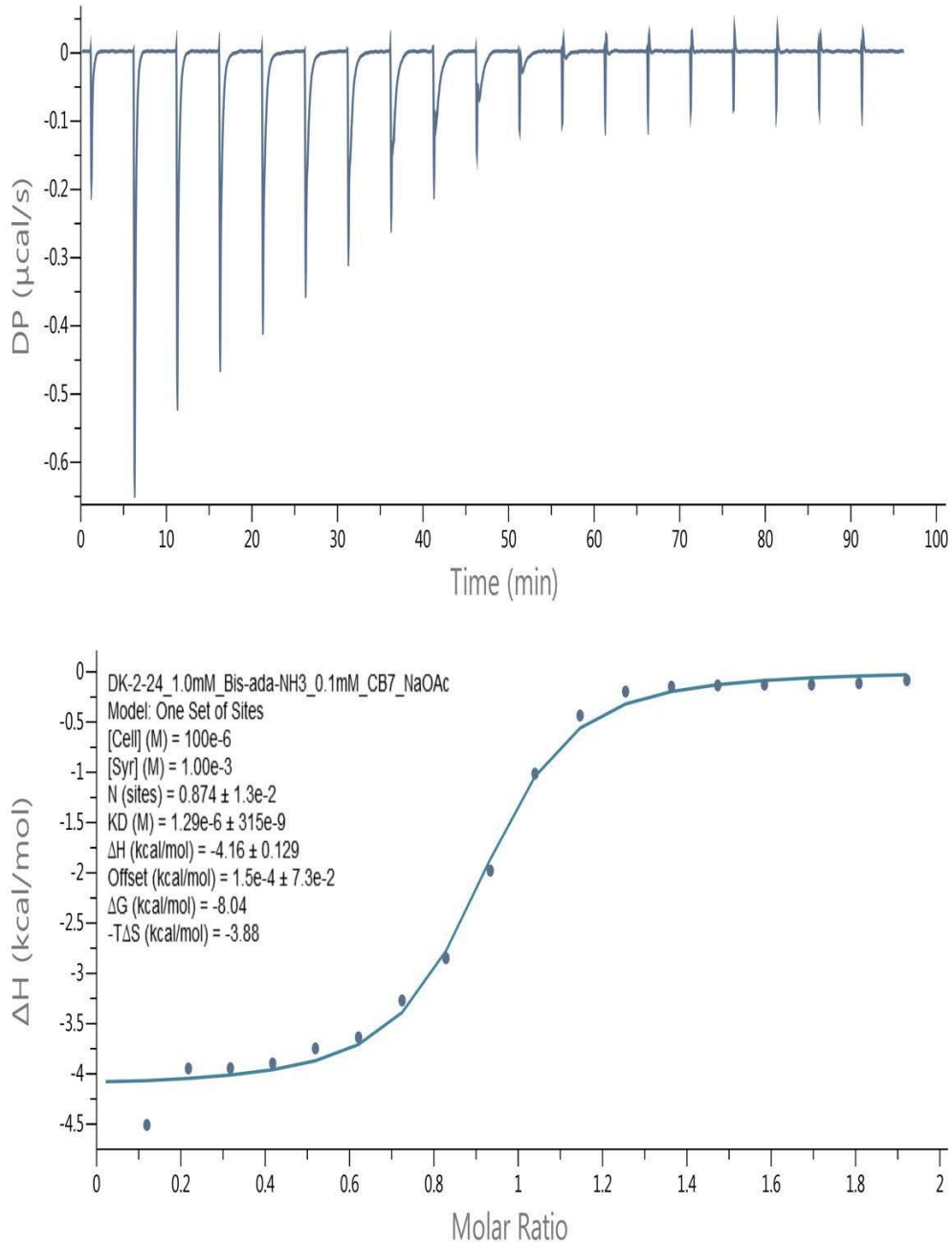

Figure SII-19. Isothermal Titration Calorimetry (ITC) curve obtained through direct binding titration studies. A solution of CB[7] (0.100 mM) in the cell was titrated with **G4** (1.00 mM) in the syringe at 298.0 K in 50 mM sodium acetate buffered water at pH 4.74. K_a = (7.75 ± 1.89) × 10^5 M^{-1}. Average of 3 measurements: K_a = (6.73 ± 1.41) × 10^5 M^{-1}; ΔH = (–3.79 ± 0.10) kcal mol^{-1}; $-T\Delta S$ = (–4.16 ± 0.15 kcal mol^{-1}); ΔG = (–7.96 ± 0.11) kcal mol^{-1}.

Determination of K_a of CB[7] and CB[8] towards 1, 7, and 8 using ^{1}H NMR Competition

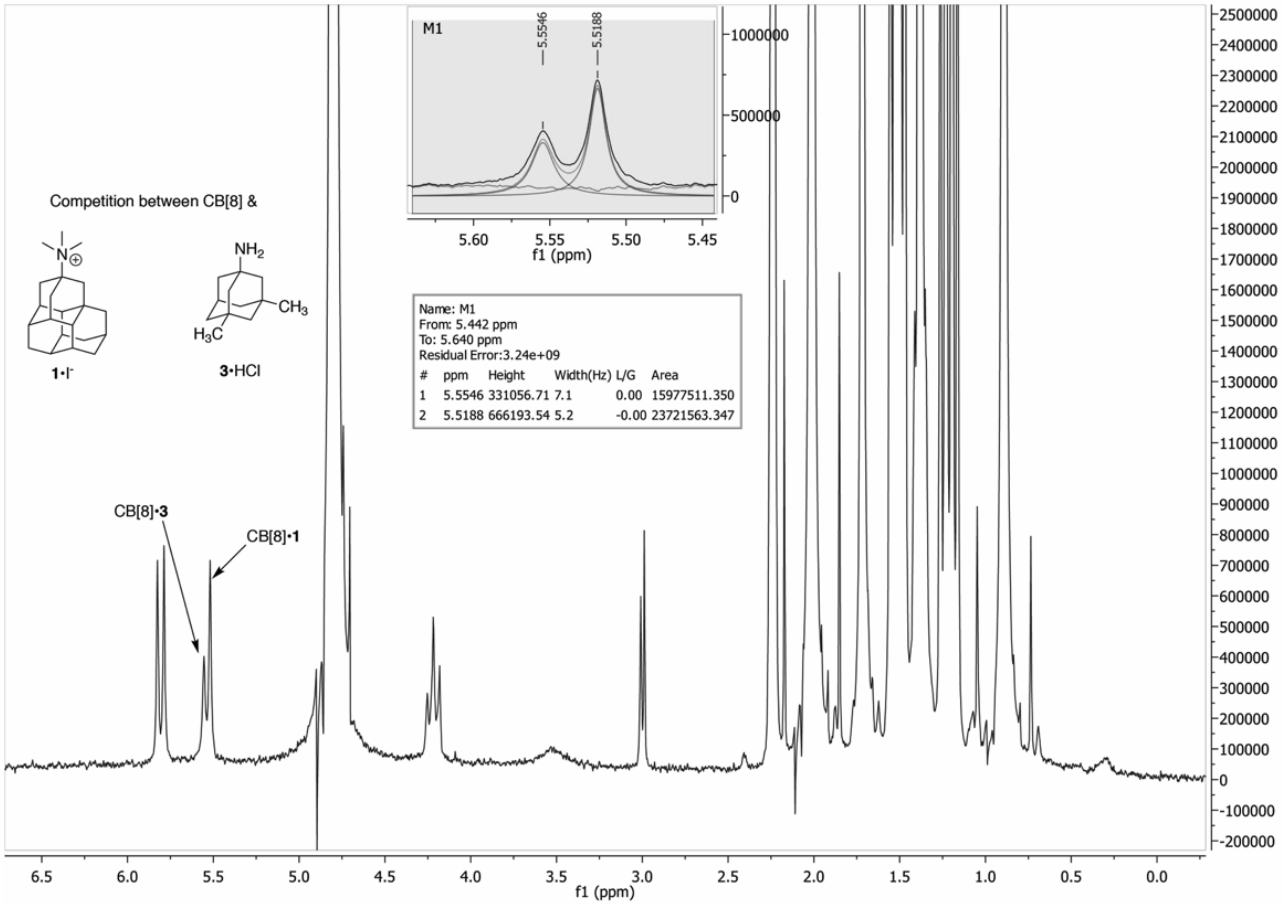

Figure SII-20. ^{1}H NMR spectra recorded (600 MHz, RT, 50 mM NaOAc Buffered D_2O, pH = 4.74) for a competitive mixture of CB[8] (0.100 mM), **C1** (16.5 mM), and **G1** (0.11 mM) at equilibrium. K_{rel} = 493.8 (Equilibrium was studied starting from both directions and gave the same K_{rel} value).

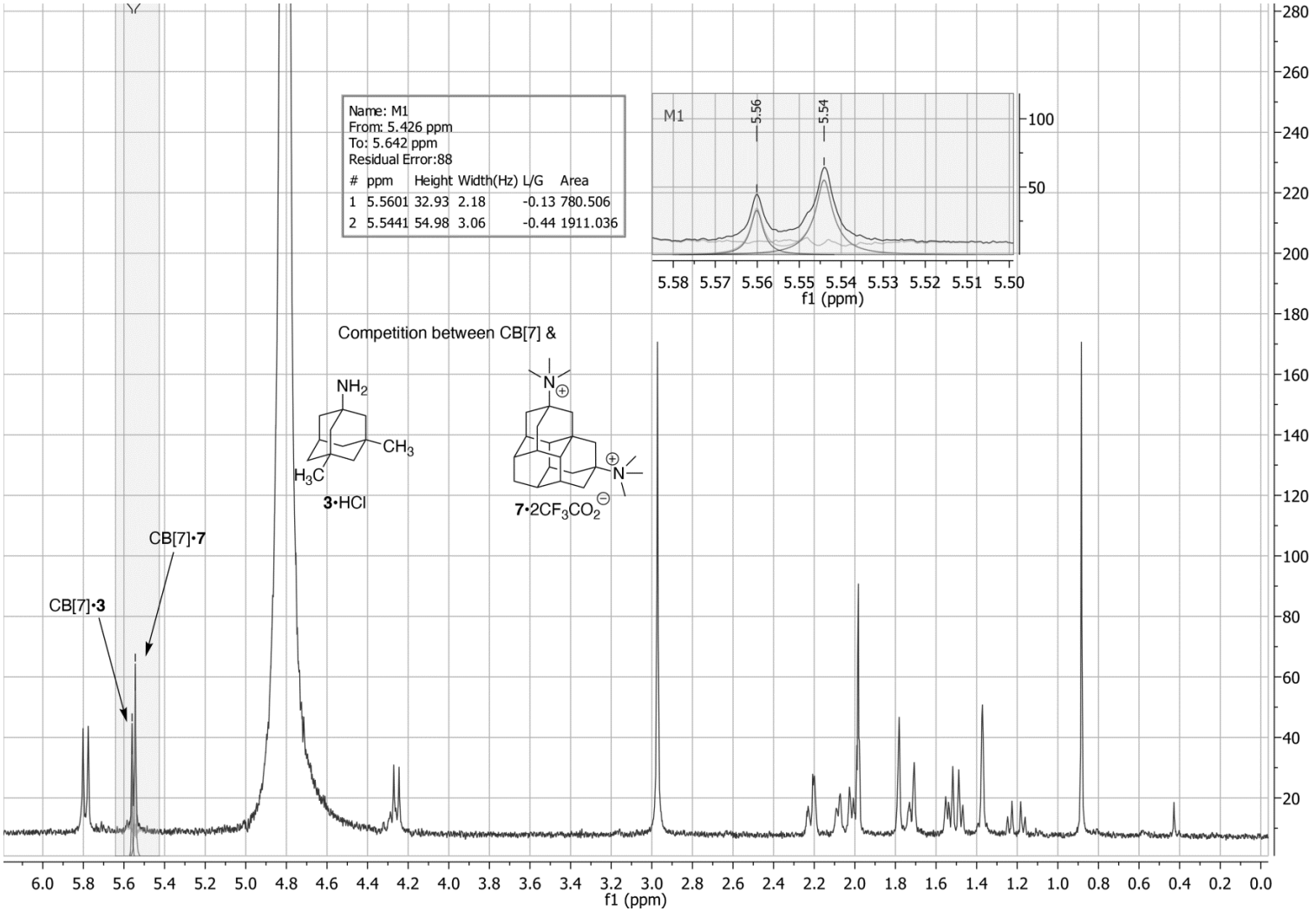

Figure SII-21. ^{1}H NMR spectra recorded (600 MHz, RT, 50 mM NaOAc Buffered D_2O, pH = 4.74) for a competitive mixture of CB[7] (0.100 mM), **C1** (0.22 mM), and **G3** (0.11 mM) at equilibrium. K_{rel} = 11.99 (Equilibrium was studied starting from both directions and gave the same K_{rel} value).

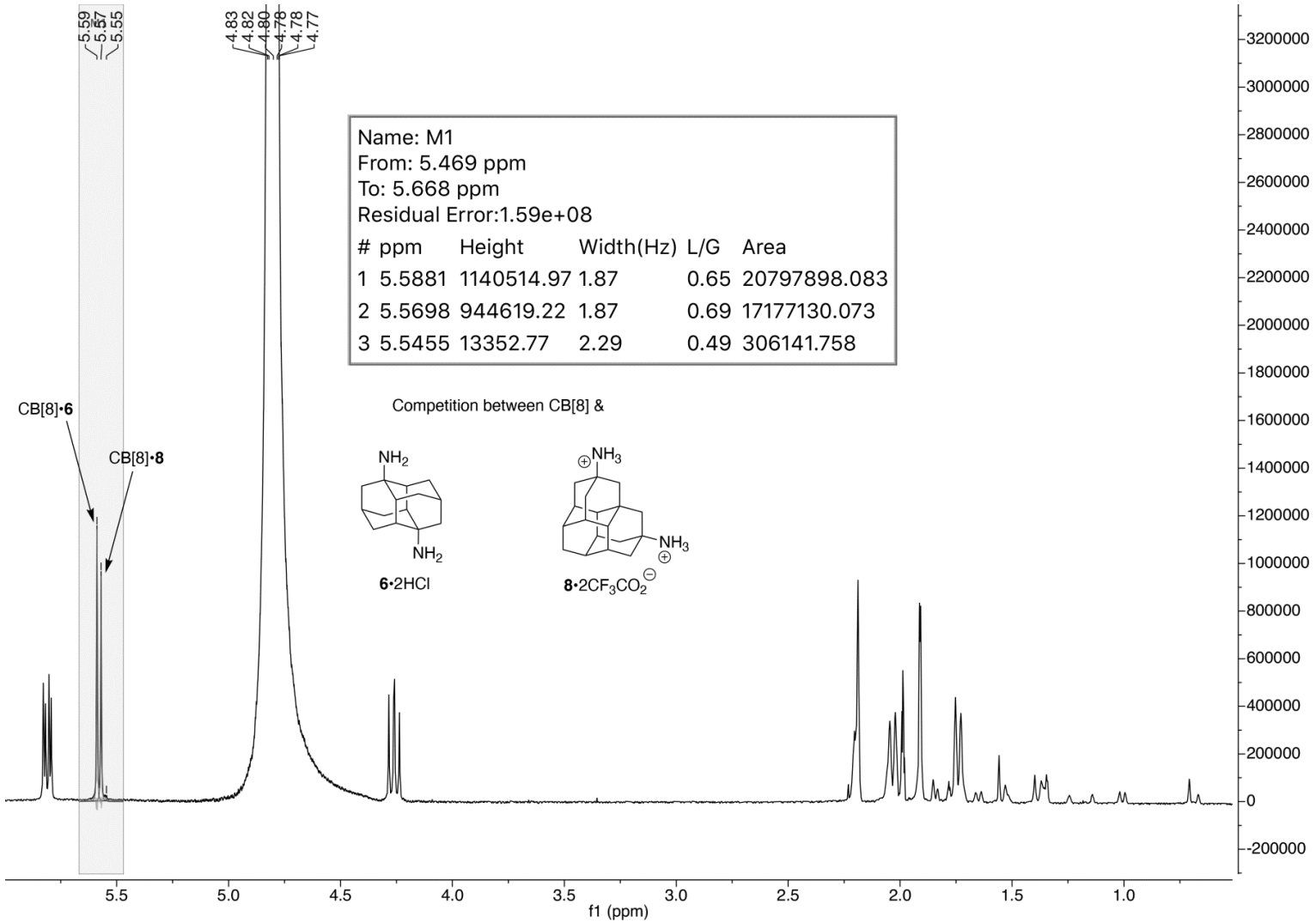

Figure SII-22. ^{1}H NMR spectra recorded (600 MHz, RT, 50 mM NaOAc Buffered D_2O, pH = 4.74) for a competitive mixture of CB[8] (0.100 mM), **C2** (0.33 mM), and **G4** (0.11 mM) at equilibrium. K_{rel} = 3.46 (Equilibrium was studied starting from both directions and gave the same K_{rel} value).

Affinimeter Output Files from the Competitive Titration of CB[8] + C3 with G3 or G4.

Experiment 1: Measuring the binding affinity of **C3** and CB[8]

Figure SII-23. Cartoon representation of the stepwise 1:2 binding model used in Affinimeter™ for both titrations of **C3** (A) and CB[8] (M) outlined in Figures **SII-24** – **SII-29**.

Results

- Global χ^2: *2.76e+00*
  - χ^2 for curve [1]: *4.15e+00*

Table 1: Correction parameters† *† fitted parameters in blue*

ΔH_{dil} [cal·mol^{-1}]	Q_{db} [cal]	r_M	r_A	r_B
(1.1029 ± 0.0081)e+03	0.000e+00	1.000e+00	(9.8192 ± 0.0309)e-01	1.000e+00

Table 2: Reaction parameters† *† fitted parameters in blue*

Reaction	K [M^{-n}]	ΔH [cal·mol^{-1}]
[1] Free species ⟺ M_1A_1	(2.6699 ± 0.3224)e+07	(-9.2300 ± 0.0419)e+03
[2] M_1A_1 + A_1 ⟺ M_1A_2	(7.4697 ± 1.7486)e+06	(-8.2808 ± 0.0638)e+03

Figure SII-24. Results from the titration of **C3** (A) titrated into CB[8] (B) as a part of the global fit for experiment 1. ΔH_{dil} = heat of dilution; r_A = % of active **C3** concentration for titration 1. Cell: CB[8] (0.02 mM); Syringe: **C3** (0.350 mM); Number of Injections: 18.

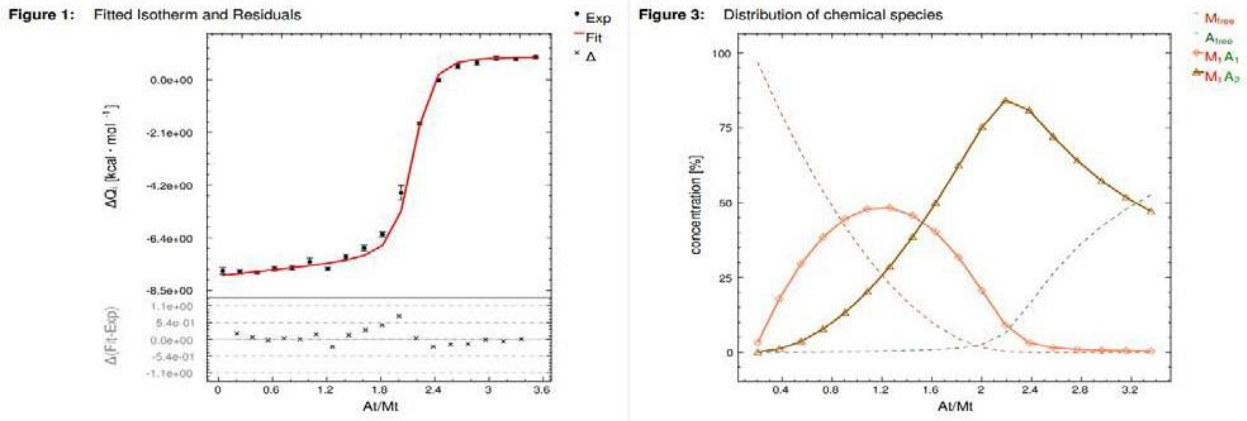

Figure SII-25. Left) Integrated signal from titration 1 and best fit line from global fit (top) and the residuals of the fit (bottom). Right) Percent concentration of each species present in the cell over time with respect to the total CB[8] concentration (M_{free}) or total **C3** concentration (A_{free}, M_1A_1, M_1A_2).

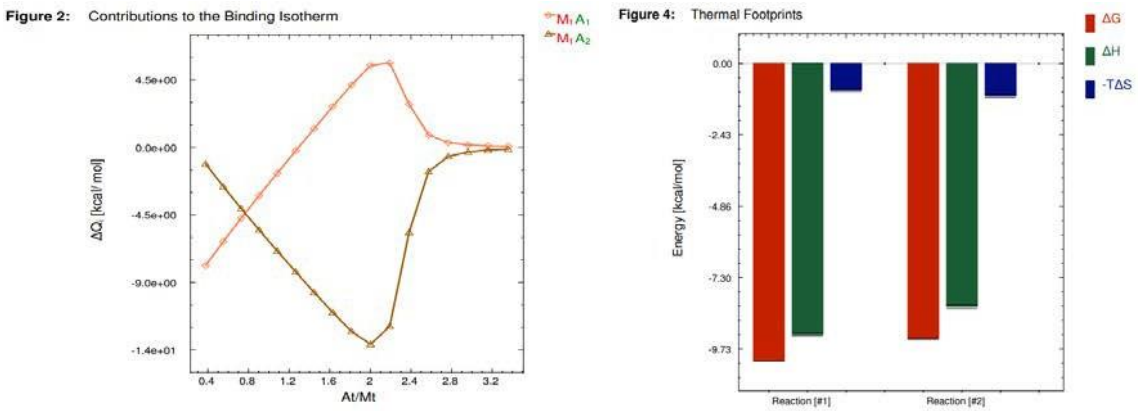

Figure SII-26. Left) Total contribution of each complexation reaction to the overall integrated signal over time for titration 2. Right) Graphical representation of ΔG, ΔH, and -TΔS for each complexation reaction.

Results

- Global χ^2: *2.76e+00*
  - χ^2 for curve [2]: *2.29e+00*

Table 3: Correction parameters† *† fitted parameters in blue*

ΔH_{dil} [cal·mol^{-1}]	Q_{db} [cal]	r_M	r_A	r_B
(-2.9819 ± 0.0212)e+03	0.000e+00	1.000e+00	(1.0325 ± 0.0023)e+00	1.000e+00

Figure SII-27. Results from the titration of **C3** (A) titrated into CB[8] (B) as a part of the global fit for experiment 1. ΔH_{dil} = heat of dilution; r_A = % of active **C3** concentration for titration 1. Cell: CB[8] (0.005 mM); Syringe: **C3** (0.040 mM); Number of Injections: 54.

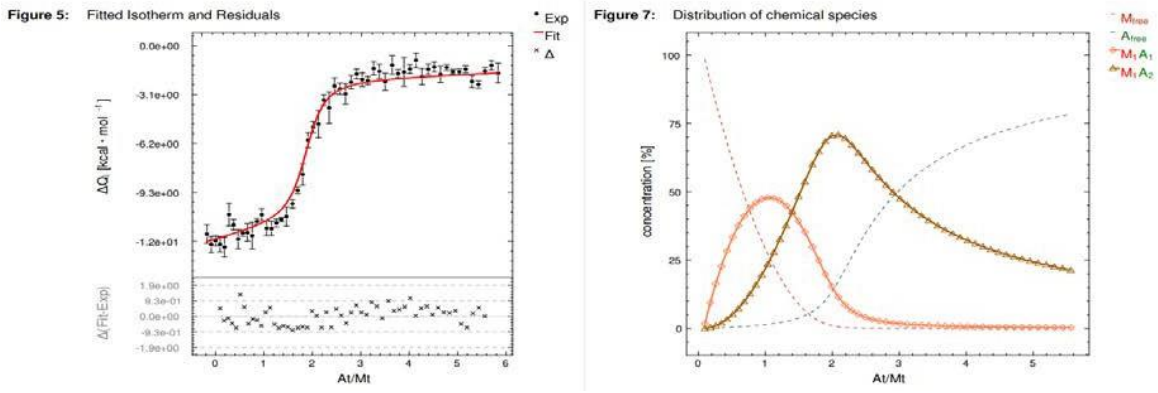

Figure S28. Left) Integrated signal from titration 2 and best fit line from global fit (top) and the residuals of the fit (bottom). Right) Percent concentration of each species present in the cell over time with respect to the total CB[8] concentration (M_{free}) or total **C3** concentration (A_{free}, M_1A_1, M_1A_2).

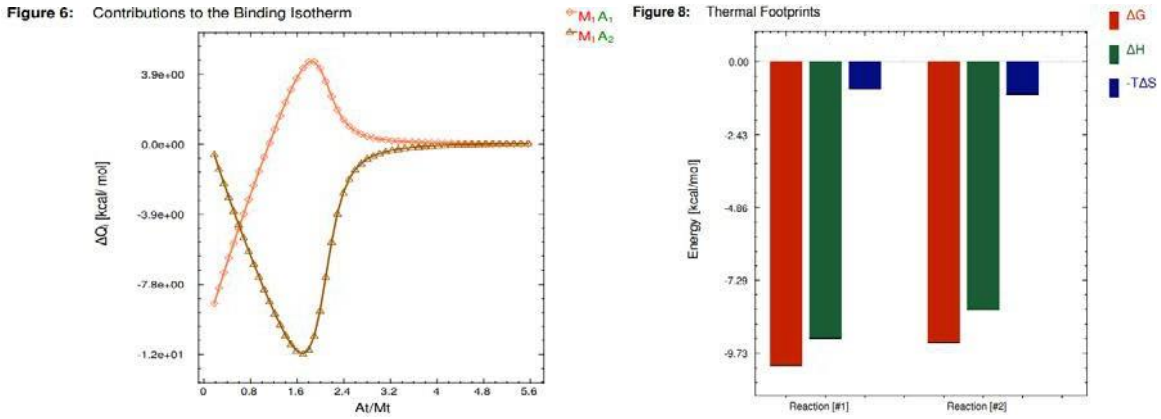

Figure SII-29. Left) Total contribution of each complexation reaction to the overall integrated signal over time for titration 2. Right) Graphical representation of ΔG, ΔH, and -TΔS for each complexation reaction.

Experiment 2: Measuring the binding affinity of **G3** and CB[8] by using **C3** as a competitor.

Figure SII-30. Cartoon representation of the stepwise 1:2 binding model used in Affinimeter™ for both titrations of **C3** (A) and CB[8] (M) outlined in Figures **SII-31** – **SII-36**.

Results

- Global χ^2: ***2.81e+00***
  - χ^2 for curve [1]: ***4.09e+00***

Table 1: Correction parameters† *† fitted parameters in blue*

ΔH_{dil} [cal·mol^{-1}]	Q_{db} [cal]	r_M	r_A	r_B
(1.1023 ± 0.0061)e+03	0.000e+00	1.000e+00	(9.8076 ± 0.0224)e-01	1.000e+00

Figure SII-31. Results from the titration of **C3** (A) titrated into CB[8] (M) as a part of the global fit for experiment 2. ΔH_{dil} = heat of dilution; r_A = % of active **C3** concentration for titration 1. Cell: CB[8] (0.02 mM); Syringe: **C3** (0.350 mM); Number of Injections: 18.

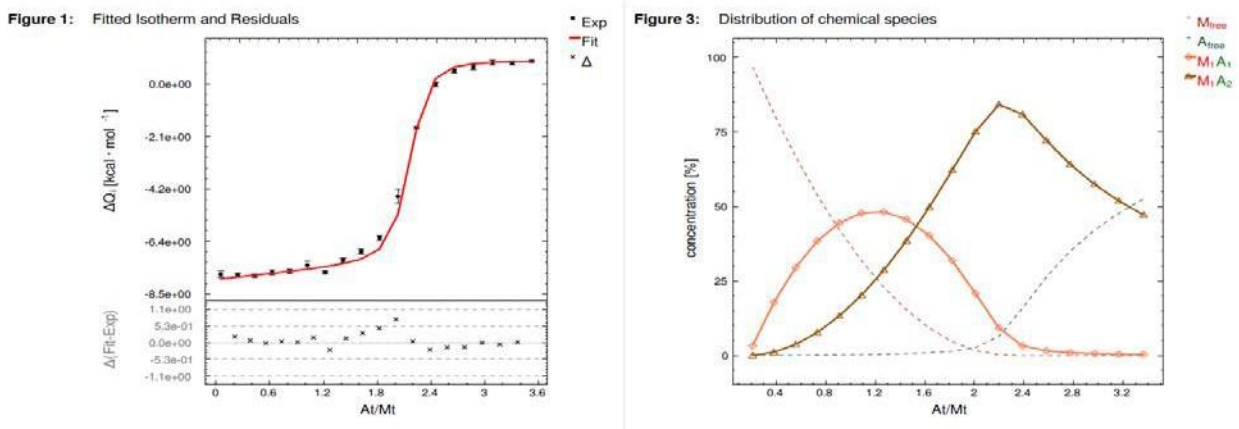

Figure SII-32. Left) Integrated signal from titration 1 and best fit line from global fit (top) and the residuals of the fit (bottom). Right) Percent concentration of each species present in the cell over time with respect to the total CB[8] concentration (M_{free}) or total **C3** concentration (A_{free}, M_1A_1, M_1A_2).

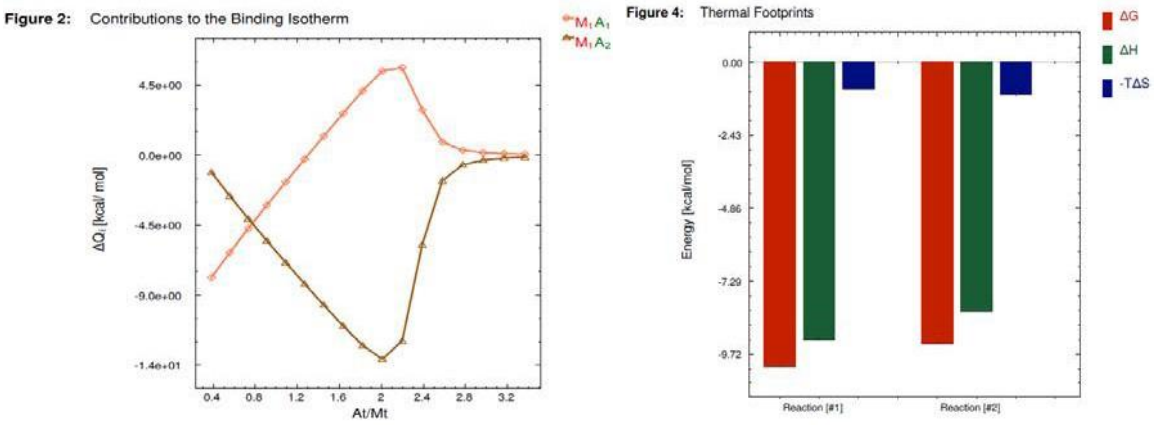

Figure SII-33. Left) Total contribution of each complexation reaction to the overall integrated signal over time for titration 1. Right) Graphical representation of ΔG, ΔH, and -TΔS for each complexation reaction.

Results

- Global χ^2: **2.81e+00**
  - χ^2 for curve [2]: **2.27e+00**

Table 3: Correction parameters† *† fitted parameters in blue*

ΔH_{dil} [cal·mol^{-1}]	Q_{db} [cal]	r_M	r_A	r_B
(-2.9759 ± 0.0157)e+03	0.000e+00	1.000e+00	(1.0323 ± 0.0017)e+00	1.000e+00

Figure SII-34. Results from the titration of **C3** (A) titrated into CB[8] (B) as a part of the global fit for experiment 2. ΔH_{dil} = heat of dilution; r_A = % of active **C3** concentration for titration 2. Cell: CB[8] (0.005 mM); Syringe: **C3** (0.040 mM); Number of Injections: 54.

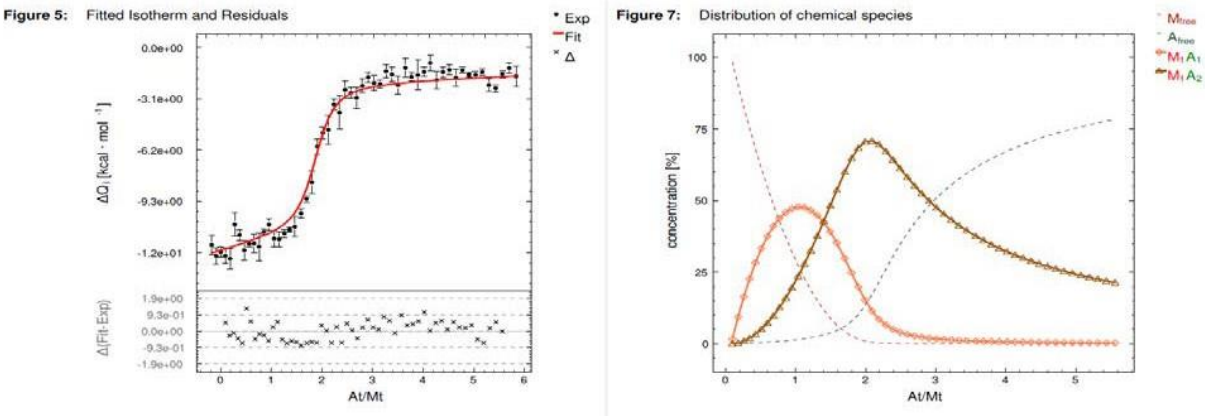

Figure SII-35. Left) Integrated signal from titration 2 and best fit line from global fit (top) and the residuals of the fit (bottom). Right) Percent concentration of each species present in the cell over time with respect to the total CB[8] concentration (M_{free}) or total **C3** concentration (A_{free}, M_1A_1, M_1A_2).

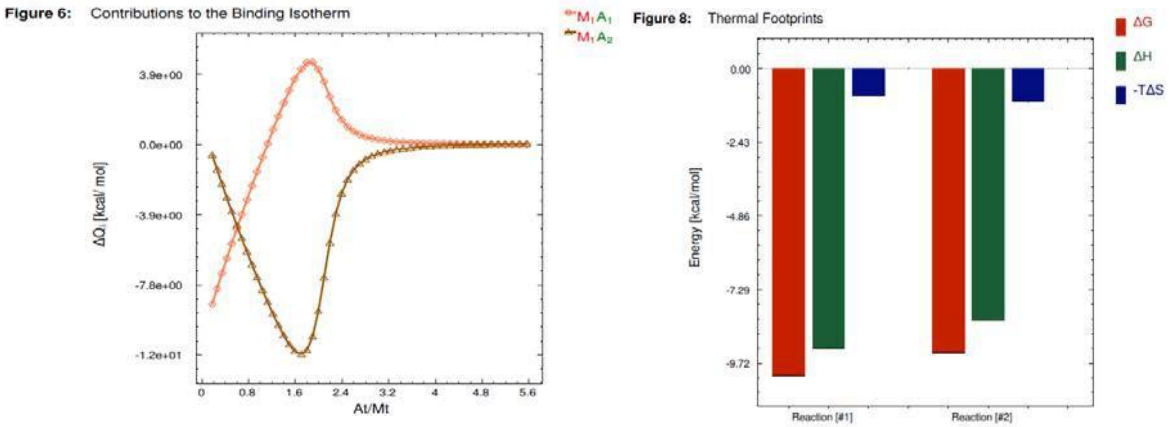

Figure SII-36. Left) Total contribution of each complexation reaction to the overall integrated signal over time for titration 2. Right) Graphical representation of ΔG, ΔH, and -TΔS for each complexation reaction.

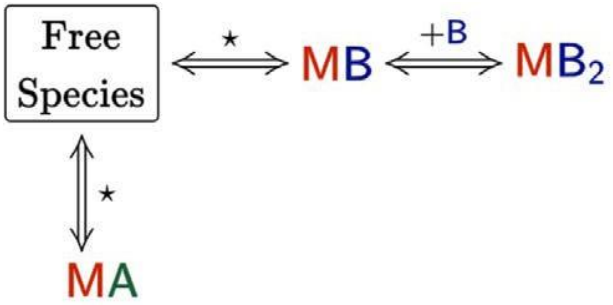

Figure SII-37. Cartoon representation of the stepwise competition binding model used in Affinimeter™ for the titration of **G3** (A) into a mixture of CB[8] (M) and **C3** (B) outlined in Figures **SII-38** - **SII-40**.

Results

- Global χ^2: *2.81e+00*
  - χ^2 for curve [3]: *2.93e+00*

Table 5: Correction parameters† *† fitted parameters in blue*

ΔH_{dil} [cal·mol^{-1}]	Q_{db} [cal]	r_M	r_A	r_B
(-8.3660 ± 0.1136)e+02	*0.000e+00*	*1.000e+00*	(8.5858 ± 0.0145)e-01	(1.4040 ± 0.0115)e+00

Table 6: Reaction parameters† *† fitted parameters in blue*

Reaction	K [M^{-n}]	ΔH [cal·mol^{-1}]
[1] Free species ⟹ M_1B_1	(2.6496 ± 0.2385)e+07	(-9.2416 ± 0.0310)e+03
[2] M_1B_1 + B_1 ⟹ M_1B_2	(7.4659 ± 1.2976)e+06	(-8.2917 ± 0.0472)e+03
[3] Free species ⟹ M_1A_1	(1.1486 ± 0.1689)e+13	(-1.0076 ± 0.0045)e+04

Figure SII-38. Results from the titration of **G3** (A) into a mixture of CB[8] (M) and **C3** (B) as a part of the global fit for experiment 2. ΔH_{dil} = heat of dilution; r_A = % of active **C3** concentration for titration 3. Cell: CB[8] (0.030 mM), **C3** (0.175 mM); Syringe: **G3** (0.100 mM); Number of Injections: 54.

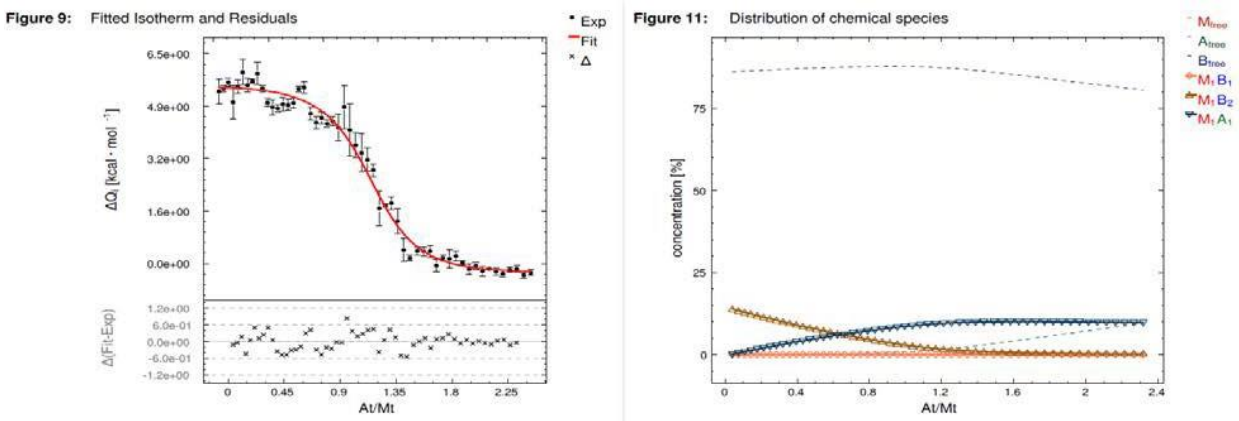

Figure SII-39. Left) Integrated signal from titration 3 and best fit line from global fit (top) and the residuals of the fit (bottom). Right) Percent concentration of each species present in the cell over time with respect to the total CB[8] concentration (M_{free}), total **C3** concentration (B_{free}, M_1B_1, M_1B_2), or total **G3** concentration (A_{free}, M_1A_1).

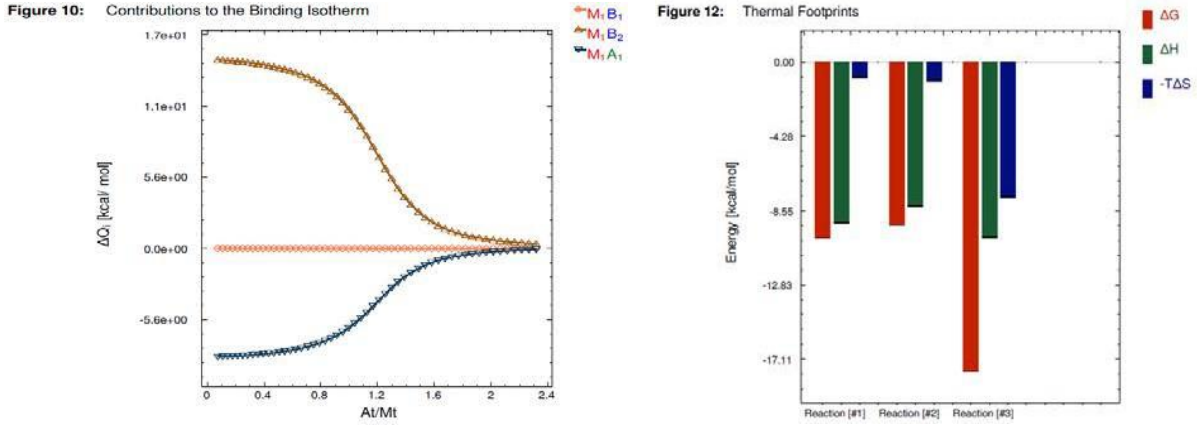

Figure SII-40. Left) Total contribution of each complexation reaction to the overall integrated signal over time for titration 3. Right) Graphical representation of ΔG, ΔH, and -TΔS for each complexation reaction.

Experiment 3: Measuring the binding affinity of **G4** and CB[8] by using **C3** as a competitor

Figure SII-41. Cartoon representation of the stepwise 1:2 binding model used in Affinimeter™ for both titrations of **C3** (A) and CB[8] (M) outlined in Figures **SII-42 - SII-47**.

Results

- Global χ^2: *3.98e+00*
  - χ^2 for curve [3]: *1.22e+01*

Table 5: Correction parameters† *† fitted parameters in blue*

ΔH_{dil} [cal·mol^{-1}]	Q_{db} [cal]	r_M	r_A	r_B
(1.4547 ± 0.0191)e+03	0.000e+00	1.000e+00	(9.7919 ± 0.0324)e-01	1.000e+00

Figure SII-42. Results from the titration of **C3** (A) titrated into CB[8] (B) as a part of the global fit for experiment 3. ΔH_{dil} = heat of dilution; r_A = % of active **C3** concentration for titration 1. Cell: CB[8] (0.02 mM); Syringe: **C3** (0.350 mM); Number of Injections: 18.

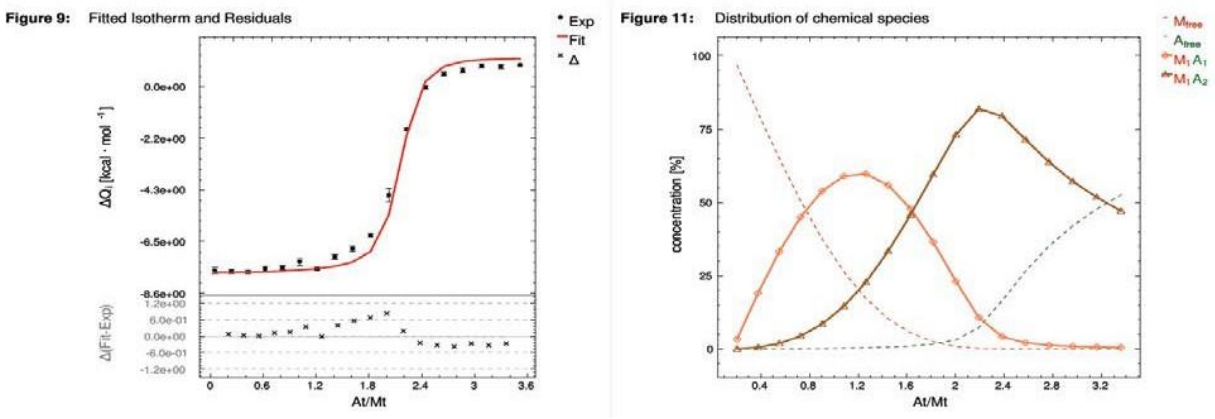

Figure S43. Left) Integrated signal from titration 1 and best fit line from global fit (top) and the residuals of the fit (bottom). Right) Percent concentration of each species present in the cell over time with respect to the total CB[8] concentration (M_{free}) or total **C3** concentration (A_{free}, M_1A_1, M_1A_2).

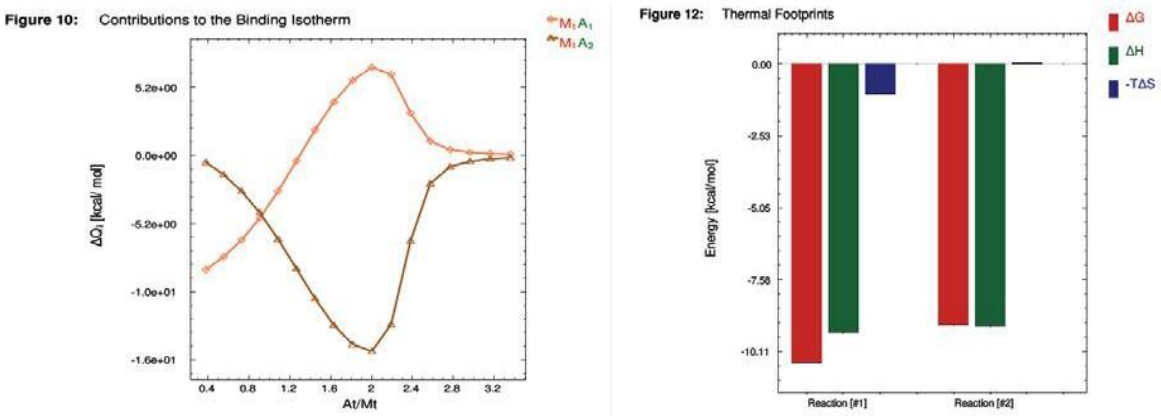

Figure SII-44. Left) Total contribution of each complexation reaction to the overall integrated signal over time for titration 1. Right) Graphical representation of ΔG, ΔH, and -TΔS for each complexation reaction.

Results

- Global χ^2: *3.98e+00*

Table 3: Correction parameters† *† fitted parameters in blue*

ΔH_{dil} [cal·mol^{-1}]	Q_{db} [cal]	r_M	r_A	r_B
(-2.7148 ± 0.0169)e+03	0.000e+00	1.000e+00	(1.0176 ± 0.0017)e+00	1.000e+00

Figure SII-45. Results from the titration of **C3** (A) titrated into CB[8] (B) as a part of the global fit for experiment 3. ΔH_{dil} = heat of dilution; r_A = % of active **C3** concentration for titration 2. Cell: CB[8] (0.005 mM); Syringe: **C3** (0.040 mM); Number of Injections: 54.

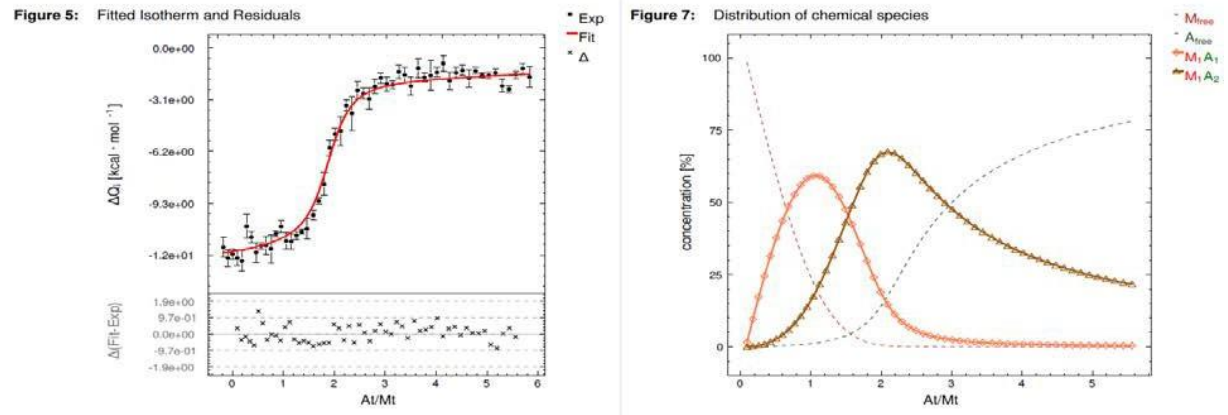

Figure SII-46. Left) Integrated signal from titration 2 and best fit line from global fit (top) and the residuals of the fit (bottom). Right) Percent concentration of each species present in the cell over time with respect to the total CB[8] concentration (M_{free}) or total **C3** concentration (A_{free}, M_1A_1, M_1A_2).

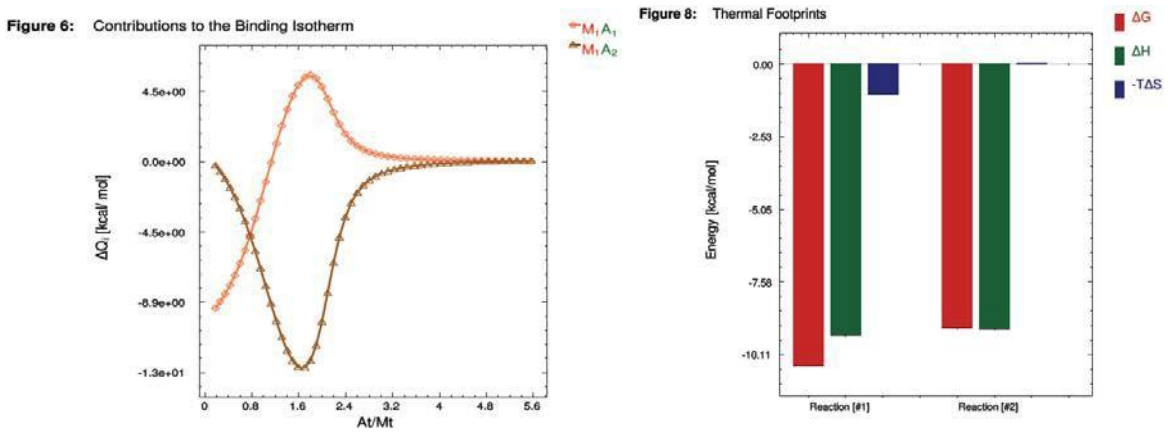

Figure SII-47. Left) Total contribution of each complexation reaction to the overall integrated signal over time for titration 2. Right) Graphical representation of ΔG, ΔH, and -TΔS for each complexation reaction.

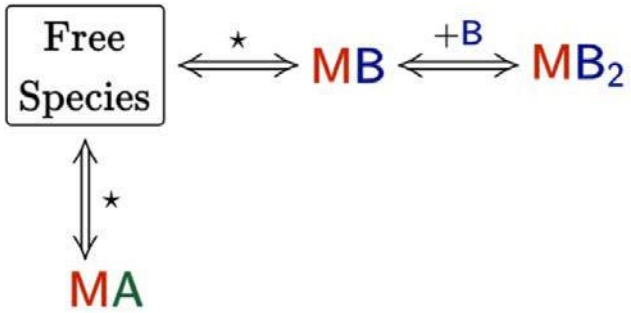

Figure SII-48. Cartoon representation of the stepwise competition binding model used in Affinimeter™ for the titration of **G4** (A) into a mixture of CB[8] (M) and **C3** (B) outlined in Figures **SII-49** – **SII-54**.

Results

- Global χ^2: *3.98e+00*
  - χ^2 for curve [1]: *4.38e+00*

Table 1: Correction parameters† *† fitted parameters in blue*

ΔH_{dil} [cal·mol^{-1}]	Q_{db} [cal]	r_M	r_A	r_B
(-1.4297 ± 0.0316)e+03	0.000e+00	1.000e+00	(9.2598 ± 0.0330)e-01	(1.0598 ± 0.0060)e+00

Table 2: Reaction parameters† *† fitted parameters in blue*

Reaction	K [M^{-n}]	ΔH [cal·mol^{-1}]
[1] Free species ⟹ M_1B_1	(4.9349 ± 0.3942)e+07	(-9.4436 ± 0.0416)e+03
[2] M_1B_1 + B_1 ⟹ M_1B_2	(5.4213 ± 0.6600)e+06	(-9.2195 ± 0.0661)e+03
[3] Free species ⟹ M_1A_1	(1.1418 ± 0.2161)e+14	(-1.1501 ± 0.0050)e+04

Figure SII-49. Results from the titration of **G4** (A) into a mixture of CB[8] (M) and **C3** (B) as a part of the global fit for experiment 3. ΔH_{dil} = heat of dilution; r_A = % of active **C3** concentration for titration 3. Cell: CB[8] (0.020 mM), **C3** (0.015 mM); Syringe: **G4** (0.070 mM); Number of Injections: 54.

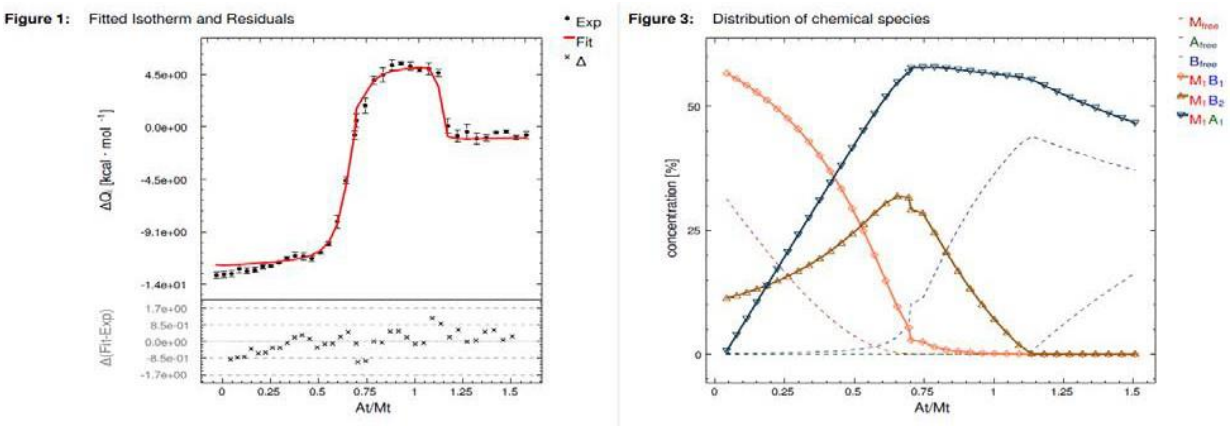

Figure SII-50. Left) Integrated signal from titration 3 and best fit line from global fit (top) and the residuals of the fit (bottom). Right) Percent concentration of each species present in the cell over time with respect to the total CB[8] concentration (M_{free}), total **C3** concentration (B_{free}, M_1B_1, M_1B_2), or total **G4** concentration (A_{free}, M_1A_1).

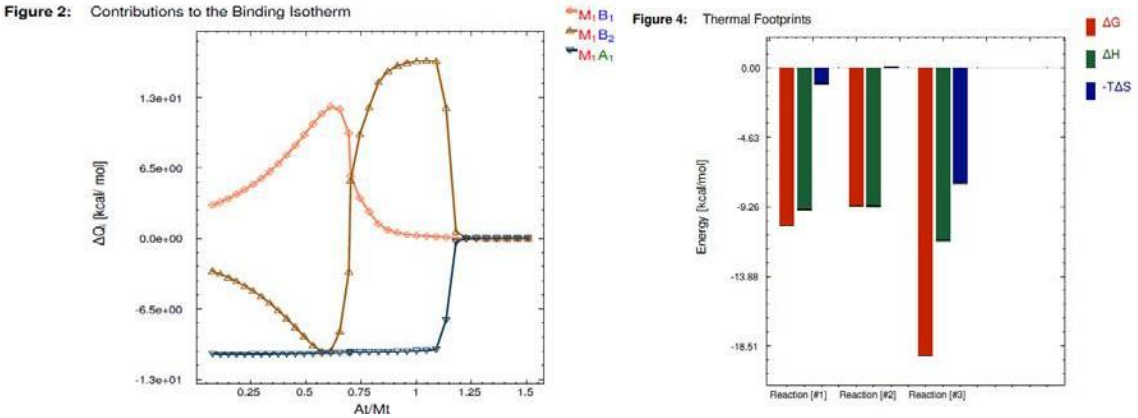

Figure SII-51. Left) Total contribution of each complexation reaction to the overall integrated signal over time for titration 3. Right) Graphical representation of ΔG, ΔH, and -TΔS for each complexation reaction.

Results

- Global χ^2: *3.98e+00*
  - χ^2 for curve [4]: *2.68e+00*

Table 7: Correction parameters[f] *fitted parameters in blue*

ΔH_{dil} [cal·mol^{-1}]	Q_{db} [cal]	r_M	r_A	r_B
(-4.8798 ± 0.0191)e+02	0.000e+00	1.000e+00	(7.9695 ± 0.0300)e-01	(8.8648 ± 0.0244)e-01

Figure SII-52. Results from the titration of **G4** (A) into a mixture of CB[8] (M) and **C3** (B) as a part of the global fit for experiment 3. ΔH_{dil} = heat of dilution; r_A = % of active **C3** concentration for titration 4. Cell: CB[8] (0.020 mM), **C3** (0.040 mM); Syringe: **G4** (0.150 mM); Number of Injections: 54.

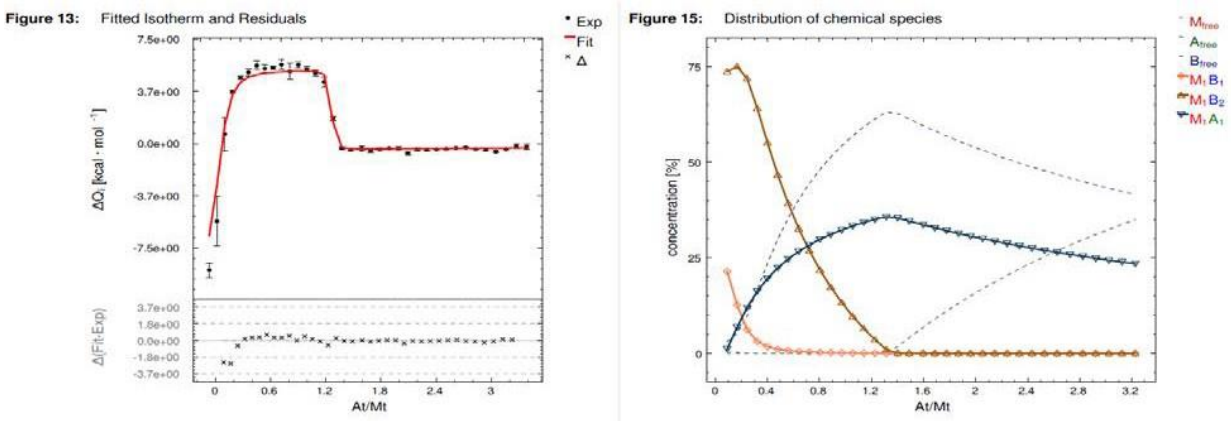

Figure SII-53. Left) Integrated signal from titration 4 and best fit line from global fit (top) and the residuals of the fit (bottom). Right) Percent concentration of each species present in the cell over time with respect to the total CB[8] concentration (M_{free}), total **C3** concentration (B_{free}, M_1B_1, M_1B_2), or total **G4** concentration (A_{free}, M_1A_1).

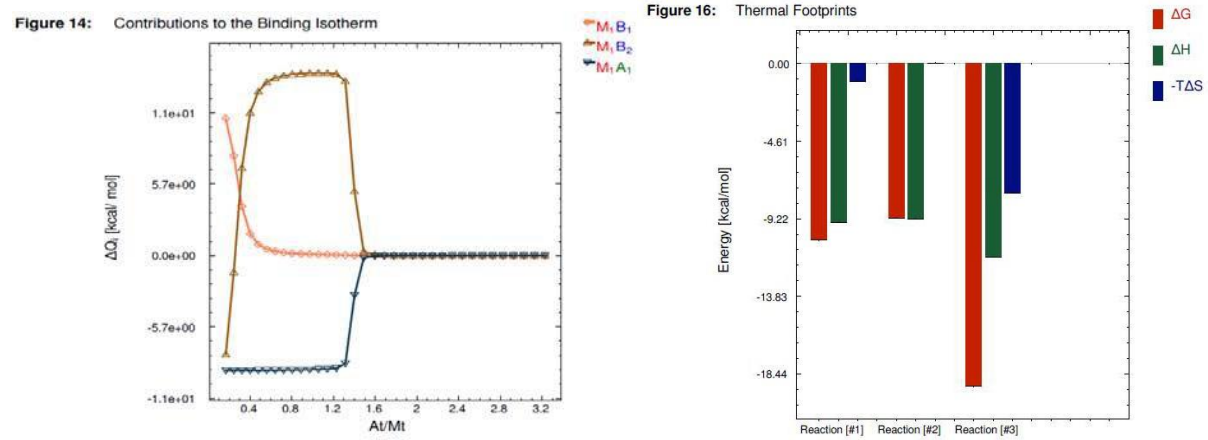

Figure SII-54. Left) Total contribution of each complexation reaction to the overall integrated signal over time for titration 4. Right) Graphical representation of ΔG, ΔH, and -TΔS for each complexation reaction.

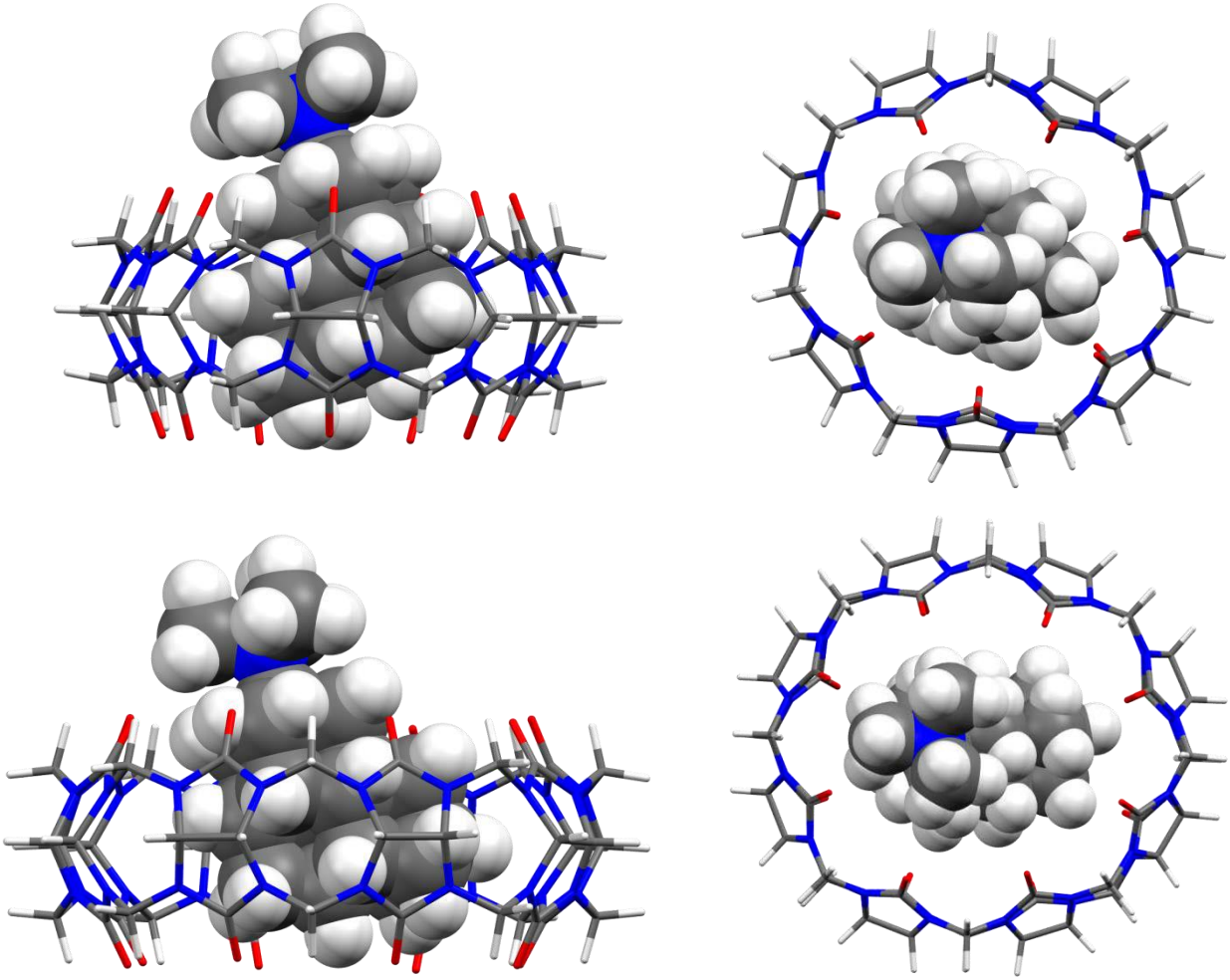

Figure SII-55. Representations of the minimized geometries of CB[7]•**G1** (top) and CB[8]•**G1** (bottom). Color coding: C, gray; H, white; O, red; N, blue.

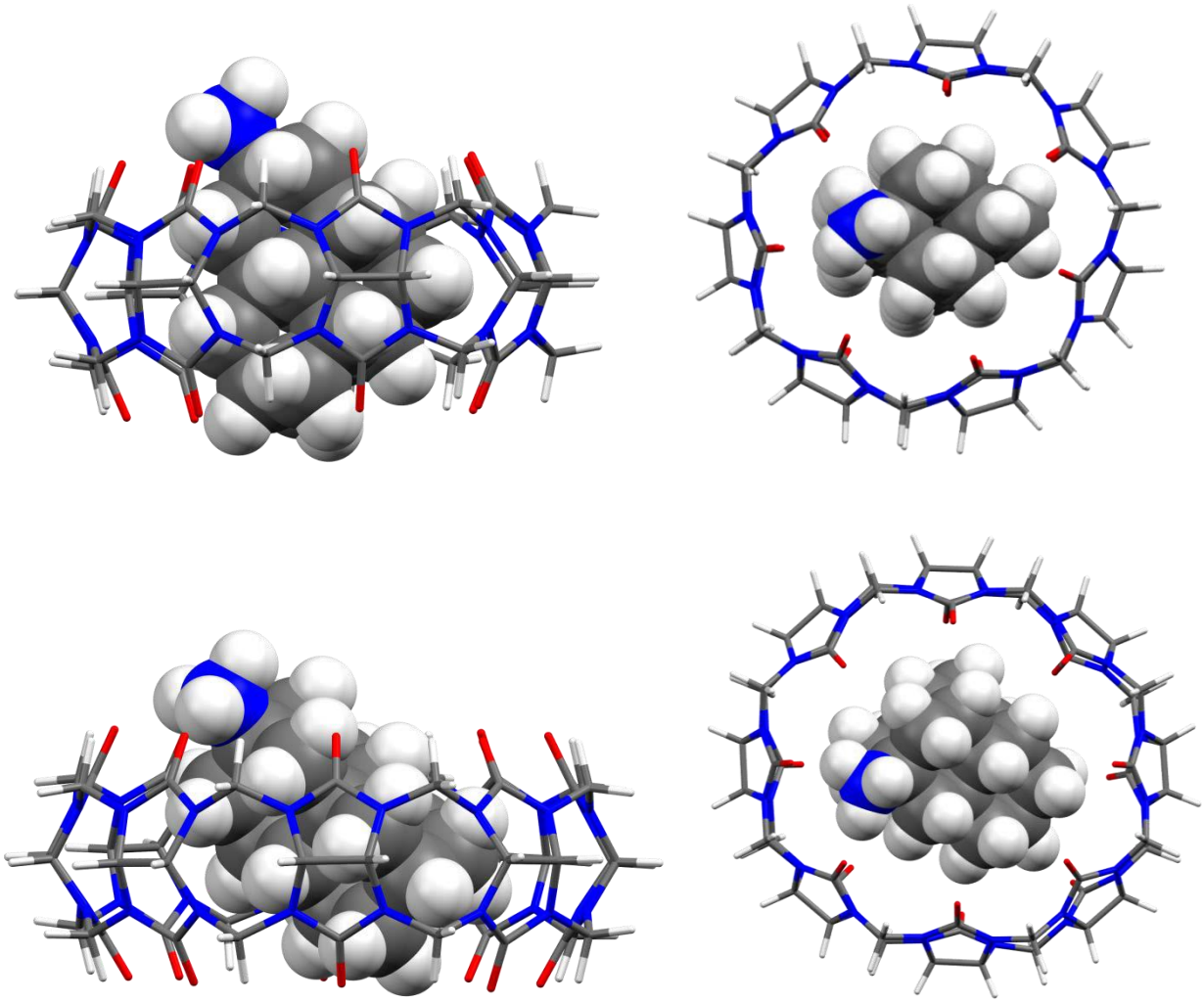

Figure SII-56. Representations of the minimized geometries of CB[7]•**G2** (top) and CB[8]•**G2** (bottom). Color coding: C, gray; H, white; O, red; N, blue.

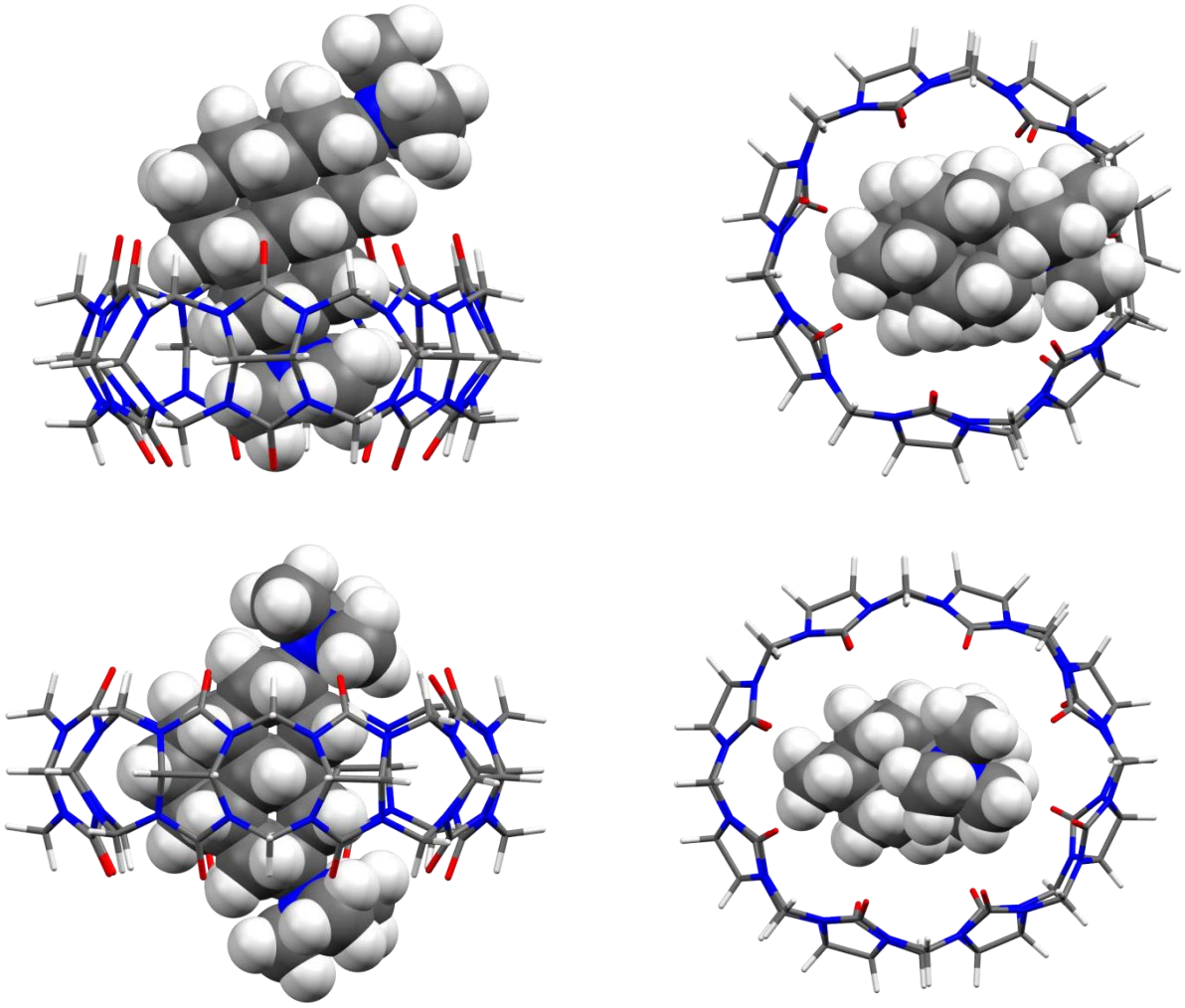

Figure SII-57. Representations of the minimized geometries of CB[7]•**G3** (top) and CB[8]•**G3** (bottom). Color coding: C, gray; H, white; O, red; N, blue.

Table SII-1 Electronic energies, zero-point vibrational energies, enthalpies and Gibbs energies of guests **G1**–**G4**, CB[7] and CB[8], and the corresponding complexes in Hartree computed using the GFN2-xTB method. The interaction energies (difference between the energy of the complex and the energy of the guest and the host molecules) for the complexes in kcal mol^{-1} are given in parentheses.

compound	*E*	*ZPVE*	*H*	*G*
G1	-64.055694	0.495235	-63.544051	-63.599693
G2	-54.570637	0.410876	-54.146303	-54.196330
G3	-77.160562	0.607646	-76.531822	-76.595677
G4	-58.192044	0.438754	-57.738041	-57.790919
CB[7]	-251.174100	0.923189	-250.186362	-250.339766
CB[8]	-287.050977	1.055132	-285.921884	-286.093340
CB[7]•G1	-315.272746 **(-27.0)**	1.424573	-313.767545 **(-23.3)**	-313.947474 **(-5.0)**
CB[7]•G2	-305.783942 **(-24.6)**	1.339440	-304.367502 **(-21.9)**	-304.540738 **(-2.9)**
CB[7]•G3 unstable	-328.322615 **(7.6)**	1.539372	-326.698337 **(12.5)**	-326.884910 **(31.7)**
CB[7]•G3 exclusion	-328.361297 **(-16.7)**	1.535884	-326.738713 **(-12.9)**	-326.931129 **(2.7)**
CB[7]•G4	-309.422823 **(-35.6)**	1.369077	-307.975832 **(-32.3)**	-308.149194 **(-11.6)**
CB[8]•G1	-351.159698 **(-33.3)**	1.554003	-349.514316 **(-30.4)**	-349.717460 **(-15.3)**
CB[8]•G2	-341.674384 **(-33.1)**	1.469324	-340.117704 **(-31.1)**	-340.312876 **(-14.6)**
CB[8]•G3	-364.265517 **(-33.9)**	1.668273	-362.501204 **(-29.8)**	-362.711852 **(-14.3)**
CB[8]•G4	-345.307439 **(-40.4)**	1.497598	-343.720905 **(-38.3)**	-343.919089 **(-21.9)**

Table S2 Geometries of guests **G1**–**G4**, CB[7] and CB[8], and the corresponding complexes in Cartesian coordinates in Å obtained using the GFN2-xTB method and from CREST sampling.

G1

6	-1.977600000	1.142300000	-1.092500000
6	-2.723300000	-0.191200000	-1.083800000
6	-2.329800000	-0.945200000	0.185500000
6	-2.345300000	1.970300000	0.143000000
6	-0.451700000	0.935200000	1.381700000
6	-2.699500000	-0.131100000	1.429700000
6	-1.959800000	1.213700000	1.421500000
6	-2.356600000	-1.009200000	-2.318900000
6	-0.090100000	0.056100000	-2.359900000
6	-0.852200000	-1.270500000	-2.331200000
6	-0.444400000	-2.043100000	-1.074900000
6	1.060900000	-2.303100000	-1.079100000
6	1.805300000	-0.969100000	-1.106000000
6	1.416000000	-0.199200000	-2.367000000
6	-0.473600000	0.874900000	-1.126100000
6	1.431500000	-0.150200000	0.128600000
6	-0.827600000	-1.222500000	0.157900000
6	-0.077200000	0.111500000	0.140000000
7	-2.327200000	2.043800000	2.676200000
1	2.885400000	-1.153500000	-1.109400000
1	-2.260900000	1.707700000	-1.986800000
1	-3.803800000	-0.009700000	-1.085200000
1	-2.869400000	-1.897900000	0.220500000
1	-1.813900000	2.917700000	0.070500000
1	-3.417000000	2.157700000	0.102800000
1	-0.133000000	0.365100000	2.253200000
1	0.119000000	1.861600000	1.336300000
1	-3.778700000	0.011400000	1.417600000
1	-2.427200000	-0.725100000	2.300500000
1	-2.897100000	-1.958800000	-2.311900000
1	-2.645700000	-0.469200000	-3.223800000
1	-0.366900000	0.611100000	-3.264300000
1	-0.592000000	-1.858100000	-3.219200000
1	-0.976700000	-3.001600000	-1.052700000
1	1.332400000	-2.898300000	-1.954200000
1	1.344400000	-2.872400000	-0.190700000
6	-1.971300000	1.339900000	3.925700000
1	-0.903500000	1.155100000	3.976500000
1	-2.508100000	0.400900000	4.008900000
1	-2.246900000	1.962600000	4.773500000
1	-4.094300000	2.911900000	1.881100000
1	-3.981800000	2.911900000	3.635900000
1	-4.351300000	1.413400000	2.793300000
1	-1.895600000	3.946000000	1.837500000
1	-0.551900000	3.206900000	2.727500000
1	-1.921300000	3.888700000	3.594600000

G2

6	-1.977000000	1.150300000	-1.094800000
6	-2.723300000	-0.186100000	-1.075900000
6	-2.331700000	-0.950600000	0.191200000
6	-2.341900000	1.975700000	0.141800000
6	-0.440300000	0.934300000	1.384200000
6	-2.698000000	-0.134900000	1.433700000
6	-1.943700000	1.191000000	1.388800000
6	-2.359600000	-1.004200000	-2.312100000
6	-0.091500000	0.059000000	-2.356400000
6	-0.855200000	-1.266800000	-2.326100000
6	-0.446100000	-2.041000000	-1.070900000
6	1.058500000	-2.305400000	-1.081900000
6	1.807400000	-0.973900000	-1.112800000
6	1.414000000	-0.200400000	-2.370500000
6	-0.470600000	0.878500000	-1.121100000
6	1.441500000	-0.155100000	0.123600000
6	-0.825000000	-1.220500000	0.163700000
6	-0.065500000	0.111600000	0.143600000
7	-2.296500000	1.995000000	2.604800000
1	2.886800000	-1.162100000	-1.122300000
1	-2.255700000	1.705200000	-1.996400000
1	-3.803500000	-0.004100000	-1.076500000
1	-2.865500000	-1.906000000	0.214200000
1	-1.812700000	2.928300000	0.100300000
1	-3.414900000	2.169400000	0.133600000
1	-0.140900000	0.378600000	2.273800000
1	0.112000000	1.874600000	1.358300000
1	-3.775400000	0.033500000	1.441000000
1	-3.435400000	-0.703700000	2.333400000

1	0.070300000	1.831200000	-1.156200000
1	1.736300000	-0.701300000	1.022400000
1	1.988300000	0.790400000	0.109100000
1	-0.540500000	-1.786400000	1.058300000
1	-1.800700000	2.894400000	2.596000000
1	-3.306500000	2.179400000	2.630700000
1	-2.035600000	1.487000000	3.458500000

G3

6	-1.971000000	1.134200000	-1.103000000
6	-2.718300000	-0.198400000	-1.092900000
6	-2.322600000	-0.953300000	0.175100000
6	-2.331000000	1.961400000	0.135700000
6	-0.429400000	0.922000000	1.365400000
6	-2.683500000	-0.138300000	1.421600000
6	-1.938100000	1.203600000	1.411600000
6	-2.352800000	-1.016300000	-2.328900000
6	-0.083000000	0.042600000	-2.367000000
6	-0.849200000	-1.279100000	-2.344600000
6	-0.434900000	-2.045100000	-1.089200000
6	1.074000000	-2.311900000	-1.095700000
6	1.846600000	-0.985600000	-1.122400000
6	1.428200000	-0.211500000	-2.380300000
6	-0.467800000	0.866300000	-1.139800000
6	1.445200000	-0.163500000	0.110700000
6	-0.821300000	-1.232400000	0.144900000
6	-0.069000000	0.097800000	0.119600000
7	-2.292400000	2.033500000	2.669400000
7	3.372800000	-1.244100000	-1.123500000
1	-2.259300000	1.702100000	-1.993700000
1	-3.798200000	-0.016700000	-1.093200000
1	-2.866500000	-1.902900000	0.213500000
1	-1.805400000	2.911900000	0.061000000
1	-3.402900000	2.148100000	0.102600000
1	-0.116400000	0.353700000	2.239500000
1	0.134800000	1.851900000	1.320400000
1	-3.761900000	0.009700000	1.413600000
1	-2.416200000	-0.733900000	2.292900000
1	-2.896200000	-1.964100000	-2.322100000
1	-2.645900000	-0.476500000	-3.232400000
1	-0.348300000	0.597400000	-3.273000000
1	-0.545500000	-1.795400000	1.042900000
6	-1.584200000	3.331000000	2.691900000
6	-3.738500000	2.328800000	2.741400000
6	-1.932800000	1.326100000	3.916600000
6	3.793200000	-2.038000000	-2.296900000
6	4.145800000	0.015600000	-1.154200000
6	3.807800000	-1.986100000	0.078900000
1	-0.864300000	1.147000000	3.968000000
1	-2.468400000	0.386400000	3.999800000
1	-2.210000000	1.944400000	4.767100000
1	-4.059800000	2.915900000	1.887400000
1	-3.939600000	2.906900000	3.640200000
1	-4.320900000	1.414900000	2.794300000
1	-1.842100000	3.930900000	1.825700000
1	-0.510000000	3.187000000	2.733800000
1	-1.883200000	3.882400000	3.580300000
1	3.922200000	0.588300000	-2.047900000
1	5.207200000	-0.220500000	-1.166100000
1	3.946800000	0.615400000	-0.272700000
1	3.319200000	-2.952800000	0.138300000
1	3.608800000	-1.416500000	0.980200000
1	4.880100000	-2.157400000	0.020700000
1	3.562900000	-1.519100000	-3.221600000
1	3.317400000	-3.013100000	-2.298800000
1	4.869200000	-2.190100000	-2.257000000

G4

6	-1.926400000	1.165400000	-1.057900000
6	-2.672000000	-0.171600000	-1.040200000
6	-2.282100000	-0.936100000	0.227500000
6	-2.291700000	1.990300000	0.179200000
6	-0.390700000	0.949900000	1.424700000
6	-2.648900000	-0.120300000	1.470100000
6	-1.894500000	1.206100000	1.427200000
6	-2.304800000	-0.989900000	-2.275800000
6	-0.039000000	0.075400000	-2.316900000
6	-0.800700000	-1.252200000	-2.288300000
6	-0.394200000	-2.025800000	-1.031300000
6	1.113700000	-2.291800000	-1.038800000
6	1.848000000	-0.953900000	-1.068800000
6	1.470100000	-0.182100000	-2.330400000

1	-0.600000000	-1.866100000	-3.234900000	6	-0.419900000	0.895600000	-1.082000000
1	-0.956200000	-3.007800000	-1.066200000	6	1.491900000	-0.136700000	0.169100000
1	1.294800000	-2.914100000	-1.975200000	6	-0.775600000	-1.205900000	0.203600000
1	1.310000000	-2.890500000	-0.204200000	6	-0.018700000	0.128200000	0.184200000
1	1.924100000	0.756200000	-2.433600000	7	-2.245500000	2.009000000	2.642700000
1	1.656300000	-0.774500000	-3.283700000	7	3.325400000	-1.204200000	-1.071400000
1	0.063900000	1.823300000	-1.172100000	1	-2.208300000	1.721600000	-1.957300000
1	1.693600000	-0.696600000	1.026700000	1	-3.752000000	0.009400000	-1.043300000
1	1.947100000	0.802500000	0.109800000	1	-2.819500000	-1.889200000	0.251300000

1	-1.767000000	2.945600000	0.139300000
1	-3.364600000	2.184900000	0.170600000
1	-0.098900000	0.396500000	2.318000000
1	0.154900000	1.893800000	1.402600000
1	-3.726300000	0.048300000	1.477200000
1	-2.382100000	-0.688400000	2.362100000
1	-2.848700000	-1.937600000	-2.270600000
1	-2.596700000	-0.450700000	-3.180400000
1	-0.317500000	0.629600000	-3.218700000
1	-0.550900000	-1.839100000	-3.178500000
1	-0.927900000	-2.981100000	-1.009700000
1	1.363500000	-2.889000000	-1.916400000
1	1.380700000	-2.859800000	-0.146900000
1	1.994900000	0.773000000	-2.372200000
1	1.723400000	-0.754700000	-3.223300000
1	0.111000000	1.852700000	-1.114800000
1	1.766500000	-0.680200000	1.073900000
1	2.020300000	0.817200000	0.158800000
1	-0.502400000	-1.769800000	1.101600000
1	-1.753200000	2.910600000	2.636400000
1	-3.255100000	2.194000000	2.669900000
1	-1.988000000	1.502500000	3.498600000
1	3.594700000	-1.753400000	-1.896200000
1	3.842200000	-0.316600000	-1.092500000
1	3.606000000	-1.725000000	-0.231600000

CB7

8	-0.920900000	3.982900000	2.927900000
8	-3.709300000	1.785700000	2.947700000
8	-3.685700000	-1.736500000	2.979000000
8	-0.879400000	-3.920800000	2.997900000
8	2.611500000	-3.143900000	2.996400000
8	4.140900000	0.030100000	2.962100000
8	2.566900000	3.196000000	2.933300000
8	-0.896900000	3.912000000	-2.997100000
8	-3.694600000	1.707500000	-2.979800000
8	-3.701800000	-1.813500000	-2.948300000
8	-0.901100000	-3.987500000	-2.927600000
8	2.583900000	-3.174000000	-2.932300000
8	4.143500000	0.002000000	-2.960900000
8	2.597800000	3.164500000	-2.995800000
7	4.094400000	-3.262000000	1.239500000
7	5.159900000	-1.083200000	1.223800000
7	5.142000000	1.131400000	1.205900000
7	4.065300000	3.304400000	1.189100000
7	2.312200000	4.658200000	1.173600000
7	-0.046400000	5.160900000	-1.260300000
7	-2.206000000	4.667300000	-1.260600000
7	-4.110600000	3.165700000	-1.247900000
7	-5.091800000	1.180100000	-1.227700000
7	-5.088100000	-1.245000000	-1.200600000
7	-4.106300000	-3.230100000	-1.179500000
7	-2.191300000	-4.718200000	-1.166600000
7	-0.025800000	-5.183700000	-1.166400000
7	2.337800000	-4.638400000	-1.173200000
7	4.082400000	-3.273500000	-1.187600000
7	5.147800000	-1.094900000	-1.203900000
7	5.156200000	1.119800000	-1.221800000
7	4.079000000	3.292800000	-1.238200000
7	2.323500000	4.643300000	-1.253000000
6	-1.043400000	4.529200000	1.852200000
6	-3.497200000	4.371400000	1.729400000
1	-3.323600000	4.160100000	2.791000000
1	-4.171300000	5.225500000	1.597600000
6	-4.220100000	2.023200000	1.874000000
6	-5.621100000	0.001800000	1.772500000
1	-5.344100000	0.014900000	2.833100000
1	-6.709300000	-0.003100000	1.644000000
6	-4.201300000	-2.004500000	1.914800000
6	-3.460100000	-4.349500000	1.823800000
1	-3.280600000	-4.109500000	2.878300000
1	-4.129300000	-5.211100000	1.719100000
6	-1.005100000	-4.492800000	1.936000000
6	1.281400000	-5.397800000	1.827400000
1	1.218300000	-5.103300000	2.881400000
1	1.522100000	-6.462200000	1.724400000
6	2.958500000	-3.599200000	1.927400000
6	5.105600000	-2.402400000	1.791200000
1	6.083200000	-2.881200000	1.664700000
1	4.858000000	-2.273800000	2.851300000
6	4.716100000	0.026000000	1.894700000
6	5.076300000	2.456300000	1.758800000

7	-0.055500000	5.185700000	1.166200000
7	-2.216900000	4.701500000	1.166100000
7	-4.121400000	3.200000000	1.178900000
7	-5.092700000	1.209700000	1.200200000
7	-5.085600000	-1.215400000	1.227300000
7	-4.096000000	-3.196800000	1.247500000
7	-2.181400000	-4.685600000	1.260200000
7	-0.017700000	-5.160700000	1.260200000
7	2.348100000	-4.624400000	1.253400000
1	6.052200000	2.939400000	1.635800000
1	4.820300000	2.337400000	2.818100000
6	2.921700000	3.642900000	1.863300000
6	1.241300000	5.436600000	1.732800000
1	1.175500000	5.158900000	2.791200000
1	1.478800000	6.500100000	1.613600000
6	-1.027900000	4.483900000	-1.935900000
6	-3.481600000	4.321700000	-1.825300000
1	-3.299300000	4.081200000	-2.879100000

1	-4.156800000	5.179000000	-1.722800000
6	-4.211100000	1.973100000	-1.915300000
6	-5.622300000	-0.039500000	-1.772600000
1	-5.345900000	-0.051300000	-2.833400000
1	-6.710400000	-0.039300000	-1.643400000
6	-4.211300000	-2.053800000	-1.874500000
6	-3.474300000	-4.397600000	-1.729500000
1	-3.302900000	-4.185800000	-2.791300000
1	-4.142300000	-5.256200000	-1.596500000
6	-1.019200000	-4.535400000	-1.852300000
6	1.272700000	-5.424100000	-1.733300000
1	1.204900000	-5.145400000	-2.791300000
1	1.518300000	-6.485900000	-1.615500000
6	2.941100000	-3.619000000	-1.862400000
6	5.088900000	-2.419900000	-1.757200000
1	6.067300000	-2.898100000	-1.634600000
1	4.832000000	-2.301900000	-2.816400000
6	4.717700000	0.008700000	-1.893000000
6	5.095800000	2.438900000	-1.788700000
1	4.850500000	2.309500000	-2.849300000
1	6.070500000	2.922900000	-1.660400000
6	2.941200000	3.622200000	-1.926600000
6	1.251000000	5.408300000	-1.827100000
1	1.483200000	6.474600000	-1.723800000
1	1.190500000	5.113600000	-2.881200000
6	-0.530500000	5.786900000	-0.055300000
1	-0.288900000	6.858400000	-0.065300000
6	-2.042900000	5.444500000	-0.057000000
1	-2.722500000	6.307200000	-0.072300000
6	-4.894500000	3.194700000	-0.038000000
1	-5.576900000	4.055300000	-0.053100000
6	-5.577500000	1.802700000	-0.021500000
1	-6.675800000	1.815600000	-0.022100000
6	-5.569200000	-1.840300000	0.021400000
1	-6.667400000	-1.858600000	0.022800000
6	-4.879500000	-3.229000000	0.037400000
1	-5.557800000	-4.092800000	0.052000000
6	-2.011300000	-5.460400000	0.056100000
1	-2.683600000	-6.328900000	0.070500000
6	-0.496100000	-5.789900000	0.054500000
1	5.218500000	4.555600000	-0.024200000
6	3.011100000	5.005600000	-0.038600000
1	3.243000000	6.079200000	-0.044200000

CB8

7	17.607200000	9.939000000	3.565200000
6	18.041400000	8.884100000	4.445200000
1	19.029900000	8.518600000	4.135400000
7	18.062200000	9.243200000	5.842000000
6	16.364000000	9.707900000	3.037600000
8	15.784100000	10.417900000	2.243400000
6	17.110900000	8.581200000	6.572800000
8	16.955400000	8.656100000	7.773200000
7	15.940600000	8.480600000	3.477000000
6	16.889700000	7.849200000	4.361400000
1	17.168500000	6.861000000	3.970900000
7	16.446300000	7.733100000	5.726900000
6	14.843000000	7.784700000	2.863800000
1	15.189900000	6.795300000	2.539100000
1	14.526600000	8.393400000	2.008700000
6	15.590100000	6.682400000	6.202700000
1	15.707100000	6.655100000	7.292100000
1	15.906200000	5.737000000	5.744900000
7	13.684100000	7.616600000	3.696900000
6	13.559300000	6.574200000	4.686200000
1	13.945800000	5.627000000	4.286200000
7	14.189200000	6.871700000	5.946900000
6	12.488300000	8.225200000	3.417300000
8	12.306900000	9.089300000	2.585700000
6	13.284100000	7.116300000	6.945800000
8	13.549400000	7.354100000	8.105100000
7	11.517000000	7.607700000	4.160800000
6	12.047100000	6.587600000	5.029200000
1	11.515800000	5.640200000	4.865400000
7	12.028300000	6.929500000	6.430200000
6	10.115600000	7.767500000	3.887800000
1	10.040200000	8.345800000	2.959700000
1	9.665500000	6.773300000	3.773700000
6	10.869000000	6.792400000	7.268100000
1	10.373100000	5.842200000	7.032900000
1	11.231800000	6.804600000	8.302400000
7	9.378900000	8.498000000	4.881600000

6	8.911000000	7.919500000	6.117100000
1	8.493000000	6.920900000	5.930800000
7	9.905500000	7.852400000	7.157500000
6	8.812800000	9.718200000	4.620900000
8	8.992300000	10.388000000	3.625900000
6	9.666700000	8.739700000	8.174200000
8	10.327400000	8.859400000	9.184300000
7	7.921600000	9.991100000	5.624800000

6	7.907600000	8.976300000	6.647200000	8	14.058300000	16.824200000	10.648900000
1	6.882000000	8.617000000	6.807400000	6	13.226200000	18.524000000	6.145200000
7	8.489300000	9.386000000	7.901900000	8	12.999500000	18.215600000	4.994200000
6	6.936400000	11.031400000	5.520600000	7	14.892400000	18.186600000	8.991500000
1	5.948800000	10.602800000	5.730900000	6	14.394600000	19.173500000	8.065500000
1	6.993600000	11.413500000	4.494900000	1	14.921700000	20.126200000	8.210900000
6	7.778800000	10.140100000	8.897900000	7	14.461400000	18.778200000	6.681400000
1	6.755200000	9.750900000	8.970300000	6	16.286200000	18.003300000	9.287700000
1	8.322500000	10.002100000	9.839700000	1	16.331200000	17.440100000	10.227000000
7	7.144000000	12.157700000	6.387500000	1	16.757800000	18.988500000	9.392600000
6	6.765900000	12.178900000	7.777400000	6	15.638800000	18.924900000	5.870800000
1	5.776300000	11.719500000	7.905200000	1	16.112500000	19.885200000	6.111100000
7	7.718000000	11.556900000	8.664800000	1	15.306700000	18.897400000	4.826500000
6	7.494400000	13.395200000	5.915400000	7	17.022600000	17.243000000	8.316000000
8	7.813500000	13.658400000	4.775400000	6	17.556700000	17.806600000	7.102200000
6	8.344800000	12.460000000	9.483300000	1	17.978500000	18.800900000	7.302400000
8	9.143500000	12.194000000	10.356400000	7	16.613700000	17.879400000	6.013500000
7	7.305800000	14.299400000	6.927200000	6	17.523100000	15.995800000	8.583700000
6	6.858500000	13.681100000	8.150900000	8	17.267700000	15.320500000	9.558400000
1	5.920500000	14.144400000	8.485800000	6	16.916300000	17.017100000	4.992500000
7	7.827400000	13.700800000	9.217400000	8	16.317500000	16.919300000	3.942300000
6	7.288400000	15.717000000	6.695900000	7	18.446000000	15.695100000	7.616300000
1	6.346400000	16.126800000	7.081400000	6	18.569800000	16.734500000	6.623900000
1	7.365900000	15.854000000	5.611200000	1	19.614400000	17.067200000	6.555400000
6	8.014400000	14.819700000	10.099500000	7	18.080300000	16.372400000	5.318400000
1	7.031500000	15.241400000	10.344100000	6	19.392500000	14.623900000	7.765500000
1	8.514200000	14.433300000	10.995300000	1	20.405000000	15.029000000	7.642900000
7	8.853400000	15.867700000	9.587900000	1	19.247600000	14.218000000	8.773400000
6	8.402400000	16.873400000	8.657800000	6	18.845200000	15.626100000	4.358300000
1	7.411100000	17.242600000	8.953700000	1	19.880000000	15.989900000	4.374000000
7	8.379700000	16.444900000	7.282300000	1	18.377300000	15.801700000	3.382800000
6	10.071800000	16.165200000	10.139500000	7	19.221900000	13.525800000	6.854500000
8	10.647400000	15.516000000	10.986900000	6	19.712200000	13.531100000	5.498100000
6	9.357900000	17.038800000	6.528400000	1	20.720800000	13.964900000	5.464000000
8	9.533100000	16.882800000	5.338400000	7	18.853600000	14.203300000	4.556400000
7	10.467100000	17.383200000	9.652600000	6	18.845400000	12.277200000	7.275400000
6	9.543100000	17.923500000	8.688400000	8	18.449700000	11.989600000	8.385300000
1	9.243900000	18.939000000	8.981400000	6	18.233100000	13.337400000	3.694900000
7	10.029800000	17.923700000	7.330600000	8	17.495100000	13.646400000	2.783500000
6	11.540700000	18.136800000	10.238200000	7	19.102000000	11.394600000	6.259100000
1	11.177200000	19.145600000	10.469500000	6	19.610400000	12.042300000	5.076500000

1	11.835800000	17.602500000	11.148600000	1	20.553700000	11.572600000	4.766200000
6	10.891700000	18.941400000	6.795300000	7	18.686300000	12.074000000	3.969900000
1	10.807400000	18.878700000	5.704100000	6	19.134000000	9.972400000	6.461600000
1	10.553900000	19.918500000	7.163600000	1	20.089400000	9.586100000	6.084700000
7	12.722200000	18.247200000	9.428400000	1	19.037400000	9.806400000	7.540700000
6	12.872200000	19.200300000	8.358700000	6	18.476600000	10.971600000	3.072700000
1	12.465400000	20.174400000	8.662300000	1	19.448300000	10.524400000	2.828700000
7	12.286200000	18.788400000	7.106700000	1	17.995900000	11.387300000	2.179500000
6	13.901900000	17.634900000	9.760600000				

CB[7]•G1

8	0.743322385	-3.874730731	3.375092227
8	3.855100683	-1.865744790	3.295860490
8	4.056349559	1.421897645	3.306556674
8	1.182351047	3.727415172	3.356192751
8	-2.614977724	3.444470444	3.507211960
8	-4.441845938	0.261984076	3.435924564
8	-2.986843132	-3.096274477	3.499727455
8	0.747113125	-4.224988232	-2.739684835
8	3.927847578	-2.035310639	-2.763270114
8	4.159355763	1.643712233	-2.749282962
8	1.286973017	4.177351829	-2.741517073
8	-2.337422846	3.231924870	-2.546398012
8	-4.418376736	0.210170335	-2.699194404
8	-2.791570169	-2.942108426	-2.545961660
7	-0.229654286	-4.953882497	1.586646132
7	1.969213329	-4.628834141	1.578161857
7	3.995968916	-3.318187402	1.516366815
7	5.267207729	-1.501912125	1.513097117
7	5.418505577	0.904215364	1.522973068
7	4.381573677	2.862505529	1.541853204
7	2.504825273	4.378483850	1.586796262
7	0.357625499	4.952891740	1.588085630
7	-2.047042137	4.674071857	1.642368078
7	-3.928716312	3.498454288	1.616886623
7	-5.149727918	1.412430520	1.572532301
7	-5.285848927	-0.805207028	1.579030988
7	-4.323878961	-3.023963015	1.627245892
7	-2.592668314	-4.413271802	1.648827615
7	-0.217910191	-5.073594451	-0.839465201
7	1.977627291	-4.712182103	-0.853856078
7	4.027341528	-3.393709331	-0.908990406
7	5.212287353	-1.505807650	-0.928684822
7	5.362624533	0.936852462	-0.918411341
7	4.428170018	2.960362731	-0.884030439
7	2.548562805	4.510759462	-0.841580537
7	0.404690621	5.101963109	-0.835544713
7	-1.978590391	4.663722470	-0.786360481
7	-3.828169459	3.425922707	-0.807410563
7	-5.142673812	1.390493605	-0.865740451
7	-5.326151928	-0.820902854	-0.859469072
1	6.996087897	-0.404104043	1.818299940
6	4.540926962	1.684597887	2.226993011
6	3.772399066	4.010540394	2.154712531
1	3.585524916	3.744294402	3.201791789
1	4.458112265	4.864426913	2.082074721
6	1.325582196	4.269183310	2.280919446
6	-0.893311227	5.327504802	2.197702194
1	-0.841567108	5.022239115	3.249360079
1	-1.017792789	6.414985022	2.111908680
6	-2.825447454	3.807452932	2.368970826
6	-5.034545058	2.734335478	2.131009372
1	-5.965854698	3.283865469	1.948733293
1	-4.855313016	2.610340077	3.205367495
6	-4.886157455	0.285405844	2.306304693
6	-5.326235274	-2.129216060	2.144122626
1	-6.317962642	-2.563911045	1.971475128
1	-5.125947674	-2.021710288	3.216610632
6	-3.254852011	-3.450014362	2.371187731
6	-1.514130090	-5.190673358	2.197456726
1	-1.424916724	-4.897599889	3.250028054
1	-1.758833084	-6.257173550	2.108009668
6	0.825128868	-4.600935682	-1.593318387
6	3.283399379	-4.511324175	-1.436712479
1	3.119304755	-4.304605534	-2.500900737
1	3.877975615	-5.423545133	-1.302223832
6	4.324592323	-2.271343137	-1.645339182
6	5.830269580	-0.315494691	-1.465218947
1	5.585662681	-0.296232868	-2.533659710
1	6.913076550	-0.383098141	-1.311526455
6	4.581472708	1.815763071	-1.628764465
6	3.829965823	4.163503205	-1.408277074
1	3.657653803	3.987487174	-2.476689806
1	4.525538514	4.997754439	-1.254940097
6	1.396271053	4.529988126	-1.589915872
6	-0.893715848	5.409059563	-1.372189172
1	-0.855440595	5.144399533	-2.435223281
1	-1.094104090	6.479556788	-1.242142026
6	-2.668191057	3.704608423	-1.482498766
6	-4.924010761	2.704255796	-1.407100149
1	-5.838219299	3.298257018	-1.294882233

7	-4.281375683	-3.005419221	-0.799263504
7	-2.543151497	-4.393243529	-0.780442305
6	0.815084084	-4.402286398	2.285962136
6	3.274719674	-4.399399347	2.131573471
1	3.128355568	-4.121642475	3.182065862
1	3.866152067	-5.320241020	2.047013566
6	4.301618831	-2.175996447	2.212566976
6	5.925431413	-0.337455699	2.035986101
1	5.738046297	-0.330151367	3.115941087

1	-0.085608289	-6.707538312	0.457592253
6	1.749816868	-5.411023827	0.388819359
1	2.364650706	-6.322592189	0.425299241
6	4.785236445	-3.458411188	0.314141208
1	5.363054597	-4.393005826	0.353958321
6	5.636785240	-2.161920060	0.287012910
1	6.724496429	-2.319601704	0.266862599
6	5.866459840	1.524165259	0.302150844
1	6.965365666	1.545216605	0.281568728
6	5.183970524	2.917046678	0.341493881
1	5.873738500	3.771675958	0.392601545
6	2.385655009	5.205430645	0.412954762
1	3.096966515	6.042295894	0.474246415
6	0.889837012	5.612694838	0.418430469
1	0.703071122	6.694775393	0.485147582
6	-2.674103439	5.076000222	0.404707626
1	-2.822366255	6.165403451	0.399449574
6	-3.975499511	4.233806536	0.376315383
1	-4.906572043	4.816331023	0.324721513
6	-5.863512518	1.117464148	0.352157893
1	-6.824972323	1.651343074	0.347779295
6	-5.974559413	-0.430154263	0.364764752
1	-7.002193398	-0.821198334	0.387130633
6	-4.478458711	-3.772707032	0.402430349
1	-5.464494368	-4.258467477	0.385144250
6	-3.267940788	-4.741561854	0.415542463
1	-3.525220748	-5.810335487	0.405021098
6	1.069720303	1.209018595	-1.555582151
6	1.916413134	-0.037943528	-1.339379171
6	1.046357511	-1.259380235	-1.593119132
6	0.550639703	1.242654380	-2.992784737
6	-1.474064014	0.027805493	-2.235778028
6	0.510855218	-1.244991607	-3.022942972
6	-0.325775382	0.014521327	-3.251029088
6	2.458453219	-0.055632903	0.083238130
6	0.458991249	1.185851101	0.884409089
6	1.308569157	-0.066698928	1.076853149
6	0.441000605	-1.299492138	0.841215774
6	-0.715593401	-1.312661704	1.827819437
6	-1.558254065	-0.057079926	1.634731950
6	-0.698569041	1.179852410	1.872042595
1	-0.009793932	2.165949286	-3.135550624
1	1.430249429	1.261413293	-3.634095583
1	-2.130664925	-0.825526170	-2.393917515
1	-2.054452360	0.941228915	-2.341395864
1	1.370346772	-1.292743618	-3.691956594
1	-0.086741261	-2.144131826	-3.152276738
1	3.073962254	-0.939581851	0.247174127
1	3.069170540	0.829029762	0.265749306
1	1.084337318	2.069716960	1.067611045
1	1.705750470	-0.087506646	2.102761248
1	1.055768160	-2.196656299	0.990489119
1	-0.343224037	-1.367430745	2.855343469
1	-1.328800937	-2.199268625	1.663019191
1	-1.302209728	2.080062393	1.743869753
1	-0.321347240	1.193176785	2.899258686
1	-0.674809509	2.119248745	-0.684318826
1	-2.739147005	-0.895474884	0.037239673
1	-2.712034951	0.876031162	0.074129393
1	-0.718397394	-2.160702456	-0.753653961
6	-1.982723031	1.005217755	-4.833950141
6	0.165594670	0.396291104	-5.658761106
6	-1.413454424	-1.287028408	-5.083385267
1	-2.079713759	-1.684296707	-4.323604191
1	-0.604034254	-1.991381078	-5.248385330
1	-1.973143413	-1.170550460	-6.007634225
1	1.058710333	-0.201490146	-5.502734178
1	0.416661321	1.448781513	-5.569705170
1	-0.208413898	0.207861617	-6.662128287
1	-1.714286332	1.967051518	-4.408460286
1	-2.879055602	0.642394801	-4.338474771
1	-2.193018553	1.135345603	-5.892019780

CB[7]•G2

8	-2.408241613	-3.065191700	3.704902424
8	0.637691644	-4.760649893	2.591069647
8	3.799026450	-3.102371965	1.812637582
8	4.781361200	0.603610292	1.944888541
8	2.695804029	3.567359771	2.811461020
8	-0.652694360	3.653025275	3.796446918
8	-3.001749403	0.786710817	4.268964586
8	-3.747375685	-2.310622450	-2.127733134

6	-0.072713773	1.212676660	-0.547374630
6	-2.104575897	-0.022471071	0.207391618
6	-0.097340259	-1.271532447	-0.588179059
6	-0.947450201	-0.017715184	-0.795506399
7	-0.881809436	0.032329447	-4.683895359
1	-2.374269967	-0.066813308	2.363766375
1	1.697761340	2.088241077	-1.394525508
1	2.741409581	-0.039869819	-2.055352844
1	1.650295621	-2.159431092	-1.462056823
8	-1.079440562	-4.122461385	-3.223134593
8	1.950725988	-2.430147858	-3.907107669
8	3.136291176	1.308612982	-3.979505176
8	1.061489876	4.190025956	-2.937614026
8	-2.294227324	4.244861737	-1.958242380
8	-4.624263664	1.398754682	-1.658321233
7	-4.085521057	-2.344962294	2.296836896
7	-2.975875106	-4.203313858	1.788340082
7	-0.978157156	-5.358828465	1.061515645

7	1.153520579	-5.393094058	0.437289872	6	-4.605993356	-1.302545646	3.143940620
7	3.232656583	-4.279421132	-0.082156698	1	-4.048736191	-1.351496944	4.086789213
7	4.541711315	-2.494753106	-0.280353390	1	-5.675816834	-1.483544141	3.317153189
7	5.134051541	-0.156280765	-0.198789974	6	-3.975458675	-2.725179633	-1.013641117
7	4.832922188	2.020854311	0.129228414	6	-3.080146766	-4.992082723	-1.385212370
7	3.571709861	3.997023997	0.726362843	1	-3.272380404	-4.686123877	-2.420090935
7	1.765840892	5.112687999	1.378117282	1	-3.590589067	-5.931755447	-1.152114225
7	-0.566868039	5.154624253	2.052331921	6	-0.786208785	-4.739457979	-2.222878520
7	-2.484992744	4.118942330	2.483585250	6	1.585462924	-5.044001084	-2.785196853
7	-3.951149575	2.203147051	2.721915331	1	1.176411860	-4.732864771	-3.753225842
7	-4.433052443	0.032569195	2.628362379	1	2.093438007	-6.010541236	-2.868055511
7	-4.689993414	-2.080501204	-0.037524528	6	2.692632550	-2.849148708	-3.042540304
7	-3.606162626	-3.954410287	-0.535936442	6	4.446135143	-1.119192529	-3.260283409
7	-1.660513728	-5.180391726	-1.270060643	1	3.869138705	-0.928298055	-4.172662550
7	0.468234615	-5.170372536	-1.887353810	1	5.480747954	-1.390481870	-3.507870559
7	2.551262706	-4.046141878	-2.396174030	6	3.835193015	1.248709425	-2.995373022
7	3.827929123	-2.235243386	-2.586057523	6	3.851452018	3.665940430	-2.521606772
7	4.445555053	0.114295423	-2.514093005	1	3.344940845	3.634243424	-3.493557030
7	4.222733441	2.308936604	-2.215056637	1	4.755228944	4.284893466	-2.567314554
7	2.925434628	4.264324415	-1.593135654	6	1.622426465	4.543345378	-1.926338114
7	1.098455535	5.360411785	-0.955327710	6	-0.191850821	5.987569248	-1.082984078
7	-1.239872413	5.414353530	-0.278819611	1	-0.094909288	7.049257321	-0.831739908
7	-3.157526325	4.383900103	0.169114387	1	-0.497572596	5.853253764	-2.127138553
7	-4.609573441	2.454834954	0.388184412	6	-2.222137647	4.615529072	-0.809737562
7	-5.080256919	0.284514949	0.298299095	6	-4.441722584	3.796224108	-0.108414086
6	-3.068542944	-3.179503826	2.693942269	1	-4.528512056	3.735423450	-1.199871926
6	-2.095973691	-5.331123532	1.969491696	1	-5.224058817	4.437356152	0.315017709
1	-1.681058377	-5.243257967	2.980472178	6	-4.731784626	1.377879382	-0.454011165
1	-2.673059960	-6.256802464	1.861522362	6	-5.522438558	-0.939896566	-0.313929004
6	0.305925430	-5.106939062	1.478322586	1	-6.545593883	-1.161020677	0.017080576
6	2.584391936	-5.383247943	0.581377106	1	-5.491040506	-0.770466001	-1.396665735
1	2.793658756	-5.273203286	1.651899811	6	-4.809229295	-2.870562613	1.161616641
1	2.994194970	-6.324520721	0.196762945	1	-5.867977679	-3.007471408	1.423627553
6	3.834577862	-3.261979540	0.611180733	6	-4.043046759	-4.173295705	0.815298456
6	5.492644480	-1.504915959	0.150265757	1	-4.636526166	-5.096126099	0.881771161
1	5.526344734	-1.550394244	1.245141683	6	-1.019160134	-5.967754361	-0.249298985
1	6.476030598	-1.739616605	-0.278682406	1	-1.490865713	-6.958532913	-0.184629752
6	4.877201257	0.798031362	0.752421072	6	0.468018452	-5.976446679	-0.690933377
6	4.792770969	3.250922303	0.876089349	1	0.882183072	-6.971955244	-0.905268010
1	4.867690424	2.976416361	1.935059830	6	3.624454146	-4.300380080	-1.472247357
1	5.636067603	3.884927671	0.574586234	1	4.114272211	-5.255377678	-1.709362259

6	2.663204158	4.141598118	1.744597884	6	4.523943240	-3.045345077	-1.613945914
6	0.772337982	5.630108877	2.281672044	1	5.551031199	-3.243207979	-1.951875235
1	0.775067523	6.724046285	2.221592123	6	5.414374296	0.420076027	-1.490542649
1	1.055818320	5.288385430	3.283937042	1	6.421222172	0.121943091	-1.820438394
6	-1.169461808	4.225146330	2.860743809	6	5.232144602	1.942461506	-1.256896813
6	-3.465010332	3.434739730	3.287223198	1	6.136737976	2.548969142	-1.414735628
1	-4.312649542	4.108897186	3.463091117	6	3.326072887	4.907015179	-0.367629666
1	-2.971857363	3.170273141	4.230076712	1	4.211900498	5.534982457	-0.538474688
6	-3.696069669	0.980879214	3.294980649	6	2.053485677	5.673924156	0.078444958

1	2.170790401	6.763224665	0.164278402
6	-1.482821660	5.744315867	1.103595155
1	-1.496388077	6.835712212	1.232058776
6	-2.824224956	5.028409519	1.413118687
1	-3.642767537	5.690128339	1.729860607
6	-5.003946038	2.138933299	1.737407520
1	-5.837714852	2.787780607	2.045421108
6	-5.339340045	0.626022429	1.672462212
1	-6.376882834	0.371295872	1.937033213
6	-1.465540804	0.898074486	-0.921154455
6	-0.223683516	1.774487780	-1.056840187
6	0.965471852	0.904057691	-1.449169055
6	-1.762005776	0.210436726	-2.255286567
6	-0.337102552	-1.691965254	-1.521672434
6	0.669764727	0.222589559	-2.780356839
6	-0.563546671	-0.656314035	-2.619878643
6	0.066289497	2.466414754	0.265071195
6	-0.921784283	0.565798381	1.520875888
6	0.317449468	1.439517971	1.357396276
6	1.507153753	0.560113116	0.984871487
6	1.747071009	-0.467153157	2.085985361
6	0.505932545	-1.340525537	2.233766413
6	-0.676622884	-0.459794164	2.620508196
6	-1.222876257	-0.123009945	0.190868995
6	0.209405760	-2.034850438	0.906799098
6	1.212154714	-0.126434905	-0.347363713
6	-0.032375981	-1.004671513	-0.192656912
7	-0.799031162	-1.386448824	-3.897798562
1	0.673266936	-2.099709510	3.007255247
1	-2.309937690	1.536768133	-0.652092990
1	-0.397323375	2.527144329	-1.833555796
1	1.847713459	1.542181668	-1.550431139
1	-2.665978099	-0.392210571	-2.177119454
1	-1.933396750	0.984325578	-3.004468861
1	0.493484764	-2.343706520	-1.786799068
1	-1.237848845	-2.294747807	-1.407629328
1	0.506636670	0.993585556	-3.534612481
1	1.521253266	-0.376175183	-3.092645556
1	0.942954039	3.103482482	0.163150306
1	-0.783764741	3.083373611	0.550815150
1	2.070165959	-0.757325801	-0.615991685
1	-1.488014877	-2.141556577	-3.763762518
1	-1.121515463	-0.748839086	-4.631090333
1	0.088797429	-1.830436111	-4.190230607

CB[7]•G3 unstable complex

8	-0.842990169	4.211123394	2.879903492
8	-3.507138596	1.743424153	2.776210821
8	-3.539224678	-1.916159158	2.854481237
8	-0.578497544	-4.669760117	2.773561327
8	3.025732731	-4.021331810	2.726308857
8	4.641370141	-0.342974439	2.760360510
8	2.703563202	3.103129074	2.686555925
8	-1.203365530	4.465903428	-3.360106845
8	-4.522958087	2.227596204	-3.353590767
8	-3.709587607	-1.639270178	-3.253460546
8	-0.637704668	-3.984872463	-3.209222567
8	2.585199626	-3.453937697	-3.282445057
8	4.028099450	-0.247194030	-3.370111729
8	2.731360559	3.380786639	-3.510373579
7	0.031846523	5.130875560	0.970270166
7	-2.153544856	4.725473060	1.067810970
7	-4.002973912	3.190786071	1.066832485
7	-4.896542022	1.146485562	1.057048945
7	-4.800948646	-1.258620694	1.057238785
7	-3.714118391	-3.207786179	0.950558536
7	-1.920982906	-4.859721999	0.914408537
7	0.163779595	-5.686007646	0.840769529
7	2.609360030	-5.247527950	0.817709203
7	4.268473848	-3.729481793	0.809755970
7	5.140270916	-1.430842948	0.780889908
7	5.096847120	0.807432783	0.824988829
7	4.011354154	2.976642162	0.804739569
7	2.344098028	4.465464401	0.878180845
7	-0.083652882	5.125435288	-1.456347732
7	-2.294752321	4.759380645	-1.358298148
7	-4.243859147	3.315928579	-1.339767260
7	-5.137967798	1.270927121	-1.352204525
7	-4.901598483	-1.142763893	-1.353306810
7	-3.823603082	-3.096709588	-1.470479774
7	-1.987416460	-4.677371100	-1.487061272
7	0.102119697	-5.438408371	-1.582772903

7	2.462980450	-5.022382204	-1.605652257
7	4.146463235	-3.574996851	-1.603898798
7	5.078656050	-1.362536739	-1.649340508
7	4.960752810	0.862224223	-1.586531259
7	3.992631345	3.072603385	-1.618404691
7	2.256282411	4.478681757	-1.538104246
6	-0.974658326	4.633012481	1.759853899
6	-3.419291635	4.368226503	1.652231688

1	-3.228495597	4.148499431	2.709298290	6	2.968910677	3.612781073	-2.357892951
1	-4.119841546	5.207608551	1.554573059	6	1.219987338	5.347600418	-2.053297474
6	-4.069789007	1.994530485	1.744401033	1	1.511533772	6.396458301	-1.898699595
6	-5.361908778	-0.082228820	1.655190172	1	1.127530136	5.138733213	-3.125743587
1	-5.032200455	-0.074686509	2.701370483	6	-0.481580305	5.754912436	-0.220535851
1	-6.457867188	-0.118194933	1.593662082	1	-0.211632860	6.824383676	-0.233532782
6	-3.957645017	-2.107187212	1.746073867	6	-2.010846901	5.485203393	-0.145402673
6	-3.153460052	-4.419818932	1.516695207	1	-2.628948044	6.397430938	-0.094440812
1	-2.929670851	-4.201782888	2.568196329	6	-4.897261898	3.220758947	-0.056980922
1	-3.901308090	-5.224681023	1.444444760	1	-5.632471303	4.034396707	0.060299477
6	-0.751736989	-5.026584174	1.643546073	6	-5.519434156	1.794242984	-0.064841135
6	1.496651493	-6.034380642	1.310711667	1	-6.616544090	1.777705093	0.045927284
1	1.476728889	-5.876485232	2.395695348	6	-5.302184034	-1.839675368	-0.154980947
1	1.680294739	-7.089245789	1.073283762	1	-6.400659298	-1.929027630	-0.114751976
6	3.263740340	-4.298004572	1.586143118	6	-4.547248719	-3.194532964	-0.231653640
6	5.220613992	-2.777055543	1.331434172	1	-5.203291588	-4.080793501	-0.241578754
1	6.237848331	-3.163819826	1.174244452	6	-1.881686080	-5.553272256	-0.346963389
1	5.007481761	-2.683258684	2.403339988	1	-2.658041498	-6.334583708	-0.386166757
6	4.922065839	-0.331222695	1.593359418	6	-0.423390213	-6.093709848	-0.416902630
6	5.039988699	2.131288044	1.379667576	1	-0.346753748	-7.187088871	-0.528762375
1	6.013452184	2.628690240	1.257309904	6	3.242689292	-5.430521862	-0.466789964
1	4.801417094	2.015034280	2.443742097	1	3.561246050	-6.479175574	-0.582717872
6	2.989096488	3.467989055	1.576862151	6	4.414596903	-4.403523333	-0.458090224
6	1.365507477	5.330964804	1.479213826	1	5.415637112	-4.857290461	-0.538397718
1	1.337198387	5.098217501	2.550206757	6	5.793144434	-1.034214747	-0.451309389
1	1.662046232	6.377243317	1.324307446	1	6.811847370	-1.455507220	-0.488073168
6	-1.194214339	4.754779689	-2.195870151	6	5.742110845	0.518164937	-0.427127360
6	-3.643633276	4.529808210	-1.844691929	1	6.730831724	1.005919086	-0.472051781
1	-3.584597656	4.423987181	-2.934547482	6	4.198970549	3.774701950	-0.383619672
1	-4.270741034	5.392162061	-1.581285622	1	5.197282688	4.243430356	-0.370337963
6	-4.625003656	2.264748973	-2.159946396	6	3.017098061	4.784512660	-0.348108989
6	-5.606653861	0.006360179	-1.874354137	1	3.325467142	5.843528348	-0.352863329
1	-5.432586202	0.036527872	-2.956799348	6	1.590494021	-0.674596460	-0.852418573
1	-6.679526660	-0.105343574	-1.664883508	6	0.726648089	-1.924860327	-0.807165074
6	-4.096769282	-1.935223998	-2.154125754	6	-0.739944873	-1.550096805	-0.674562686
6	-3.218561955	-4.248879705	-2.093494005	6	1.242072524	0.124086642	-2.090993193
1	-2.977725576	-3.954787661	-3.122301944	6	-0.490961553	1.333085961	-0.790506681
1	-3.938271420	-5.081065767	-2.086530880	6	-1.134887383	-0.782378192	-1.914200396
6	-0.806784758	-4.620034741	-2.206464292	6	-0.249244365	0.450950317	-2.062603684
6	1.371024625	-5.755193756	-2.176928375	6	1.150556805	-2.735560301	0.386871426
1	1.308927052	-5.451373446	-3.229524924	6	1.741558565	-0.699228975	1.634768366

1	1.557149679	-6.831810343	-2.086372697	6	0.894049705	-1.961570427	1.666712284
6	3.004236456	-3.951029909	-2.275595207	6	-0.566295851	-1.555973141	1.789282799
6	5.077955419	-2.679058859	-2.225959061	6	-0.764079924	-0.788287164	3.086538778
1	6.090600940	-3.100503095	-2.172970512	6	0.097903208	0.471627298	3.080741608
1	4.753698730	-2.561493746	-3.267594071	6	1.570752235	0.099237472	2.918217795
6	4.611570113	-0.258047058	-2.323414828	6	1.367944138	0.138317028	0.416206051
6	4.961244586	2.167684589	-2.189988405	6	-0.301848232	1.334176875	1.845632375
1	4.679077672	2.038172852	-3.242191309	6	-0.957833117	-0.720127525	0.579999513
1	5.964380879	2.610526551	-2.110799249	6	-0.102130987	0.545509515	0.512402999

7	-0.606751413	1.065651252	-3.438316835	8	-0.794200000	4.186500000	2.303800000
7	-0.089112003	1.176880126	4.457850200	8	-3.397000000	1.482600000	2.111000000
1	2.641523646	-0.970089904	-0.907474806	8	-3.638600000	-2.415500000	1.965300000
1	0.869833290	-2.493006322	-1.729349327	8	-0.773100000	-5.020700000	1.589300000
1	-1.343920473	-2.457867661	-0.605322383	8	3.175000000	-4.107400000	1.439600000
1	1.835134274	1.038505500	-2.101553197	8	4.585900000	-0.497700000	1.641000000
1	1.523527268	-0.472303081	-2.956918069	8	2.626800000	2.905100000	1.855600000
1	-1.543227010	1.614847474	-0.706778119	8	-0.962800000	3.801600000	-3.761300000
1	0.105316662	2.248290063	-0.837153567	8	-4.001400000	1.822300000	-3.897400000
1	-1.038831083	-1.463939778	-2.754964251	8	-3.885800000	-1.688800000	-4.088900000
1	-2.171863966	-0.466814882	-1.823374020	8	-1.068300000	-3.728100000	-4.407200000
1	0.616278566	-3.671451028	0.396130208	8	2.375600000	-2.874600000	-4.500900000
1	2.212851389	-2.917720313	0.291762621	8	4.066500000	0.175800000	-4.402900000
1	2.781931551	-0.999396153	1.550285135	8	2.617300000	3.350500000	-4.150800000
1	1.175342654	-2.577314127	2.524632685	7	0.045700000	5.098800000	0.372900000
1	-1.193474584	-2.445491852	1.829390115	7	-2.107200000	4.560400000	0.455400000
1	-0.482078323	-1.469587501	3.885329668	7	-3.922600000	2.966000000	0.440000000
1	-1.819711796	-0.544636915	3.188287693	7	-4.788400000	0.912100000	0.365900000
1	2.191321808	0.990046305	2.857187377	7	-4.835000000	-1.507600000	0.226300000
1	1.939129341	-0.520557515	3.733288853	7	-3.957500000	-3.541800000	-0.020000000
1	1.995321613	1.038970558	0.388172268	7	-2.084800000	-5.060700000	-0.294900000
1	-1.346395511	1.627957379	1.930548251	7	0.091900000	-5.511900000	-0.492200000
1	0.316562382	2.230609035	1.815755606	7	2.461300000	-4.965500000	-0.579600000
1	-2.015700035	-0.436878732	0.658565934	7	4.219500000	-3.592600000	-0.539000000
6	0.333041259	2.133603727	-3.799548219	7	5.236600000	-1.395300000	-0.378800000
6	-0.557754518	0.078566616	-4.546448188	7	5.126000000	0.820400000	-0.161700000
6	-1.970937540	1.597164863	-3.436281146	7	4.020900000	2.973000000	0.019800000
6	0.111879149	0.229504934	5.577843810	7	2.367300000	4.460000000	0.189400000
6	0.857222307	2.285841709	4.661449200	7	-0.039800000	5.026500000	-2.045000000
6	-1.436233607	1.742256101	4.631287741	7	-2.203900000	4.528400000	-1.962600000
1	-2.096771718	2.296555411	-2.620453668	7	-4.114900000	3.071000000	-1.968500000
1	-2.689166182	0.787070875	-3.359508546	7	-5.139100000	1.109700000	-2.026500000
1	-2.171957160	2.128714485	-4.363310813	7	-5.085600000	-1.283300000	-2.167300000
1	0.352182982	-0.514026898	-4.522628019	7	-4.124700000	-3.262500000	-2.426200000
1	-0.581970898	0.630555879	-5.483946738	7	-2.238000000	-4.713700000	-2.688500000
1	-1.419412401	-0.583991238	-4.527064386	7	-0.075000000	-5.141300000	-2.886400000
1	1.286596190	1.725436334	-4.120530368	7	2.251600000	-4.584600000	-2.965700000
1	0.487479015	2.790190859	-2.953926217	7	4.012700000	-3.242200000	-2.926300000
1	-0.073560543	2.733604377	-4.609756162	7	5.086700000	-1.105400000	-2.785500000
1	1.881878649	1.933058255	4.701305860	7	5.098100000	1.098000000	-2.564100000
1	0.623888926	2.786734890	5.598774133	7	4.096900000	3.269900000	-2.387700000

1	0.757644567	3.009823329	3.861538751	7	2.311400000	4.566800000	-2.222100000
1	-2.204739828	1.007345793	4.422436153	6	-0.933200000	4.555400000	1.161800000
1	-1.566585400	2.592837743	3.971773713	6	-3.356900000	4.149500000	1.041700000
1	-1.551976007	2.083530317	5.657868608	1	-3.143800000	3.911000000	2.089500000
1	1.029716496	-0.338716050	5.461028846	1	-4.085100000	4.965000000	0.969900000
1	-0.729493960	-0.451983946	5.664627793	6	-3.966800000	1.752700000	1.078700000
1	0.183330588	0.796605386	6.504363322	6	-5.281700000	-0.325700000	0.923400000
				1	-4.887200000	-0.402500000	1.943300000
CB[7]•G3 exclusion complex				1	-6.378600000	-0.302700000	0.934400000

6	-4.080100000	-2.478600000	0.841900000	6	-1.995300000	5.313100000	-0.771800000
6	-3.345700000	-4.793400000	0.358400000	1	-2.678900000	6.173200000	-0.757200000
1	-3.134300000	-4.738200000	1.432600000	6	-4.801900000	3.012900000	-0.698900000
1	-4.044100000	-5.611800000	0.145300000	1	-5.505500000	3.852100000	-0.608100000
6	-0.901700000	-5.164700000	0.396100000	6	-5.456600000	1.607600000	-0.714000000
6	1.434300000	-5.847400000	-0.069600000	1	-6.544200000	1.596900000	-0.558300000
1	1.454600000	-5.759000000	1.022800000	6	-5.462900000	-2.000100000	-0.977200000
1	1.660800000	-6.877000000	-0.375800000	1	-6.556700000	-2.004700000	-0.866000000
6	3.261700000	-4.199000000	0.237500000	6	-4.818500000	-3.397300000	-1.171000000
6	5.275800000	-2.781500000	0.021700000	1	-5.528800000	-4.235000000	-1.219900000
1	6.246800000	-3.207800000	-0.258500000	6	-1.980400000	-5.636100000	-1.614900000
1	5.143300000	-2.807900000	1.109600000	1	-2.639800000	-6.512100000	-1.701700000
6	4.928800000	-0.374700000	0.488300000	6	-0.465900000	-5.941300000	-1.756400000
6	5.043300000	2.086400000	0.525300000	1	-0.220700000	-6.998000000	-1.937900000
1	6.014900000	2.593800000	0.470900000	6	3.048400000	-5.117700000	-1.892900000
1	4.787400000	1.854800000	1.565800000	1	3.282000000	-6.175400000	-2.082800000
6	2.965300000	3.385200000	0.797900000	6	4.277100000	-4.171300000	-1.860300000
6	1.390500000	5.296200000	0.844800000	1	5.247300000	-4.664200000	-2.019000000
1	1.388000000	5.025800000	1.906300000	6	5.857400000	-0.900900000	-1.585300000
1	1.679300000	6.344400000	0.712500000	1	6.859600000	-1.337500000	-1.701400000
6	-1.058000000	4.386000000	-2.704100000	6	5.827700000	0.640000000	-1.411300000
6	-3.510300000	4.260600000	-2.503200000	1	6.815300000	1.121300000	-1.370300000
1	-3.392000000	4.090200000	-3.579400000	6	4.249200000	3.874500000	-1.091400000
1	-4.160900000	5.123000000	-2.316800000	1	5.240200000	4.340700000	-1.005400000
6	-4.366800000	1.976500000	-2.752600000	6	3.050400000	4.853700000	-1.013800000
6	-5.721000000	-0.068300000	-2.602000000	1	3.320100000	5.918000000	-0.974300000
1	-5.569200000	0.002200000	-3.685200000	6	1.674700000	-1.243300000	1.398200000
1	-6.788500000	-0.109000000	-2.357700000	6	0.697800000	-2.372200000	1.686300000
6	-4.305900000	-2.035000000	-3.007500000	6	-0.716100000	-1.840100000	1.514600000
6	-3.554400000	-4.365200000	-3.145100000	6	1.490300000	-0.701800000	-0.025200000
1	-3.457100000	-4.045100000	-4.189200000	6	-0.183000000	0.929100000	0.829300000
1	-4.211000000	-5.238700000	-3.061100000	6	-0.914800000	-1.329000000	0.082900000
6	-1.118400000	-4.435800000	-3.426400000	6	0.059600000	-0.180300000	-0.199800000
6	1.169400000	-5.297900000	-3.581600000	6	0.896800000	-2.894500000	3.105700000
1	1.030600000	-4.867500000	-4.580400000	6	1.641700000	-0.629200000	3.841200000
1	1.423400000	-6.362900000	-3.643900000	6	0.661700000	-1.769800000	4.104100000
6	2.824100000	-3.489600000	-3.559400000	6	-0.757900000	-1.227100000	3.954300000
6	5.001100000	-2.358100000	-3.478500000	6	-0.995900000	-0.093400000	4.956100000
1	5.977700000	-2.855200000	-3.465300000	6	-0.015000000	1.053300000	4.683900000
1	4.690200000	-2.128700000	-4.504600000	6	1.418300000	0.526000000	4.821800000
6	4.669300000	0.067000000	-3.358300000	6	1.454500000	-0.126800000	2.411200000

6	5.098100000	2.461500000	-3.020300000	6	-0.216700000	1.535000000	3.246800000
1	4.857500000	2.440700000	-4.089400000	6	-0.954100000	-0.726600000	2.525800000
1	6.087000000	2.901600000	-2.849400000	6	0.034600000	0.401200000	2.254800000
6	2.963400000	3.679100000	-3.037500000	7	-0.151900000	0.366800000	-1.638900000
6	1.203700000	5.353100000	-2.691900000	7	-0.261500000	2.223600000	5.657500000
1	1.417500000	6.418700000	-2.547200000	1	2.690700000	-1.625800000	1.506200000
1	1.090600000	5.121700000	-3.757300000	1	0.867500000	-3.190300000	0.982300000
6	-0.488000000	5.674500000	-0.836900000	1	-1.422200000	-2.649600000	1.706000000
1	-0.268900000	6.750500000	-0.877800000	1	2.218400000	0.096900000	-0.168700000

1	1.708600000	-1.502100000	-0.736200000	8	2.956040658	1.997673988	-3.614744505
1	-1.208700000	1.288700000	0.784700000	8	4.134639586	-1.817801607	2.407823483
1	0.497500000	1.767000000	0.678800000	8	1.356114828	-4.219609723	2.857265211
1	-0.742800000	-2.164400000	-0.597600000	8	-2.010510230	-3.512826300	3.437456477
1	-1.950600000	-1.002600000	-0.021600000	8	-3.629558769	-0.192617744	3.810529294
1	0.200000000	-3.714800000	3.284300000	8	-1.839282275	3.326469794	3.368843917
1	1.910200000	-3.286100000	3.204800000	8	1.473691246	4.382571001	2.767045100
1	2.667500000	-0.995700000	3.950700000	8	3.890832458	2.042980005	2.258261578
1	0.806100000	-2.157500000	5.118600000	7	4.502020797	-1.137743415	-2.023539125
1	-1.478600000	-2.028700000	4.146000000	7	3.747877038	-3.228450013	-1.870695599
1	-0.855500000	-0.507900000	5.952800000	7	1.970969723	-4.834839667	-1.511108980
1	-2.027300000	0.239200000	4.846400000	7	-0.126859529	-5.483966019	-1.155788962
1	2.141800000	1.298000000	4.568500000	7	-2.469968205	-4.981145292	-0.764910568
1	1.615600000	0.163000000	5.830300000	7	-4.109565340	-3.506006426	-0.490553301
1	2.171700000	0.677300000	2.224200000	7	-5.045456526	-1.283474737	-0.333235948
1	-1.238800000	1.869000000	3.090700000	7	-4.938321900	0.937259535	-0.359307918
1	0.469100000	2.345000000	3.009600000	7	-3.968961030	3.139492371	-0.524662953
1	-1.977600000	-0.355600000	2.420100000	7	-2.431182086	4.720207679	-0.800152729
6	0.931500000	1.291100000	-2.032600000	7	-0.187992746	5.468558729	-1.246410070
6	-0.195400000	-0.709600000	-2.649100000	7	1.938913585	4.957798161	-1.619685009
6	-1.422200000	1.110200000	-1.744400000	7	3.728894598	3.368424413	-1.949072729
6	-0.401400000	1.753200000	7.049400000	7	4.510902351	1.288936871	-2.067309679
6	0.849700000	3.195900000	5.627100000	7	4.904678005	-1.095010878	0.366585136
6	-1.491900000	2.965600000	5.311000000	7	4.112170505	-3.165314362	0.538736841
1	-1.365000000	2.038800000	-1.185100000	7	2.366226353	-4.802193390	0.874382467
1	-2.248600000	0.506800000	-1.379400000	7	0.277902876	-5.464952105	1.247620827
1	-1.612100000	1.349500000	-2.790700000	7	-2.062438748	-4.948717540	1.637905875
1	0.648800000	-1.386100000	-2.548900000	7	-3.716331589	-3.483482565	1.895391465
1	-0.146000000	-0.274300000	-3.645700000	7	-4.692708417	-1.274332225	2.078696345
1	-1.121700000	-1.274200000	-2.588300000	7	-4.542392543	0.947917774	2.032293524
1	1.837700000	0.742000000	-2.274700000	7	-3.576189729	3.167833604	1.861401766
1	1.132000000	2.004900000	-1.238800000	7	-2.027252869	4.738865358	1.574262405
1	0.633200000	1.837300000	-2.927700000	7	0.243574577	5.440738002	1.139144988
1	1.730900000	2.786900000	6.110800000	7	2.389505840	5.020683746	0.761681125
1	0.546200000	4.093400000	6.160200000	7	4.135250487	3.399016144	0.424830715
1	1.087500000	3.465900000	4.602900000	7	4.903732102	1.316341559	0.318742940
1	-2.321800000	2.284200000	5.153000000	6	3.731037181	-2.094331073	-2.643854445
1	-1.331200000	3.553600000	4.411900000	6	3.122601642	-4.455189901	-2.291640516
1	-1.741900000	3.634300000	6.130700000	1	2.768847638	-4.288171117	-3.315916010
1	0.413500000	1.086700000	7.315300000	1	3.858129186	-5.267995054	-2.259492909
1	-1.347800000	1.239300000	7.185500000	6	0.695634787	-4.805853727	-2.020114036

1	-0.375200000	2.610100000	7.718700000

CB[7]•G4

8	3.175657078	-1.968812860	-3.710667652
8	0.368475228	-4.313233694	-3.075911154
8	-2.987267201	-3.555197693	-2.497912526
8	-4.560301184	-0.210761607	-2.314064081
8	-2.785481631	3.223595697	-2.501540691
8	0.357746327	4.342059218	-3.170092271
6	-1.501154318	-5.781775645	-1.467439353
1	-1.632177844	-5.562647036	-2.533566676
1	-1.693467302	-6.839436140	-1.256638759
6	-3.154732144	-3.955999618	-1.368872134
6	-5.164484652	-2.608684433	-0.883723679
1	-5.098427048	-2.502793949	-1.973214075
1	-6.129194200	-3.040530423	-0.590625013
6	-4.803365665	-0.191314572	-1.129025319
6	-5.011135263	2.245830425	-0.954589979

1	-4.894047297	2.102768754	-2.035084449	6	-2.964985668	-5.273104213	0.559120294
1	-5.987224177	2.696275202	-0.729690859	1	-3.262359025	-6.329203127	0.623285021
6	-3.033344127	3.642036615	-1.392764765	6	-4.119341050	-4.252642351	0.742970734
6	-1.587772333	5.633539532	-1.529856305	1	-5.110029219	-4.698719164	0.910197971
1	-1.889072959	6.660735210	-1.302041994	6	-5.537700377	-0.907729358	0.970349666
1	-1.724815773	5.416590167	-2.595313361	1	-6.548674275	-1.316062793	1.119586917
6	0.668275995	4.859519136	-2.119340761	6	-5.452565748	0.641437832	0.953684171
6	3.096046873	4.587396517	-2.393834366	1	-6.413825323	1.154275150	1.110233570
1	3.829813043	5.399536421	-2.365504935	6	-4.039707611	3.897095725	0.701255637
1	2.751916490	4.414065061	-3.419663748	1	-5.060964395	4.266082262	0.866124026
6	3.657577345	2.192982670	-2.641991006	6	-2.964101695	4.997611678	0.508164999
6	4.911938050	0.062327501	-2.713156487	1	-3.335986667	6.029582383	0.564341978
1	4.430435420	0.035197610	-3.697471215	6	0.495261215	6.077844423	-0.133866254
1	6.004702378	0.062071322	-2.824127952	1	0.256515074	7.148706209	-0.078765912
6	4.343005218	-2.002103911	1.230362568	6	1.987419680	5.752006712	-0.412778688
6	3.699717064	-4.372755775	1.206091022	1	2.634478482	6.627837520	-0.557729808
1	3.702141769	-4.153680397	2.280591476	6	4.710351053	3.322336818	-0.892755013
1	4.404390144	-5.179417401	0.969900290	1	5.464181574	4.108782578	-1.032954026
6	1.327606487	-4.751833308	1.771271906	6	5.249790531	1.870189293	-0.967863560
6	-0.917564846	-5.744114430	2.000026019	1	6.329998105	1.781951189	-1.145825234
1	-0.689907173	-5.502777089	3.044887531	6	0.935362999	-1.069533335	-1.311880210
1	-1.169727718	-6.804169293	1.887043311	6	-0.459691378	-1.666944642	-1.165676577
6	-2.527395928	-3.923955843	2.423446064	6	-1.487582884	-0.539803874	-1.120482661
6	-4.604197776	-2.606421259	2.617935160	6	1.000490366	-0.268729596	-2.605717465
1	-4.194085101	-2.505510509	3.629767244	6	0.265782950	1.761482574	-1.339324654
1	-5.604436684	-3.055342499	2.644279169	6	-1.421079367	0.272819824	-2.413461310
6	-4.208293196	-0.178661396	2.748858481	6	-0.020715798	0.859584565	-2.540142422
6	-4.423793059	2.267488321	2.605373260	6	-0.520599289	-2.482023015	0.114990223
1	-3.975757102	2.136672935	3.597141882	6	1.166771127	-0.989458035	1.191430384
1	-5.422631640	2.715460906	2.695272945	6	-0.225771370	-1.601078113	1.317144854
6	-2.421204758	3.700092830	2.369681860	6	-1.261307076	-0.484097669	1.383940563
6	-0.950360387	5.635511754	1.921472465	6	-0.975777566	0.386683273	2.600395702
1	-1.297006439	6.667892757	1.808186453	6	0.410701979	1.000317342	2.454175104
1	-0.685703938	5.429745215	2.964745772	6	1.455690745	-0.107399224	2.405954237
6	1.377267905	4.885919574	1.669026456	6	1.232162630	-0.181127904	-0.103655224
6	3.742943211	4.634636311	1.055160956	6	0.487646715	1.831295532	1.173156011
1	3.801333363	4.476097063	2.137980481	6	-1.199327167	0.338070631	0.096547600
1	4.426664051	5.430142806	0.742906151	6	0.198870997	0.948428285	-0.043822559
6	4.264985056	2.226843226	1.121549657	7	0.092520257	1.667400705	-3.786674906
6	5.507360346	0.121383457	0.845329790	7	0.653939085	1.892619835	3.622021264
1	6.577886837	0.120493402	0.599946387	1	1.661244980	-1.885891709	-1.349690276

1	5.362481170	0.133432408	1.931847590	1	-0.673848707	-2.315510640	-2.022427827
6	5.232783883	-1.686867830	-0.905412017	1	-2.481834105	-0.983552321	-1.030690442
1	6.315934382	-1.618419960	-1.088807976	1	1.999884190	0.132068212	-2.749677686
6	4.689393392	-3.135095859	-0.783647131	1	0.789210902	-0.937440563	-3.441786334
1	5.448909193	-3.925914083	-0.877577039	1	-0.478301921	2.557386724	-1.306918046
6	2.052697247	-5.595875687	-0.287918519	1	1.255887383	2.205658367	-1.439402648
1	2.777817330	-6.414906661	-0.396583167	1	-1.644395759	-0.394450652	-3.247456661
6	0.589484953	-6.046680699	-0.036069647	1	-2.172804339	1.061678204	-2.408404618
1	0.436765617	-7.134502861	-0.001214915	1	-1.511216001	-2.918348302	0.223151577

1	0.209822736	-3.286571561	0.064282268
1	1.897816637	-1.800670642	1.159730882
1	-0.273758313	-2.202523237	2.231745400
1	-2.252768489	-0.934079676	1.480384937
1	-1.034826932	-0.233736418	3.496185012
1	-1.727773255	1.165573446	2.689747030
1	2.460382802	0.310075951	2.345011331
1	1.408214907	-0.731549118	3.299745189
1	2.236469451	0.246301652	-0.208518288
1	-0.239242972	2.642150138	1.215105219
1	1.487690923	2.255783756	1.084232237
1	-1.945856770	1.139768731	0.144493925
1	1.090551462	1.886401454	-3.961046621
1	-0.279339454	1.149547526	-4.587135047
1	-0.405975058	2.566592542	-3.699955166
1	1.469263450	2.505234543	3.465364690
1	-0.169284400	2.507672759	3.757943379
1	0.801950252	1.342052651	4.471798113

CB[8]•G1

7	0.775654155	5.523730327	-0.897951829
6	1.212489738	6.178854910	0.308465111
1	1.002946838	7.255914001	0.258500232
7	0.648532478	5.618686386	1.512074185
6	1.783014523	4.834502102	-1.519144546
8	1.687469626	4.229185749	-2.564318406
6	1.570443414	4.917079846	2.244910008
8	1.367738864	4.369784326	3.308744474
7	2.933416471	5.022912400	-0.800798202
6	2.711737199	5.792931212	0.394606609
1	3.415095474	6.635200564	0.443639292
7	2.779586040	5.018519309	1.610438504
6	4.241403484	4.745081064	-1.332686907
1	4.865875673	5.637916760	-1.208939408
1	4.108662877	4.501441852	-2.392896369
6	4.015175118	4.668525249	2.252532896
1	3.765025304	4.392039408	3.283392965
1	4.687750513	5.535861195	2.230844054
7	4.909549114	3.619044602	-0.741795391
6	5.574540610	3.645172271	0.534966030
1	6.195010355	4.547379872	0.624294115
6	6.608233964	0.498116729	-1.211672822
1	6.365269289	0.470961360	-2.280257257
1	7.691481163	0.557292042	-1.055220384
6	6.440770966	0.499919960	2.348741342
1	7.529304546	0.617355615	2.289136533
1	6.102407051	0.480767494	3.391146073
7	6.127860682	-0.732967149	-0.640422104
6	6.651668978	-1.304638365	0.573947593
1	7.744794983	-1.202628314	0.604451914
7	6.071718545	-0.763977628	1.778656227
6	5.357291357	-1.620324528	-1.342691098
8	4.814075248	-1.403255271	-2.403243197
6	5.270617806	-1.659957304	2.433819544
8	4.708320724	-1.474935281	3.492318013
7	5.375066661	-2.820836211	-0.685151627
6	6.119242965	-2.761059601	0.546237354
1	6.888006185	-3.545148668	0.567530763
7	5.302857699	-2.836662924	1.733578538
6	4.960280834	-4.048604022	-1.309089683
1	5.758539427	-4.790594444	-1.187356549
1	4.787552395	-3.827101598	-2.368551968
6	4.779054029	-4.059658321	2.268657516
1	5.551797162	-4.836781636	2.215222515
1	4.501728690	-3.851388765	3.308517244
7	3.730286884	-4.596028288	-0.807153425
6	3.627739654	-5.347789380	0.416061498
1	4.443549161	-6.080940843	0.483291103
7	3.594516399	-4.536700789	1.608023424
6	2.595816842	-4.673488829	-1.571839929
8	2.453389509	-4.205387525	-2.677852004
6	2.373334845	-4.558540864	2.226419825
8	2.091373732	-4.003619372	3.268011059
7	1.691818539	-5.460237298	-0.906156147
6	2.199056128	-5.947141005	0.350011546
1	2.146092527	-7.044135827	0.384777375
7	1.545810922	-5.383480012	1.507727240
6	0.508477830	-5.969145728	-1.541003248
1	0.536314024	-7.066854130	-1.523514138
1	0.524947410	-5.593013587	-2.570245150
6	0.363436878	-5.951138729	2.094344309
1	0.448846763	-7.046852857	2.077885313

7	4.686451060	3.541295071	1.668479099
6	5.158066112	2.469189125	-1.440382914
8	4.777654298	2.225015747	-2.563048116
6	4.835007052	2.360154327	2.348876686
8	4.252445817	2.048553720	3.366394505
7	5.991348713	1.685934249	-0.688833407
6	6.348152427	2.300937286	0.564342996
1	7.440010572	2.388101072	0.649255618
7	5.814926372	1.634175013	1.726412567

1	0.307592027	-5.580345884	3.124351972
7	-0.862110811	-5.569163512	1.452980292
6	-1.310799894	-6.147323071	0.209643111
1	-1.125305382	-7.230073485	0.206556256
7	-0.730663281	-5.533210567	-0.955354205
6	-1.855354455	-4.895355902	2.114903135
8	-1.753815307	-4.370383280	3.204033806
6	-1.633084281	-4.760584497	-1.640883373
8	-1.405447974	-4.130742040	-2.649343026

7	-3.002982394	-5.003582602	1.375083851	6	-2.641051486	4.675186160	2.152141222
6	-2.800866069	-5.725209013	0.142843621	8	-2.467104076	4.218630452	3.262332289
1	-3.523922776	-6.548545299	0.065414452	6	-2.459689394	4.416666234	-1.601015545
7	-2.854570242	-4.897685245	-1.033646510	8	-2.161280299	3.775371105	-2.583315944
6	-4.301365861	-4.721133683	1.923512512	7	-1.765905254	5.475119976	1.465394835
1	-4.937822693	-5.607087044	1.799928741	6	-2.285311826	5.906670625	0.192357239
1	-4.151471291	-4.490431266	2.984391261	1	-2.236479308	7.001278526	0.114366554
6	-4.084880713	-4.541416224	-1.682201151	7	-1.635141985	5.289962772	-0.936073245
1	-3.823454264	-4.201814280	-2.691217440	6	-0.600777577	6.050218503	2.075558188
1	-4.733566133	-5.426517939	-1.720057576	1	-0.663773323	7.144636537	2.001680065
7	-4.968221518	-3.587260674	1.348762591	1	-0.605933276	5.728834564	3.123243239
6	-5.661735506	-3.620235745	0.085801667	6	-0.459720325	5.834070666	-1.559973131
1	-6.248147319	-4.545343924	0.001774870	1	-0.566487343	6.925933389	-1.619818291
7	-4.804458465	-3.462866030	-1.063204877	1	-0.399099048	5.392248332	-2.561118538
6	-5.204522929	-2.435685506	2.052126261	6	1.491627874	0.920658882	-0.614535836
8	-4.782390010	-2.179505138	3.160590373	6	1.805001118	-0.479701838	-0.088893783
6	-5.024942620	-2.281415388	-1.725793649	6	1.053839467	-1.485558385	-0.959699142
8	-4.465449001	-1.926977117	-2.739126298	6	1.935243151	1.034216324	-2.073797304
7	-6.083912287	-1.674590392	1.330223280	6	-0.338899113	0.317833829	-2.798507231
6	-6.486938454	-2.307383139	0.095223221	6	1.454802259	-1.369128158	-2.432538914
1	-7.577785095	-2.435290492	0.078674028	6	1.160440327	0.044183057	-2.948089372
7	-6.048467520	-1.629476894	-1.093871666	6	1.372715936	-0.603983741	1.370190043
6	-6.713391657	-0.502450748	1.873248403	6	-0.461259571	1.061124336	0.977841795
1	-6.456503459	-0.479478747	2.938799511	6	-0.129458764	-0.346474219	1.480121974
1	-7.797648830	-0.578994383	1.729400598	6	-0.894936592	-1.365534582	0.633303334
6	-6.717518435	-0.493500321	-1.665244125	6	-2.396433652	-1.114869727	0.735250874
1	-7.797415401	-0.618647098	-1.533863233	6	-2.711471026	0.290249409	0.227714515
1	-6.444768988	-0.466269001	-2.726586415	6	-1.964086441	1.318145233	1.073379076
7	-6.257559879	0.739802912	1.309762679	6	-0.008080525	1.182695673	-0.478442590
6	-6.813561765	1.326636944	0.112966619	6	-2.273174038	0.418842828	-1.227499024
1	-7.910098649	1.264289128	0.141262661	6	-0.447171438	-1.239447475	-0.822910587
7	-6.318635390	0.771659953	-1.119017373	6	-0.768796290	0.166361752	-1.335622119
6	-5.464860898	1.614599781	2.007638430	7	1.589604583	0.188833382	-4.416256879
8	-4.940472945	1.398986888	3.079784906	1	-3.790203524	0.468418873	0.310220090
6	-5.500988001	1.632811575	-1.800748105	1	2.039144236	1.660554058	-0.013734541
8	-4.998586267	1.434605813	-2.883002721	1	2.885013595	-0.665037394	-0.160774463
7	-5.445886383	2.805406448	1.328227535	1	1.281948284	-2.501561285	-0.612465919
6	-6.228721468	2.763047860	0.116812003	1	1.780084119	2.059709145	-2.405514945
1	-6.971781220	3.572525879	0.121107918	1	2.998779655	0.810530872	-2.114251270
7	-5.451116887	2.805704315	-1.094648168	1	-0.934019692	-0.378579501	-3.390306668
6	-5.005065441	4.029152398	1.940573910	1	-0.590875029	1.336503644	-3.092335412

1	-5.800532283	4.779383140	1.841547497	1	2.513750087	-1.605566302	-2.527038275
1	-4.806977435	3.804151232	2.994886702	1	0.882017791	-2.121943272	-2.972194781
6	-4.887998868	3.998826308	-1.657217289	1	1.603369396	-1.600538424	1.762147148
1	-5.636127362	4.800795956	-1.627889198	1	1.917521308	0.114645584	1.992871565
1	-4.617736475	3.748483281	-2.689740765	1	0.068695336	1.796415071	1.601240907
7	-3.785503323	4.568436858	1.406066189	1	-0.437680698	-0.442614648	2.529919545
6	-3.711475599	5.299129600	0.162773231	1	-0.671244647	-2.374690633	1.009499610
1	-4.534396809	6.024081102	0.102646333	1	-2.723423165	-1.223541977	1.774379405
7	-3.693931591	4.464159553	-1.007775643	1	-2.931404437	-1.853859207	0.130977149

1	-2.186633217	2.326810679	0.710947586
1	-2.292560235	1.265337127	2.116477926
1	-0.232482514	2.194950124	-0.840365108
1	-2.817715209	-0.297122281	-1.849190089
1	-2.506160641	1.417336360	-1.605829218
1	-0.989660776	-1.973362379	-1.431346954
6	1.041549157	1.419717640	-5.023216509
6	3.058521023	0.255057981	-4.561079642
6	1.125390413	-0.955649920	-5.226048451
1	1.687692227	-1.849696186	-4.972520130
1	1.281089158	-0.727813707	-6.277492121
1	0.067833215	-1.141767529	-5.064566645
1	3.443215142	1.198837800	-4.185669472
1	3.308125241	0.169592305	-5.615002782
1	3.542453741	-0.554601731	-4.024181589
1	-0.029769894	1.330742635	-5.173917871
1	1.519066214	1.574174251	-5.987324967
1	1.245460460	2.284385293	-4.397047986

CB[8]•G2

7	-6.243851264	0.786983128	-0.954626446
6	-6.713212778	1.272680928	0.319802048
1	-7.804309349	1.168059630	0.388709689
7	-6.083365317	0.654143706	1.459914299
6	-5.542886106	1.728857812	-1.649096336
8	-5.084984008	1.595793372	-2.764617427
6	-5.256475897	1.511739870	2.136689905
8	-4.653423477	1.263479306	3.158823481
7	-5.506982667	2.875404255	-0.904860955
6	-6.180395873	2.728976505	0.360859041
1	-6.947231595	3.506224771	0.479855468
7	-5.292646360	2.725767174	1.499469810
6	-5.055414288	4.133512055	-1.433810131
1	-5.822543906	4.894109388	-1.249758972
1	-4.903172639	3.986427791	-2.508882739
6	-4.812450647	3.922388760	2.133241156
1	-4.527166790	3.647957033	3.155385951
1	-5.611241489	4.674639523	2.138002063
7	-3.804591189	4.601381515	-0.890036213
6	-3.695381605	5.329808536	0.348752300
1	-4.514343501	6.055404207	0.442230049
6	-0.589454767	5.995121336	-1.619839516
1	-0.605640368	5.634625478	-2.654840077
1	-0.644299261	7.091227129	-1.587009005
6	-0.419381382	5.919919272	2.017330300
1	-0.498496165	7.016027501	2.024404333
1	-0.350117113	5.529114617	3.038998106
7	0.664868418	5.573704208	-1.058099271
6	1.236544511	6.164655188	0.123378525
1	1.035466984	7.244547758	0.151833552
7	0.794305766	5.542341540	1.347687666
6	1.592591256	4.873875388	-1.792784273
8	1.381816265	4.321009758	-2.847252690
6	1.802022241	4.872709821	1.993282085
8	1.708768161	4.319664396	3.068830207
7	2.804605955	4.994760939	-1.165939086
6	2.733895408	5.770814304	0.044515474
1	3.441864872	6.609891949	0.000999381
7	2.946399981	5.009831304	1.251977319
6	4.039978457	4.611536044	-1.787966567
1	4.713251991	5.478471483	-1.806318548
1	3.788866936	4.287729200	-2.804734609
6	4.248932065	4.762258220	1.808600221
1	4.866280613	5.660494728	1.677966788
1	4.104179136	4.536418268	2.871407108
7	4.722482050	3.510504021	-1.161054917
6	5.605718281	3.658377953	-0.031086508
1	6.201345508	4.576485551	-0.128833176
7	4.940257163	3.636818703	1.247325785
6	4.907305299	2.318458164	-1.814702031
8	4.325938302	1.964589905	-2.816468487
6	5.202265544	2.498356826	1.964458092
8	4.818220316	2.262653680	3.090523308
7	5.923883748	1.645383017	-1.191429000
6	6.418309294	2.337489454	-0.031996587
1	7.508753270	2.454525439	-0.096427235
7	6.063855132	1.728320163	1.228527279
6	6.568529097	0.502115749	-1.775657835
1	7.653656581	0.628917524	-1.692195629
1	6.252715402	0.460855504	-2.824760670
6	6.701981634	0.558764101	1.766505264
1	7.782403146	0.628778173	1.594420810

7	-3.643133673	4.482561208	1.514379868
6	-2.657287844	4.668164032	-1.626873750
8	-2.490683149	4.155843746	-2.716522333
6	-2.425345651	4.514724892	2.140258949
8	-2.136728452	3.944469368	3.170555855
7	-1.756702106	5.455192230	-0.971623569
6	-2.269309138	5.938536008	0.287552554
1	-2.220907646	7.034840045	0.326570138
7	-1.611800150	5.368005269	1.437681737

1	6.471982582	0.549280028	2.838347627
7	6.229869862	-0.689444155	1.229309010
6	6.746931130	-1.288977538	0.023542997
1	7.842893904	-1.212869378	0.008762306
7	6.196812101	-0.758010130	-1.196919154
6	5.427992764	-1.543120994	1.939000265
8	4.913892333	-1.312342754	3.013979701
6	5.404447863	-1.657711160	-1.859607682
8	4.868334212	-1.480039890	-2.930517801

7	5.385657621	-2.740585302	1.271348744	6	-5.000751975	-2.531420850	2.091594301
6	6.181527045	-2.732630929	0.066178531	8	-4.514898666	-2.298985551	3.178496602
1	6.934191821	-3.531986254	0.107875625	6	-4.945810268	-2.293030893	-1.673533432
7	5.418869830	-2.829739316	-1.150428999	8	-4.407089477	-1.906206237	-2.686703054
6	4.877249251	-3.937093533	1.883103695	7	-5.911194929	-1.750610020	1.432650726
1	5.658537316	-4.708485765	1.858088792	6	-6.354016412	-2.331672101	0.188582466
1	4.620027631	-3.674192996	2.915929852	1	-7.447507206	-2.434091589	0.187256527
6	4.951943046	-4.064019758	-1.715207890	7	-5.912367242	-1.613496667	-0.977655830
1	4.729418280	-3.859220949	-2.768874532	6	-6.514642137	-0.592903742	2.029514405
1	5.739230819	-4.821719719	-1.616314317	1	-7.604791499	-0.668941948	1.940286220
7	3.683717742	-4.468448214	1.281262271	1	-6.205188632	-0.589796591	3.081083858
6	3.702848225	-5.304783380	0.104682264	6	-6.611175209	-0.480358915	-1.525889567
1	4.542693706	-6.011148143	0.157541876	1	-7.687598919	-0.635310003	-1.393283467
7	3.742645002	-4.574900937	-1.133538560	1	-6.351318965	-0.427577784	-2.589422789
6	2.493905167	-4.543009574	1.958850448	6	-0.403436641	-1.294581675	-1.871344944
8	2.238848366	-3.991212274	3.008826207	6	-1.295879197	-1.510128935	-0.646876013
6	2.556928538	-4.628990374	-1.818389138	6	-1.768245876	-0.147270131	-0.135691591
8	2.325718370	-4.115498440	-2.889823795	6	-1.188352158	-0.576510209	-2.968365553
7	1.676376900	-5.417196705	1.290457709	6	-0.423327539	1.619584139	-2.046940552
6	2.291247504	-5.944767262	0.098126353	6	-2.540918153	0.587273250	-1.231501327
1	2.270789539	-7.043186213	0.115475566	6	-1.636000550	0.785381424	-2.446411069
7	1.707346674	-5.450698555	-1.122086286	6	-0.516448423	-2.240543464	0.441702317
6	0.521507341	-6.017905926	1.900574897	6	1.605416197	-1.184910711	-0.362573967
1	0.483980989	-5.657873896	2.935158187	6	0.696522392	-1.407703428	0.847545137
1	0.637715929	-7.110270953	1.870525302	6	0.242994766	-0.044762200	1.375298285
6	0.537350766	-6.024426778	-1.728419750	6	1.457855601	0.785959364	1.782344308
1	0.621656441	-7.118865577	-1.698922301	6	2.347438785	1.007007699	0.561334499
1	0.512754188	-5.659715778	-2.761949582	6	2.816038005	-0.344420863	0.030839894
7	-0.734964528	-5.662916261	1.301315484	6	0.815163995	-0.467379561	-1.456773766
6	-1.230230544	-6.241560113	0.073198242	6	1.564034991	1.737165148	-0.523219273
1	-1.044439964	-7.324600383	0.066059489	6	-0.547346746	0.675302961	0.280161487
7	-0.704855121	-5.638297260	-1.122187659	6	0.354246613	0.900946440	-0.939973175
6	-1.717320181	-5.028787777	2.017298074	7	-2.393761450	1.496527391	-3.516826339
8	-1.591370205	-4.540293698	3.120725233	1	3.215647814	1.603387852	0.862448632
6	-1.636630495	-4.880971993	-1.784798214	1	-0.067151091	-2.264831798	-2.252339139
8	-1.466603216	-4.301384382	-2.832847409	1	-2.163212531	-2.112559017	-0.938546427
7	-2.886073060	-5.129989744	1.312368791	1	-2.413652986	-0.291869827	0.742025904
6	-2.723117045	-5.821570071	0.060189132	1	-0.542666335	-0.461566780	-3.839226375
1	-3.443559320	-6.648622099	-0.009786198	1	-2.052932075	-1.183611561	-3.242179239
7	-2.821307037	-4.971539151	-1.100377830	1	-0.739127487	2.597601573	-1.681867960
6	-4.167356509	-4.832468764	1.889549619	1	0.240753449	1.781518010	-2.897500045

1	-4.827063476	-5.699228602	1.755301091	1	-3.405765306	-0.008080924	-1.521729423
1	-3.993719970	-4.632309189	2.953114100	1	-2.878521768	1.551884999	-0.847588250
6	-4.069785567	-4.592626445	-1.706701144	1	-1.147679087	-2.415805325	1.319414496
1	-4.736498199	-5.464581368	-1.724571000	1	-0.180073501	-3.212013704	0.069050928
1	-3.830047794	-4.261597806	-2.724018127	1	1.948974828	-2.154844824	-0.747437025
7	-4.809071208	-3.667573047	1.349619316	1	1.249333722	-1.930081368	1.640206985
6	-5.561198120	-3.662332658	0.119128702	1	-0.401602669	-0.193404390	2.252671182
1	-6.170912393	-4.572777970	0.045662875	1	2.024404701	0.266936126	2.562351330
7	-4.751206877	-3.503513552	-1.063034021	1	1.141575885	1.745654180	2.203491691

1	3.459290590	-0.200926002	-0.841806344
1	3.386733419	-0.859798580	0.807301485
1	1.474278696	-0.327238534	-2.322377969
1	1.227864713	2.703797799	-0.136069371
1	2.200265855	1.916825469	-1.392831518
1	-0.879404648	1.644202170	0.679112236
1	-2.409695802	2.519966560	-3.332796643
1	-3.380135539	1.189523197	-3.537565048
1	-1.962857153	1.335862223	-4.430843189

CB[8]•G3

7	-3.310685868	5.121025149	-0.991117037
6	-3.195983663	5.924961476	0.199247287
1	-4.068107346	6.585432299	0.300933717
7	-3.007425560	5.151538293	1.402762217
6	-2.226524830	5.250248446	-1.821755336
8	-2.092876367	4.716447667	-2.899774027
6	-1.762275809	5.332264368	1.951688911
8	-1.369969476	4.847330146	2.988922485
7	-1.362071085	6.146612756	-1.250049617
6	-1.836264168	6.648800017	0.016445976
1	-1.887173198	7.745929846	-0.007596234
7	-1.073843492	6.212766252	1.159096562
6	-0.228422445	6.675655104	-1.958032691
1	-0.214785892	7.765759449	-1.849166561
1	-0.354250549	6.385151921	-3.007542892
6	0.186979200	6.781536961	1.549751362
1	0.316254581	6.554935421	2.614475463
1	0.158907634	7.863098194	1.377030599
7	1.039449537	6.147448307	-1.535008670
6	1.795942890	6.659695749	-0.420433308
1	1.832881473	7.756895408	-0.461078397
7	1.327848334	6.226892543	0.873703188
6	1.738734989	5.229795612	-2.274040755
8	1.352493933	4.679040676	-3.280259857
6	2.204230078	5.377876898	1.497218934
8	2.077451119	4.907455294	2.605173670
7	2.986011679	5.097979487	-1.716350846
6	3.164925048	5.943910862	-0.561051616
1	4.028393210	6.608308887	-0.702941421
7	3.290380282	5.214533137	0.675315093
7	4.849483222	3.375919818	0.563696186
6	4.464453865	2.051434175	-2.479200354
8	3.836315888	1.824269324	-3.488602586
6	4.927026805	2.233793288	1.318990070
8	4.548613317	2.106945572	2.461757245
7	5.262061190	1.154027126	-1.814250736
6	5.974925811	1.761568829	-0.717733759
1	7.059210468	1.637336038	-0.849480834
7	5.566387039	1.275800173	0.575274165
6	5.669659870	-0.084895518	-2.421724626
1	6.762475618	-0.087628103	-2.535671195
1	5.179659182	-0.128946828	-3.401196963
6	6.118994153	0.094667106	1.181238154
1	7.206753999	0.086054838	1.031172973
1	5.874471480	0.149049169	2.248231832
7	5.273439270	-1.263163639	-1.698551910
6	5.985747951	-1.758287092	-0.544624863
1	7.069667404	-1.654860903	-0.684241407
7	5.570175439	-1.134928854	0.684563232
6	4.451662722	-2.210935262	-2.250946365
8	3.748774423	-2.052263063	-3.225350217
6	4.813365362	-1.967674865	1.464674181
8	4.315192115	-1.685877401	2.531129122
7	4.587870355	-3.372227058	-1.537077575
6	5.465077278	-3.213381935	-0.405249308
1	6.238654247	-3.992353046	-0.401842133
7	4.756088239	-3.191618380	0.850942223
6	4.202637567	-4.661690396	-2.051686147
1	5.073339486	-5.328641113	-2.013795563
1	3.872538569	-4.513225657	-3.086083561
6	4.361914390	-4.381776377	1.555190739
1	5.190653607	-5.101689749	1.535238461
1	4.139385094	-4.078236594	2.584436695
7	3.180670869	-5.013799289	1.033135673
6	3.202678925	-5.929577547	-0.080798260
1	4.098262909	-6.564057334	-0.043115858
7	3.100352460	-5.273345671	-1.361667426
6	2.032626507	-5.126040608	1.777378723
8	1.764147161	-4.474146143	2.760680273
6	1.910751807	-5.534670312	-1.990055289
8	1.601770105	-5.173464510	-3.102831027

6	4.072753044	4.479373392	-2.426892403
1	3.689723230	4.218740481	-3.420538508
1	4.903487904	5.193176491	-2.503061528
6	4.525033014	4.649803590	1.144479963
1	5.341081080	5.356326158	0.944782643
1	4.405905344	4.484089317	2.221635319
7	4.552339998	3.259574036	-1.835471053
6	5.473854532	3.228728920	-0.727091809
1	6.253721905	3.991726357	-0.860687513
7	1.264463996	-6.122259913	1.238670342
6	1.851983922	-6.683810789	0.049514265
1	1.931128201	-7.775497845	0.138507615
7	1.161328521	-6.328086887	-1.165474789
6	0.168561873	-6.725883166	1.954262871
1	0.222568891	-7.812198437	1.829218945
1	0.270999516	-6.447185474	3.009407011
6	-0.127985178	-6.833381698	-1.545920629
1	-0.232773079	-6.620225203	-2.616006332

1	-0.171400580	-7.910639744	-1.355329689	1	-4.922745300	5.281125171	2.190003806
7	-1.125393764	-6.257321501	1.544184413	1	-3.700562627	4.367026146	3.156873100
6	-1.812239001	-6.692980326	0.353452154	6	-4.539435924	4.519298103	-1.428821492
1	-1.880269085	-7.788779079	0.330696657	1	-5.361007340	5.231888620	-1.278686495
7	-1.230106513	-6.198359323	-0.867852768	1	-4.413929821	4.285973030	-2.492633015
6	-1.880829308	-5.419126609	2.317352350	6	-1.326111767	1.361202030	-1.192630667
8	-1.573165038	-4.983555344	3.403543093	6	-0.086724820	2.242877202	-1.310160134
6	-2.009262035	-5.245495789	-1.466279079	6	1.142016712	1.339694085	-1.388772224
8	-1.747660041	-4.652069057	-2.487725789	6	-1.449855439	0.447453217	-2.409056175
7	-3.074070958	-5.210671624	1.676326630	6	-0.097993925	-1.283664441	-1.227365066
6	-3.170523439	-5.945980838	0.438654949	6	1.039351878	0.440554340	-2.618696789
1	-4.059611447	-6.590593930	0.441430025	6	-0.208608341	-0.445275692	-2.518610653
7	-3.158564772	-5.100666195	-0.729756028	6	0.014249753	3.156059804	-0.096592110
6	-4.182021023	-4.569136097	2.329102873	6	-1.126278485	1.433495631	1.309245477
1	-3.853270393	-4.355526976	3.352483144	6	0.108269222	2.321803642	1.173110782
1	-5.046292758	-5.245412732	2.331747339	6	1.341802263	1.426295188	1.112560366
6	-4.346046355	-4.511757962	-1.286880381	6	1.460299244	0.591582222	2.384945245
1	-5.168536345	-5.236017276	-1.220878947	6	0.213525271	-0.284529976	2.551064542
1	-4.127775928	-4.270089156	-2.333296074	6	-1.028695850	0.613828357	2.593991436
7	-4.579222509	-3.316478966	1.738535835	6	-1.233954989	0.529976114	0.085540817
6	-5.457526311	-3.233365877	0.599469742	6	0.097115319	-1.203017110	1.316093147
1	-6.225690260	-4.016421668	0.644264720	6	1.244056094	0.515629707	-0.109789920
7	-4.749154875	-3.283787153	-0.656308111	6	0.002181985	-0.371291410	0.016504149
6	-4.452566677	-2.113380673	2.381364190	7	-0.319440819	-1.333490947	-3.772813421
8	-3.752814489	-1.890858158	3.345386959	7	0.319143780	-1.091413815	3.859599621
6	-4.815182972	-2.100107286	-1.343712692	1	-2.215387419	2.000185730	-1.152739063
8	-4.320601095	-1.880924869	-2.426408655	1	-0.154708924	2.853816704	-2.218036903
7	-5.280799327	-1.206999359	1.772147318	1	2.034918838	1.965236478	-1.493444896
6	-5.988401094	-1.776111936	0.649973991	1	-2.355801019	-0.146434956	-2.292175073
1	-7.073161215	-1.672020195	0.782503348	1	-1.569883145	1.078958022	-3.289690429
7	-5.576217116	-1.225950431	-0.614808791	1	0.795695402	-1.906377033	-1.260703989
6	-5.682788190	0.011941899	2.420810345	1	-0.971033386	-1.930822942	-1.126004759
1	-6.775926491	0.013350499	2.530596201	1	0.996730176	1.105161399	-3.479257224
1	-5.196300296	0.028627648	3.402896965	1	1.944402646	-0.163037097	-2.702584224
6	-6.128821254	-0.029869397	-1.183953518	1	0.898351196	3.790126247	-0.184711048
1	-7.216150821	-0.031437070	-1.031189240	1	-0.863985050	3.802379699	-0.049797152
1	-5.886489670	-0.040255846	-2.252788581	1	-2.015270463	2.069994464	1.374202401
7	-5.275838626	1.212555155	1.740448469	1	0.180383787	2.989151240	2.040009438
6	-5.987262298	1.751795126	0.608038116	1	2.234968774	2.055793040	1.031770276
1	-7.071719189	1.636453462	0.745989646	1	1.584251936	1.277506373	3.223323172
7	-5.577525443	1.187002706	-0.652038987	1	2.362465028	-0.014194536	2.306473123

6	-4.476016436	2.147546158	2.348152379	1	-1.937602242	0.022582905	2.715928918
8	-3.846163741	1.981284589	3.368243845	1	-0.981740157	1.331753632	3.410329571
6	-4.934460964	2.096104432	-1.451717720	1	-2.135037465	-0.090522346	0.174782018
8	-4.551344878	1.897738600	-2.582631139	1	0.966011359	-1.860843874	1.256379767
7	-4.563462989	3.314485680	1.632189438	1	-0.800427211	-1.816701314	1.389353755
6	-5.484946006	3.216344549	0.527606197	1	2.141078621	-0.115120191	-0.158856184
1	-6.264211555	3.986727498	0.613539484	6	-1.674623325	-1.887755118	-3.947083196
7	-4.859030015	3.283339477	-0.769051574	6	-0.003457550	-0.577938358	-5.002178263
6	-4.088304497	4.568419663	2.151361760	6	0.600083731	-2.482842105	-3.719075911

6	0.006827170	-0.256905940	5.037805605
6	-0.606257768	-2.237166054	3.879169619
6	1.671434050	-1.640354144	4.070048736
1	0.236660817	-3.226357564	-3.017736726
1	1.611207060	-2.179749738	-3.465596279
1	0.639075064	-2.961370825	-4.693814959
1	-0.558155695	0.355346823	-5.037244611
1	-0.288428562	-1.179513868	-5.861675993
1	1.061781845	-0.374046222	-5.062186161
1	-2.389928416	-1.118306727	-4.217765571
1	-2.012868653	-2.385437876	-3.044987477
1	-1.648300165	-2.636041129	-4.734565128
1	-1.615737237	-1.946261274	3.605582929
1	-0.648209193	-2.651453629	4.882782721
1	-0.246728154	-3.026391637	3.227419130
1	2.390724209	-0.858646750	4.290243330
1	2.006713336	-2.197465212	3.202215624
1	1.640894879	-2.335501094	4.904685289
1	-1.057195812	-0.043219910	5.083674236
1	0.567028153	0.673434832	5.013502260
1	0.287738102	-0.803792889	5.934382191

CB[8]•G4

7	4.792018330	-3.513998647	-1.482892533
6	5.169162521	-4.208562760	-0.275160554
1	6.216563710	-4.535624280	-0.330428148
7	4.940244364	-3.440148653	0.919863751
6	3.739369279	-4.110655259	-2.127672246
8	3.278940357	-3.771064023	-3.195029363
6	3.894384903	-3.924666612	1.664037174
8	3.520664174	-3.478158754	2.724560341
7	3.354589305	-5.197393816	-1.387790067
6	4.123697972	-5.350171934	-0.179895920
1	4.537386532	-6.366036061	-0.120515821
7	3.401770472	-5.033151358	1.029494822
6	2.446981709	-6.188324760	-1.893141487
1	2.874346924	-7.184317606	-1.728898084
1	2.320202359	-5.984930708	-2.962771110
6	2.476742355	-5.925458403	1.669686823
1	2.368834633	-5.575166732	2.703022555
1	2.879053566	-6.945681724	1.640211497
6	-0.758437401	-6.681634386	-0.031793707
1	-1.262553389	-7.656616779	0.009759705
7	-1.060398869	-5.910092693	1.146405163
6	-2.394630149	-5.923507669	-1.823221285
1	-2.268695152	-5.615487927	-2.867724965
1	-2.877459859	-6.907040825	-1.759291708
6	-2.348710426	-5.907421274	1.781934974
1	-2.767354447	-6.921268415	1.736718515
1	-2.194693538	-5.593151430	2.820813833
7	-3.244121904	-4.950232201	-1.195160272
6	-4.012285867	-5.219451836	-0.008522300
1	-4.401068954	-6.246672023	-0.029988461
7	-3.290432878	-4.980864694	1.217950675
6	-3.637235579	-3.797775970	-1.824520113
8	-3.160647517	-3.341470681	-2.839888668
6	-3.812597428	-3.944279521	1.947064983
8	-3.437138850	-3.583775102	3.040314015
7	-4.715007391	-3.289693080	-1.144883501
6	-5.084913931	-4.100119609	-0.008933041
1	-6.124316549	-4.442793092	-0.104767573
7	-4.888244931	-3.448639278	1.258465267
6	-5.598226903	-2.331800895	-1.751205038
1	-6.609315562	-2.759150271	-1.800582402
1	-5.208113775	-2.138654165	-2.757387532
6	-5.843398191	-2.557653609	1.853342456
1	-6.849713502	-2.976947228	1.727364539
1	-5.580612078	-2.479476962	2.914579074
7	-5.659209860	-1.064275713	-1.079253194
6	-6.464522328	-0.833702427	0.095744474
1	-7.437339761	-1.334292026	-0.001329064
7	-5.822792932	-1.222963809	1.324683735
6	-5.275369749	0.100792534	-1.692921176
8	-4.629779528	0.189068899	-2.713376805
6	-5.415318257	-0.147545617	2.070261052
8	-4.860678988	-0.192944135	3.145921547
7	-5.805094859	1.148171621	-0.984621781
6	-6.515684444	0.712865978	0.188776970
1	-7.522747754	1.150778742	0.213671304
7	-5.816718828	0.988349882	1.419957157
6	-5.923205808	2.473208488	-1.532537650
1	-6.955742123	2.818131323	-1.397390697

7	1.134725906	-6.139499673	-1.310760799
6	0.791331804	-6.732467569	-0.044283135
1	1.230516375	-7.735969020	0.037839600
7	1.158109968	-5.927258064	1.094945191
6	0.040305311	-5.688745942	-1.998693823
8	0.048572350	-5.169329507	-3.092864154
6	0.067792693	-5.448611169	1.775565082
8	0.098215540	-4.786606028	2.788439875
7	-1.073898236	-6.006136637	-1.266943017
1	-5.669128081	2.407121515	-2.596802818
6	-5.784644602	2.280334631	2.046227564
1	-6.790834539	2.717192967	2.027219552
1	-5.449344858	2.113288490	3.076583609
7	-4.862737430	3.200254632	1.442406654
6	-5.197727201	4.049420333	0.328793228
1	-6.225225893	4.424236361	0.432043268
7	-5.018562490	3.430843742	-0.962998903
6	-3.704146144	3.582416703	2.067583112

8	-3.213625688	3.060858782	3.042872935	6	6.409601126	0.669695044	-0.441575336
6	-4.031862555	4.023097369	-1.702783528	1	7.384653377	1.157025153	-0.568620021
8	-3.735094051	3.758221827	-2.845805848	7	5.534371492	0.972392648	-1.546831803
7	-3.227435023	4.700762793	1.430883336	6	5.446879028	-0.089033641	1.541514430
6	-4.087984266	5.132021671	0.355594735	8	4.888495326	-0.073982282	2.620900091
1	-4.439470846	6.158273378	0.530500016	6	5.063449029	-0.157436095	-2.168910795
7	-3.477872713	5.021031626	-0.943275152	8	4.321632792	-0.175548762	-3.125243194
6	-2.263356934	5.562677713	2.059723105	7	5.839029477	-1.200555583	0.855704388
1	-2.690094008	6.568992608	2.162964865	6	6.438083837	-0.880922486	-0.418743399
1	-2.049890430	5.128632253	3.043492541	1	7.431198156	-1.339917266	-0.502893496
6	-2.600632562	6.011635015	-1.501891578	7	5.614669105	-1.245975766	-1.544031458
1	-2.572530954	5.826181067	-2.581754886	6	5.887629830	-2.504509297	1.458714186
1	-2.996509162	7.011435773	-1.288625367	1	6.899551318	-2.912597528	1.345861921
7	-1.012697651	5.648369657	1.359328267	1	5.635112285	-2.376107971	2.517584808
6	-0.796381000	6.511371806	0.221409434	6	5.631252075	-2.551414630	-2.142713260
1	-1.261663865	7.491623313	0.383420009	1	6.664332683	-2.922192822	-2.161114723
7	-1.247419265	5.935824003	-1.021109999	1	5.237240620	-2.447188712	-3.160264028
6	0.158573210	5.198062676	1.911185323	6	-0.236636826	-0.863982336	-1.280871523
8	0.268139886	4.472133731	2.873014494	6	-1.651321582	-0.545874563	-0.787761540
6	-0.213349668	5.489219482	-1.788831420	6	-1.742231350	0.951649492	-0.484849782
8	-0.312658834	4.907293196	-2.852150401	6	0.076952976	-0.059213500	-2.545857139
7	1.196653121	5.746692224	1.202641472	6	0.983305146	1.779065906	-1.128906421
6	0.747817621	6.516363651	0.074585636	6	-1.435776033	1.758693733	-1.747927983
1	1.217770551	7.507772107	0.063568257	6	-0.022211350	1.429557792	-2.221757633
7	0.959747981	5.833227205	-1.181737988	6	-1.953496926	-1.350208107	0.473883864
6	2.542525467	5.781571648	1.704388987	6	0.470852857	-1.319283353	1.100861042
1	2.503619863	5.481956680	2.757655624	6	-0.950286151	-0.997518163	1.570459539
1	2.934240789	6.800195647	1.605286049	6	-1.033874886	0.496515546	1.895953499
6	2.224140979	5.807440426	-1.869524658	6	-0.023939761	0.868110016	2.986177528
1	2.678783610	6.803925272	-1.819981058	6	1.381731701	0.531168142	2.495452087
1	2.014812963	5.531421882	-2.908942885	6	1.478347360	-0.961982467	2.195128316
7	3.427830528	4.861131102	1.046636456	6	0.763240030	-0.522172032	-0.173102901
6	4.034964667	5.101016088	-0.239445366	6	1.681356064	1.336674398	1.235228314
1	4.430323106	6.123708588	-0.293572615	6	-0.743726606	1.295378342	0.622600942
7	3.151647276	4.838835928	-1.350140659	6	0.676561710	0.977470905	0.138460286
6	3.957978375	3.779683665	1.687278839	7	0.298739270	2.239143774	-3.434161126
8	3.638535963	3.372461069	2.784613807	7	2.390742347	0.894596257	3.532396166
6	3.531872881	3.738025996	-2.069840567	1	-0.172640283	-1.932730501	-1.519590569
8	2.973650216	3.314048984	-3.060165034	1	-2.373484700	-0.808224647	-1.569999653
7	4.941994747	3.254079509	0.896112229	1	-2.757534533	1.186077017	-0.141736485
6	5.093552375	3.971617890	-0.345858020	1	1.078642767	-0.312955000	-2.900195987

1	6.130459043	4.308623794	-0.473742889	1	-0.643276711	-0.334746829	-3.318035615
7	4.659812103	3.219336759	-1.499348816	1	0.935834292	2.846477666	-0.906783684
6	5.912714406	2.327540989	1.408525244	1	1.989130026	1.532719902	-1.473473202
1	6.920562215	2.724094713	1.236404486	1	-2.171192879	1.514617112	-2.517143656
1	5.718481362	2.222752091	2.481495338	1	-1.518049028	2.824944113	-1.532348125
6	5.488319639	2.262624839	-2.180868225	1	-2.967062950	-1.138067357	0.826823653
1	6.507952761	2.659942348	-2.262740621	1	-1.899631318	-2.421464380	0.253229998
1	5.052580746	2.111651580	-3.174999085	1	0.541620780	-2.392997746	0.888455661
7	5.825862654	1.013596230	0.830175583	1	-1.186744434	-1.587497747	2.463772524

1	-2.041205525	0.732672956	2.257497194
1	-0.263710309	0.304608036	3.888379234
1	-0.111157132	1.933808752	3.208152462
1	2.486879645	-1.220320441	1.868529972
1	1.260299346	-1.557562129	3.082694526
1	1.773538095	-0.765121693	-0.525621213
1	1.595886946	2.399893832	1.464318842
1	2.694349860	1.125002672	0.888422651
1	-0.820668817	2.363469939	0.859184962
1	-0.159655320	1.852655471	-4.263598440
1	-0.019318562	3.223150748	-3.315748003
1	1.318453200	2.284574049	-3.590055918
1	2.546018070	1.915912427	3.555649379
1	3.309774402	0.464286180	3.308460563
1	2.097495559	0.571106293	4.457671221

Appendix 2

Molecular Recognition of Methylated Amino Acids and Peptides by Pillar[6]MaxQ

David King,[a] Chelsea R. Wilson,[b] Lukas Herron,[c,d] Chun-Lin Deng,[a] Shams Mehdi,[c,d] Pratyush Tiwary,[a,d,*] Fraser Hof,[b,*]Lyle Isaacs[a,*]

[a]Department of Chemistry and Biochemistry, University of Maryland, College Park, MD 20742, United States; [b]Department of Chemistry, University of Victoria, Victoria, BC, V8W 3V6, Canada; [c]Biophysics Program, University of Maryland, College Park, MD 20742, United States; [d]Institute for Physical Science and Technology, University of Maryland, College Park, MD 20742, United States

Table of Contents **Pages**

General experimental details.

Amino acids and amino acid amides were purchased from commercial suppliers and were used without further purification. 4′,6-diamidino-2-phenylindole dihydrochloride (DAPI) was purchased from Sigma-Aldrich (D9542, ≥98%). Trimethyllysine was purchased from Sigma-Aldrich (55528-53-5, ≥97%). Peptide sequences were purchased from GenScript with the exception of H3K4Me_2 which was obtained as described in literature (*Org. Biomol. Chem.* **2021**, *19*, 4691-4696). P5MQ and P6MQ were synthesized according to the literature procedures (*Angew. Chem. Int. Ed.* **2020**, *59*, 13313). ^{1}H NMR spectra were recorded on a commercial spectrometer operating at 600 MHz. ITC data was collected on a Malvern Microcal PEAQ-ITC instrument and analyzed using the software provided by the manufacturer. All fluorescence assays were performed in a Thermo Scientific™ Nunc MicroWell 96-Well Optical-Bottom, Black-walled Plate (265031). All plates were read on a BioTek Cytation-5 cell imaging and multi-mode reader plate reader.

Peptide sequences: H3K4 = (ARTKQTAY), H-K-OH = lysine, H3K4Me = (ART(KMe)QTAY), H-K(Me)-OH = monomethyl lysine, H3K4Me_2 = (ART(KMe_2)QTAY), H-K(Me_2)-OH = dimethyl lysine, H3K4Me_3 = (ART(KMe_3)QTAY), H-K(Me_3)-OH = trimethyl lysine, H-K-NH_2 = lysine amide, Ac-K-NH_2 = acetyl lysine amide, H-R-OH = arginine, H-R(Me)-OH = monomethyl arginine, H3R2Me_2a = (A(RMe_2a)TKQTAY), Asym-H-R(Me_2) = asymmetric dimethylarginine, H3R2Me_2s = (A(RMe_2s)TKQTAY), Sym-H-R(Me_2) = symmetric dimethylarginine, H-R-NH_2 = arginine amide, Ac-R-NH_2 = acetyl arginine amide.

Determination of the thermodynamic parameters of binding between P5MQand the guests by isothermal titration calorimetry

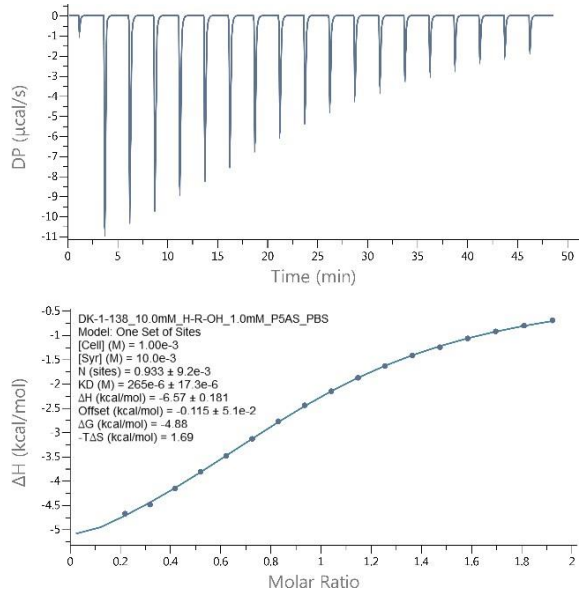

Figure SIII-1. Isothermal Titration Calorimetry (ITC) curve obtained through direct binding titration studies. A solution of P5MQ (1.00 mM) in the cell was titrated with **H-R-OH** (10.0 mM) in the syringe at 298.0 K in 10 mM sodium phosphate buffered saline at pH 7.4. K_a = (3.77 ± 0.24) x 10^3 M^{-1}.

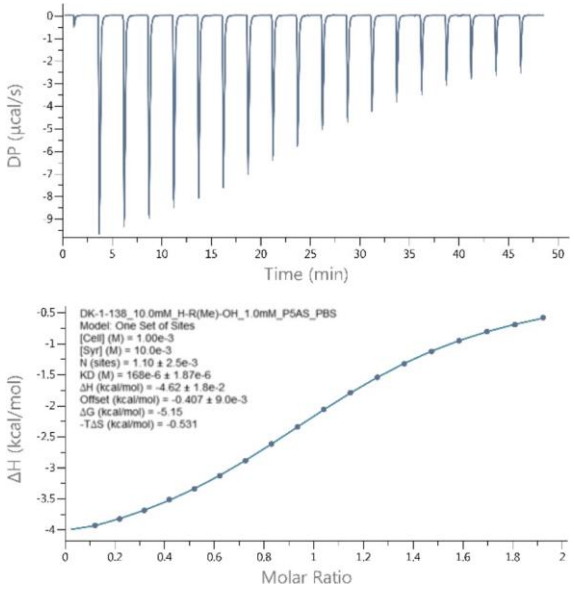

Figure SIII-2. ITC curve obtained through direct binding titration studies. A solution of P5MQ (0.1 mM) in the cell was titrated with **H-R(Me)-OH** (1.00 mM) in the syringe at 298.0 K in 10 mM sodium phosphate buffered saline at pH 7.4. K_a = (5.95 ± 0.07) x 10^3 M^{-1}.

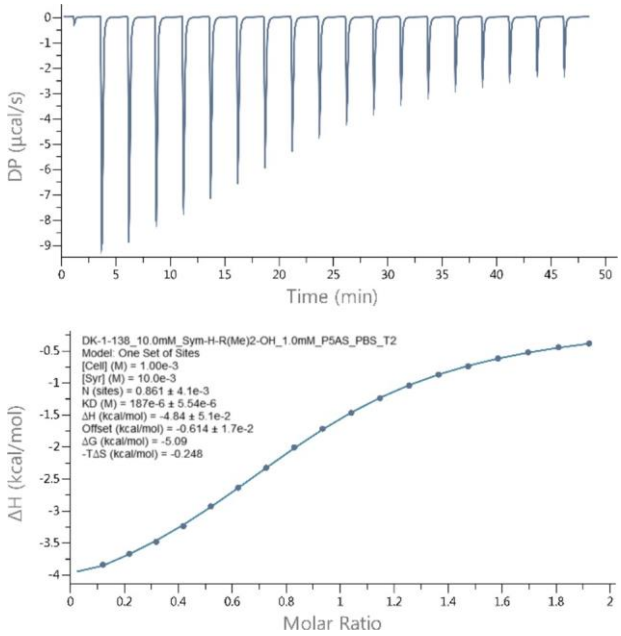

Figure SIII-3. Isothermal Titration Calorimetry (ITC) curve obtained through direct binding titration studies. A solution of P5MQ (0.1 mM) in the cell was titrated with **Sym-H-R(Me$_2$)-OH** (1.00 mM) in the syringe at 298.0 K in 10 mM sodium phosphate buffered saline at pH 7.4. K_a = (5.35 ± 0.16) x 10^3 M^{-1}.

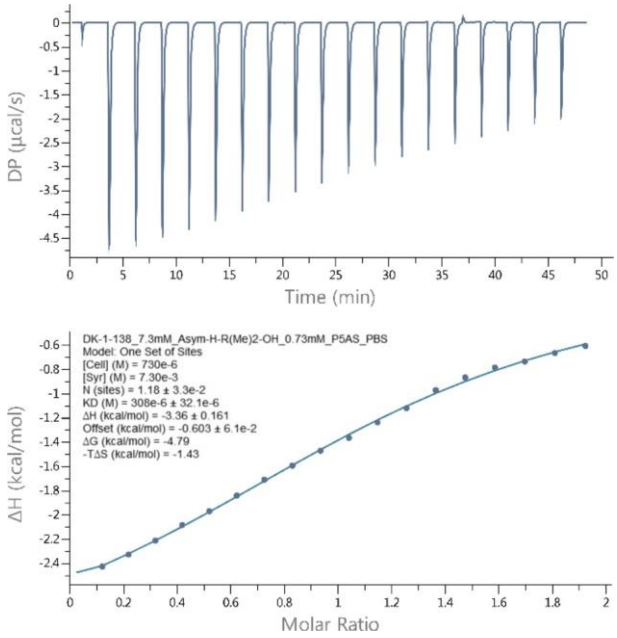

Figure SIII-4. Isothermal Titration Calorimetry (ITC) curve obtained through direct binding titration studies. A solution of P5MQ (0.73 mM) in the cell was titrated with **Asym-H-R(Me$_2$)-OH** (7.30 mM) in the syringe at 298.0 K in 10 mM sodium phosphate buffered saline at pH 7.4. K_a = (3.25 ± 0.34) x 10^3 M^{-1}.

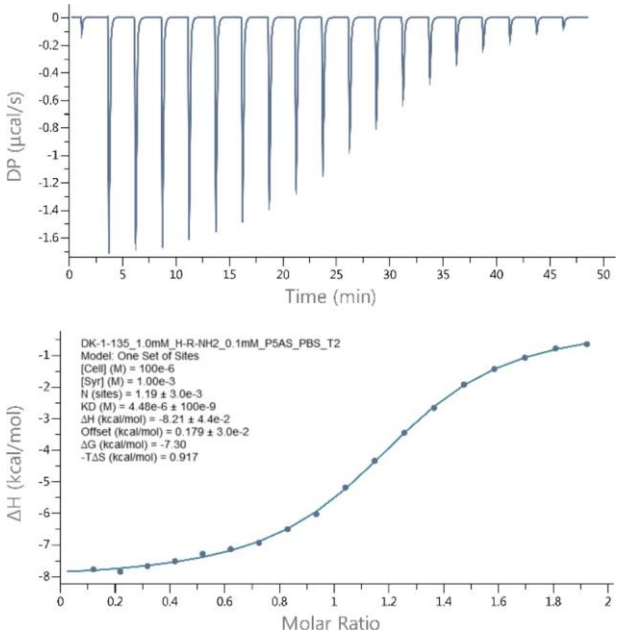

Figure SIII-5. Isothermal Titration Calorimetry (ITC) curve obtained through direct binding titration studies. A solution of P5MQ (0.1 mM) in the cell was titrated with **H-R-NH$_2$** (1.00 mM) in the syringe at 298.0 K in 10 mM sodium phosphate buffered saline at pH 7.4. K_a = (2.23 ± 0.05) x 10^5 M^{-1}.

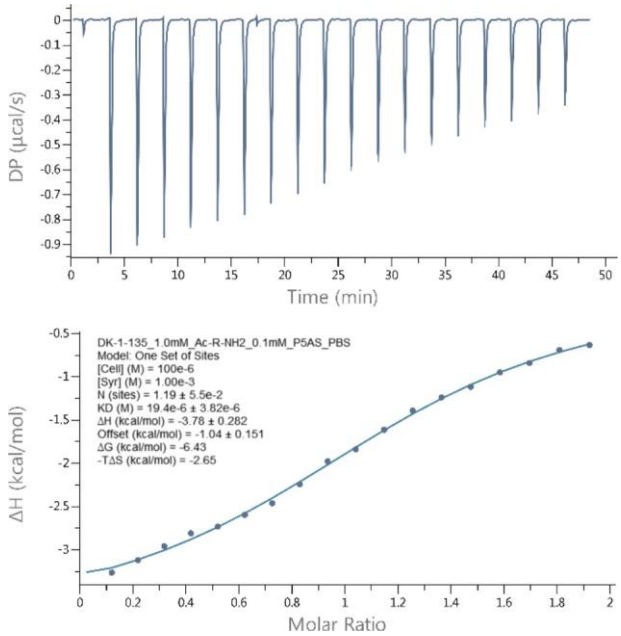

Figure SIII-6. Isothermal Titration Calorimetry (ITC) curve obtained through direct binding titration studies. A solution of P5MQ (0.1 mM) in the cell was titrated with **Ac-R-NH$_2$** (1.00 mM) in the syringe at 298.0 K in 10 mM sodium phosphate buffered saline at pH 7.4. K_a = (5.15 ± 1.01) x 10^4 M^{-1}.

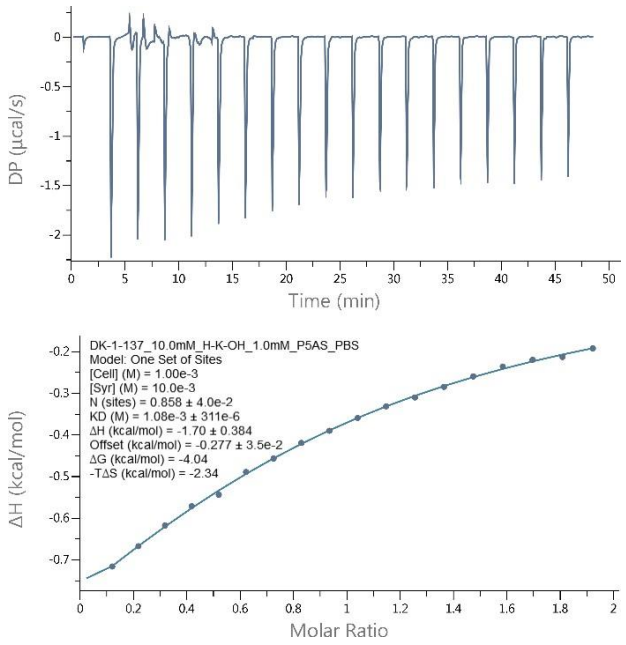

Figure SIII-7. Isothermal Titration Calorimetry (ITC) curve obtained through direct binding titration studies. A solution of P5MQ (1.0 mM) in the cell was titrated with **H-K-OH** (10.0 mM) in the syringe at 298.0 K in 10 mM sodium phosphate buffered saline at pH 7.4. K_a = (9.26 ± 2.67) x 10^2 M^{-1}.

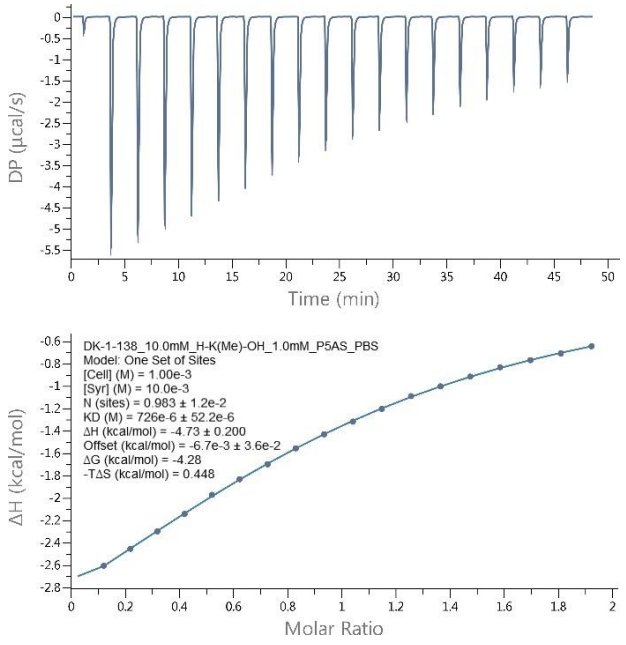

Figure SIII-8. Isothermal Titration Calorimetry (ITC) curve obtained through direct binding titration studies. A solution of P5MQ (1.0 mM) in the cell was titrated with **H-K(Me)-OH** (10.0 mM) in the syringe at 298.0 K in 10 mM sodium phosphate buffered saline at pH 7.4. K_a = (1.38 ± 0.10) x 10^3 M^{-1}.

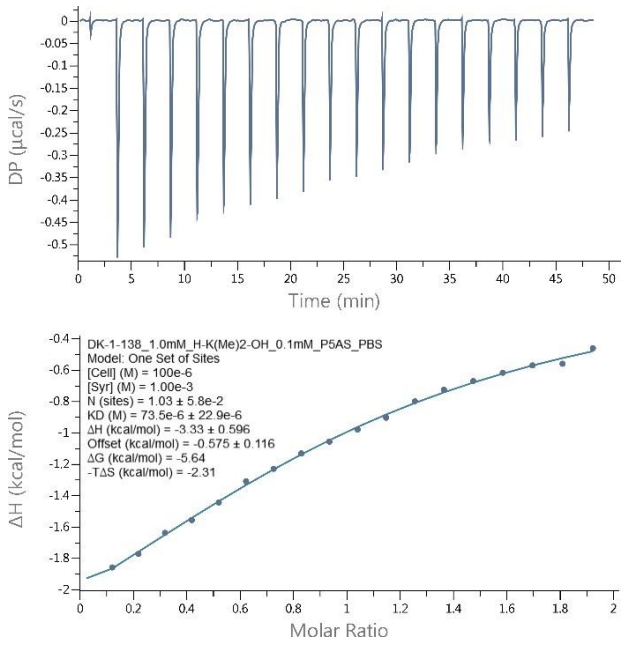

Figure SIII-9. Isothermal Titration Calorimetry (ITC) curve obtained through direct binding titration studies. A solution of P5MQ (0.1 mM) in the cell was titrated with **H-K(Me$_2$)-OH** (1.00 mM) in the syringe at 298.0 K in 10 mM sodium phosphate buffered saline at pH 7.4. K_a = (1.36 ± 0.42) x 10^4 M^{-1}.

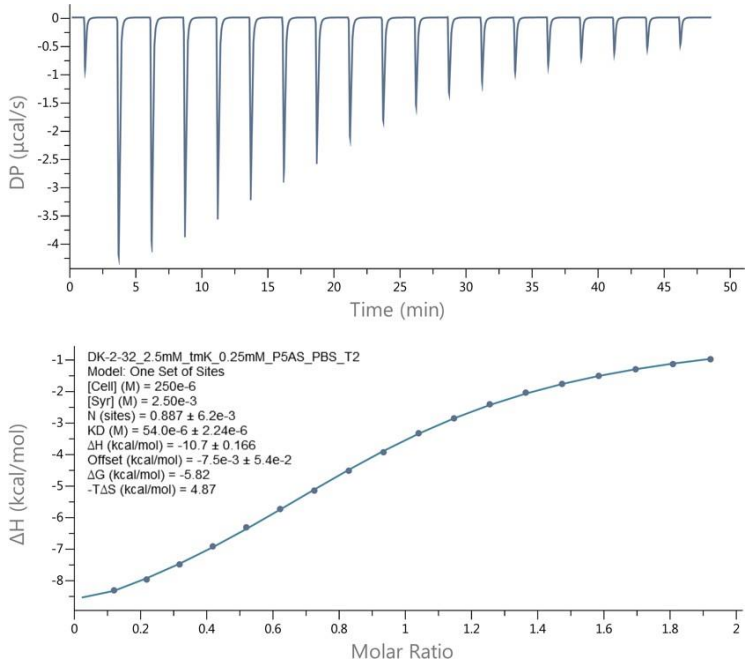

Figure SIII-10. Isothermal Titration Calorimetry (ITC) curve obtained through direct binding titration studies. A solution of P5MQ (0.25 mM) in the cell was titrated with **H-K(Me$_3$)-OH** (2.50 mM) in the syringe at 298.0 K in 10 mM sodium phosphate buffered saline at pH 7.4. K_a = (1.81 ± 0.26) x 10^4 M^{-1}.

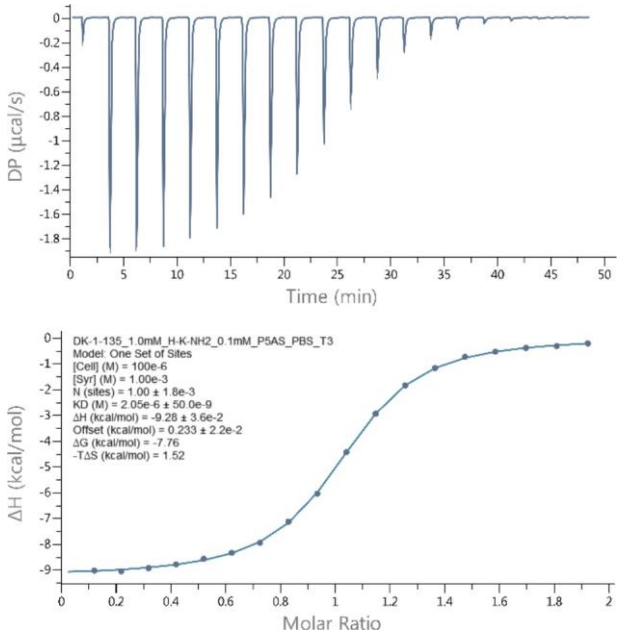

Figure SIII-11. Isothermal Titration Calorimetry (ITC) curve obtained through direct binding titration studies. A solution of P5MQ (0.1 mM) in the cell was titrated with **H-K-NH$_2$** (1.00 mM) in the syringe at 298.0 K in 10 mM sodium phosphate buffered saline at pH 7.4. K_a = (4.88 ± 0.12) x 10^5 M^{-1}.

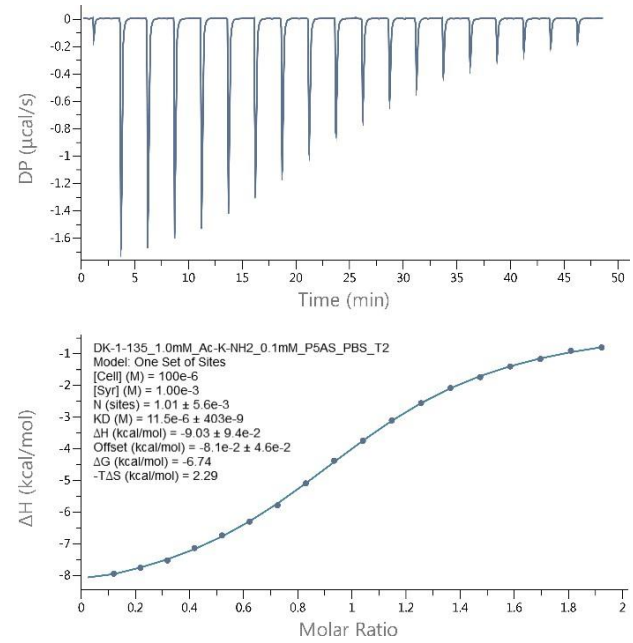

Figure SIII-12. Isothermal Titration Calorimetry (ITC) curve obtained through direct binding titration studies. A solution of P5MQ (0.1 mM) in the cell was titrated with **Ac-K-NH$_2$** (1.00 mM) in the syringe at 298.0 K in 10 mM sodium phosphate buffered saline at pH 7.4. K_a = (8.70 ± 0.30) x 10^4 M^{-1}.

Determination of the thermodynamic parameters of binding between P6MQ and the guests by isothermal titration calorimetry

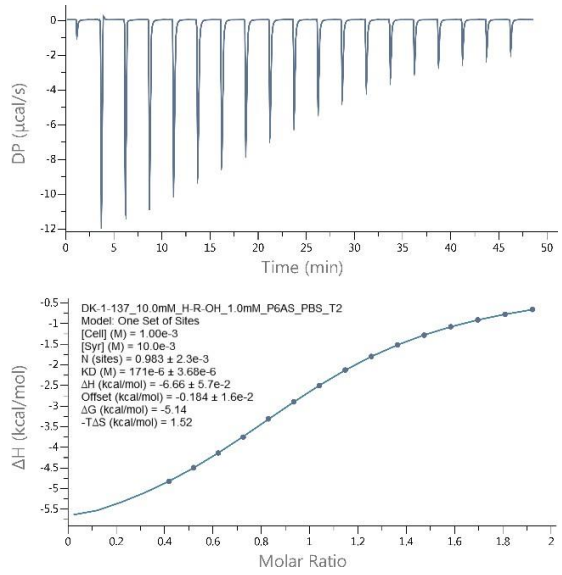

Figure SIII-13. Isothermal Titration Calorimetry (ITC) curve obtained through direct binding titration studies. A solution of P6MQ (1.0 mM) in the cell was titrated with **H-R-OH** (10.0 mM) in the syringe at 298.0 K in 10 mM sodium phosphate buffered saline at pH 7.4. K_a = (5.85 ± 0.13) x 10^3 M^{-1}.

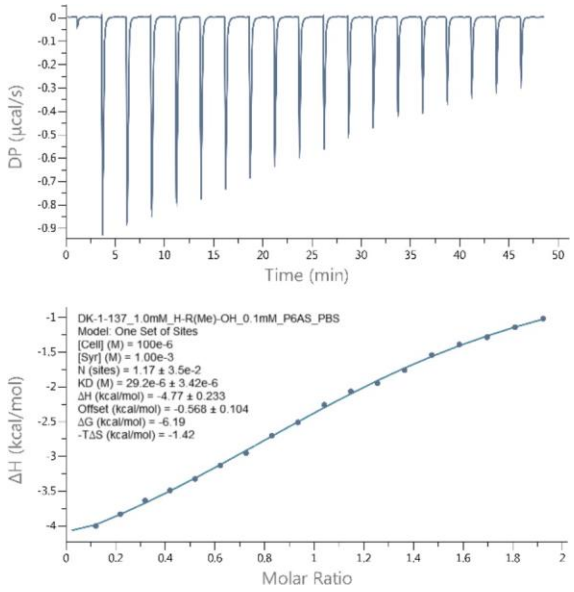

Figure SIII-14. Isothermal Titration Calorimetry (ITC) curve obtained through direct binding titration studies. A solution of P6MQ (0.1 mM) in the cell was titrated with **H-R(Me)-OH** (1.00 mM) in the syringe at 298.0 K in 10 mM sodium phosphate buffered saline at pH 7.4. K_a = (3.42 ± 0.40) x 10^4 M^{-1}.

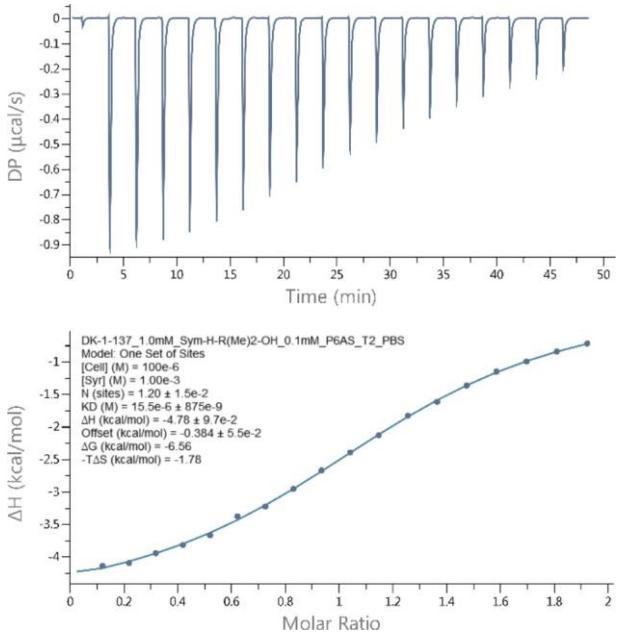

Figure SIII-15. Isothermal Titration Calorimetry (ITC) curve obtained through direct binding titration studies. A solution of P6MQ (0.1 mM) in the cell was titrated with **Sym-H-R(Me$_2$)-OH** (1.00 mM) in the syringe at 298.0 K in 10 mM sodium phosphate buffered saline at pH 7.4. K_a = (6.45 ± 0.36) x 10^4 M^{-1}.

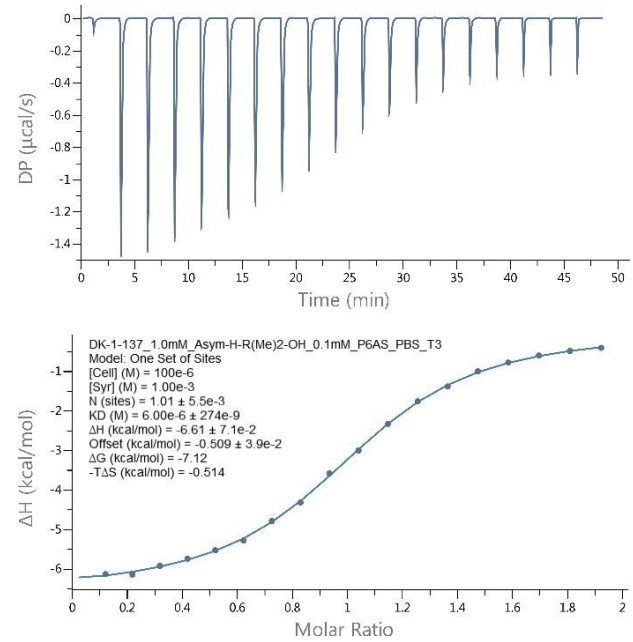

Figure SIII-16. Isothermal Titration Calorimetry (ITC) curve obtained through direct binding titration studies. A solution of P6MQ (0.1 mM) in the cell was titrated with **Asym-H-R(Me$_2$)-OH** (1.00 mM) in the syringe at 298.0 K in 10 mM sodium phosphate buffered saline at pH 7.4. K_a = (1.67 ± 0.08) x 10^5 M^{-1}.

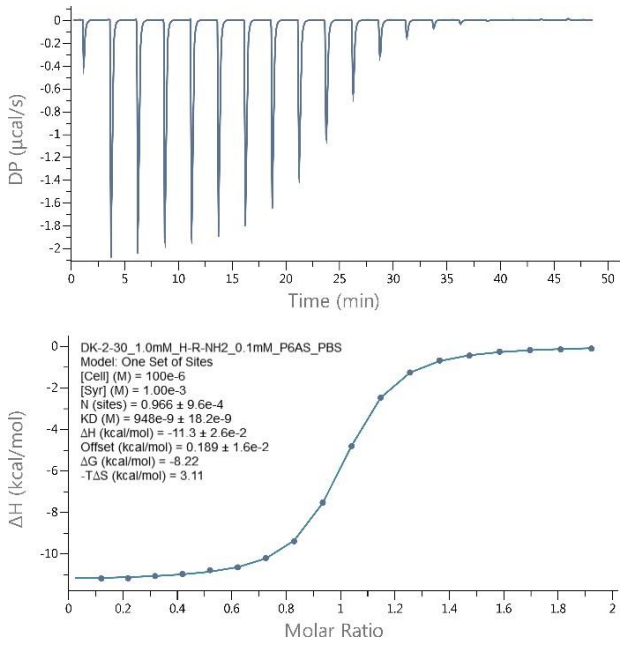

Figure SIII-17. Isothermal Titration Calorimetry (ITC) curve obtained through direct binding titration studies. A solution of P6MQ (0.1 mM) in the cell was titrated with **H-R-NH$_2$** (1.00 mM) in the syringe at 298.0 K in 10 mM sodium phosphate buffered saline at pH 7.4. K_a = (1.05 ± 0.02) x 10^6 M^{-1}.

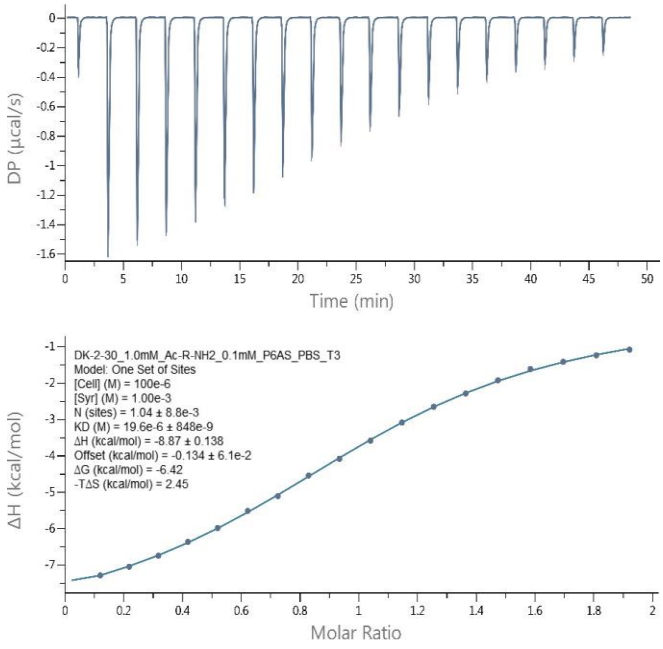

Figure SIII-18. Isothermal Titration Calorimetry (ITC) curve obtained through direct binding titration studies. A solution of P6MQ (0.1 mM) in the cell was titrated with **Ac-R-NH$_2$** (1.00 mM) in the syringe at 298.0 K in 10 mM sodium phosphate buffered saline at pH 7.4. K_a = (5.10 ± 0.02) x 10^4 M^{-1}.

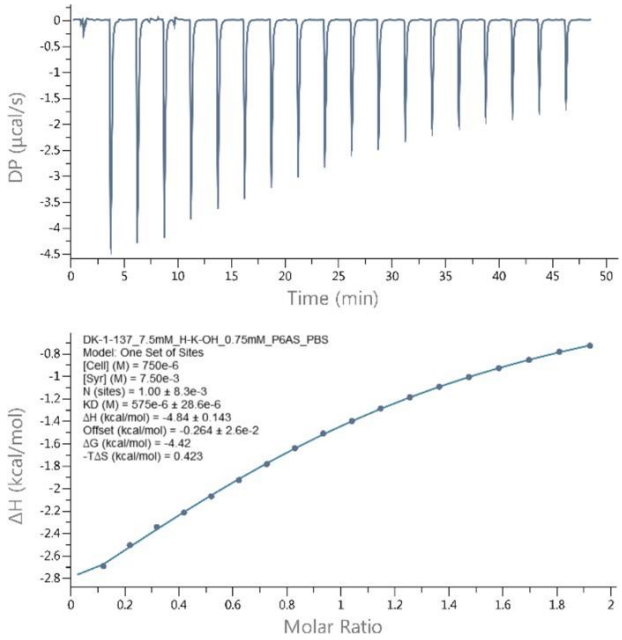

Figure SIII-19. Isothermal Titration Calorimetry (ITC) curve obtained through direct binding titration studies. A solution of P6MQ (0.75 mM) in the cell was titrated with **H-K-OH** (7.5 mM) in the syringe at 298.0 K in 10 mM sodium phosphate buffered saline at pH 7.4. K_a = (1.74 ± 0.09) x 10^3 M^{-1}.

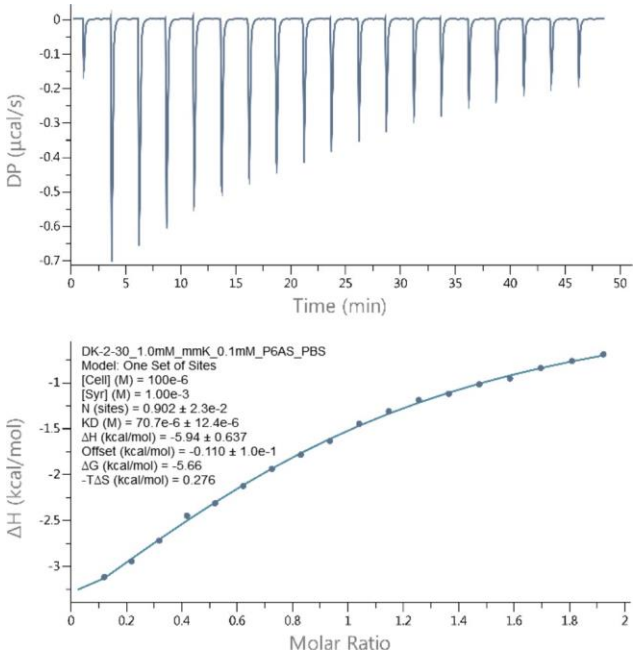

Figure SIII-20. Isothermal Titration Calorimetry (ITC) curve obtained through direct binding titration studies. A solution of P6MQ (0.1 mM) in the cell was titrated with **H-K(Me)-OH** (1.00 mM) in the syringe at 298.0 K in 10 mM sodium phosphate buffered saline at pH 7.4. K_a = (1.40 ± 0.03) x 10^4 M^{-1}.

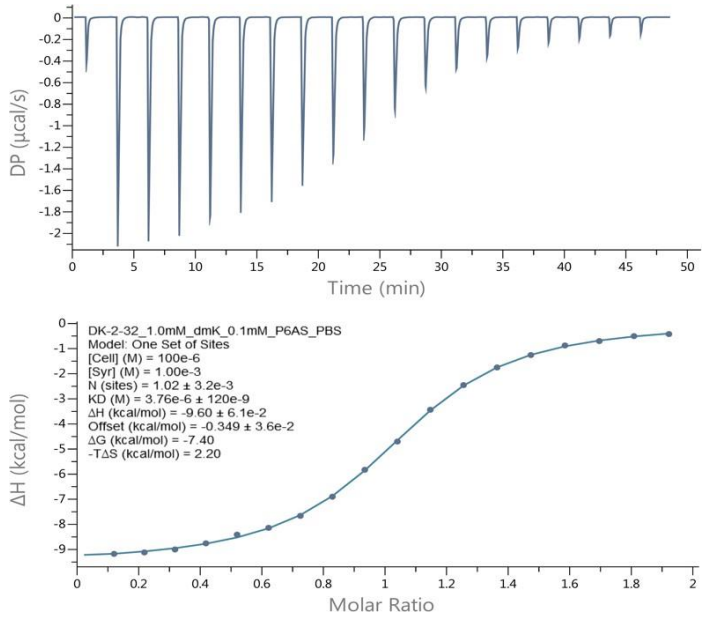

Figure SIII-21. Isothermal Titration Calorimetry (ITC) curve obtained through direct binding titration studies. A solution of P6MQ (0.1 mM) in the cell was titrated with **H-K(Me$_2$)-OH** (1.00 mM) in the syringe at 298.0 K in 10 mM sodium phosphate buffered saline at pH 7.4. K_a = (2.39 ± 0.07) x 10^5 M^{-1}.

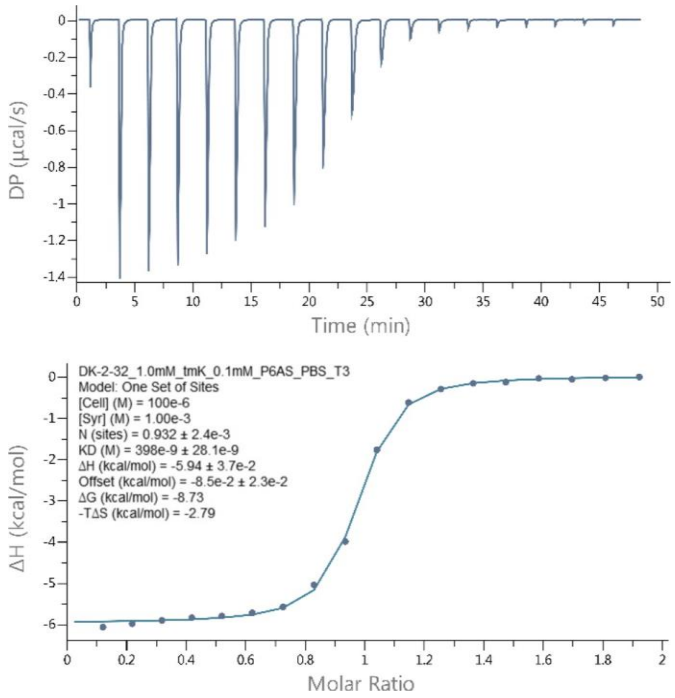

Figure SIII-22. Isothermal Titration Calorimetry (ITC) curve obtained through direct binding titration studies. A solution of P6MQ (0.1 mM) in the cell was titrated with **H-K(Me$_3$)-OH** (1.00 mM) in the syringe at 298.0 K in 10 mM sodium phosphate buffered saline at pH 7.4. K_a = (3.39 ± 0.15) x 10^6 M^{-1}.

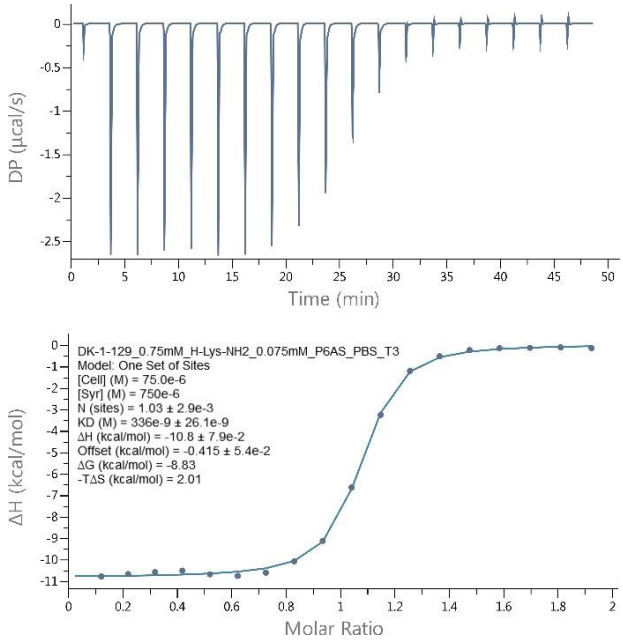

Figure SIII-23. Isothermal Titration Calorimetry (ITC) curve obtained through direct binding titration studies. A solution of P6MQ (0.075 mM) in the cell was titrated with **H-K-NH₂** (0.75 mM) in the syringe at 298.0 K in 10 mM sodium phosphate buffered saline at pH 7.4. K_a = (4.78 ± 0.80) x 10^6 M^{-1}.

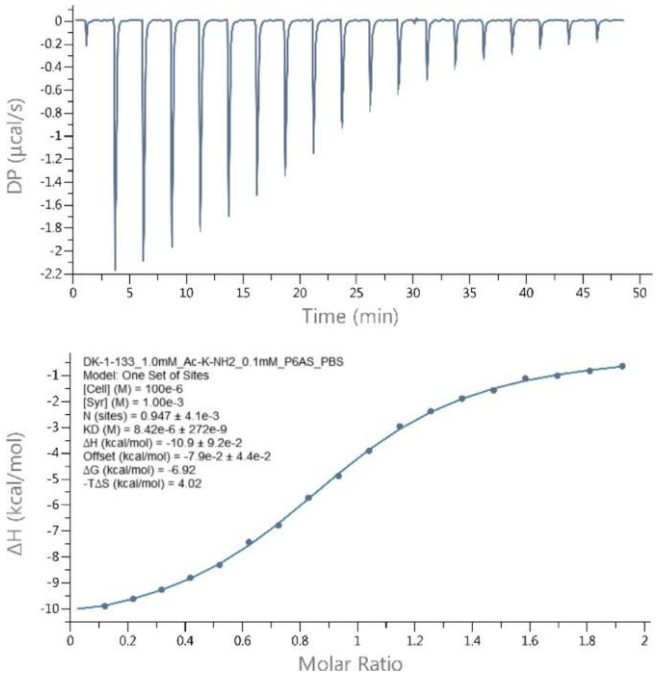

Figure SIII-24. Isothermal Titration Calorimetry (ITC) curve obtained through direct binding titration studies. A solution of P6MQ (0.1 mM) in the cell was titrated with Ac-K-NH_2 (1.00 mM) in the syringe at 298.0 K in 10 mM sodium phosphate buffered saline at pH 7.4. K_a = (1.19 ± 0.04) x 10^5 M^{-1}.

Direct and competitive fluorescence binding assays of P6MQ with H3K4 peptides.

Direct fluorescence titration assays. A direct titration of P6MQ into indicator was performed via serial dilutions as follows. All solutions were made using Milli-Q® ultrapure water and 10 mM PBS buffer (137 mM NaCl, 2.7 mM KCl, 10 mM Na_2HPO_4, 1.8 mM KH_2PO_4) at pH 7.4. In the 96-well plate, row 12 contained 200 μL of a solution of 100 nM **DAPI** and 4 μM P6MQ in 10 mM PBS buffer. Row 1 – 11 contained 100 μL of a solution of 100 nM **DAPI** in 10 mM PBS buffer. 100 μL of the solution in well 12 was added to well 11 and mixed, then 100 μL was taken from row 11 and added to row 10. These dilutions continued to well 1, whereupon 100 μL was discarded after mixing, leaving the total volume of all wells (1 – 12) at 100 μL. In a separate column of the 96-well plate, three wells contained the buffer blank (10 mM PBS), three wells contained the host blank (4 μM P6MQ in 10 mM PBS) and three wells contained the dye blank (100 nM **DAPI** in 10 mM PBS) all at a volume of 100 μL. Following the serial dilution of P6MQ across the plate, the plates were centrifuged (1300 rpm, pulse approximately 10 seconds) to remove any air bubbles. The plate was read on a BioTek Cytation-5 cell imaging and multi-mode plate reader, λ_{ex} 360/20 nm and λ_{em} 450/20 nm.

Two sets of triplicates were performed on two different days for a total of six replicates. The data for each triplicate was plotted and a K_d with standard error was determined using GraphPad Prism 9. The fluorescence (RFU) as a function of host concentration was plotted and a direct one site binding equation was used (equation S1). The fitting was constrained to the concentration of **DAPI** (100 nM). The graphs were plotted with standard error and a second plot of x residuals was determined. The IC_{90} point from the direct titrations was selected as the host concentration used in subsequent competitive titrations, this was determined to be 125 nM. The average K_d values of the

two sets of triplicates was reported along with the propagated standard error. For the direct assays, some of the data points (0 to 2 points) representing the highest P6MQ concentrations had to be excluded due to aggregation.

Equation SII-1: Curve fit for direct titration

$$Y = F_{min} + (F_{max} - F_{min})\left(\frac{D+x+K_{d\,DAPI}-\sqrt{(D+x+K_{d\,DAPI})^2-(4xD)}}{2D}\right) \quad \text{(SII-1)}$$

Where: Y = Fitted data point; F_{max} = Maximum signal; F_{min} = Minimum signal; D = Concentration of DAPI in micromolar (0.100 μM); x = Concentration of titrant in micromolar; $K_{\mathrm{d\,DAPI}}$ = Dissociation constant of **DAPI**

Competitive fluorescence titration assays. Competitive titration assays were performed in a 96-well plate with 4′,6-diamidino-2-phenylindole (**DAPI**) as the indicator. Solutions were made using Milli-Q® ultrapure water and 10 mM PBS buffer (137 mM NaCl, 2.7 mM KCl, 10 mM Na_2HPO_4, 1.8 mM KH_2PO_4) at pH 7.4. Two solutions were used, solution A and solution B. Solution B contained P6MQ (125 nM), **DAPI** (100 nM), and the guest of interest (between 1 – 100 μM) in 10 mM PBS buffer. Solution A contained P6MQ (125 nM) and **DAPI** (100 nM) in 10 mM PBS buffer at pH 7.4. In the 96 well plate, row 12 contained 200 μL solution B, row 1 – 11 contained 100 μL solution A. 100 μL from well 12 was added to row 11 and mixed, then 100 μL was taken from row 11 and added to row 10. These dilutions continued to row 1, whereupon 100 μL was discarded after mixing, leaving the total volume of all wells (1 – 12) at 100 μL. In a separate column of the 96 well plate three wells contained a buffer blank (10 mM PBS), three wells contained a host blank (125 nM P6MQ in 10 mM PBS), three wells contained a dye blank (100 nM **DAPI** in 10 mM PBS), three wells contained a guest blank (guest at highest concentration used in assay in 10 mM PBS buffer) and three wells contained a solution A blank (solution A not diluted by solution B) all

at a volume of 100 μL. Following serial dilution of P6MQ across the plate, the plates were centrifuged (1300 rpm, pulse approximately 10 seconds) to remove any air bubbles. The plate was read on a BioTek Cytation-5 cell imaging and multi-mode reader plate reader, λ_{ex} 360/20 nm and λ_{em} 450/20 nm.

Two sets of triplicates for each guest were performed on two different days for a total of six replicates. The data for each triplicate was plotted and a K_d with standard error was determined. The logarithm of the guest concentration against the fluorescence response from **DAPI** displacement (Fl-Fl_o, RFU) was plotted. A blank containing only the host (Fl_o) was subtracted from each triplicate experiment. The data was analyzed in GraphPad Prism 9 using the competitive one site binding equation (Equation SII-2). The fitting was constrained by the direct dissociation constant of **DAPI** ($K_{d\ DAPI}$, 15 nM) and the concentration of **DAPI** (100 nM). This model fits the K_d directly and does not report the EC_{50}, EC_{50} in equation SII-2 is solved by equation SII-3. This analysis also assumes a 1 : 1 stoichiometry. Graphs were plotted with standard error and a second plot of x residuals were determined. The average K_d values of the two sets of triplicates was reported along with the propagated standard error. For the competative assays with KMe_3, some of the data points (0 to 2 points) representing the highest KMe_3 concentrations had to be excluded due to aggregation.

Equation SII-2: Curve fit for competitive titration

$$Y = \frac{(F_{max} - F_{min})}{1+10^{(x-logEC_{50})}} + F_{min} \quad \text{(SII-2)}$$

Where: Y = Fitted data point; F_{max} = Maximum signal; F_{min} = Minimum signal; $logEC_{50}$ is solved by the equation below;

Equation SII-3: Curve fit for competitive titration

$$logEC_{50} = log\left(10^{logK_{d\ guest}\left(1+\frac{D}{K_{d\ DAPI}}\right)}\right) \quad \text{(SII-2)}$$

Where: $K_{\text{d guest}}$ = Dissociation constant for guest; D = Concentration of DAPI in nM; $K_{\text{d DAP}}$ = Dissociation constant of the DAPI in nM.

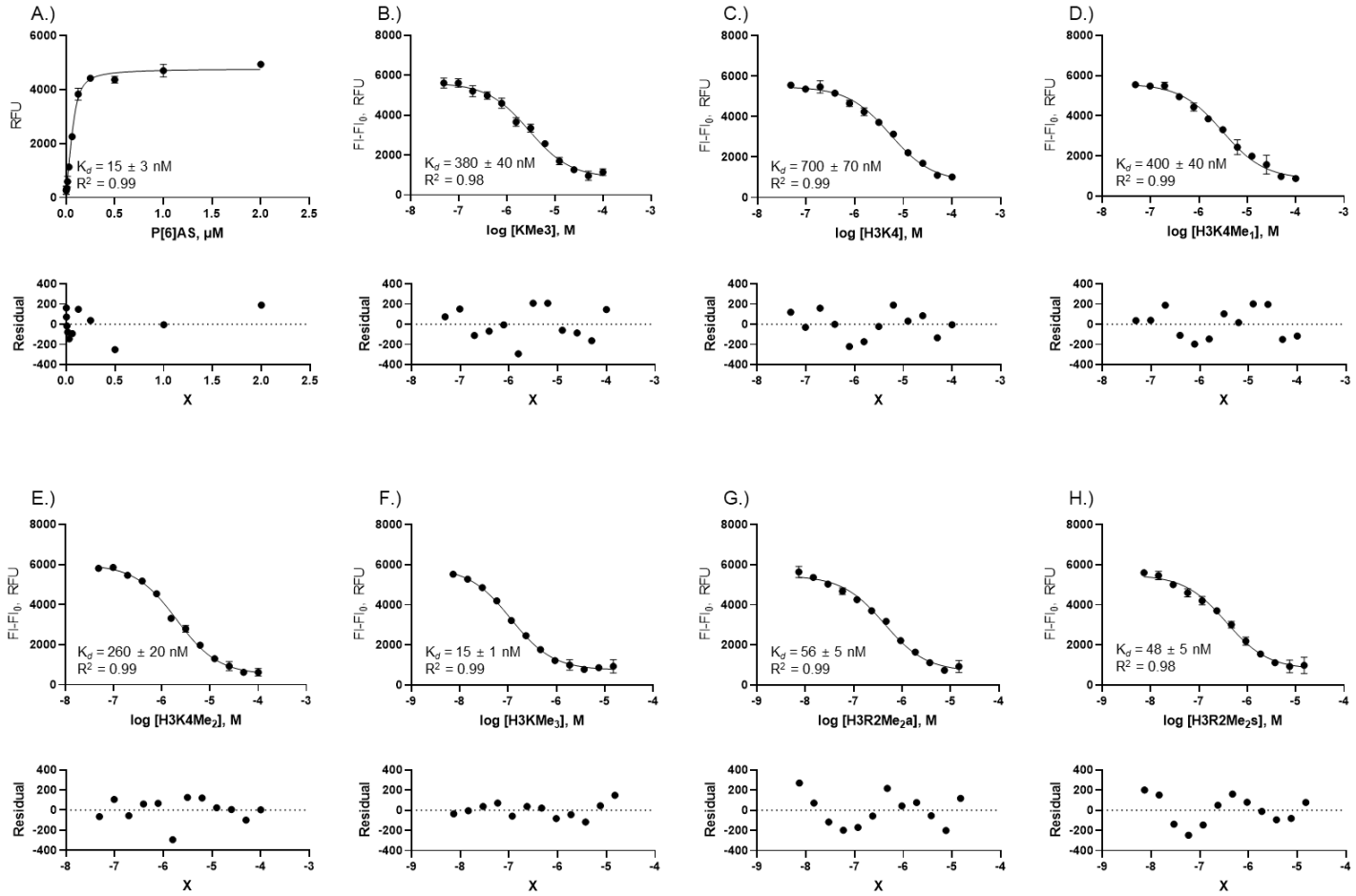

Figure SIII-25. Representative titration curves of direct and competitive titrations with residuals. Reported dissociation constants and R^2 are for an exemplary set of triplicates. A.) Direct titration of P6MQ into **DAPI** (100 nM). B.) Competitive titration of **H-K(Me$_3$)-OH** (100 μM) into P6MQ (125 nM) and **DAPI** (100 nM). C.) Competitive titration of **H3K4** (100 μM) into P6MQ (125 nM) and **DAPI** (100 nM). D.) Competitive titration of **H3K4Me** (100 μM) into P6MQ (125 nM) and **DAPI** (100 nM). E.) Competitive titration of **H3K4Me$_2$** (100 μM) into P6MQ (125 nM) and **DAPI** (100 nM). F.) Competitive titration of **H3K4Me$_3$** (15 μM) into P6MQ (125 nM) and **DAPI** (100 nM). G.) Competitive titration of Asym-H3R2Me$_2$ (15 μM) into P6MQ (125 nM) and **DAPI** (100 nM) H.) Competitive titration of **Sym-H3R2Me$_2$** (15 μM) into P6MQ (125 nM) and **DAPI** (100 nM).

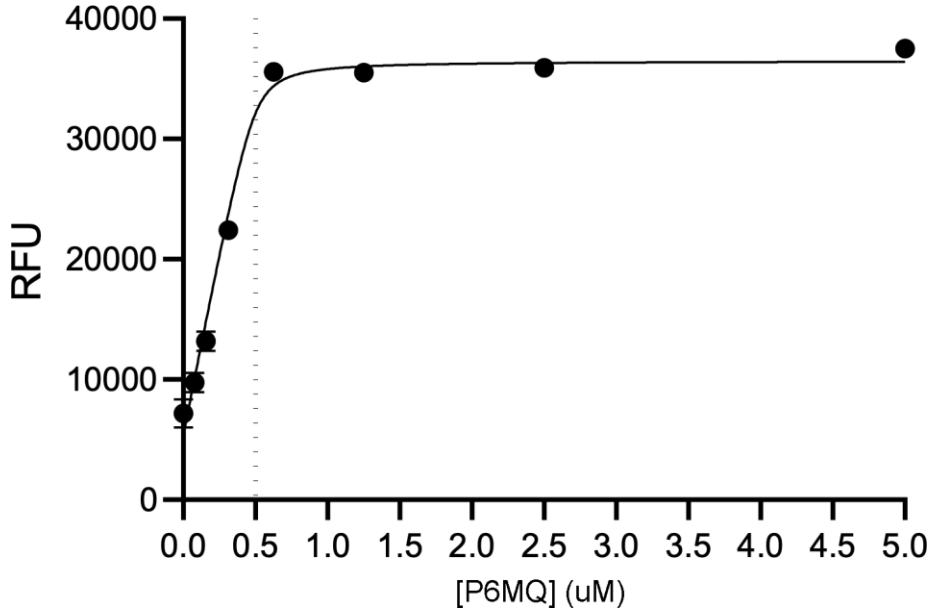

Figure SIII-26. Determination of P[6]AS•DAPI stoichiometry. Direct titration of P[6]AS into **DAPI** (0.5 μM). Preformed in duplicate in 10 mM phosphate buffer, pH 7.4. Saturation reached at 0.5 μM P[6]AS indicating 1:1 complexation.

^{1}H NMR spectra of P5MQ with selected guests.

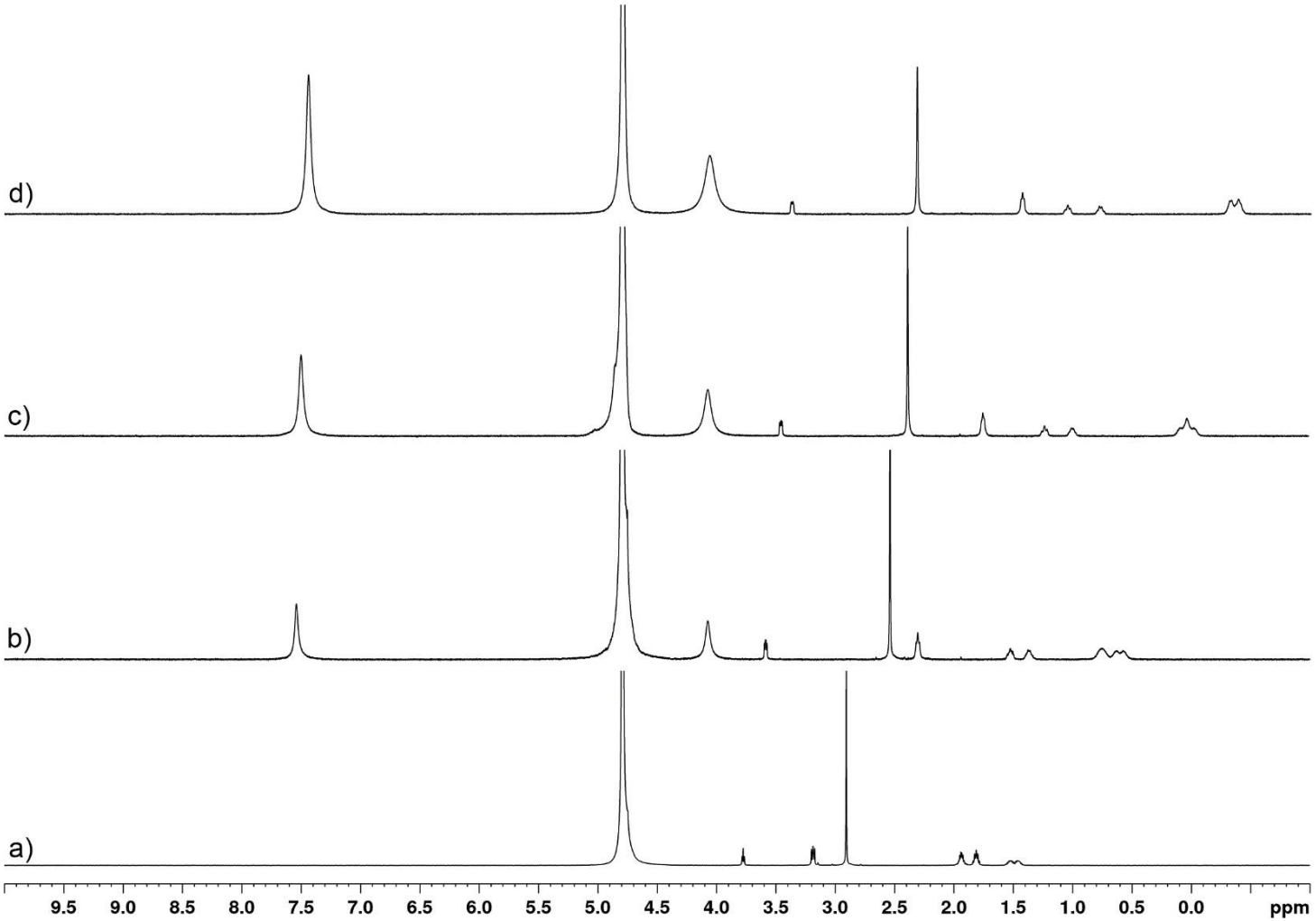

Figure SIII-27. ^{1}H NMR spectra recorded for (600 MHz, RT, phosphate buffered saline D_2O, pD 7.4) for: a) **H-K(Me$_2$)-OH** (1.0 mM), b) a mixture of **H-K(Me$_2$)-OH** (1.0 mM) and P5MQ (0.5 mM), c) an equimolar mixture of **H-K(Me$_2$)-**OH and P5MQ (1.0 mM), and d) a mixture of **H-K(Me$_2$)-OH** (1.0 mM) and P5MQ (2.0 mM).

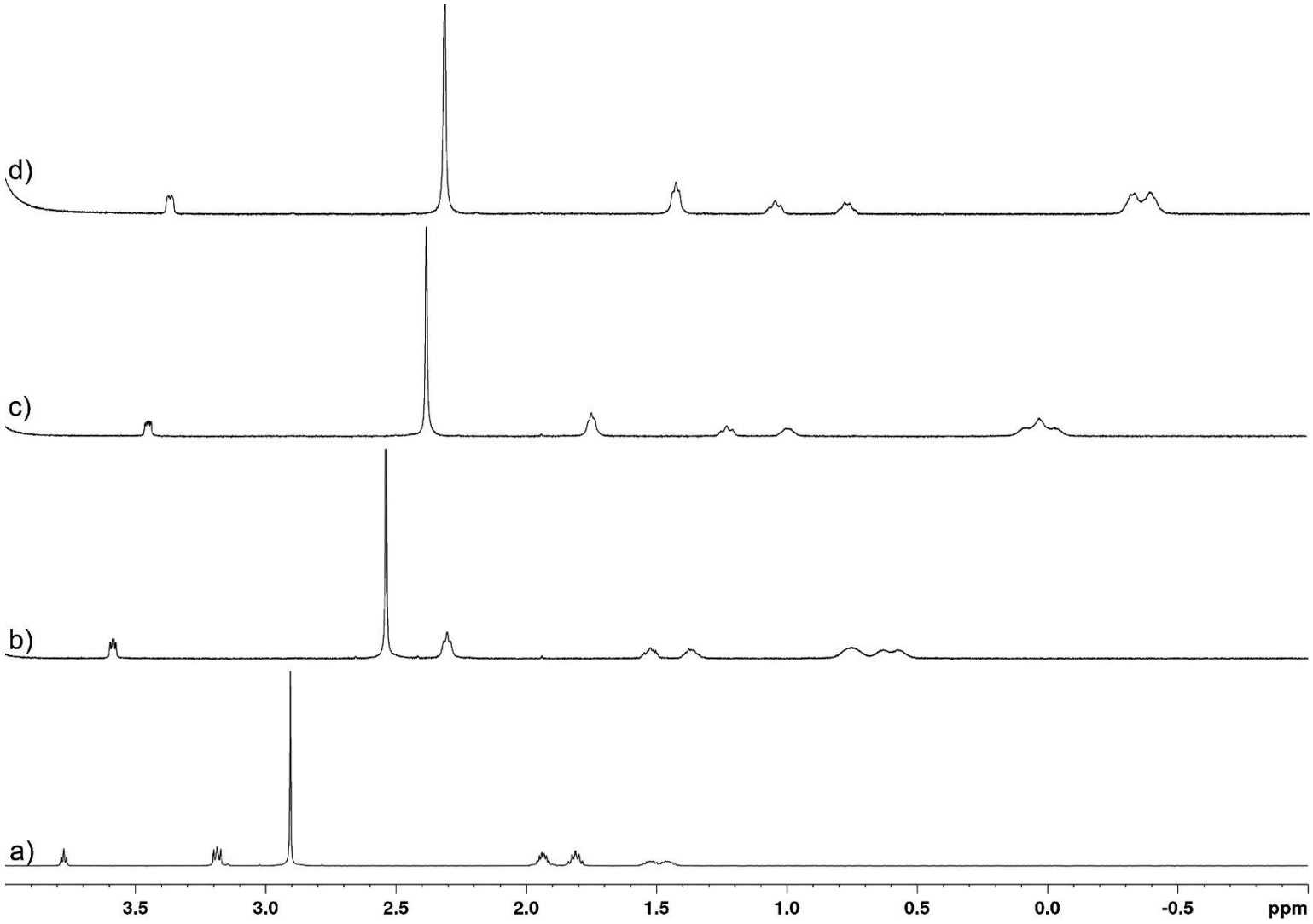

Figure SIII-28. Guest region of ^{1}H NMR spectra recorded for (600 MHz, RT, phosphate buffered saline D_2O, pD 7.4) for: a) **H-K(Me$_2$)- OH** (1.0 mM), b) a mixture of **H-K(Me$_2$)-OH** (1.0 mM) and P5MQ (0.5 mM), c) an equimolar mixture of **H-K(Me$_2$)-OH** and P5MQ (1.0 mM), and d) a mixture of **H-K(Me$_2$)-OH** (1.0 mM) and P5MQ (2.0 mM).

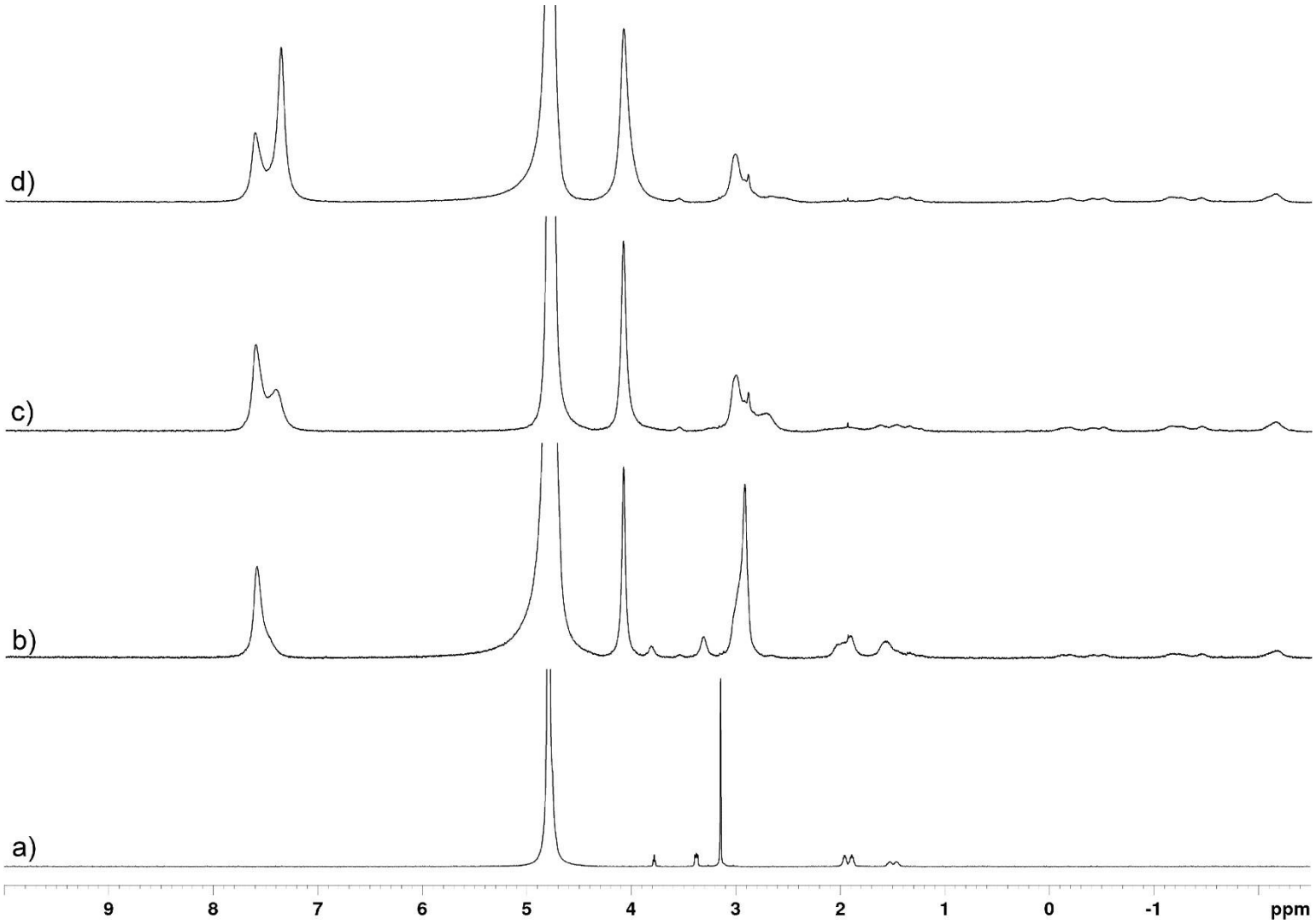

Figure SIII-29. ^{1}H NMR spectra recorded for (600 MHz, RT, phosphate buffered saline D_2O, pD 7.4) for: a) **H-K(Me$_3$)-OH** (1.0 mM), b) a mixture of **H-K(Me$_3$)-OH** (1.0 mM) and P5MQ (0.5 mM), c) an equimolar mixture of **H-K(Me$_3$)-OH** and P5MQ (1.0 mM), and d) a mixture of **H-K(Me$_3$)-OH** (1.0 mM) and P5MQ (2.0 mM).

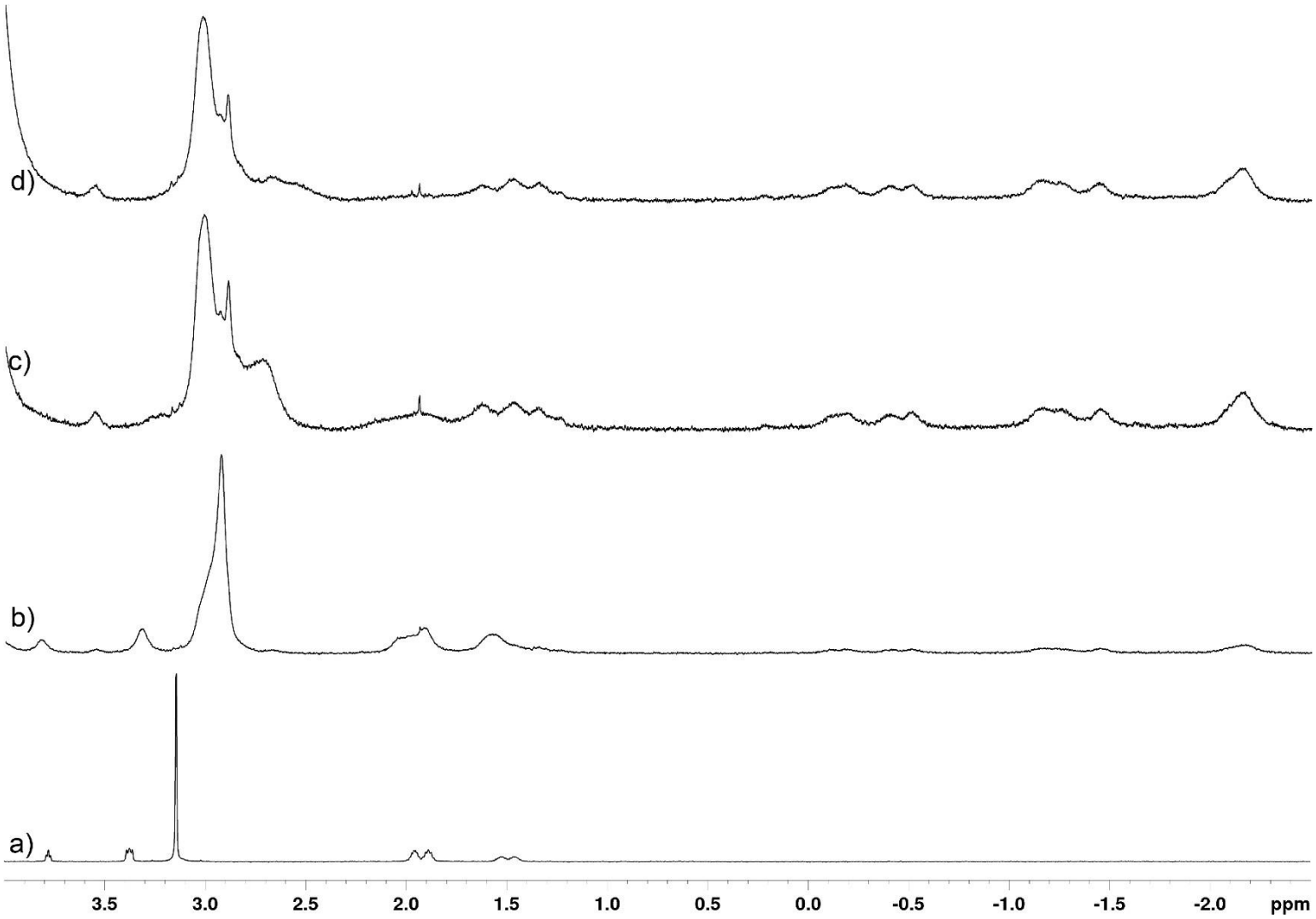

Figure SIII-30. Guest region of ^{1}H NMR spectra recorded for (600 MHz, RT, phosphate buffered saline D_2O, pD 7.4) for: a) **H-K(Me$_3$)- OH** (1.0 mM), b) a mixture of **H-K(Me$_3$)-OH** (1.0 mM) and P5MQ (0.5 mM), c) an equimolar mixture of **H-K(Me$_3$)-OH** and P5MQ (1.0 mM), and d) a mixture of **H-K(Me$_3$)-OH** (1.0 mM) and P5MQ (2.0 mM).

^{1}H NMR spectra of P6MQ with selected guests.

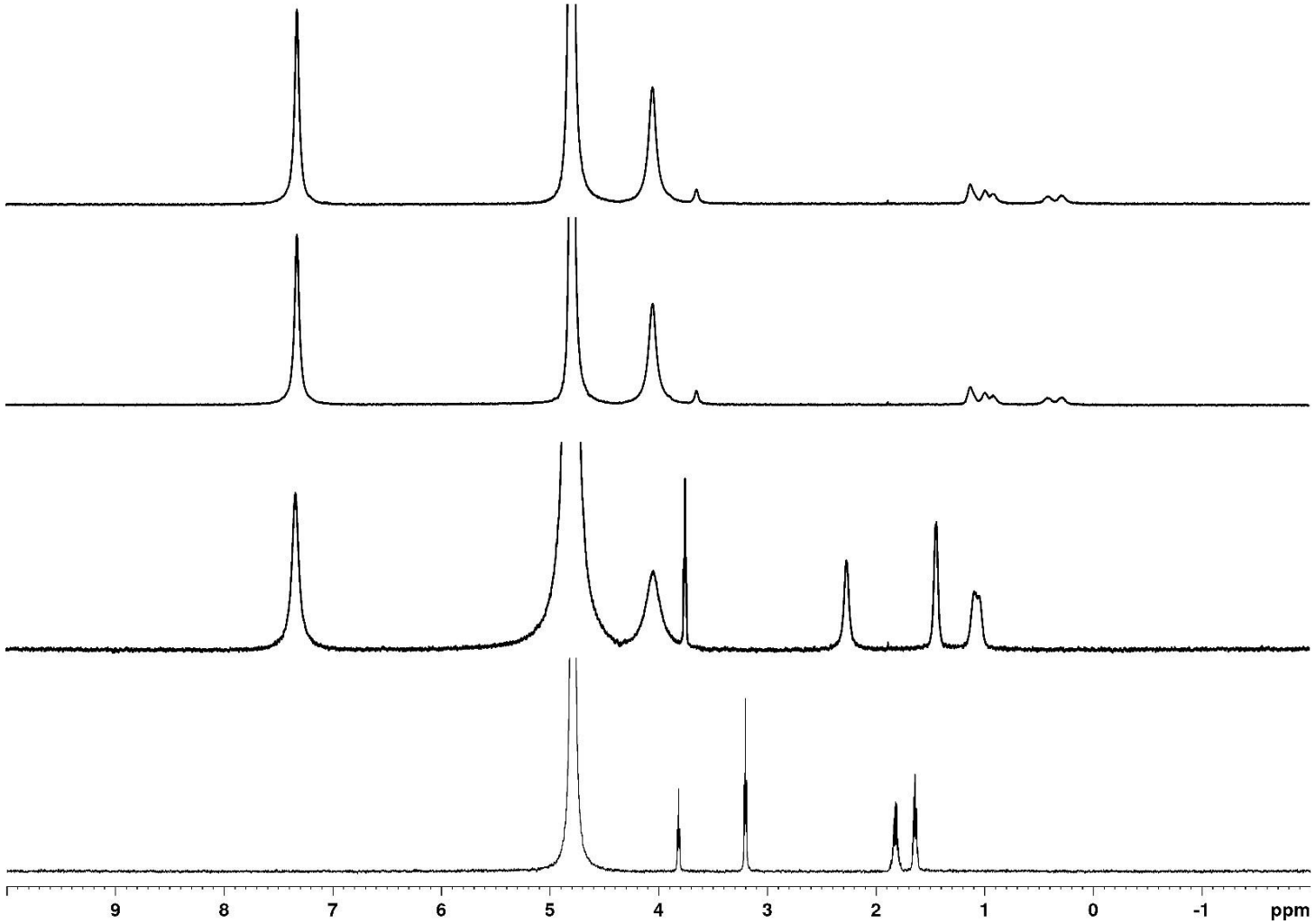

Figure SIII-31. ^{1}H NMR spectra recorded for (600 MHz, RT, phosphate buffered saline D_2O, pD 7.4) for: a) **H-R-NH$_2$** (1.0 mM), b) a mixture of **H-R-NH$_2$** (1.0 mM) and P6MQ (0.5 mM), c) an equimolar mixture of **H-R-NH$_2$** and P6MQ (1.0 mM), and d) a mixture of **H-R-NH$_2$** (1.0 mM) and P6MQ (2.0 mM).

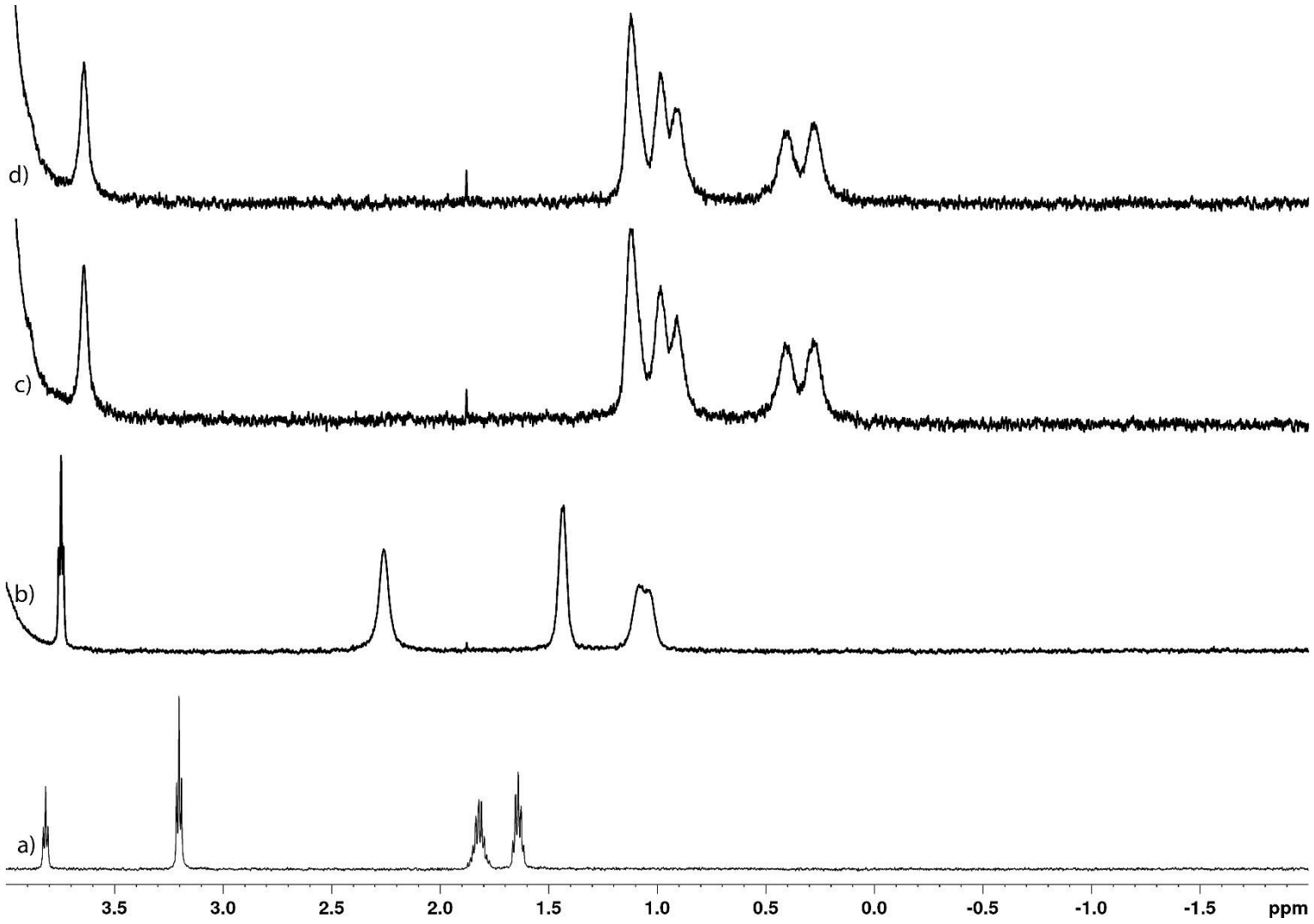

Figure SIII-32. Guest region of ^{1}H NMR spectra recorded for (600 MHz, RT, phosphate buffered saline D_2O, pD 7.4) for: a) **H-R-NH$_2$** (1.0 mM), b) a mixture of **H-R-NH$_2$** (1.0 mM) and P6MQ (0.5 mM), c) an equimolar mixture of **H-R-NH$_2$** and P6MQ (1.0 mM), and d) a mixture of **H-R-NH$_2$** (1.0 mM) and P6MQ (2.0 mM).

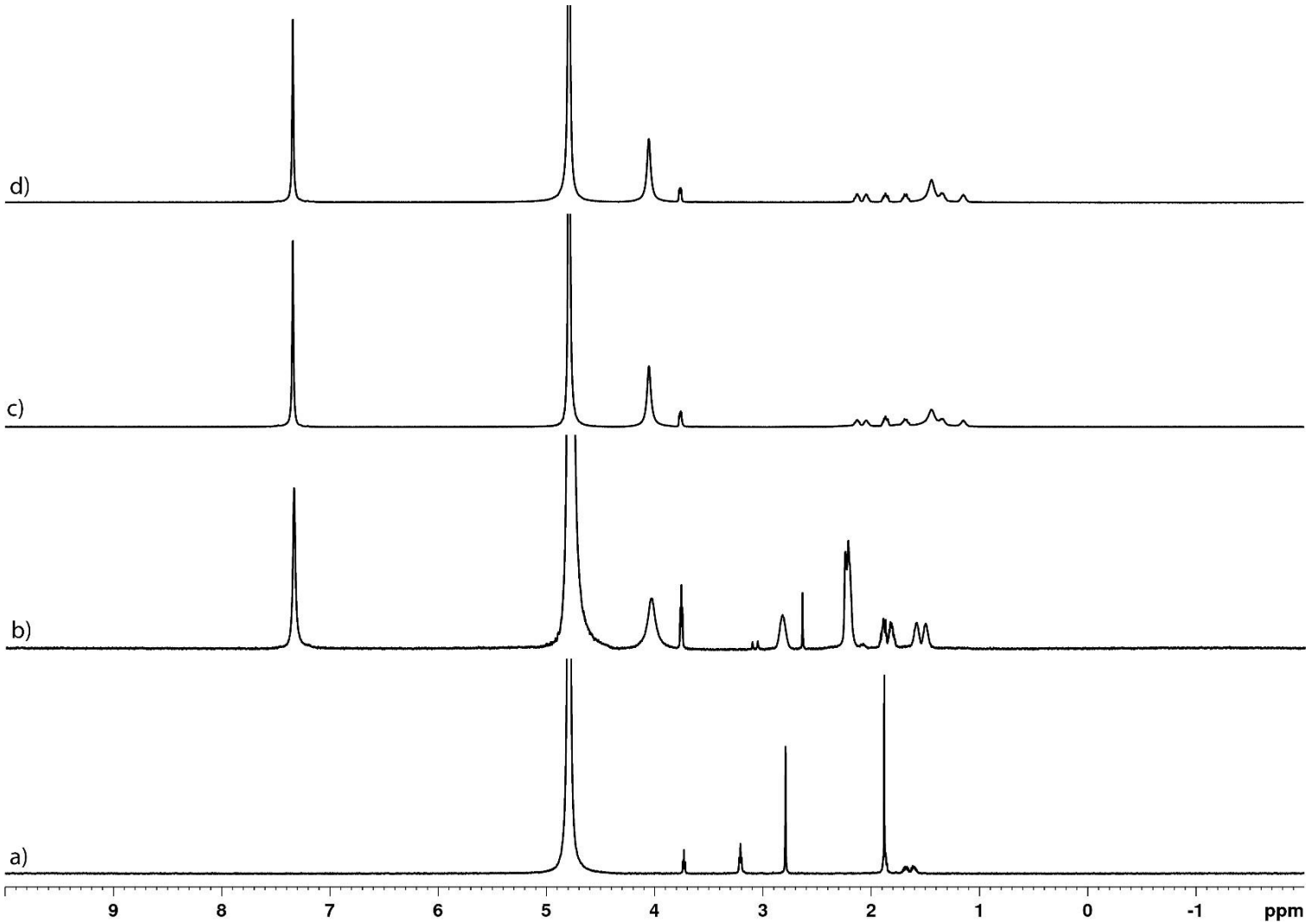

Figure SIII-33. ^{1}H NMR spectra recorded for (600 MHz, RT, phosphate buffered saline D_2O, pD 7.4) for: a) **Sym-H-R(Me$_2$)-OH** (1.0 mM), b) a mixture of **Sym-H-R(Me$_2$)-OH** (1.0 mM) and P6MQ (0.5 mM), c) an equimolar mixture of **Sym-H-R(Me$_2$)-OH** and P6MQ (1.0 mM), and d) a mixture of **Sym-H-R(Me$_2$)-OH** (1.0 mM) and P6MQ (2.0 mM).

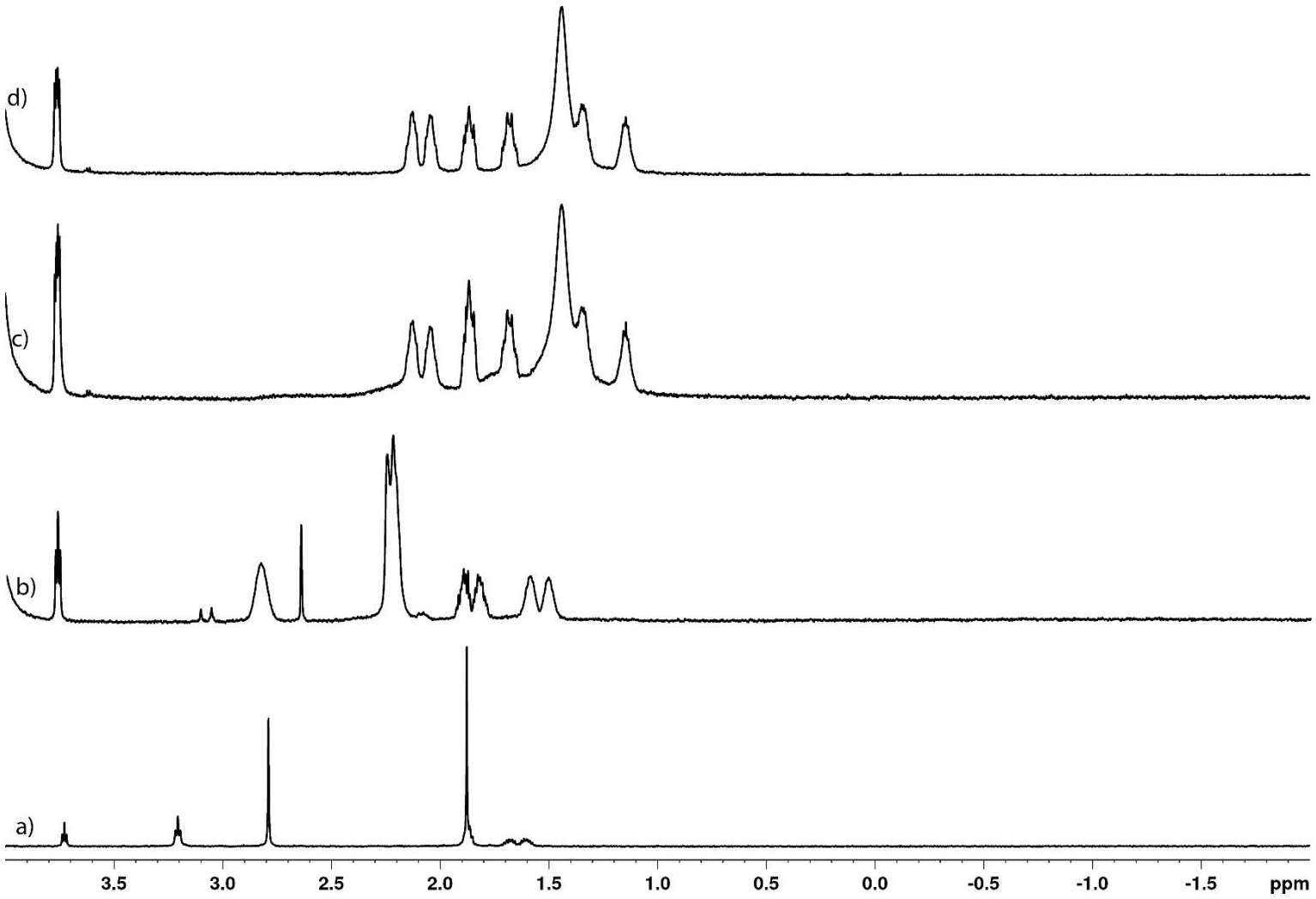

Figure SIII-34. Guest region of ^{1}H NMR spectra recorded for (600 MHz, RT, phosphate buffered saline D_2O, pD 7.4) for: a) **Sym-H- R(Me$_2$)-OH** (1.0 mM), b) a mixture of **Sym-H-R(Me$_2$)-OH** (1.0 mM) and P6MQ (0.5 mM), c) an equimolar mixture of **Sym-H- R(Me$_2$)-OH** and P6MQ (1.0 mM), and d) a mixture of **Sym-H-R(Me$_2$)-OH** (1.0 mM) and P6MQ (2.0 mM).

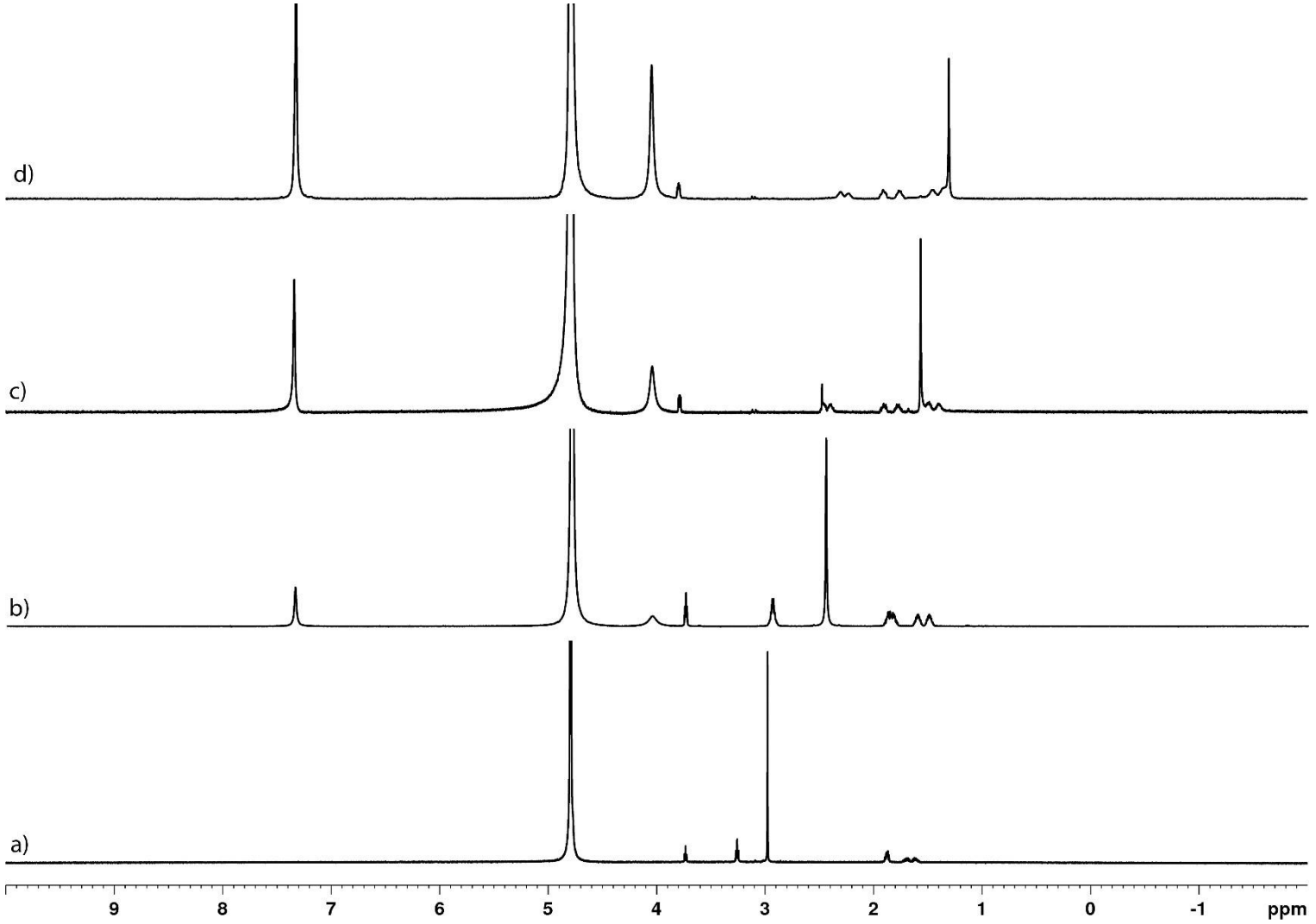

Figure SIII-35. ^{1}H NMR spectra recorded for (600 MHz, RT, phosphate buffered saline D_2O, pD 7.4) for: a) **Asym-H-R(Me$_2$)-OH** (1.0 mM), b) a mixture of **Asym-H-R(Me$_2$)-OH** (1.0 mM) and P6MQ (0.5 mM), c) an equimolar mixture of **Asym-H-R(Me$_2$)-OH** and P6MQ (1.0 mM), and d) a mixture of **Asym-H-R(Me$_2$)-OH** (1.0 mM) and P6MQ (2.0 mM).

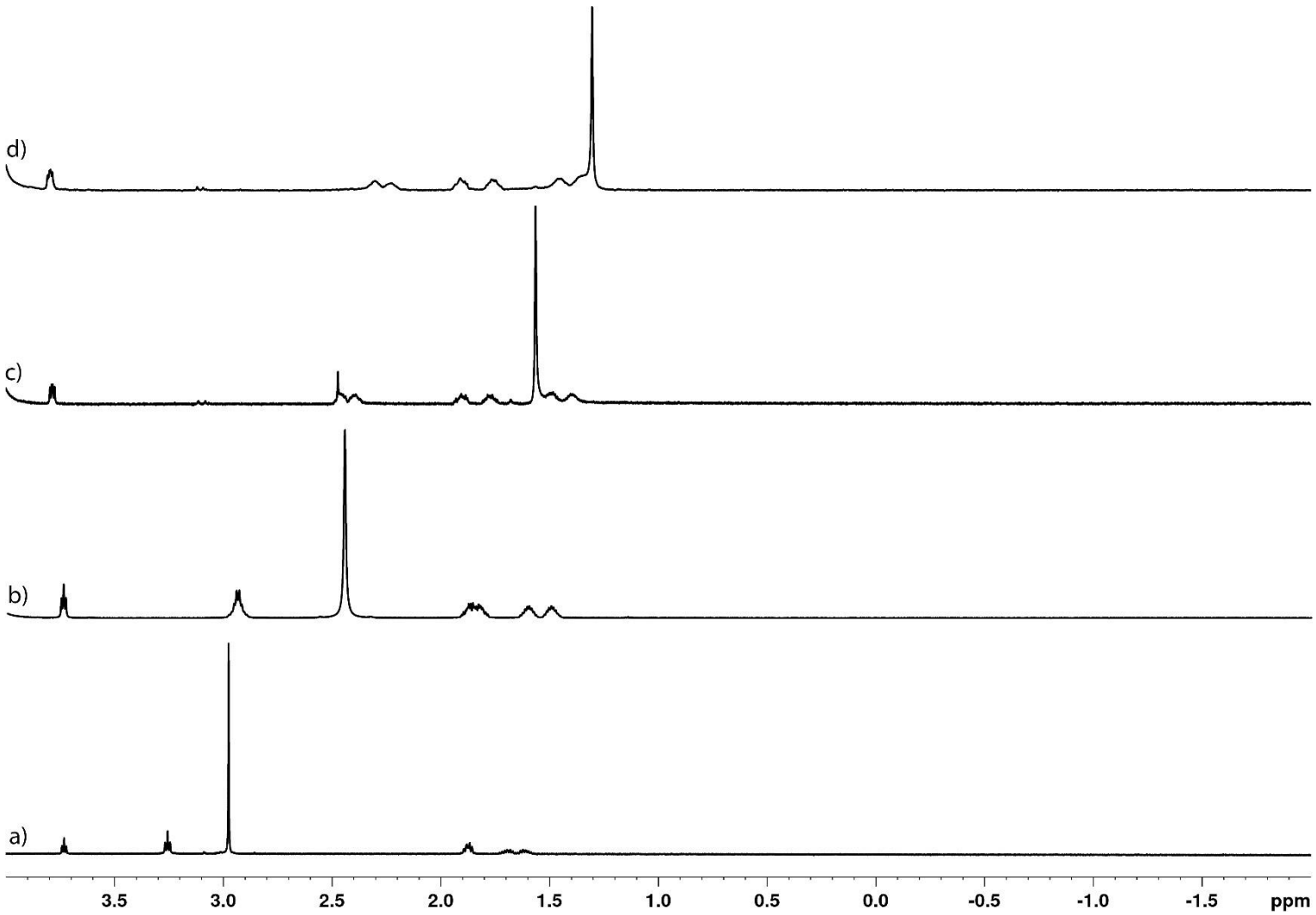

Figure SIII-36. Guest region of ^{1}H NMR spectra recorded for (600 MHz, RT, phosphate buffered saline D_2O, pD 7.4) for: a) **Asym-H- R(Me$_2$)-OH** (1.0 mM), b) a mixture of **Asym-H-R(Me$_2$)-OH** (1.0 mM) and P6MQ (0.5 mM), c) an equimolar mixture of **Asym-H- R(Me$_2$)-OH** and P6MQ (1.0 mM), and d) a mixture of **Asym-H-R(Me$_2$)-OH** (1.0 mM) and P6MQ (2.0 mM).

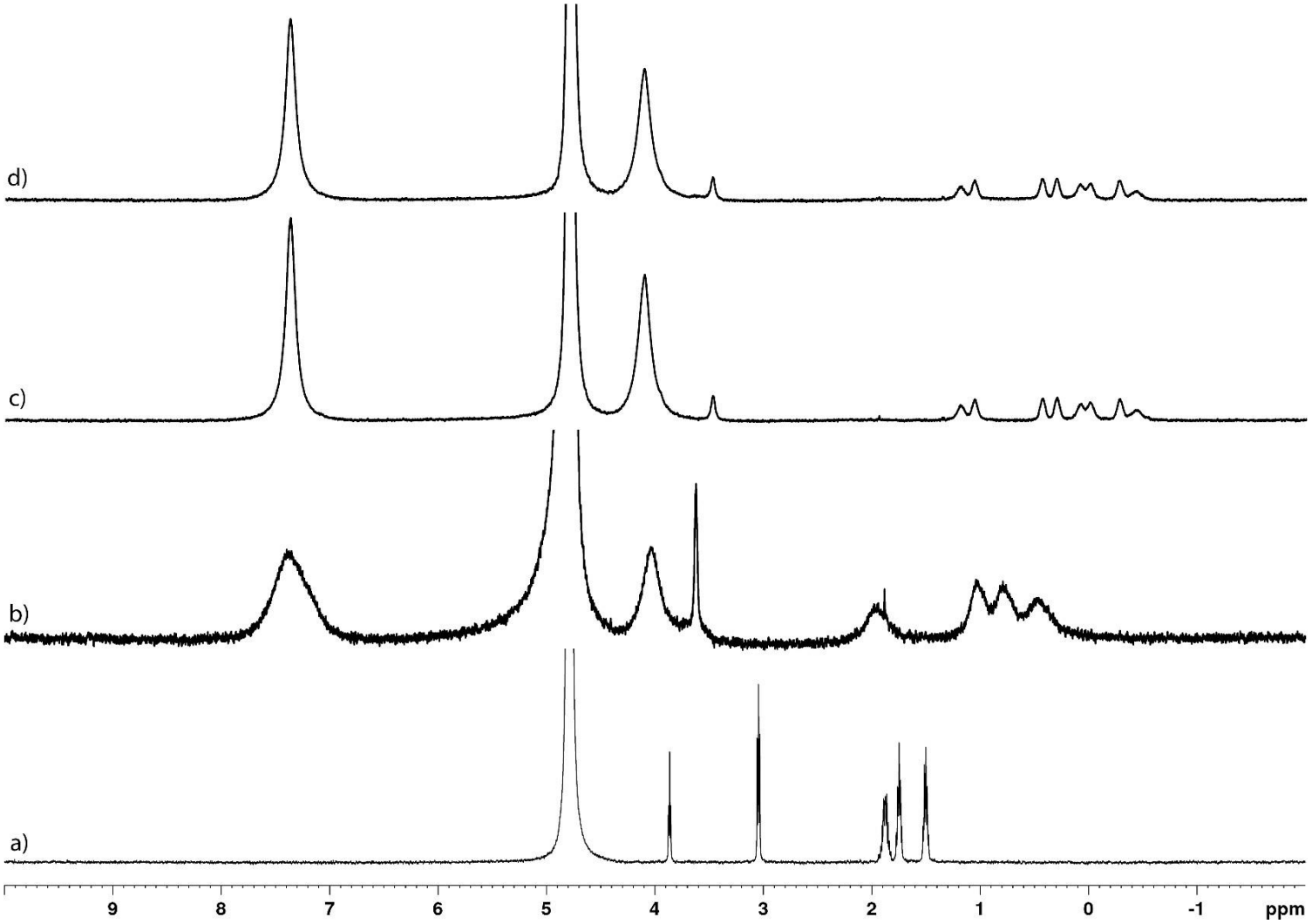

Figure SIII-37. ^{1}H NMR spectra recorded for (600 MHz, RT, phosphate buffered saline D_2O, pD 7.4) for: a) **H-K-NH$_2$** (1.0 mM), b) a mixture of **H-K-NH$_2$** (1.0 mM) and P6MQ (0.5 mM), c) an equimolar mixture of **H-K-NH$_2$** and P6MQ (1.0 mM), and d) a mixture of **H-K-NH$_2$** (1.0 mM) and P6MQ (2.0 mM).

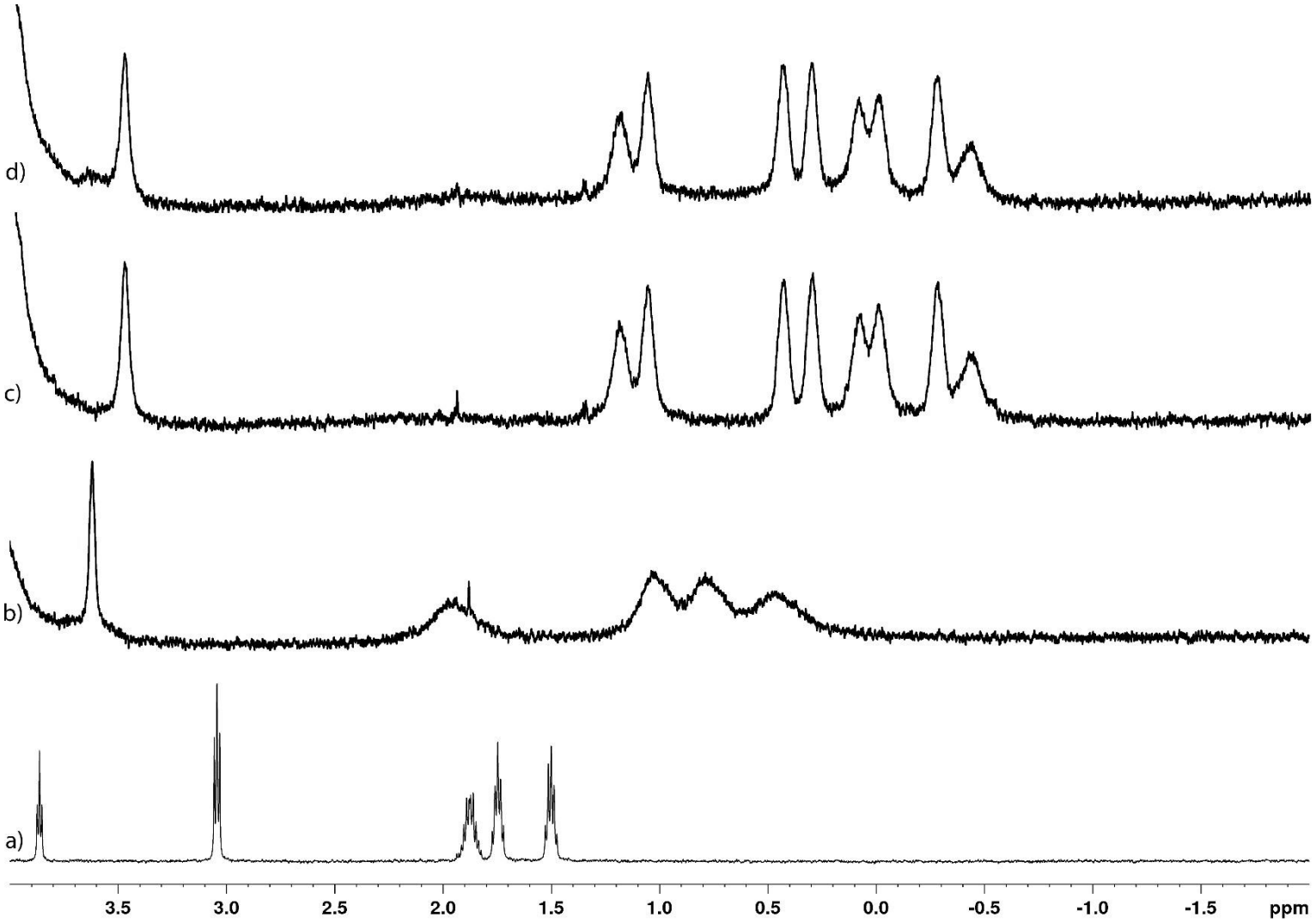

Figure SIII-38. Guest region of ^{1}H NMR spectra recorded for (600 MHz, RT, phosphate buffered saline D_2O, pD 7.4) for: a) **H-K-NH$_2$** (1.0 mM), b) a mixture of **H-K-NH$_2$** (1.0 mM) and P6MQ (0.5 mM), c) an equimolar mixture of **H-K-NH$_2$** and P6MQ (1.0 mM), and d) a mixture of **H-K-NH$_2$** (1.0 mM) and P6MQ (2.0 mM).

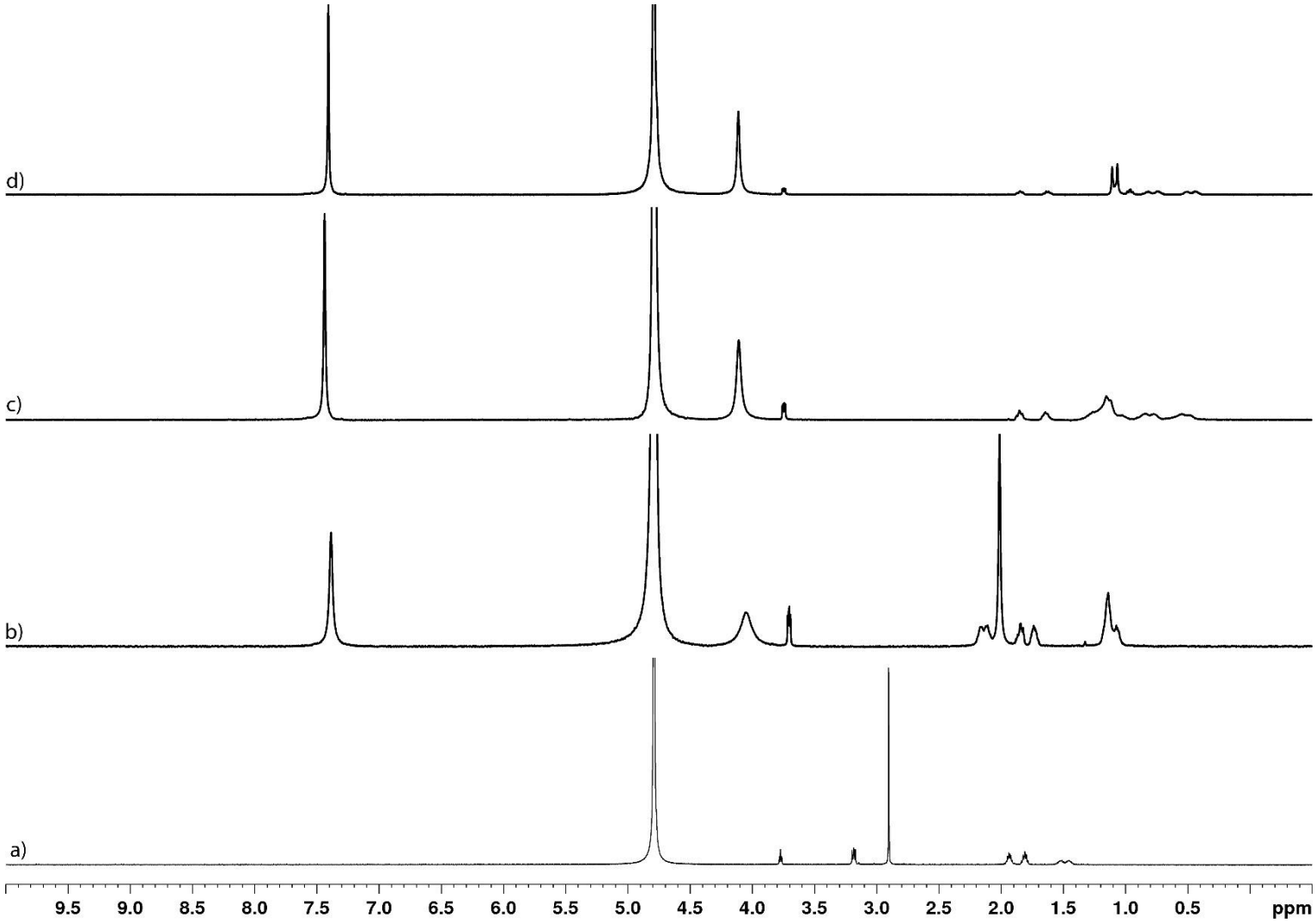

Figure SIII-39. ^{1}H NMR spectra recorded for (600 MHz, RT, phosphate buffered saline D_2O, pD 7.4) for: a) **H-K(Me$_2$)-OH** (1.0 mM), b) a mixture of **H-K(Me$_2$)-OH** (1.0 mM) and P6MQ (0.5 mM), c) an equimolar mixture of **H-K(Me$_2$)-OH** and P6MQ (1.0 mM), and d) a mixture of **H-K(Me$_2$)-OH** (1.0 mM) and P6MQ (2.0 mM).

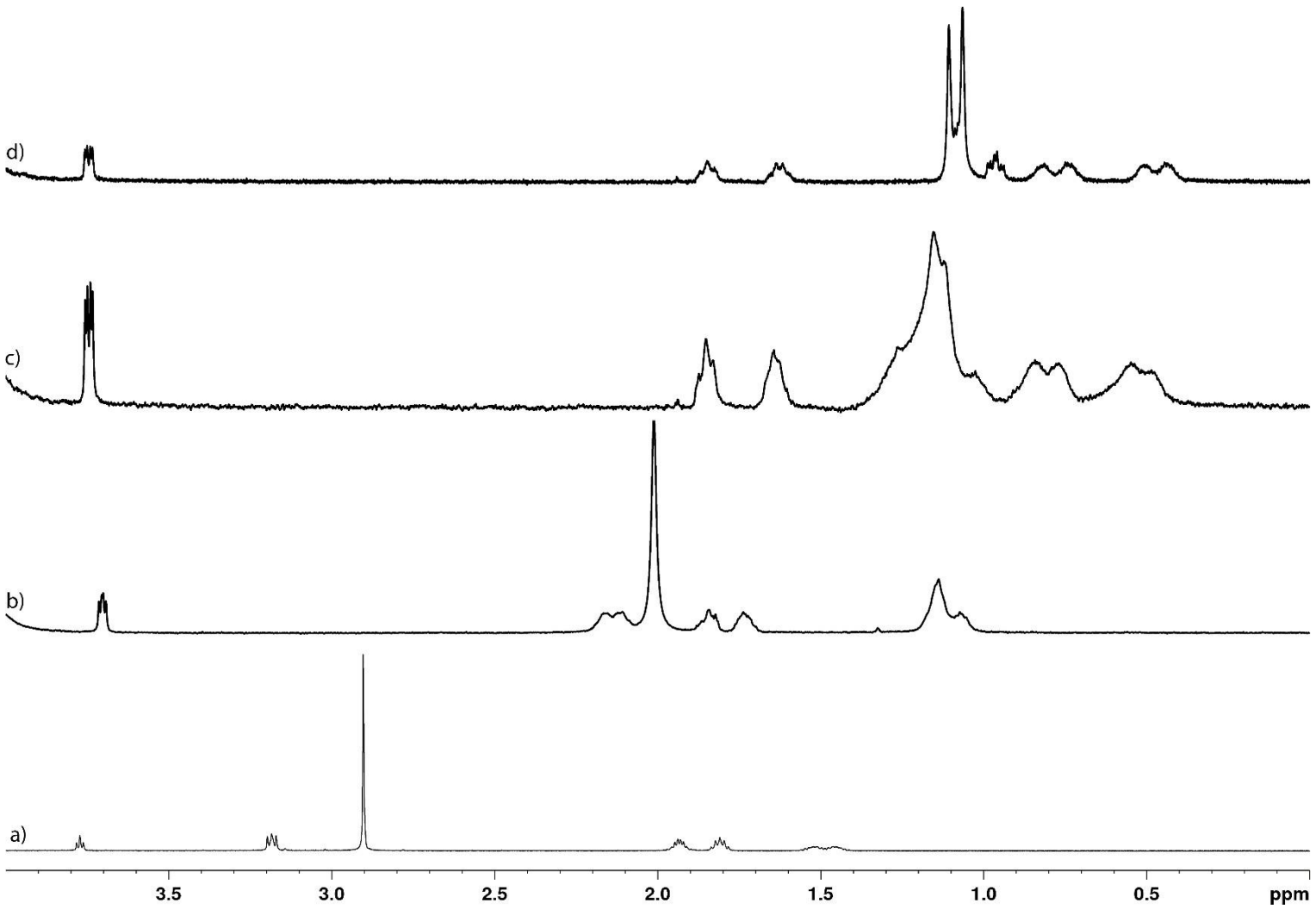

Figure SIII-40. Guest region of ^{1}H NMR spectra recorded for (600 MHz, RT, phosphate buffered saline D_2O, pD 7.4) for: a) **H-K(Me$_2$)-OH** (1.0 mM), b) a mixture of **H-K(Me$_2$)-OH** (1.0 mM) and P6MQ (0.5 mM), c) an equimolar mixture of **H-K(Me$_2$)-OH** and P6MQ (1.0 mM), and d) a mixture of **H-K(Me$_2$)-OH** (1.0 mM) and P6MQ (2.0 mM).

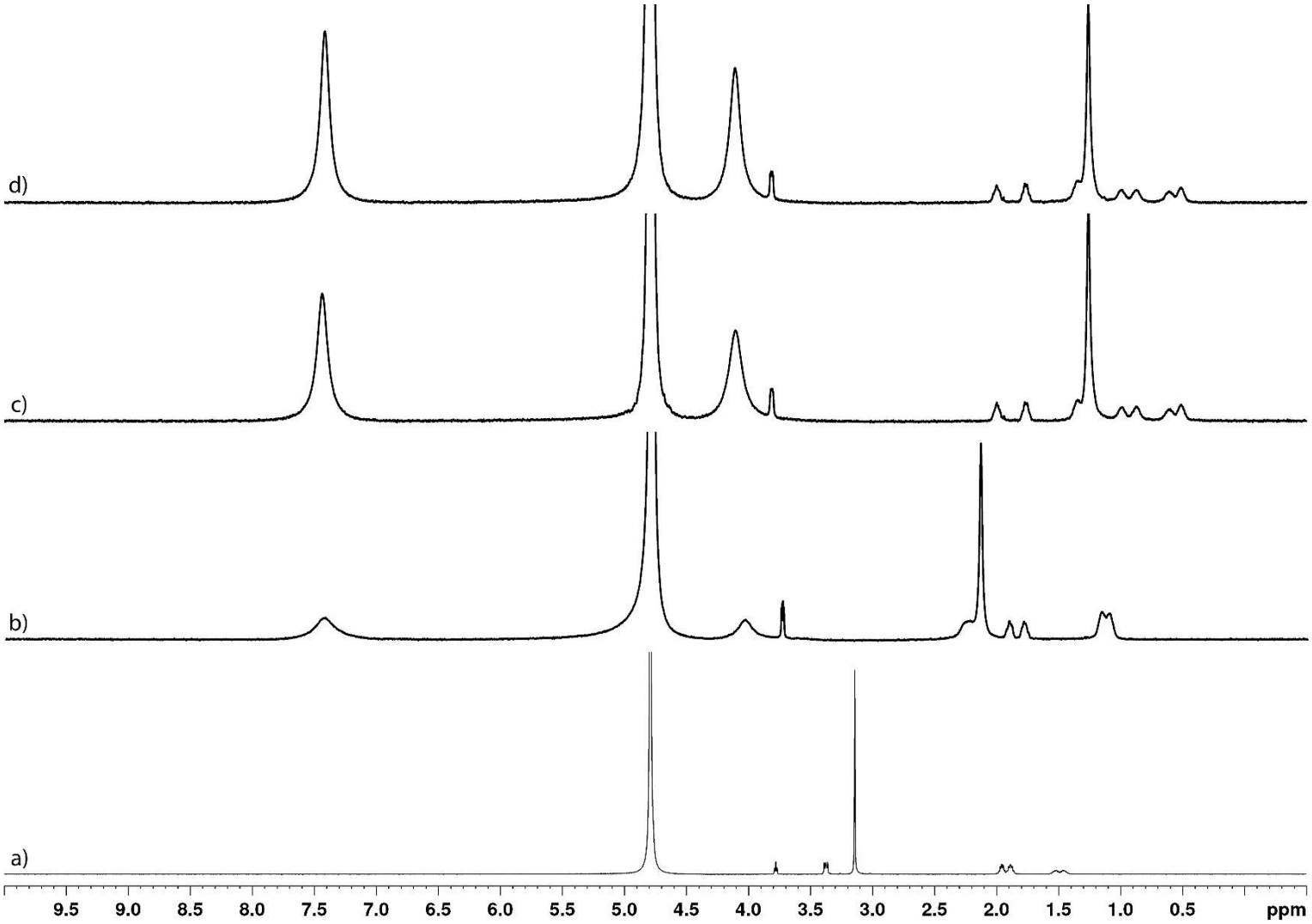

Figure SIII-41. Guest region of ^{1}H NMR spectra recorded for (600 MHz, RT, phosphate buffered saline D_2O, pD 7.4) for: a) **H-K(Me$_3$)-OH** (1.0 mM), b) a mixture of **H-K(Me$_3$)-OH** (1.0 mM) and P6MQ (0.5 mM), c) an equimolar mixture of **H-K(Me$_3$)-OH** and P6MQ (1.0 mM), and d) a mixture of **H-K(Me$_3$)-OH** (1.0 mM) and P6MQ (2.0 mM).

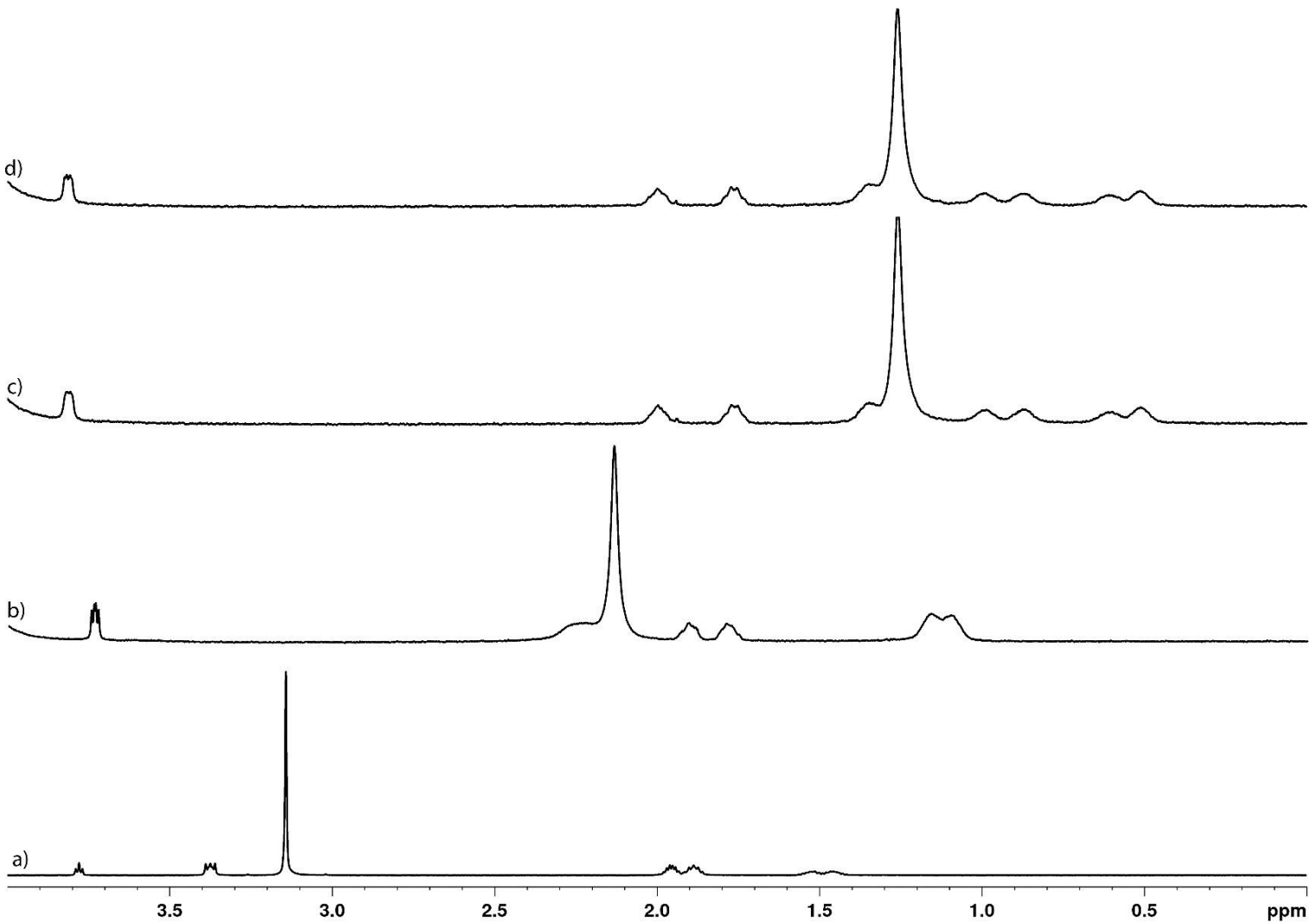

Figure SIII-42. Guest region of ^{1}H NMR spectra recorded for (600 MHz, RT, phosphate buffered saline D_2O, pD 7.4) for: a) **H-K(Me$_3$)-OH** (1.0 mM), b) a mixture of **H-K(Me$_3$)-OH** (1.0 mM) and P6MQ (0.5 mM), c) an equimolar mixture of **H-K(Me$_3$)-OH** and P6MQ (1.0 mM), and d) a mixture of **H-K(Me$_3$)-OH** (1.0 mM) and P6MQ (2.0 mM).

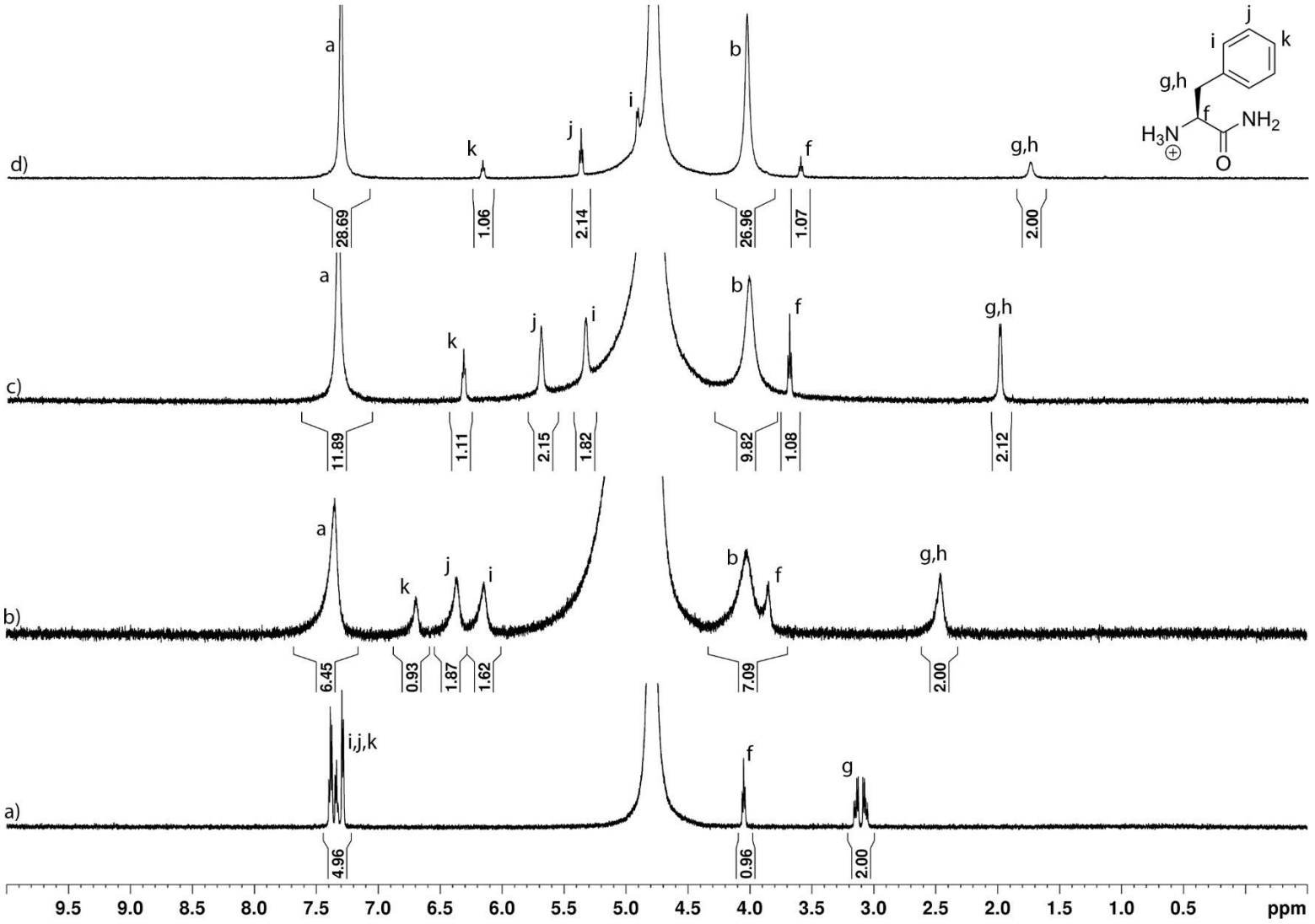

Figure SIII-43. ^{1}H NMR spectra recorded for (600 MHz, RT, phosphate buffered saline D_2O, pD 7.4) for: a) **H-F-NH$_2$** (1.0 mM), b) a mixture of **H-F-NH$_2$** (1.0 mM) and P6MQ (0.5 mM), c) an equimolar mixture of **H-F-NH$_2$** and P6MQ (1.0 mM), and d) a mixture of **H-F-NH$_2$** (1.0 mM) and P6MQ (2.0 mM).

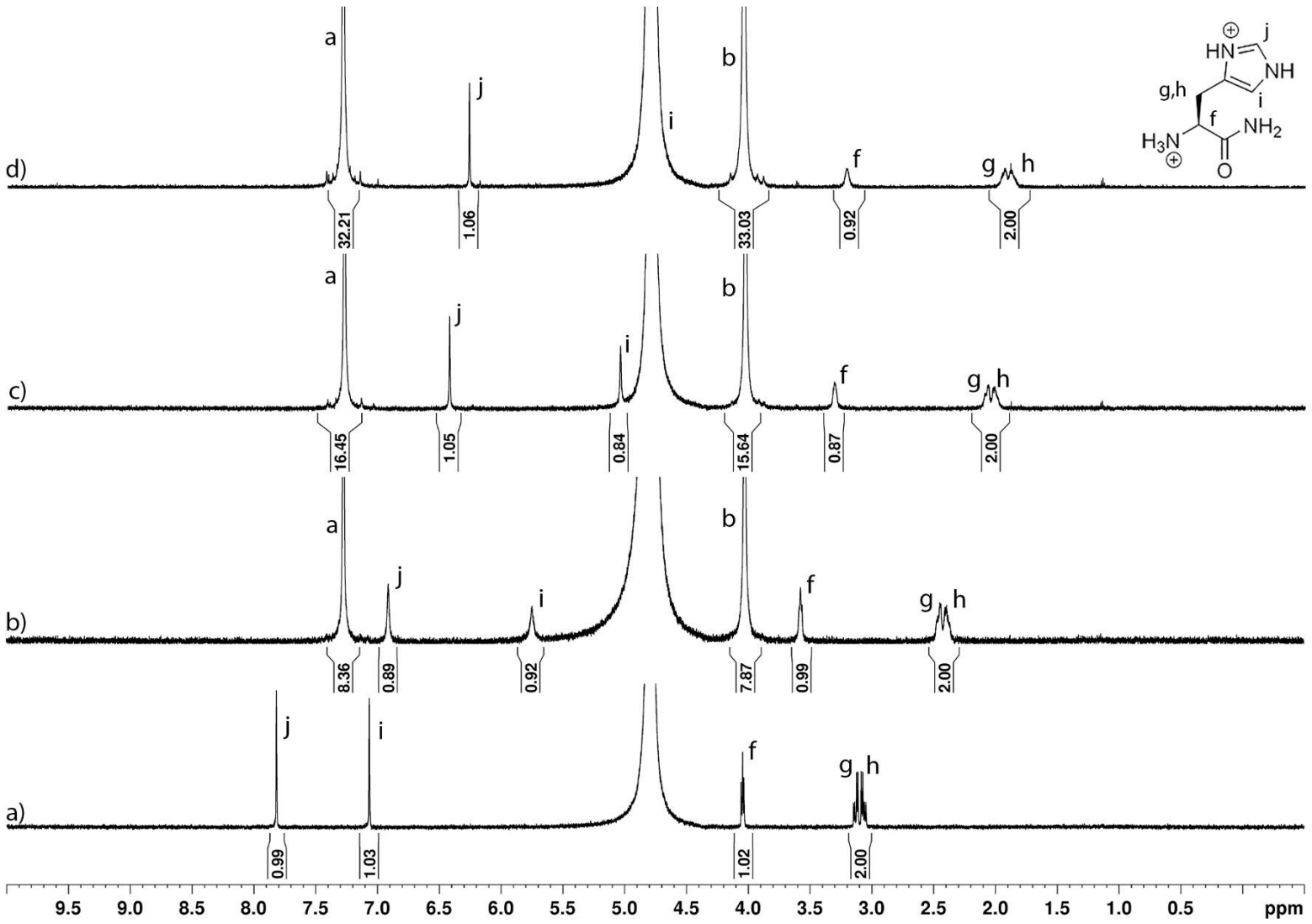

Figure SIII-44. ^{1}H NMR spectra recorded for (600 MHz, RT, phosphate buffered saline D_2O, pD 7.4) for: a) **H-H-NH$_2$** (1.0 mM), b) a mixture of **H-H-NH$_2$** (1.0 mM) and P6MQ (0.5 mM), c) an equimolar mixture of **H-H-NH$_2$** and P6MQ (1.0 mM), and d) a mixture of **H-H-NH$_2$** (1.0 mM) and P6MQ (2.0 mM).

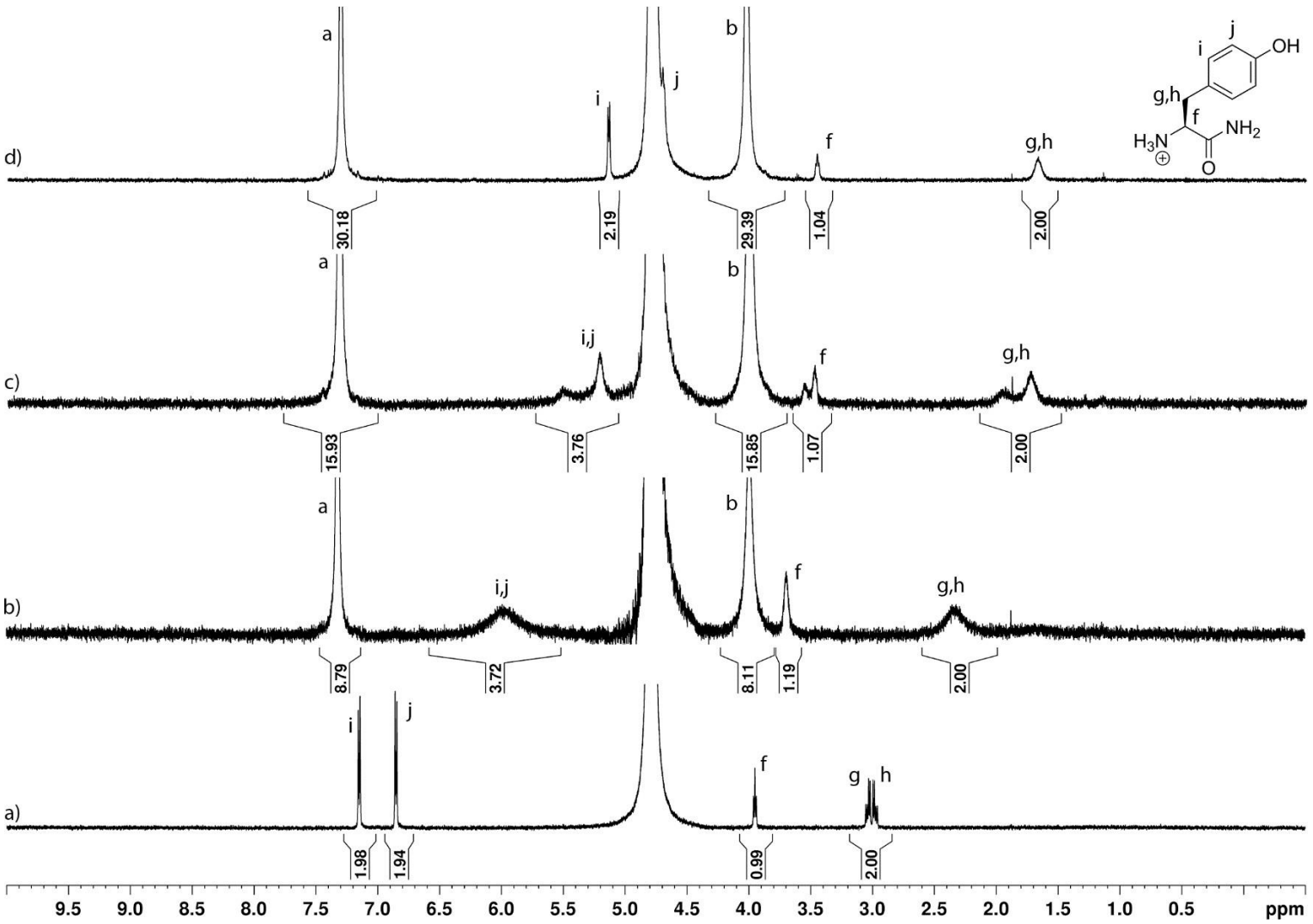

Figure SIII-45. ^{1}H NMR spectra recorded for (600 MHz, RT, phosphate buffered saline D_2O, pD 7.4) for: a) **H-Y-NH$_2$** (1.0 mM), b) a mixture of **H-Y-NH$_2$** (1.0 mM) and P6MQ (0.5 mM), c) an equimolar mixture of **H-Y-NH$_2$** and P6MQ (1.0 mM), and d) a mixture of **H-Y-NH$_2$** (1.0 mM) and P6MQ (2.0 mM).

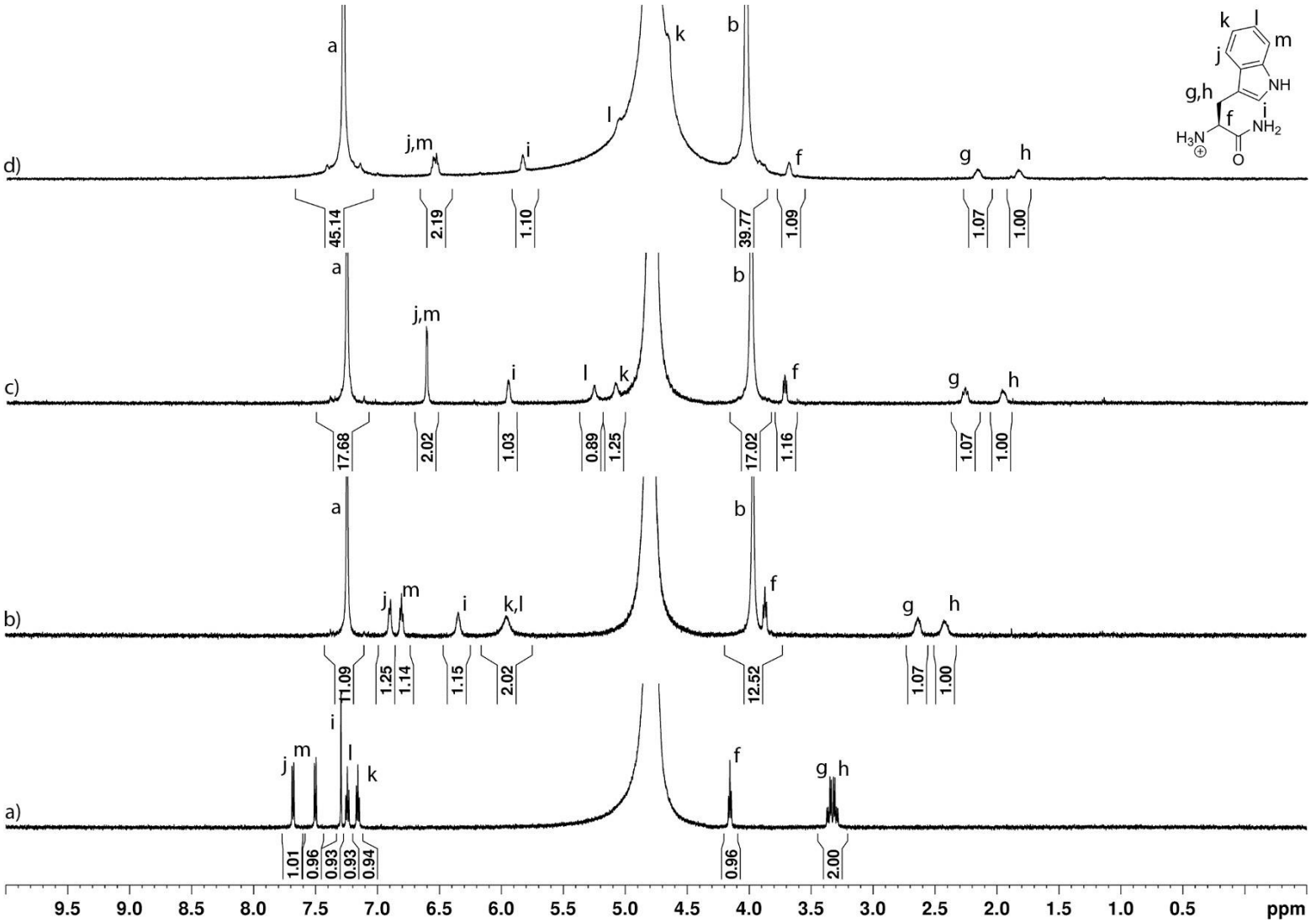

Figure SIII-46. ^{1}H NMR spectra recorded for (600 MHz, RT, phosphate buffered saline D_2O, pD 7.4) for: a) **H-W-NH$_2$** (1.0 mM), b) a mixture of **H-W-NH$_2$** (1.0 mM) and P6MQ (0.5 mM), c) an equimolar mixture of **H-W-NH$_2$** and P6MQ (1.0 mM), and d) a mixture of **H-W-NH$_2$** (1.0 mM) and P6MQ (2.0 mM).

Details of the molecular dynamics simulations

System Setup for Computations. We analyzed a total of eight systems to characterize P6MQ binding. We studied an empty P6MQ host, three free amino acids, **H3K4** and **H3K4Me$_3$** system. The **H3K4** and **H3K4Me$_3$** systems are bound in two different configurations, and the different bound configurations are treated as separate systems.

Using the NMR studies as a guide, all systems were initialized in a physically reasonable state. The **H3** systems were further minimized from the initial structure using SPARTAN software. The systems were then prepared for further minimization, equilibration, and production simulation via the following procedure.

The systems were parameterized using the AMBER GAFF2 force field, the state-of-the-art force field for parameterizing novel systems. Subsequently, each system was solvated in TIP3P water and neutralized with NaCl counter-ions at a concentration of 0.15 mM to emulate the experimental conditions. Due to the method used to calculate electrostatic interactions during simulation, the system is required to be electrically neutral. The system was prepared for simulation with periodic boundary conditions, and the size of the box is chosen such that the Van der Waals interaction strength is zero between periodic images of the system. Specific values for the simulation box size, and water, and ion counts can be found in **Table SIII-1**.

The variation in the number of water molecules in **Table SIII-1** is due to the Monte-Carlo algorithm used to fill the simulation box. The difference between the number of Na^+ and Cl^- ions is such that the system is electrically neutral and the desired concentration of ions is retained.

Table SIII-1 Values for box size and number of water and ions in each simulation

System	Box Size (Å)	Water Count	Na^+ Count	Cl^- Count
P6MQ	37	4308	16	4
H-K-OH	37	4302	16	4
H-K-NH2	37	4314	14	4
H-K(Me_3)-OH	37	4740	15	4
H3K4 (Lys bound)	42	6501	15	6
H3K4 (Arg bound)	42	6492	15	6
H3K4Me_3 (TMK bound)	42	5985	14	5
H3K4Me_3 (Arg bound)	42	5967	14	5

Simulation Details. Each of the systems were minimized using the steepest descent algorithm, and the equilibrated to 298K over 125ps. Then a 1μs production simulation was performed at 298K. In both the equilibration and production simulations a Nose-Hoover thermostat was used along with a Parrinello-Rahman barostat held at 1bar, placing the simulation under the NPT ensemble. In all cases the GROMACS simulation engine was used to perform simulations. Calculations were performed over recorded trajectories consisting of 100,000 frames each using PLUMED except where noted.

Order Parameters. We examined order parameters which aimed to characterize geometry, electrostatics, and the role of water. All calculations except for the H-bond calculations were performed using PLUMED. The order parameters included

- Bound depth: depth of the ligand in the binding cavity relative to the P6MQ center of mass
- Electrostatic distances: minimum distance between functional groups on the ligand and sulfates on P6MQ
- Na^+ Distance: minimum distance between a Na^+ ion and the P6MQ center of mass
- H-bonds: average number of H-bonds formed in the P6MQ binding cavity
- Local Density: radial distribution of water molecules within the cavity

Bound depth. The bound depth of the ligand is characterized by

$$d_{bound} = D(COM_{LIG}, COM_{OSO3^-,BOT}) - D(COM_{LIG}, COM_{OSO3^-,TOP}), \qquad \text{(Eq. SIII-4)}$$

where $COM_{OSO3^-,TOP}$ and $COM_{OSO3^-,BOT}$ refer to the center of mass of sulfates along the top portal and bottom portals respectively, and COM_{LIG} refers to the center of mass of the bound ligand. The function $D(X, Y)$ computes the 2 distance between points X and Y. The orientation of the molecule is such that the top portal is taken to be the one containing the C_α of the bound sidechain. Thus, the quantity defined in Eq. SIII-4 is positive when the center of mass of the bound sidechain is closer to the top portal and negative when the center of mass is closer to the bottom portal. The numerical value of the quantity will be accurate so long as the center of mass is located between and co-linear with the top and bottom portal. In simulations these conditions were observed to hold

approximately for all systems except for **H3K4Me$_3$** with arginine bound. When the center of mass of the ligand is located outside the binding cavity the displacements are accurate in a relative sense.

Electrostatic distances.

Functional groups were identified on each ligand and considered to study the electrostatic interaction between the host-guest complexes. These include amine groups, amide groups, and the backbone nitrogen where applicable. The minimum distance between the functional groups and P6MQ sulfates is calculated as

$$d_{FG} = \min_{\{FG\}} D(COM_{FG}, O_{P6MQ}), \quad \text{(Eq. SIII-5)}$$

where {FG} represents the set of functional groups for a ligand. The purpose of this order parameter is to quantify electrostatic interactions between the host and bound ligand.

Na$^+$ Distance. Similarly, the minimum distance between the center of P6MQ and a sodium ion is calculated as:

$$dNa = \min_{\{Na^+\}} D(Na^+, COM_{P6MQ}), \quad \text{(Eq. SIII-6)}$$

where COM_{P6MQ} represents the center of mass of the host P6MQ, and {Na^+} represents the set of sodium ions present in the system. The presence of sodium in the binding cavity was observed to play a role in deciding the hydrogen bonding structure of water in the cavity.

H-bonds. We analyzed the number of hydrogen bonds, n_{HB}, each water molecule participates in within a distance r of the P6MQ center of mass as:

$$n_{HB}(r) = 2 \times \text{Hbonds}(H_2O_{int}, H_2O_{int}) + \text{Hbonds}(H_2O_{int}, H_2O_{ext}) +$$

$$\text{Hbonds}(H_2O_{int}, \text{P6MQ}) + \text{Hbonds}(H_2O_{int, \text{LIG}})' \qquad \text{(Eq. SIII-7)}$$

where the function Hbonds(X,Y) counts the number of hydrogen bonds formed between the groups X and Y. In Eq. SIII-7 P6MQ and LIG represent the atoms of the host and bound ligand which are able to accept and donate hydrogen bonds (N, O, H), and H_2O_{int} and H_2O_{ext} respectively refer to water molecules within and outside of the region of interest defined by r. The number of hydrogen bonds between groups was calculated using GROMACS' built-in hbond tool. Importantly, the number of hydrogen bonds formed between water molecules within the region of interest must be counted twice since two water molecules participate in a hydrogen bond.

Local Density. We also computed local density plots derived from radial distribution functions which aim to quantify the structure of water within the binding cavity. Since the radial distribution function $g(r)$ is related to the local density $\rho(r)$ through $\rho(r) = \rho_{bulk} g(r)$, we may directly interpret $g(r)$ as the local density $\rho(r)$ because $\rho_{bulk} = 1$ for water.

Free Energy Calculation: The free energy for a collective variable $\boldsymbol{z}$ is defined as

$$F(\boldsymbol{z}) = -k_A T \log p(\boldsymbol{z}), \qquad \text{(Eq. SIII-8)}$$

where $p(\boldsymbol{z})$ is the Boltzmann probability of observing $\boldsymbol{z}$.

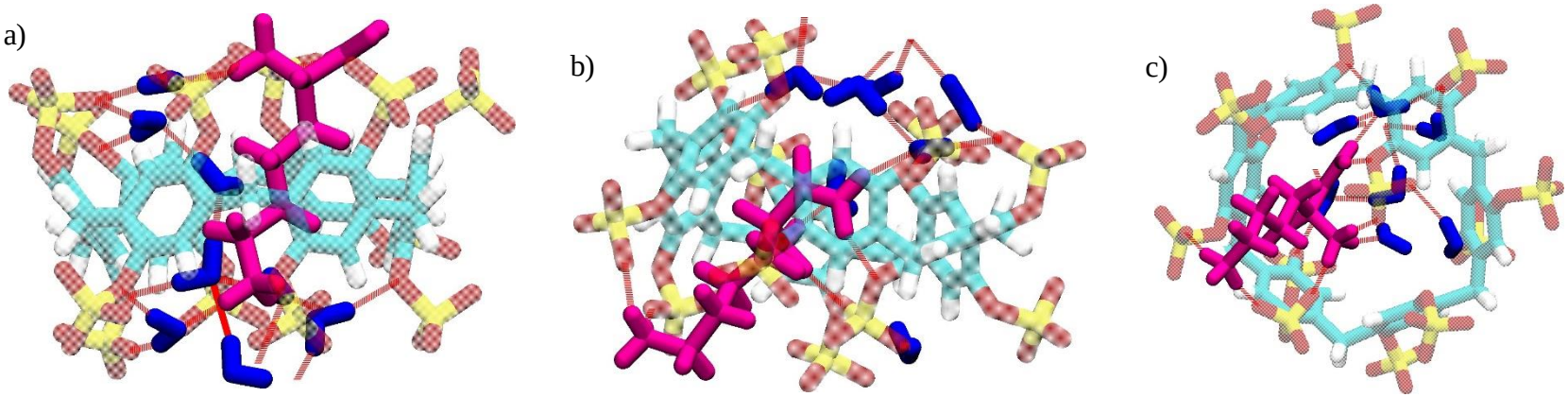

Figure SIII-47. Representative structures of P6MQ·**H-K-NH$_2$**. In all panes water molecules are depicted in blue, the ligand in magenta, and sodium ions in pink, and H-bonds in red. a) Side view of **H-K-NH$_2$** interacting with the upper portal of P6MQ. b) Side view **of H-K-NH$_2$** interacting with the lower portal of P6MQ. c) View of **H-K-NH$_2$** interacting with the lower portal of P6MQ. **H-K-NH$_2$** is capable of forming multiple H-bonds with P6MQ sulfate groups and is permissive of water in the cavity. In simulations the conformations observed in a) and b) were observed with approximately equal frequency.

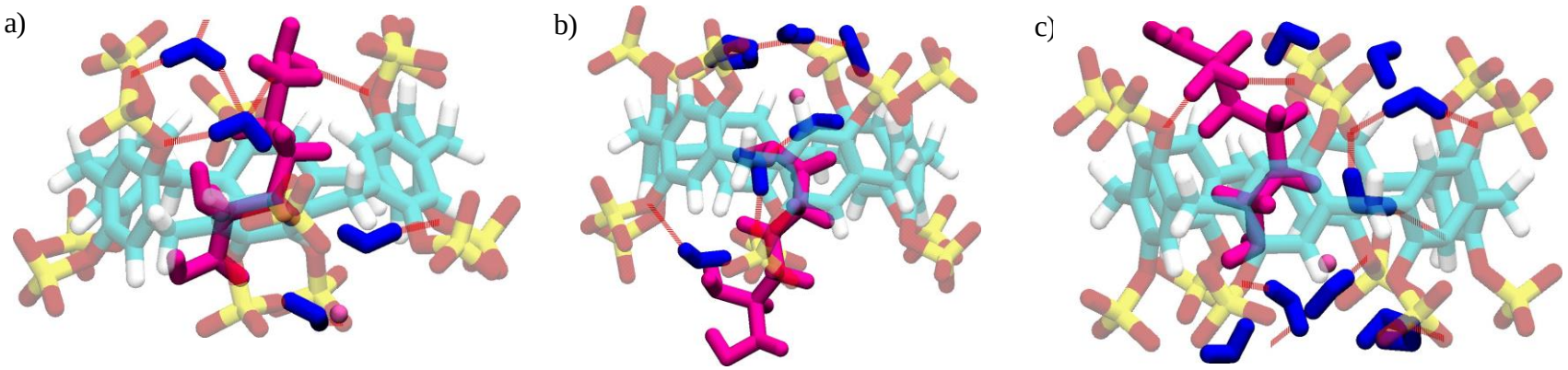

Figure SIII-48. Representative structures of P6MQ·**H-K-OH**. In all panes water molecules are depicted in blue, the ligand in magenta, and sodium ions in pink, and H-bonds in red. a) Side view of **H-K-OH** bound to the upper portal of P6MQ. c) Side view of **H-K-OH** bound to the lower portal of P6MQ. c) Side view illustrating that **H-K-OH** is permissive of water and sodium in the binding cavity. **H-K-OH** often binds to one side of the binding cavity allowing water and ions to enter the cavity. The states depicted in a) and b) were observed with approximately equal frequency during simulation.

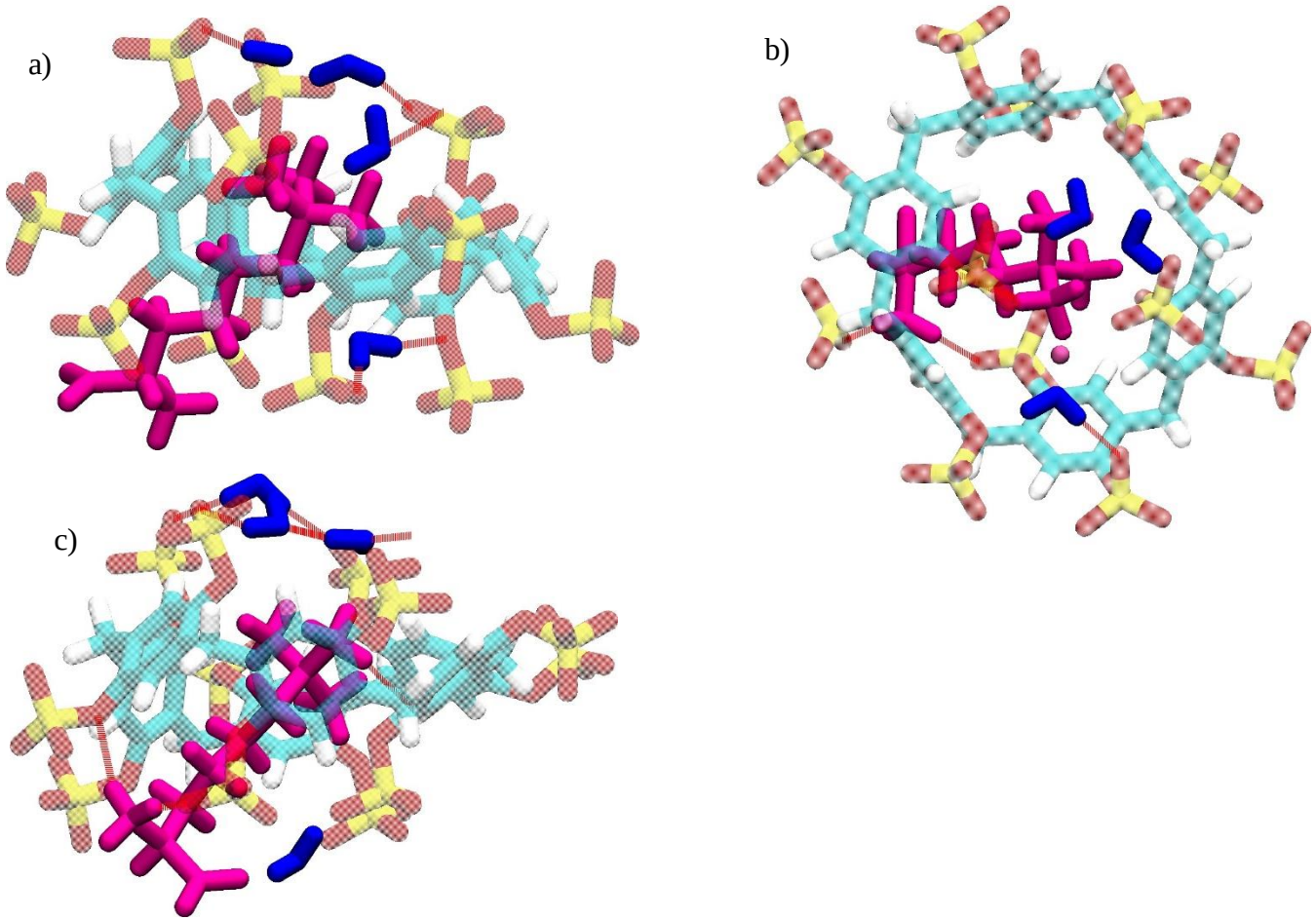

Figure SIII-49. Representative structures of P6MQ·**H-K(Me$_3$)-OH**. In all panes water molecules are depicted in blue, the ligand in magenta, and sodium ions in pink, and H-bonds in red. a) Side view of **H-K(Me$_3$)-OH** bound to the lower portal of P6MQ. b) Top view of **H-K(Me$_3$)-OH** bound to the lower portal of **H-K(Me$_3$)-OH**. The ligand is bound at an angle in the cavity. c) Side view of **H-K(Me$_3$)-OH** bound to the lower portal of P6MQ highlighting the angle at which the ligand is bound, as well as the resulting deformation of the P6MQ host. The NMe$_3$ group largely excludes water from the cavity (c.f. **H-K-NH$_2$** and **H-K-OH**). The conformation depicted in (a-c) was the only conformation observed in simulation.

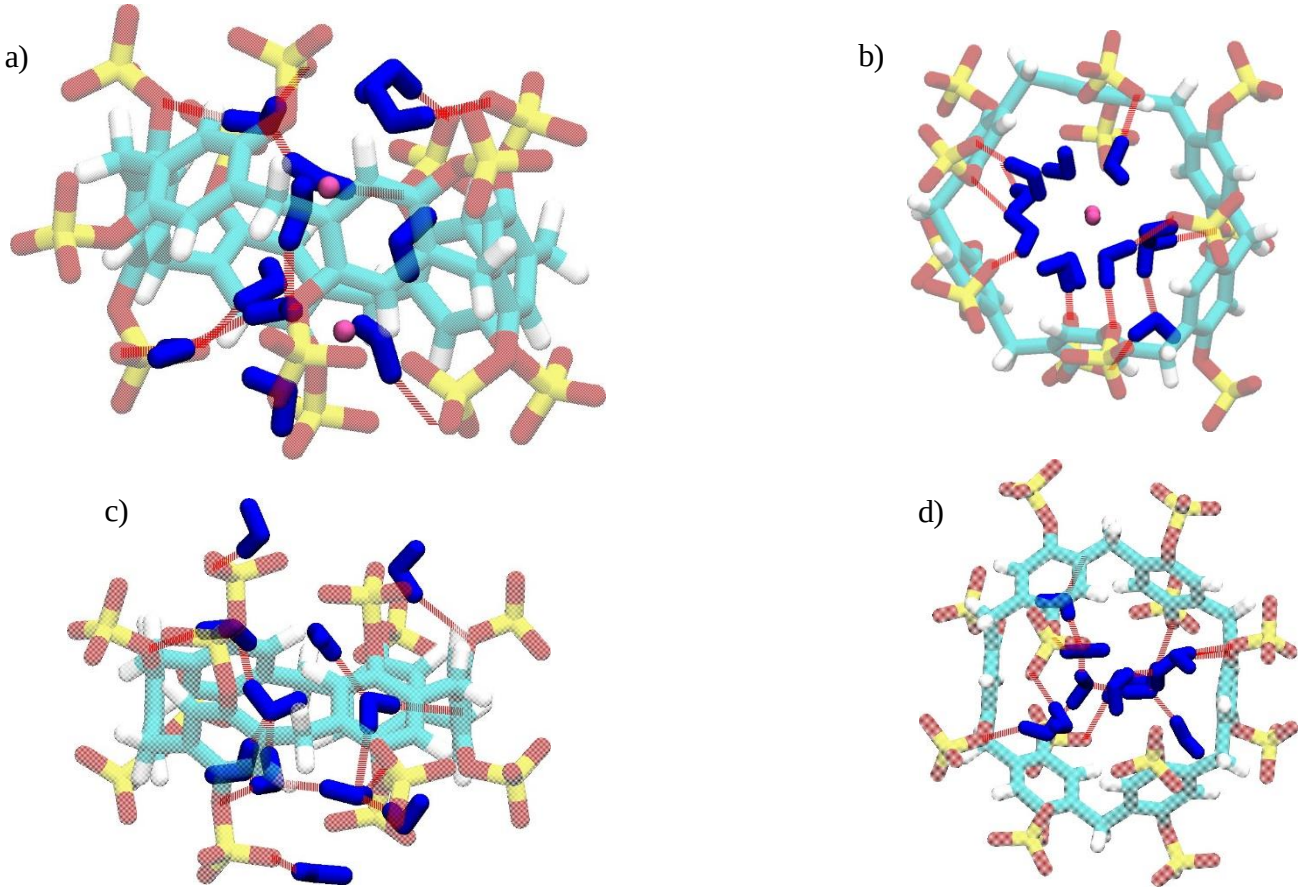

Figure SIII-50. Representative structures of unbound P6MQ. In all panes water molecules are depicted in blue, sodium ions in pink, and H-bonds in red. a) Side view of unbound P6MQ with two sodium ions in the binding cavity. b) Top view of sodium ions in the unbound P6MQ cavity. Observe how the sodium ions coordinate the water oxygens so that H-bonds are mainly formed between water hydrogens and P6MQ sulfate oxygens. c) Side view of the unbound P6MQ cavity in the absence of sodium ions. d) Top view of the unbound P6MQ cavity in the absence of sodium. Note that more hydrogen bonds are formed between waters when sodium ions are absent (c-d) compared to when sodium is present (a-b). The resulting network of hydrogen bonds is more connected in panels (c-d). The unbound state where sodium ions are absent is observed exceedingly rarely in simulation.

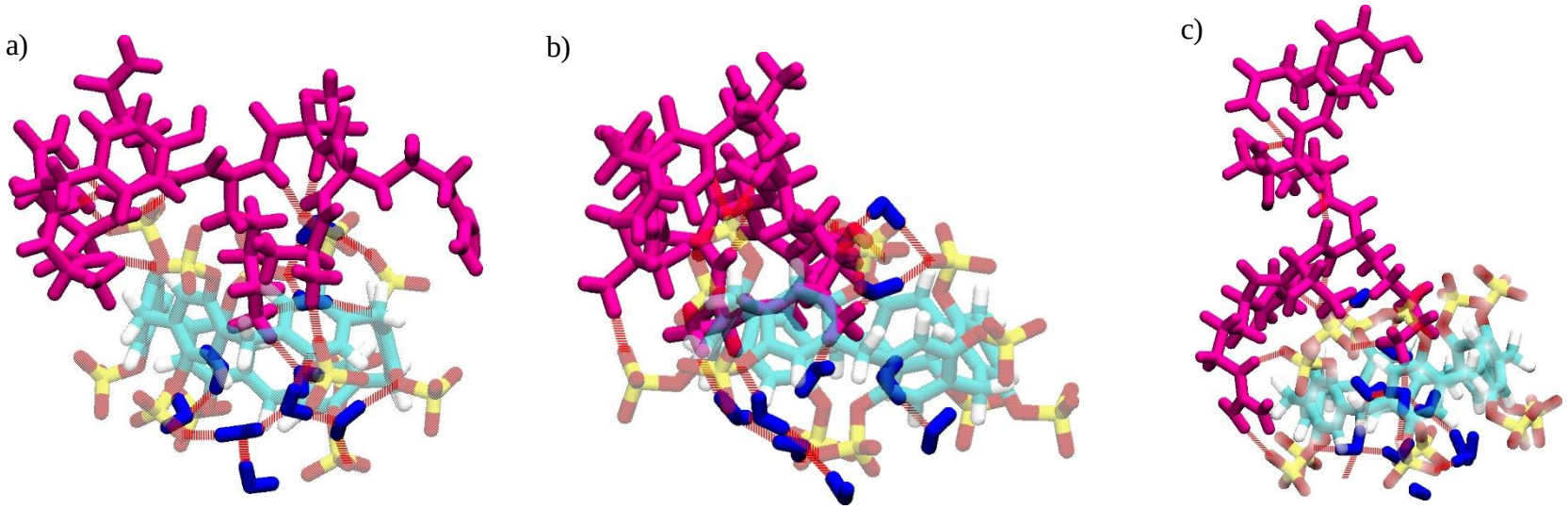

Figure SIII-51. Representative structures of P6MQ·**H3K4** (Lys bound). In all panes water molecules are depicted in blue, the ligand in magenta, and sodium ions in pink, and H-bonds in red. a) The first of two metastable states observed in simulation. The backbone and unbound sidechains participate in H-bonds with P6MQ. b) Alternative view of metastable state depicted in (a). Note the deformation of P6MQ due to the H-bond interactions between **H3K4** and P6MQ. c) The second metastable state is depicted. Here the half of the ligand containing the tyrosine ring is not interacting with P6MQ and is stabilized by H-bonds between the unbound sidechains and the backbone. Here the arginine sidechain is within π-stacking distance of the P6MQ aromatic walls. H-bonding between the arginine sidechain and P6MQ further stabilizes the π-stacking interaction.

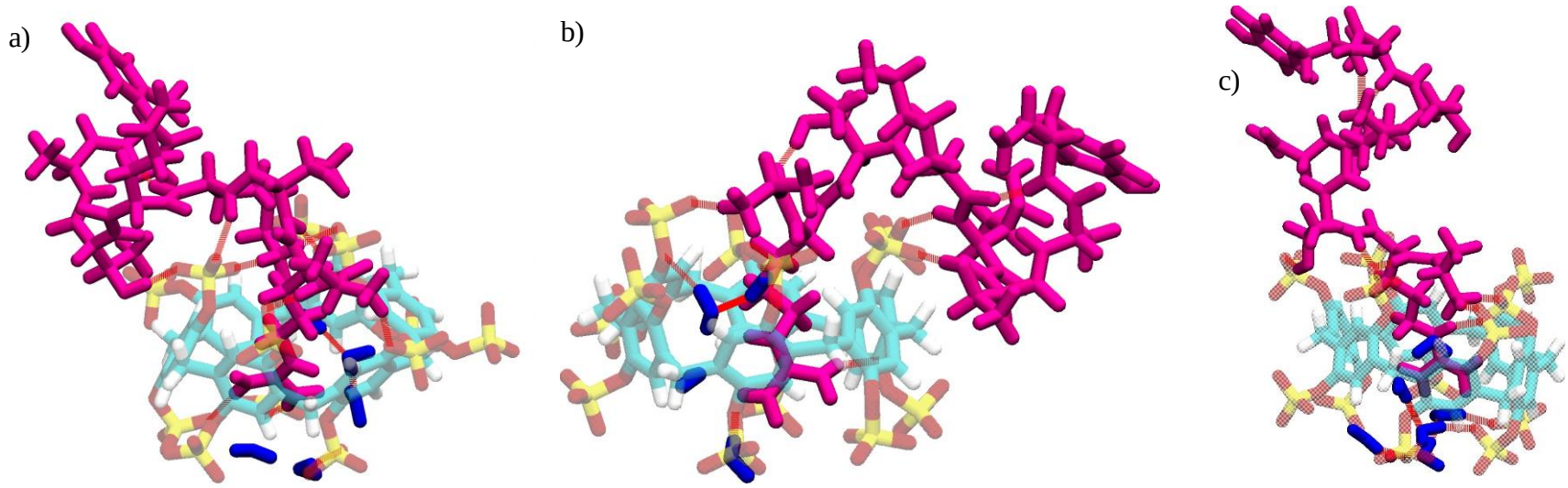

Figure SIII-52. Representative structures of P6MQ·**H3K4** (Arg bound). In all panes water molecules are depicted in blue, the ligand in magenta, and sodium ions in pink, and H-bonds in red. a) One of two metastable states observed in simulation. The bound arginine sidechain is H-bonded to the lower portal of P6MQ and the unbound sidechains and backbone for H-bonds with the upper and lower portals. b) Alternative view of the first metastable state. c) Second metastable state observed in simulation. Here the unbound sidechains and residues are stabilized away from P6MQ from H-bonds between the sidechains and backbone. H-bonding may still occur between the unbound sidechains and backbone and P6MQ.

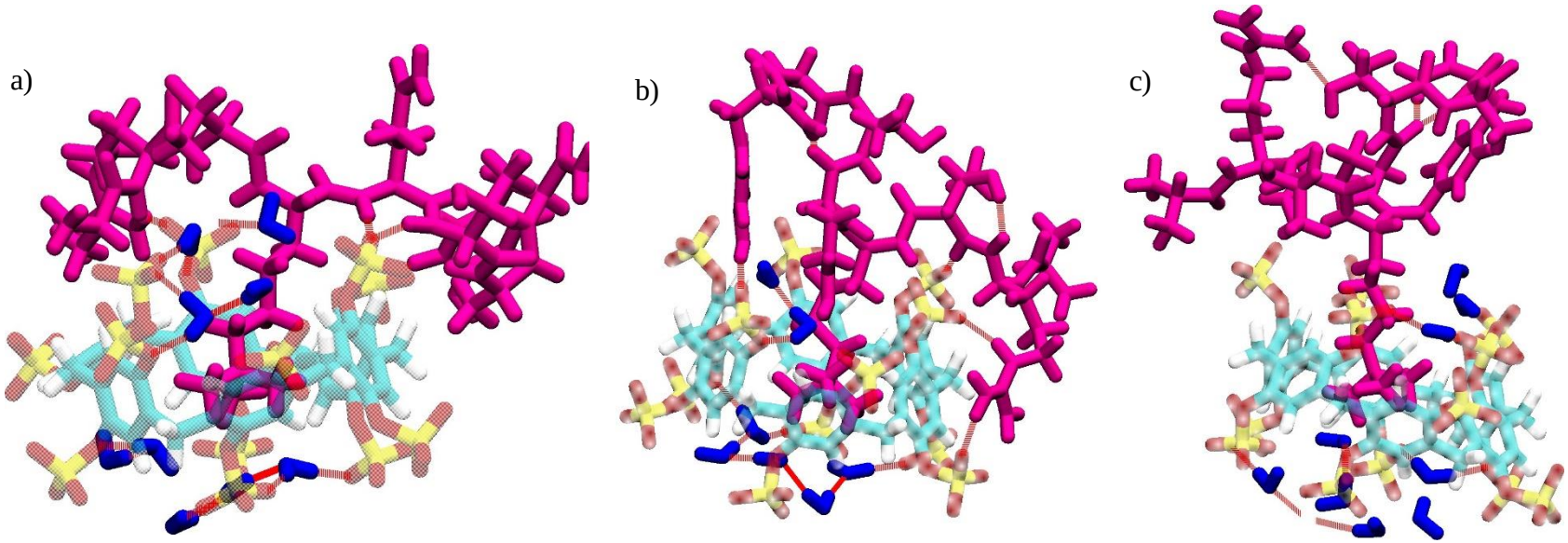

Figure SIII-53. Representative structures of P6MQ·**H3K4Me3** (KMe_3 bound). In all panes water molecules are depicted in blue, the ligand in magenta, and sodium ions in pink, and H-bonds in red. a) The first of two metastable states observed in simulation. The backbone and unbound sidechains engage in H-bonding with P6MQ. b) Alternative view of the first metastable state where arginine is within π-stacking distance of the P6MQ aromatic walls. Arginine is observed within π-stacking distance more rarely when KMe_3 is bound compared to lysine. c) The second metastable state observed. The unbound portion of the molecule is stabilized by H-bonds between the sidechains and backbone. H-bond interactions are still present between the unbound sidechains and the top portal of P6MQ.

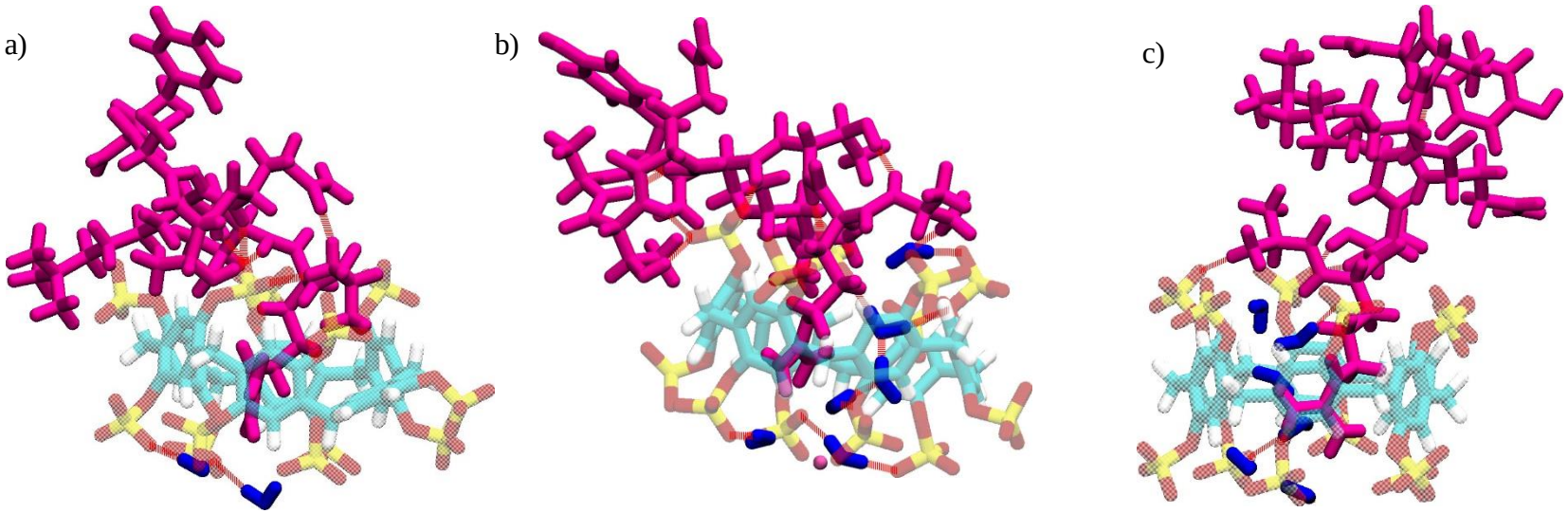

Figure SIII-54. Representative structures of P6MQ·**H3K4Me$_3$** (Arg bound) In all panes water molecules are depicted in blue, the ligand in magenta, and sodium ions in pink, and H-bonds in red. a) The first of two metastable states observed in simulation. The backbone and unbound sidechains engage in H-bonding with P6MQ. Here the deformation of P6MQ due to the ligand is evident. b) Alternative view of the first metastable state. c) The second metastable state observed. Here the unbound portion of the molecule is stabilized by H-bonds between the sidechains and backbone. H-bond interactions are still present between the unbound sidechains and the top portal of P6MQ. It is clear from (a-c) that arginine is bound deeper within the cavity compared to Lys/KMe$_3$ for **H3K4** and **H3K4Me$_3$**.

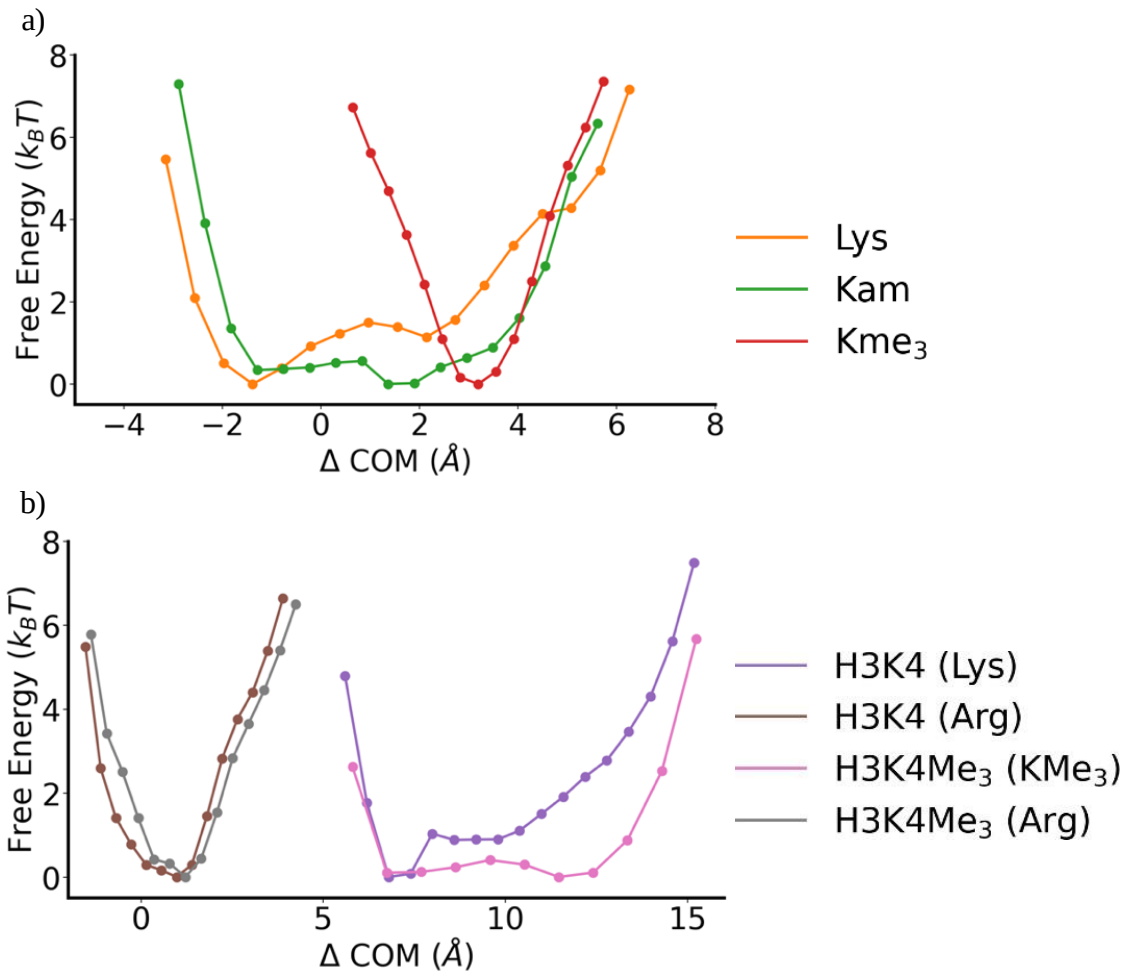

Figure SIII-55. Bound depth of P6MQ complexes. a) Bound depth for amino acids (Lys = **H-K-OH**; Kam = **H-K-NH$_2$**; KMe$_3$ = **H-K(Me$_3$)-OH**). b) Bound depth for **H3K4** and **H3K4Me$_3$**. Note that the bound depth calculation is only accurate when the center of mass of the bound ligand is between the P6MQ portals. For **H3K4** (Lys) and **H3K4Me$_3$** (KMe$_3$) bound the center of mass is outside of the portals, so the distances are accurate only in a relative sense. That is, arginine is bound deeper in the P6MQ cavity compared to lysine and KMe$_3$.

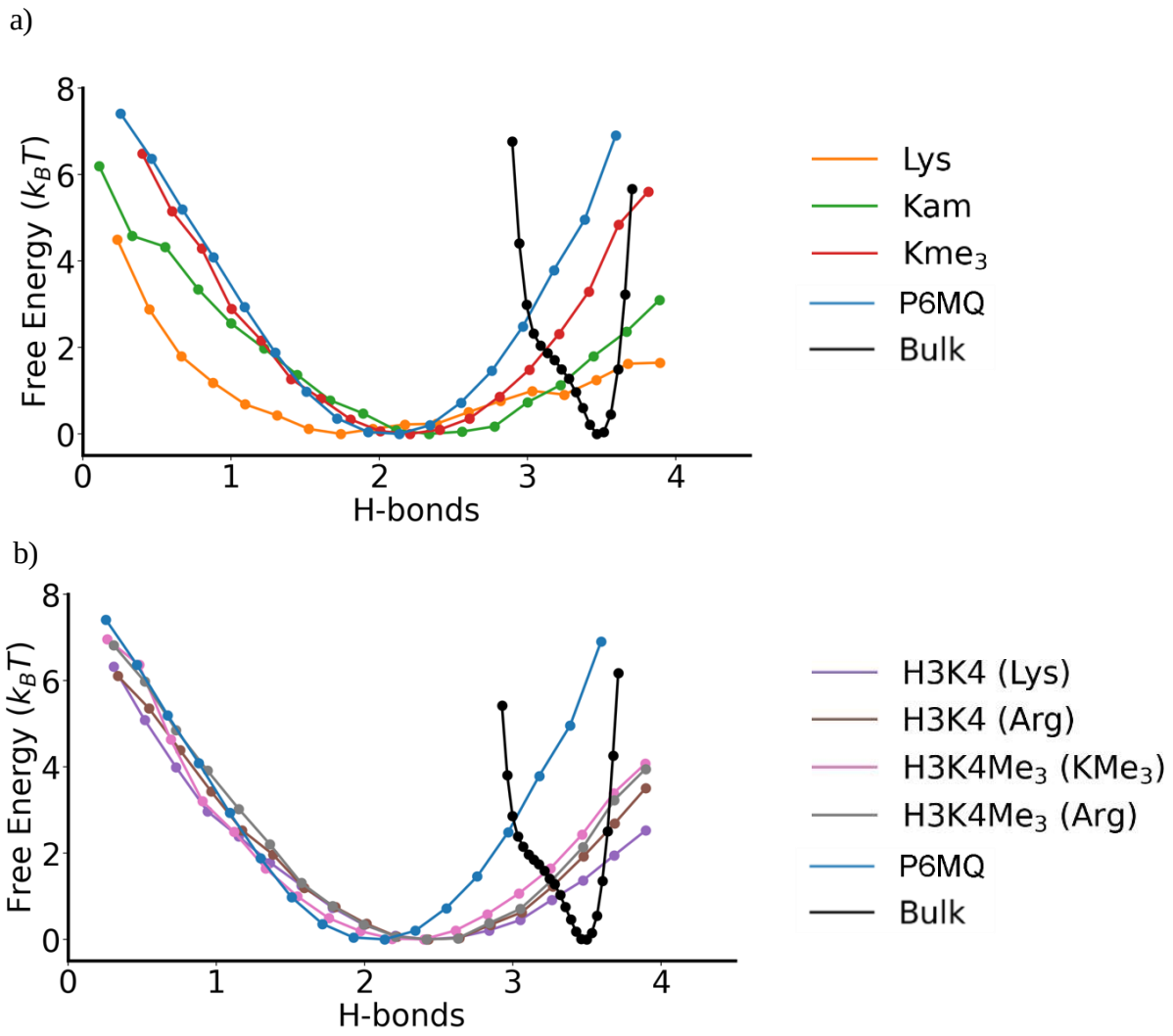

Figure SIII-56. Number of H-bonds within P6MQ cavity. a) The average number of H-bonds formed per water molecule within 6 Angstroms of the P6MQ center of mass is depicted for amino acids bound to P6MQ, unbound P6MQ, and a bulk-water reference. (Lys = **H-K-OH**; Kam = **H-K-NH$_2$**; KMe$_3$ = **H-K(Me$_3$)-OH**). b) The number of H-bonds is depicted for P6MQ□**H3K4** complexes, unbound P6MQ, and a bulk-water reference.

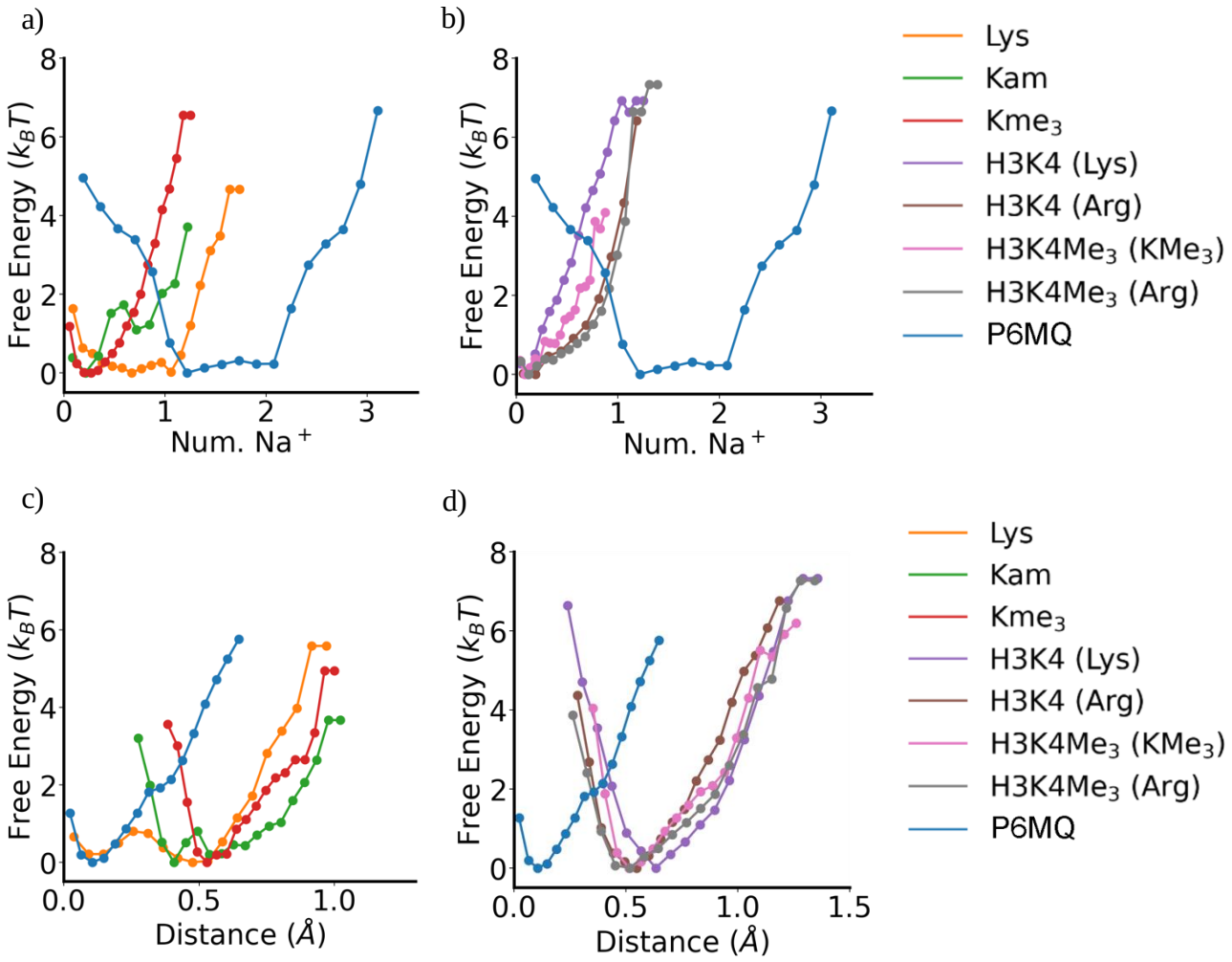

Figure SIII-57. Quantifying Na^+ presence in P6MQ. a) Number of Na^+ ions present within 4 Angstroms of the P6MQ center of mass for amino acid complexes and unbound P6MQ. (Lys = **H-K-OH**; Kam = **H-K-NH_2**; KMe_3 = **H-K(Me_3)-OH**). b) Number of Na^+ ions present within 4 Angstroms of the P6MQ center of mass for **H3** complexes and unbound P6MQ. c) Minimum distance between any Na^+ ion and the P6MQ center of mass for amino acid complexes and unbound P6MQ. d) Minimum distance between any Na^+ ion and the P6MQ center of mass for **H3** complexes and unbound P6MQ.

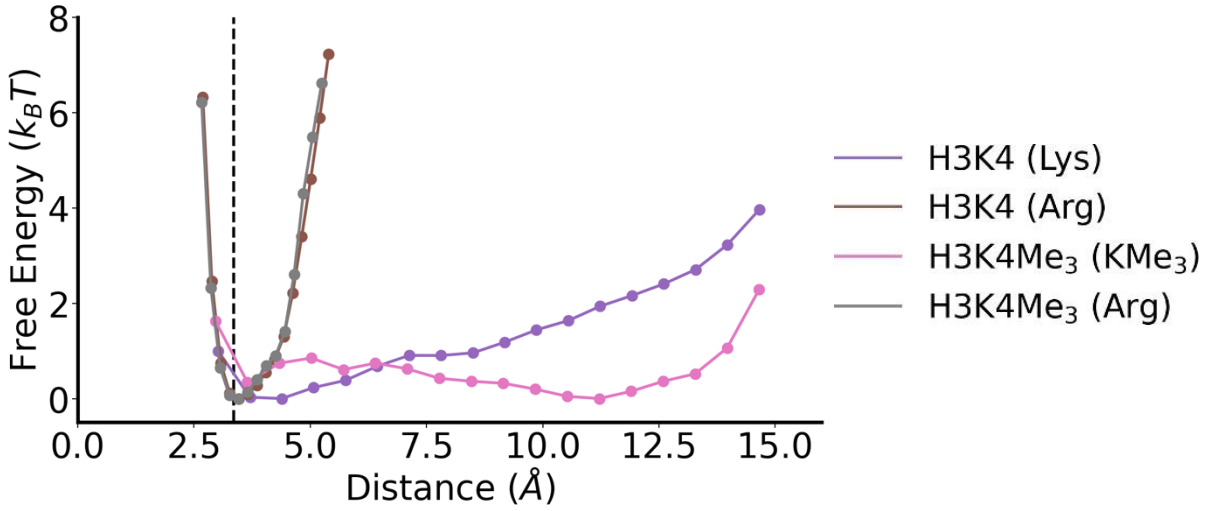

Figure SIII-58. Arginine π-stacking in **H3K4** complexes. The minimum distance between the arginine π-bond and the center of mass of the P6MQ aromatic walls is shown. The characteristic distance of π-stacking interactions (3.35 Angstroms) is depicted by the dashed line.

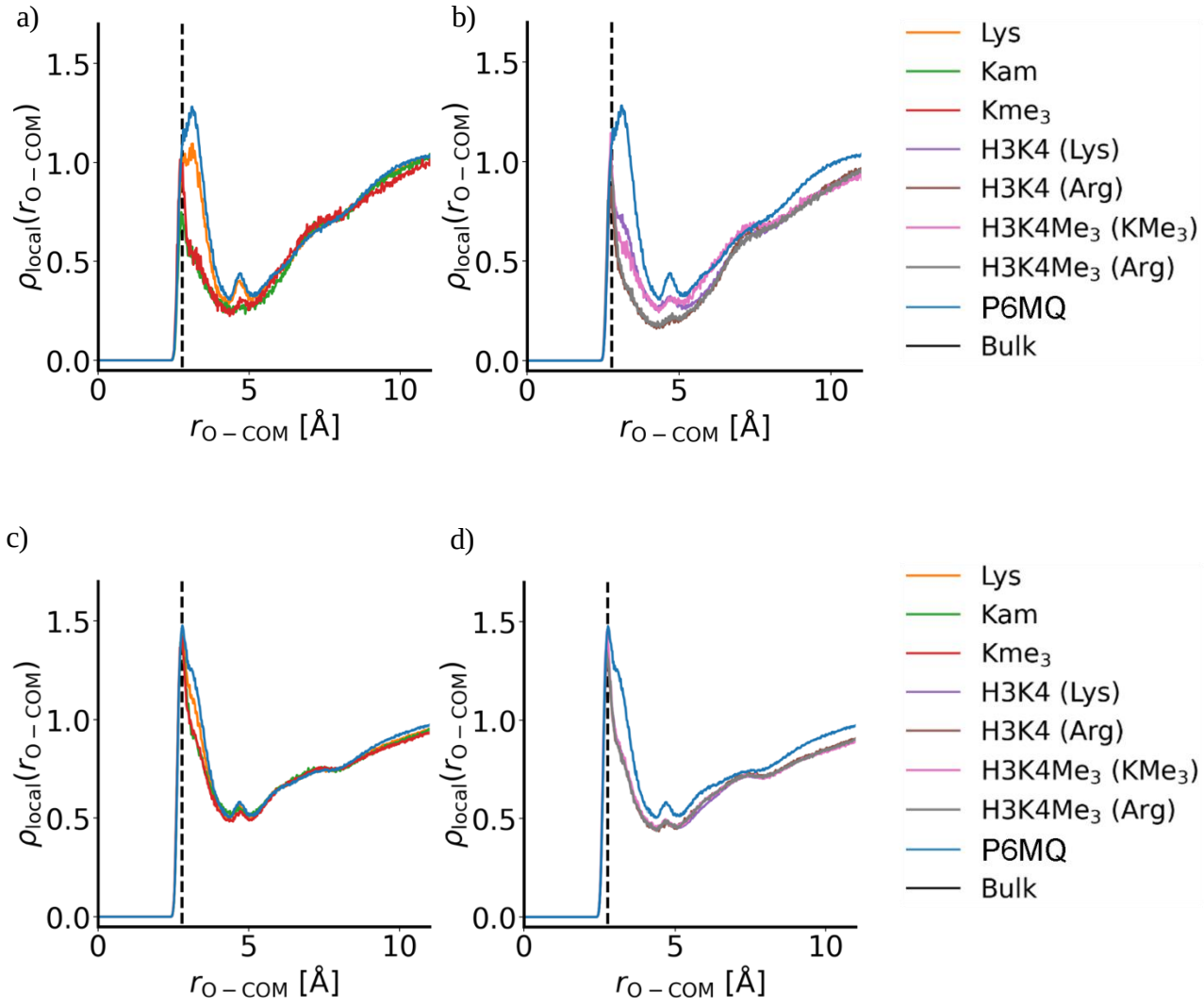

Figure SIII-59. Local density of water measured from P6MQ center of mass**.** a) Local density of water oxygens within 4 Angstroms of the P6MQ center of mass for amino acid complexes. (Lys = **H-K-OH**; Kam = **H-K-NH$_2$**; KMe$_3$ = **H-K(Me$_3$)-OH**). b) Local density of water oxygens within 4 Angstroms of the P6MQ center of mass for **H3K4** complexes. c) Local density of water oxygens between 4 and 7 Angstroms of the P6MQ center of mass for amino acid complexes. d) Local density of water oxygens between 4 and 7 Angstroms of the P6MQ center of mass for **H3K4** complexes. The black dashed line represents the dominant peak for bulk water at 2.78 Angstroms, and unbound P6MQ is included as a reference for all panes.

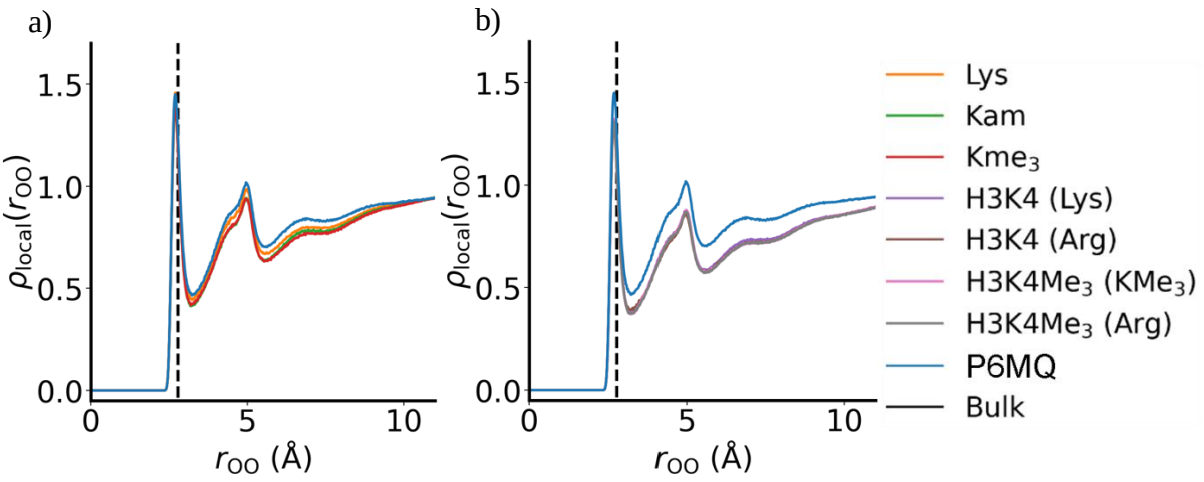

Figure SIII-60. Local density of water measured from P6MQ sulfate oxygens. a) The local density of water is measured for oxygens within 7 Angstroms of a P6MQ sulfate oxygen for amino acid complexes. (Lys = **H-K-OH**; Kam = **H-K-NH$_2$**; KMe$_3$ = **H-K(Me$_3$)-OH**). b) The local density of water is measured for oxygens within 7 Angstroms of a P6MQ sulfate oxygen for **H3K4** complexes. The black dashed line represents the dominant peak for bulk water at 2.78 Angstroms, and unbound P6MQ is included as a reference for both panes

Appendix 3

Detection of WADA Banned Substances in Simulated Urine Using a Pillar[*n*]MaxQ Based Assay

By David King,[a] Chun-lin Deng,[a] and Lyle Isaacs[a,]*

[a] Department of Chemistry and Biochemistry, University of Maryland, College Park, Maryland 20742, United States

*To whom correspondence should be addressed. Prof. Lyle Isaacs, Email: LIsaacs@umd.edu

Table of Contents

General Experimental Details.

Chemicals were purchased from commercial suppliers and used without further purification or were prepared by literature procedures. Simulated urine was purchased from Flinn Scientific ("Artificial Urine, Normal" Lot#294189). PBS buffer was made by dissolving MP Biomedicals brand tablets (Lot#S7091) in HPLC grade H_2O and using minimal NaOH or HCl to adjust the pH as needed. ^{1}H NMR spectra were measured on commercial instruments operating at 600 MHz for using sodium phosphate buffered D_2O saline (pD 7.4) as the solvent. Chemical shifts (δ) are referenced relative to the residual resonances for HOD (4.79 ppm). ITC data were collected on a Malvern Microcal PEAQ-ITC instrument and analyzed using the software provided by the vendor All fluorescence measurements were performed using in a Greiner Bio-One black, flat-bottomed, polystyrene 96 well plate and measured with a SpectraMax 5^e multimode plate reader. Curve fitting for fluorescence based binding titrations were performed using Scientist^{TM}. Data analysis and machine learning algorithms were implemented in Python using pandas,[174] numPy,[175] and scikit-learn[176] libraries. All data analysis files and csv files for the calibration curves and LDA plot can be found on GitHub: https://github.com/daking11/WADA_sensor.git

Determination of K_a of P5AS towards various guests using Isothermal Titration Calorimetry (ITC).

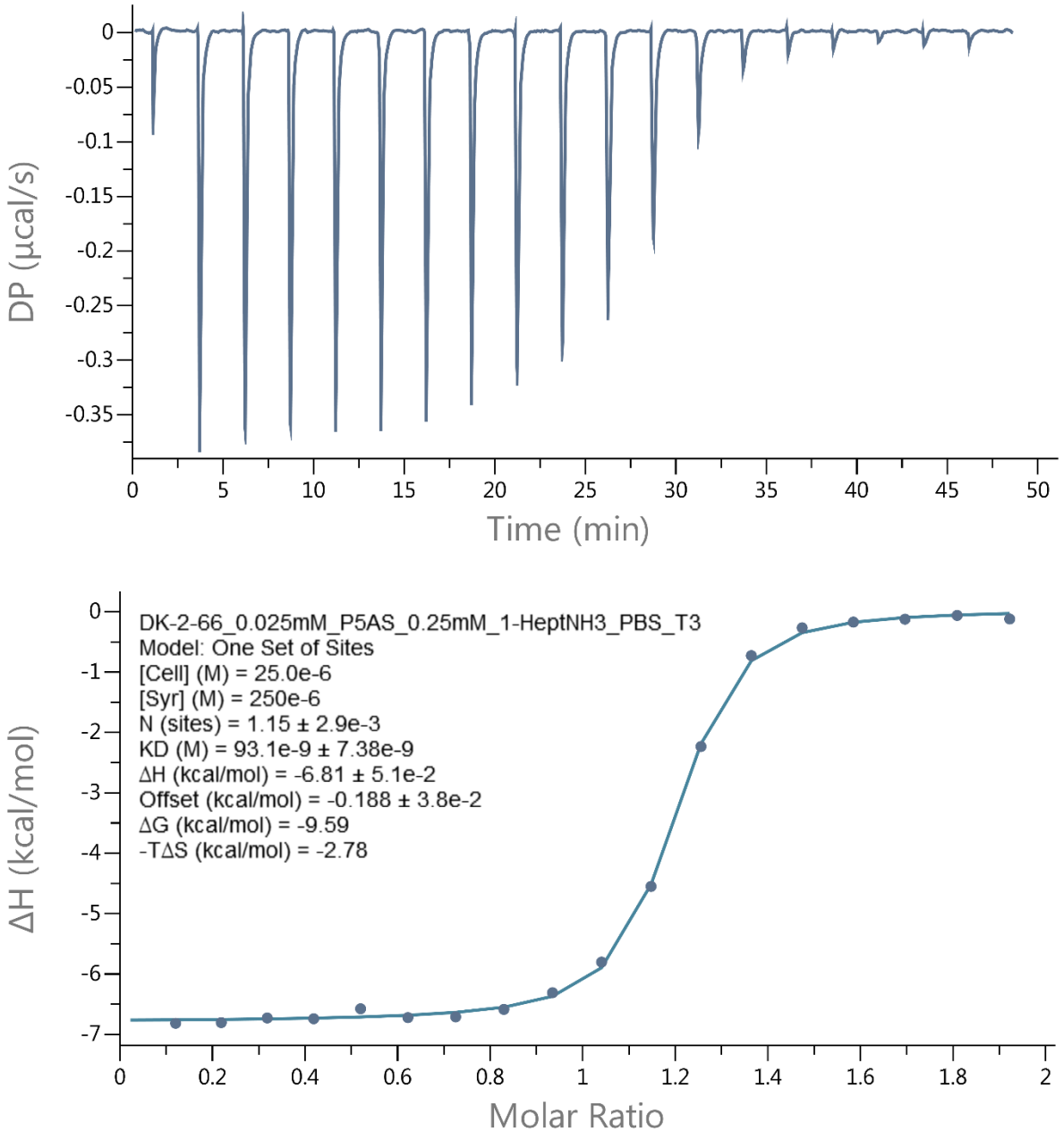

Figure SIV-1. Isothermal Titration Calorimetry (ITC) curve obtained through direct binding titration studies. A solution of P5AS (0.025 mM) in the cell was titrated with **1HeptNH3** (0.25 mM) in the syringe at 298.0 K in 10 mM sodium phosphate buffered saline at pH 7.4. The solid line represents the best non-linear fit of the data to a 1:1 binding model. (K_a = (1.12 ± 0.06) × 10^7 M^{-1}; ΔH = (–6.84 ± 0.03) kcal mol^{-1}).

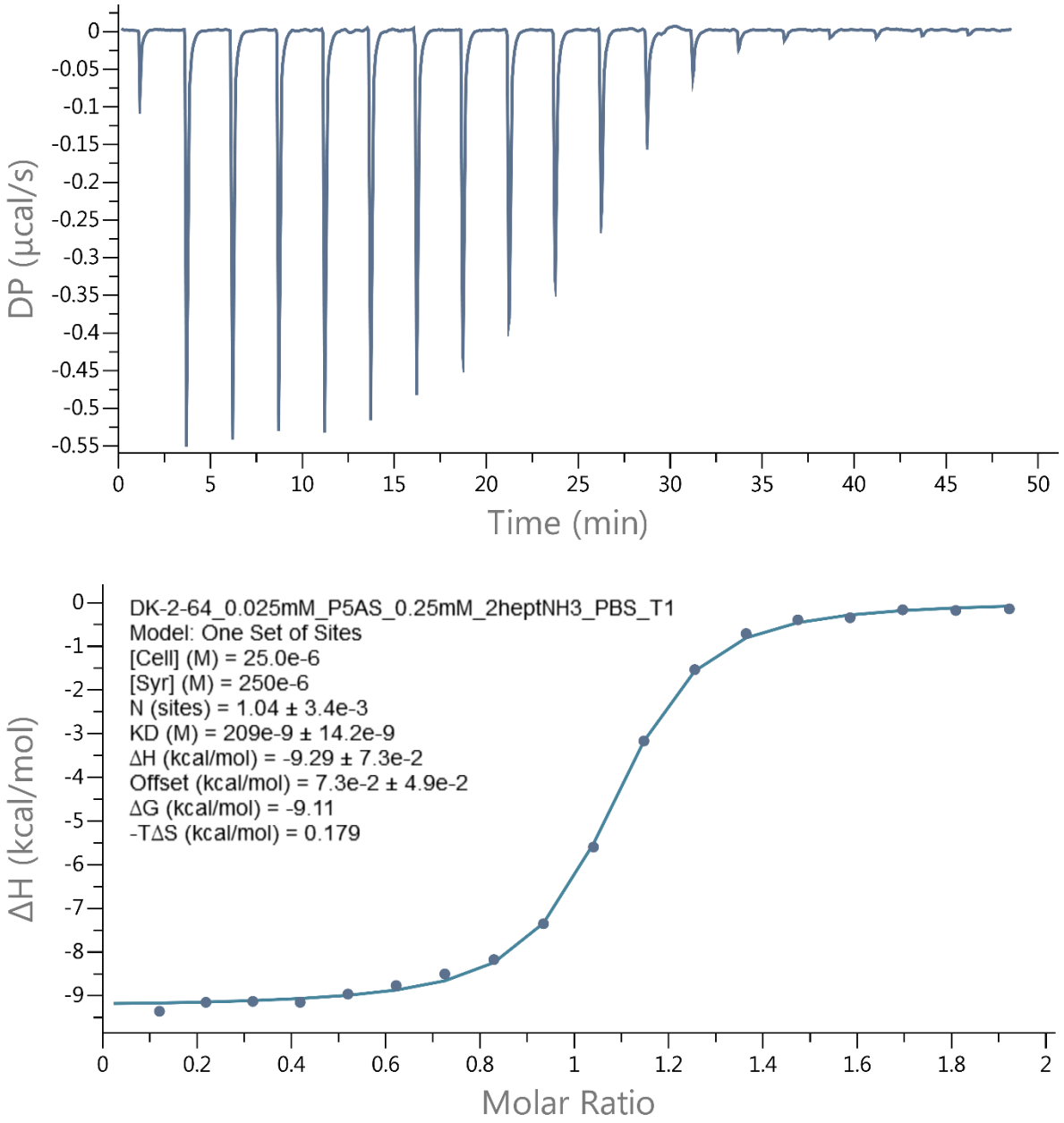

Figure SIV-2. Isothermal Titration Calorimetry (ITC) curve obtained through direct binding titration studies. A solution of P5AS (0.025 mM) in the cell was titrated with **2HeptNH3** (0.25 mM) in the syringe at 298.0 K in 10 mM sodium phosphate buffered saline at pH 7.4. The solid line represents the best non-linear fit of the data to a 1:1 binding model. (K_a = (5.59 ± 0.32) × 10^6 M^{-1}; ΔH = (–9.17 ± 0.06) kcal mol^{-1}).

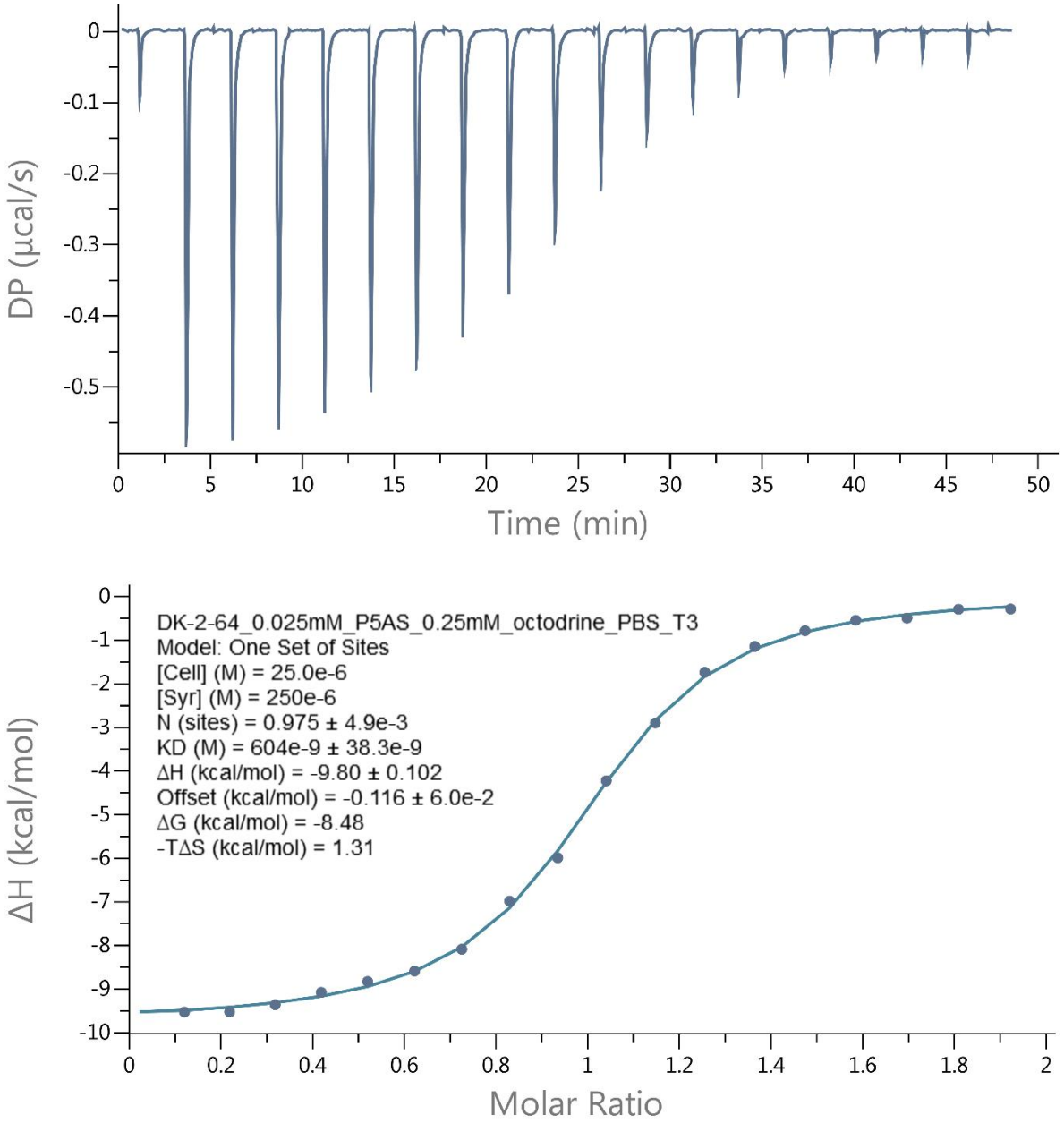

Figure SIV-3. Isothermal Titration Calorimetry (ITC) curve obtained through direct binding titration studies. A solution of P5AS (0.025 mM) in the cell was titrated with **1,5dmHexNH3** (0.25 mM) in the syringe at 298.0 K in 10 mM sodium phosphate buffered saline at pH 7.4. The solid line represents the best non-linear fit of the data to a 1:1 binding model. (K_a = (1.53 ± 0.08) × 10^6 M^{-1}; ΔH = (–9.87 ± 0.08) kcal mol^{-1}).

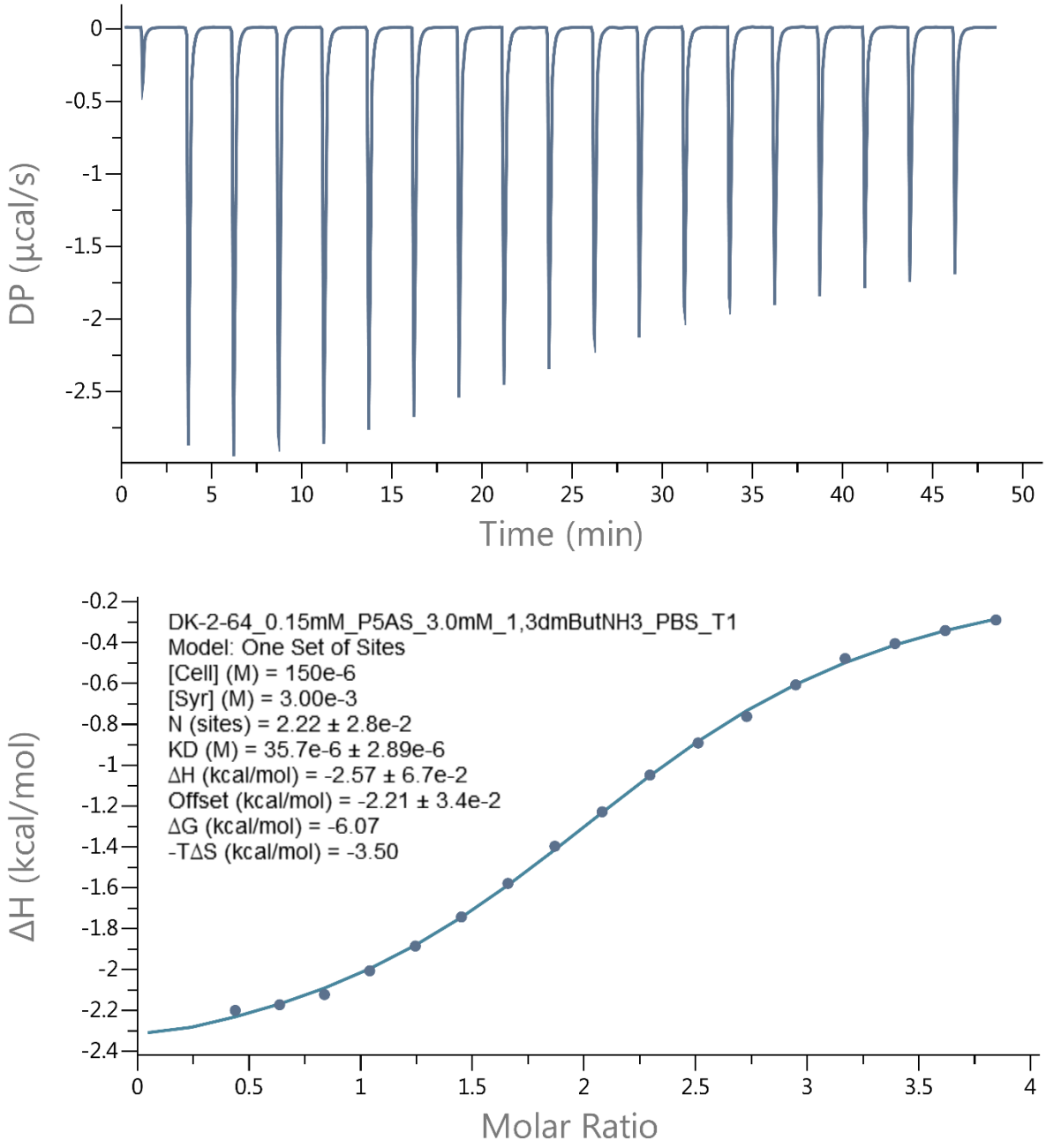

Figure SIV-4. Isothermal Titration Calorimetry (ITC) curve obtained through direct binding titration studies. A solution of P5AS (0.15 mM) in the cell was titrated with **1,3dmButNH3** (3.0 mM) in the syringe at 298.0 K in 10 mM sodium phosphate buffered saline at pH 7.4. The solid line represents the best non-linear fit of the data to a 1:1 binding model. (K_a = (4.64 ± 0.34) × 10^4 M^{-1}; ΔH = (–5.29 ± 0.13) kcal mol^{-1}).

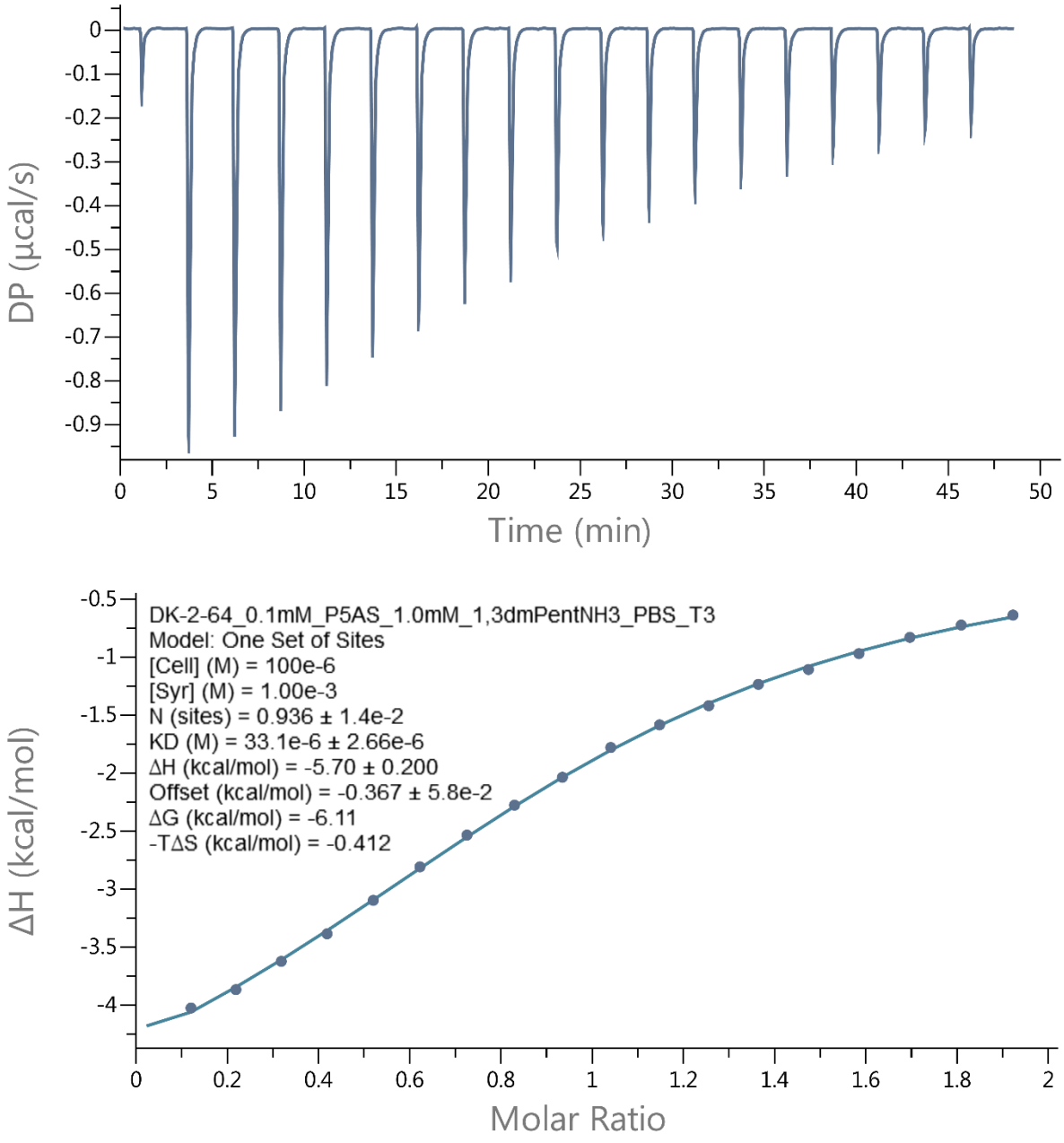

Figure SIV-5. Isothermal Titration Calorimetry (ITC) curve obtained through direct binding titration studies. A solution of P5AS (0.10 mM) in the cell was titrated with **1,3dmPentNH3** (1.0 mM) in the syringe at 298.0 K in 10 mM sodium phosphate buffered saline at pH 7.4. The solid line represents the best non-linear fit of the data to a 1:1 binding model. (K_a = (2.95 ± 0.15) × 10^4 M^{-1}; ΔH = (–5.70 ± 0.13) kcal mol^{-1}).

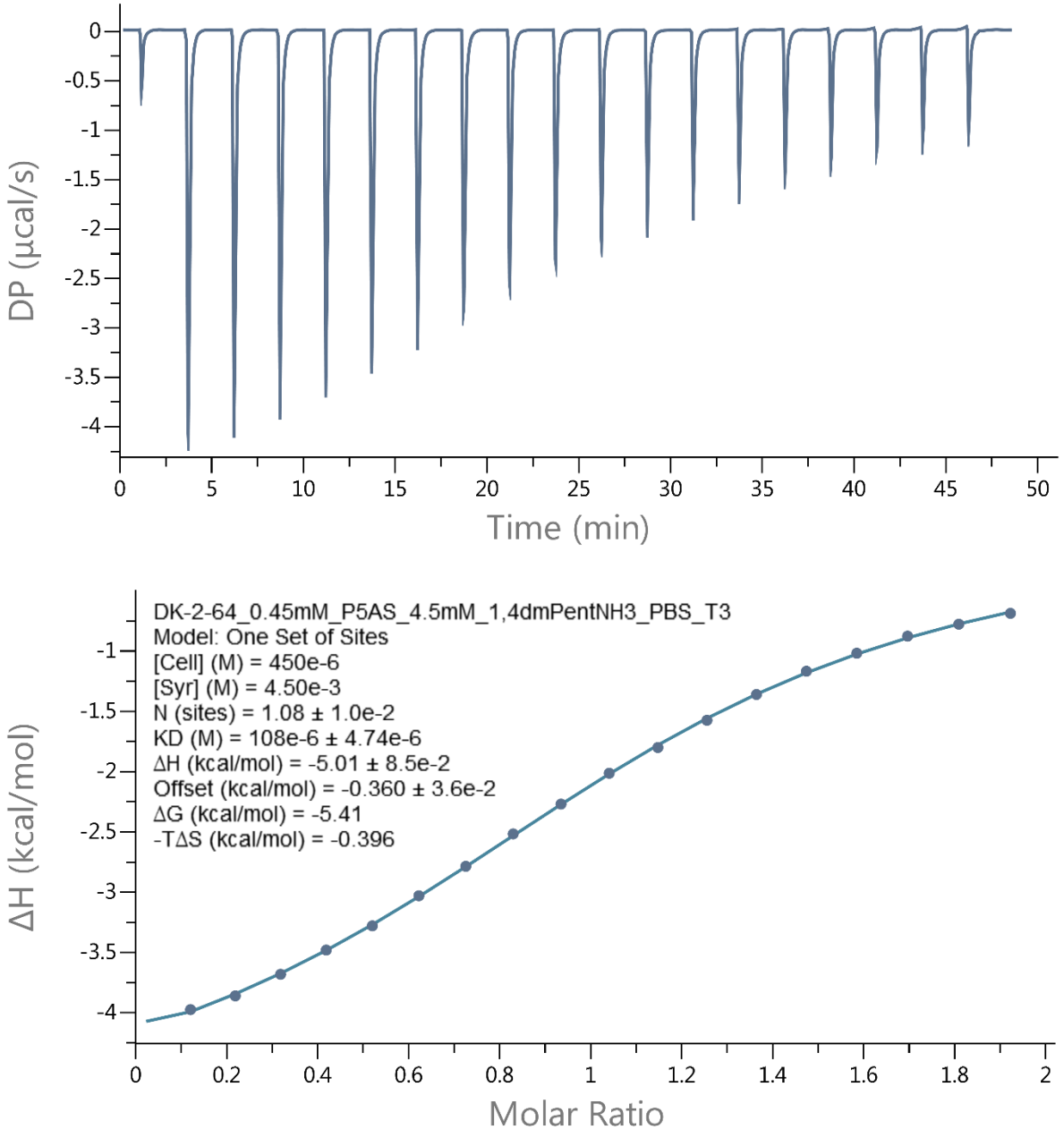

Figure SIV-6. Isothermal Titration Calorimetry (ITC) curve obtained through direct binding titration studies. A solution of P5AS (0.45 mM) in the cell was titrated with **1,4dmPentNH3** (4.5 mM) in the syringe at 298.0 K in 10 mM sodium phosphate buffered saline at pH 7.4. The solid line represents the best non-linear fit of the data to a 1:1 binding model. (K_a = (9.90 ± 0.28) × 10^3 M^{-1}; ΔH = (–5.08 ± 0.23) kcal mol^{-1}).

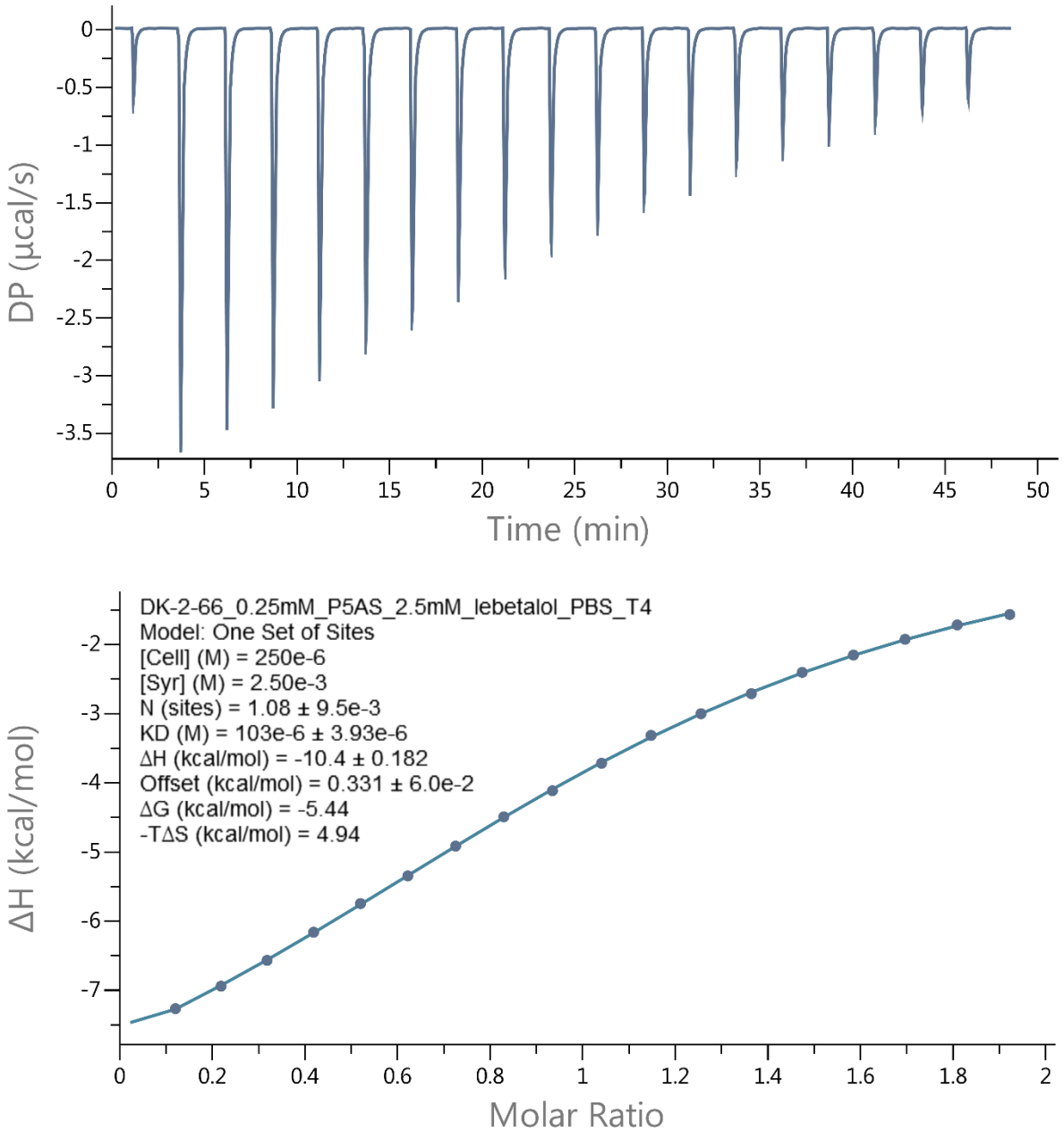

Figure SIV-7. Isothermal Titration Calorimetry (ITC) curve obtained through direct binding titration studies. A solution of P5AS (0.25 mM) in the cell was titrated with **labetalol** (2.5 mM) in the syringe at 298.0 K in 10 mM sodium phosphate buffered saline at pH 7.4. The solid line represents the best non-linear fit of the data to a 1:1 binding model. (K_a = (9.65 ± 0.27) × 10^3 M^{-1}; ΔH = (–10.6 ± 0.1) kcal mol^{-1}).

Determination of Ka of P6AS towards various guests using Isothermal Titration Calorimetry (ITC).

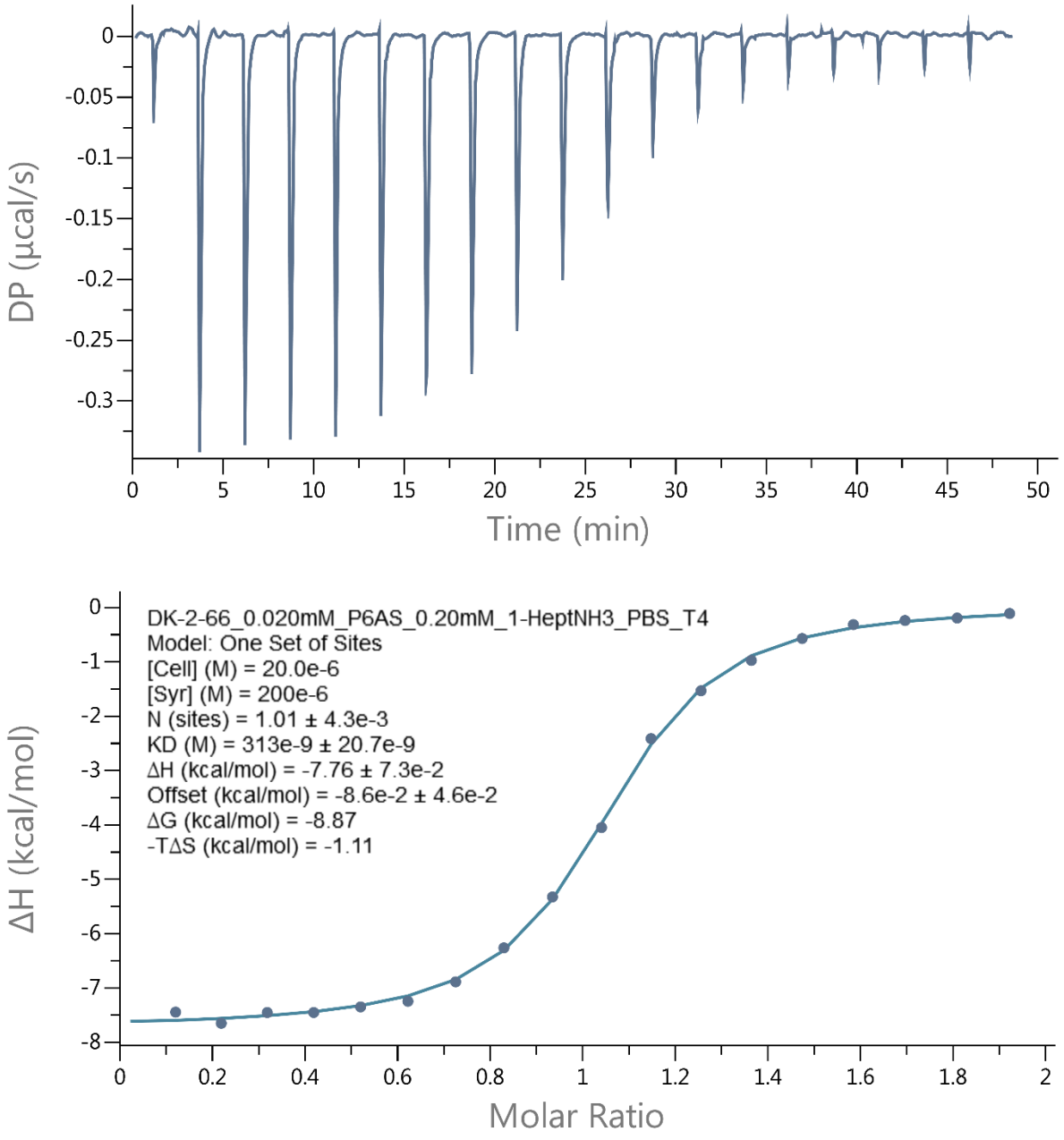

Figure SIV-8. Isothermal Titration Calorimetry (ITC) curve obtained through direct binding titration studies. A solution of P6AS (0.020 mM) in the cell was titrated with **1HeptNH3** (0.20 mM) in the syringe at 298.0 K in 10 mM sodium phosphate buffered saline at pH 7.4. The solid line represents the best non-linear fit of the data to a 1:1 binding model. (K_a = (3.65 ± 0.22) × 10^6 M^{-1}; ΔH = (–7.68 ± 0.07) kcal mol^{-1}).

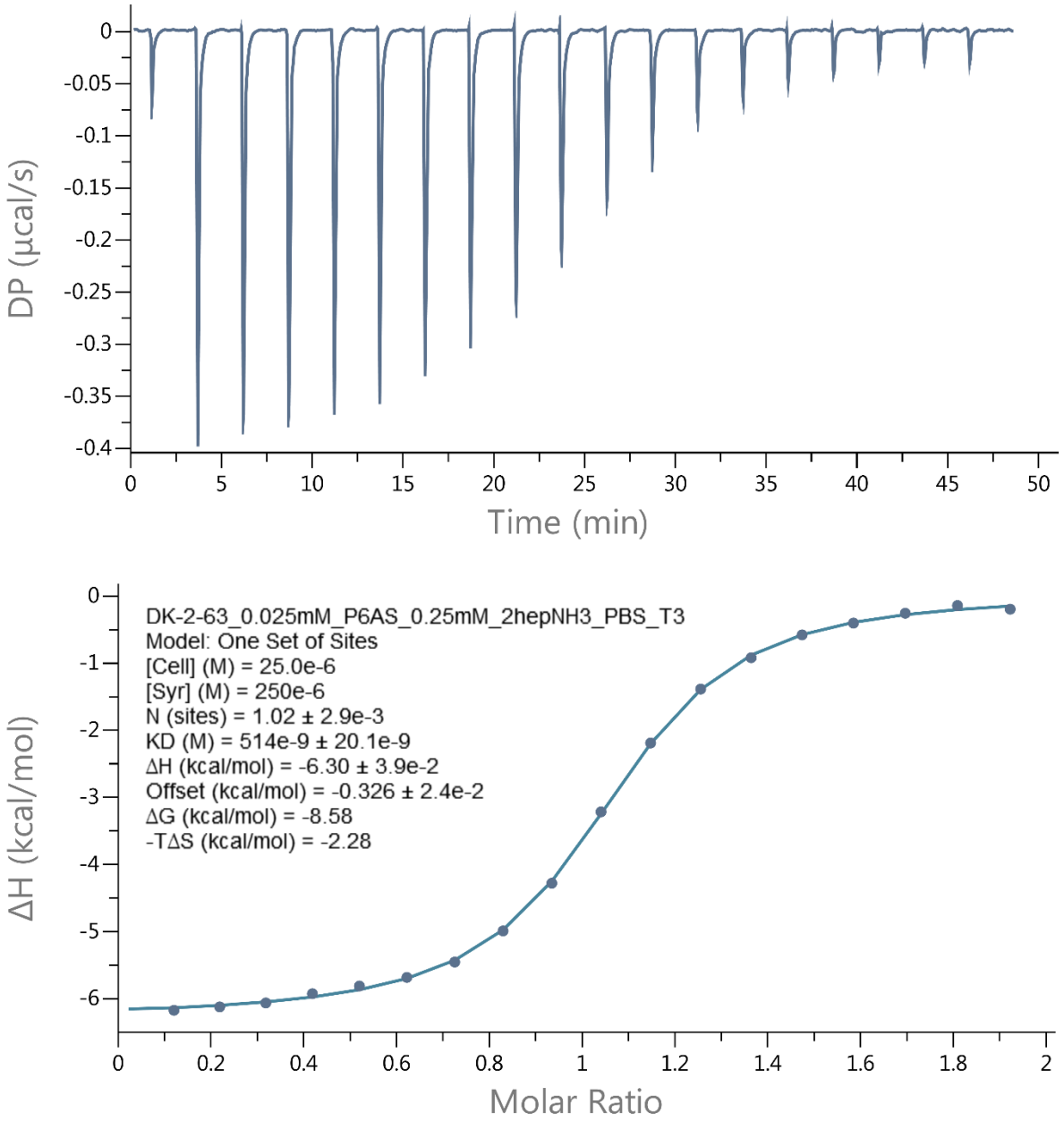

Figure SIV-9. Isothermal Titration Calorimetry (ITC) curve obtained through direct binding titration studies. A solution of P6AS (0.025 mM) in the cell was titrated with **2HeptNH3** (0.25 mM) in the syringe at 298.0 K in 10 mM sodium phosphate buffered saline at pH 7.4. The solid line represents the best non-linear fit of the data to a 1:1 binding model. (K_a = (1.82 ± 0.06) × 10^6 M^{-1}; ΔH = (–6.38 ± 0.03) kcal mol^{-1}).

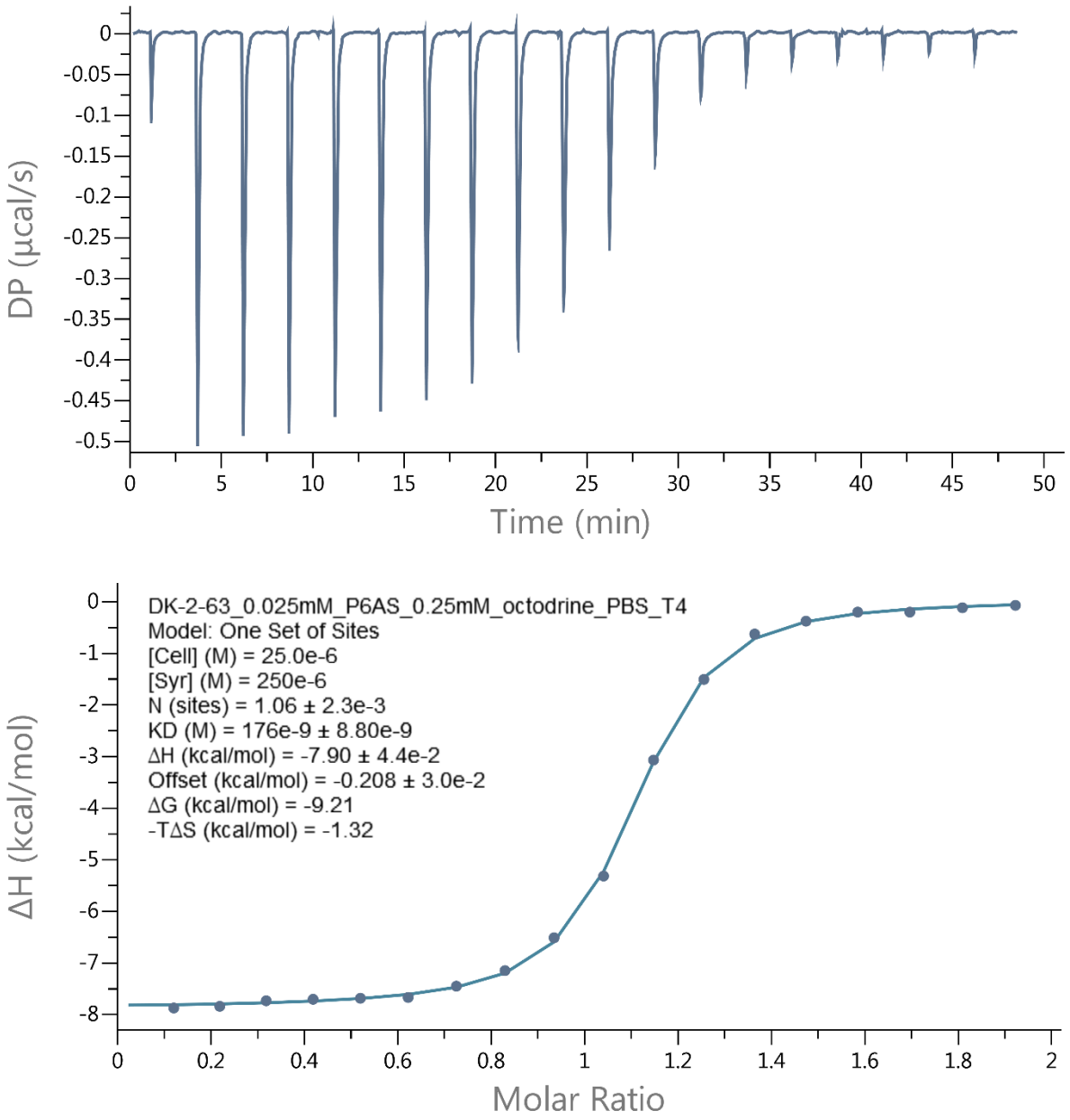

Figure SIV-10. Isothermal Titration Calorimetry (ITC) curve obtained through direct binding titration studies. A solution of P6AS (0.025 mM) in the cell was titrated with **1,5dmHexNH3** (0.25 mM) in the syringe at 298.0 K in 10 mM sodium phosphate buffered saline at pH 7.4. The solid line represents the best non-linear fit of the data to a 1:1 binding model. (K_a = (6.37 ± 0.43) × 10^6 M^{-1}; ΔH = (–7.88 ± 0.05) kcal mol^{-1}).

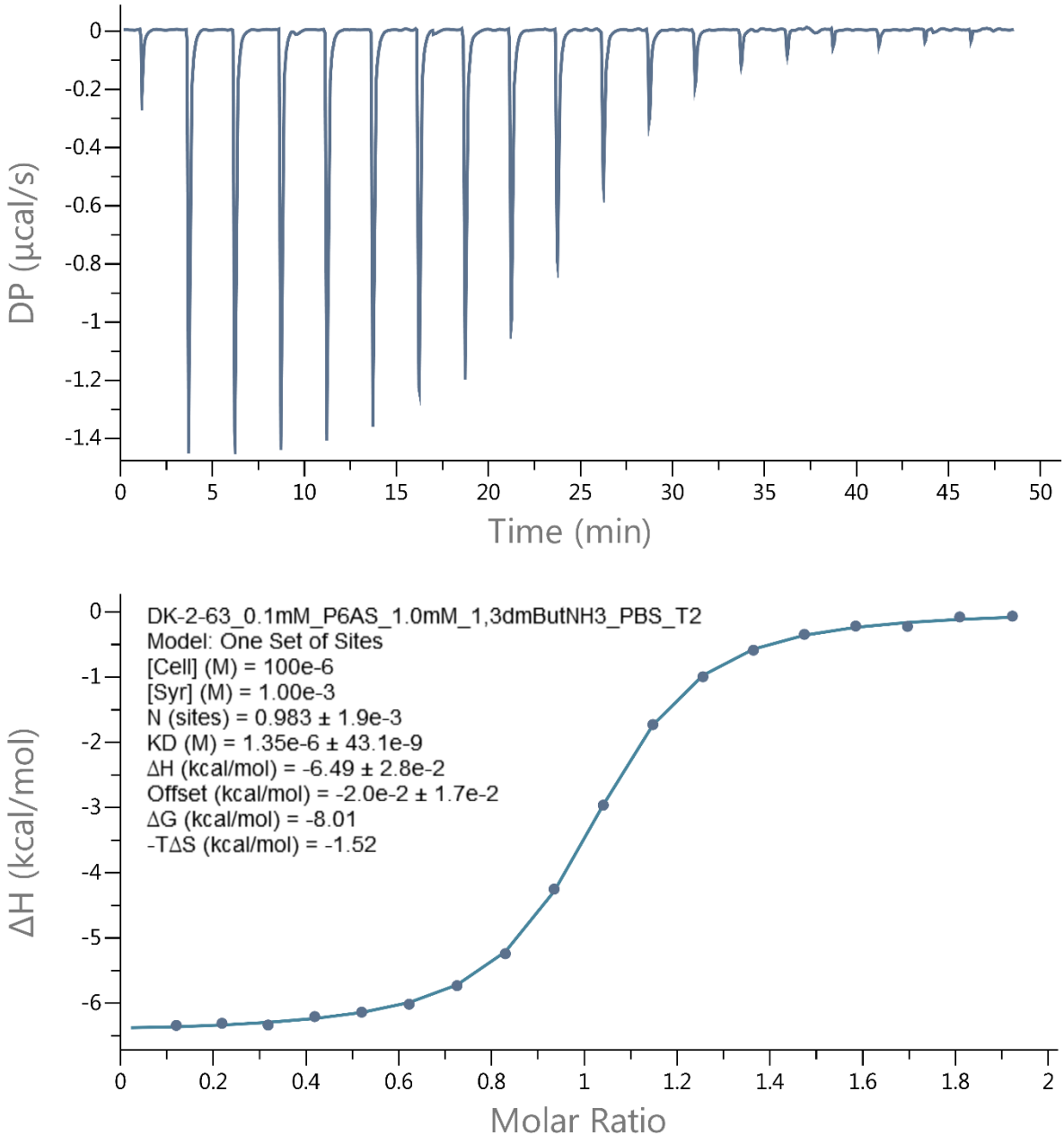

Figure SIV-11. Isothermal Titration Calorimetry (ITC) curve obtained through direct binding titration studies. A solution of P6AS (0.10 mM) in the cell was titrated with **1,3dmButNH3** (1.0 mM) in the syringe at 298.0 K in 10 mM sodium phosphate buffered saline at pH 7.4. The solid line represents the best non-linear fit of the data to a 1:1 binding model. (K_a = (7.89 ± 0.17) × 10^5 M^{-1}; ΔH = (–6.43 ± 0.02) kcal mol^{-1}).

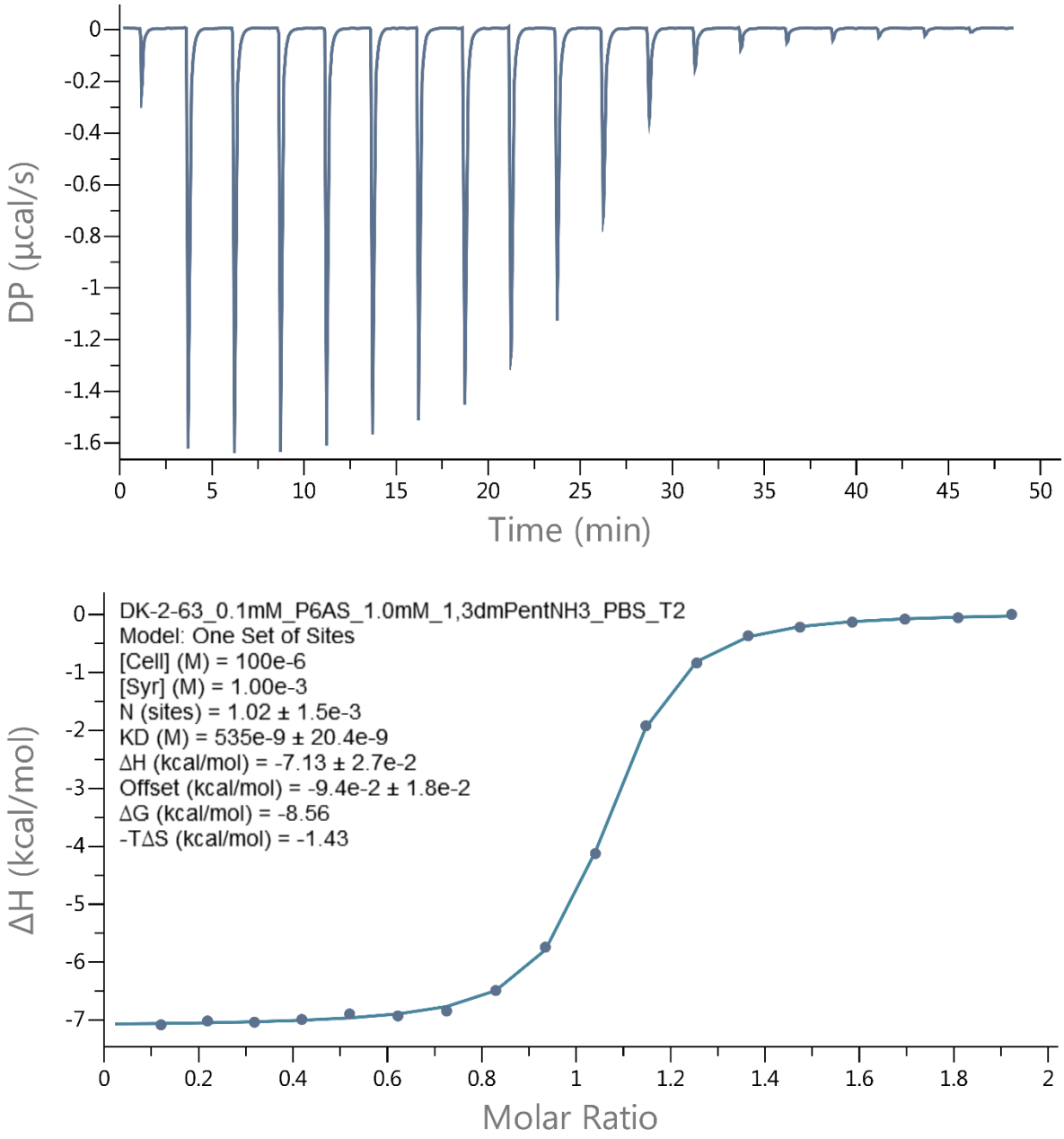

Figure SIV-12. Isothermal Titration Calorimetry (ITC) curve obtained through direct binding titration studies. A solution of P6AS (0.10 mM) in the cell was titrated with **1,3dmPentNH3** (1.0 mM) in the syringe at 298.0 K in 10 mM sodium phosphate buffered saline at pH 7.4. The solid line represents the best non-linear fit of the data to a 1:1 binding model. (K_a = (1.89 ± 0.05) × 10^6 M^{-1}; ΔH = (–7.11 ± 0.02) kcal mol^{-1}).

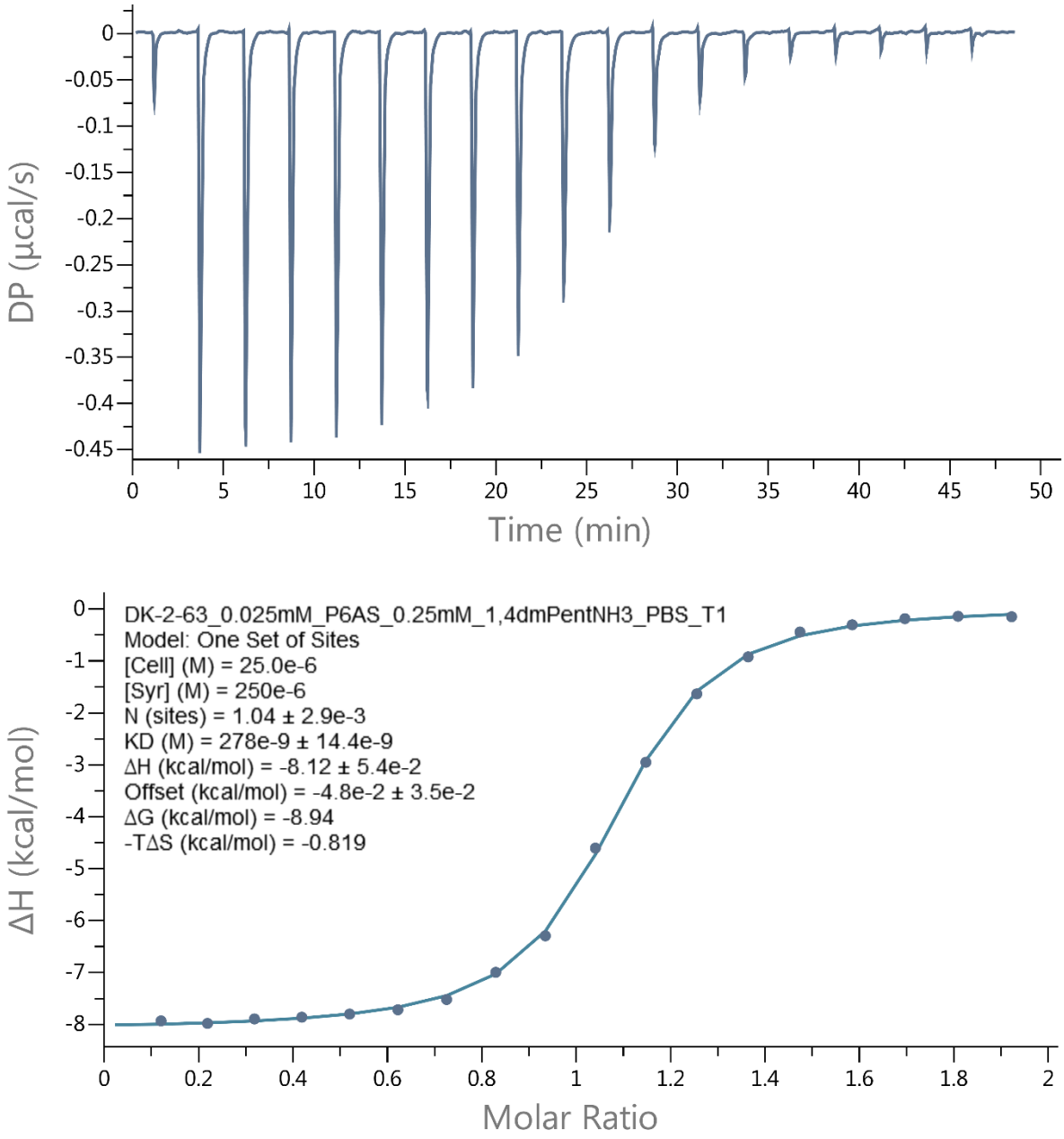

Figure SIV-13. Isothermal Titration Calorimetry (ITC) curve obtained through direct binding titration studies. A solution of P6AS (0.025 mM) in the cell was titrated with **1,4dmPentNH3** (0.25 mM) in the syringe at 298.0 K in 10 mM sodium phosphate buffered saline at pH 7.4. The solid line represents the best non-linear fit of the data to a 1:1 binding model. (K_a = (3.55 ± 0.13) × 10^6 M^{-1}; ΔH = (–8.01 ± 0.04) kcal mol^{-1}).

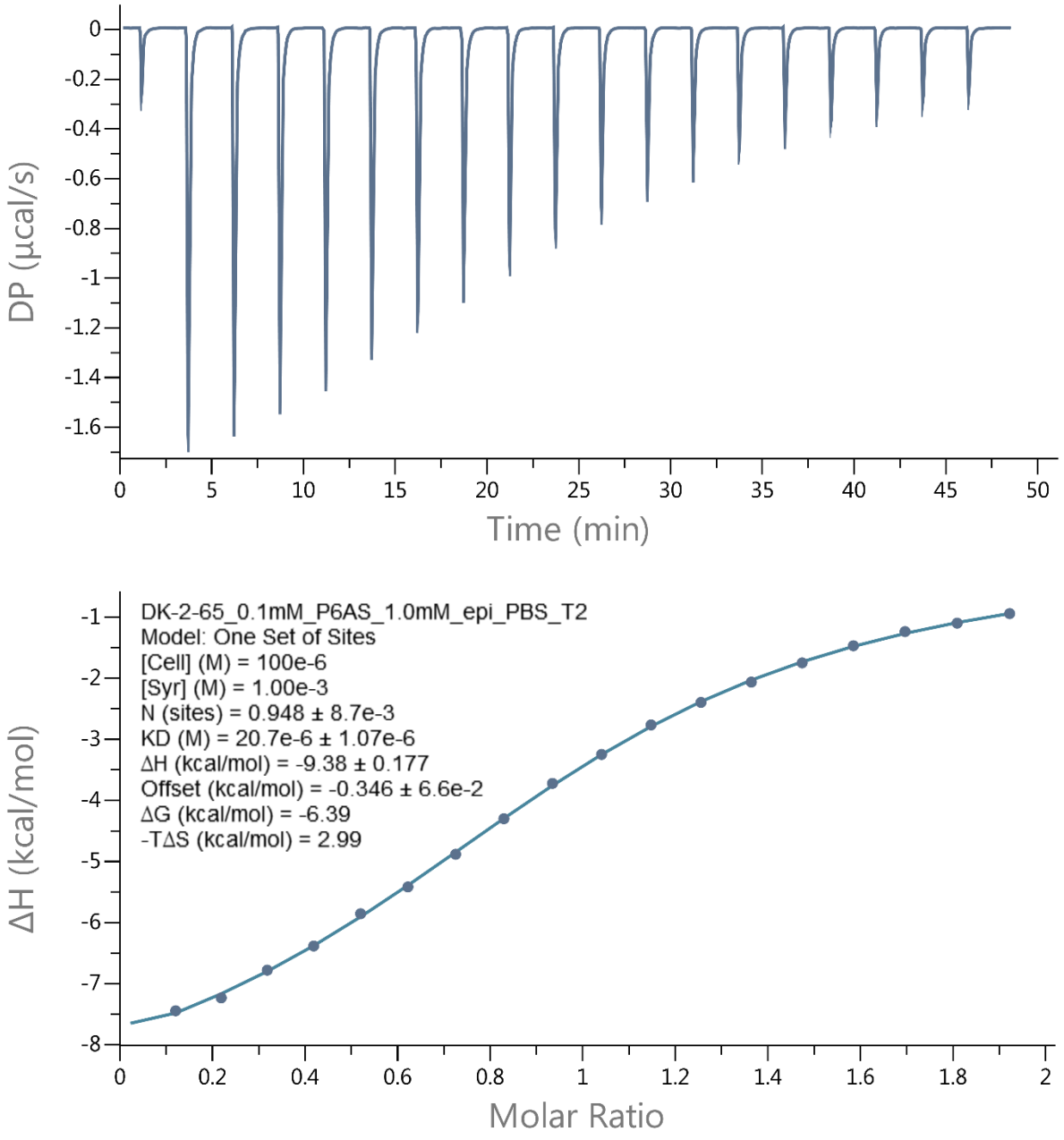

Figure SIV-14. Isothermal Titration Calorimetry (ITC) curve obtained through direct binding titration studies. A solution of P6AS (0.10 mM) in the cell was titrated with **Epi** (1.0 mM) in the syringe at 298.0 K in 10 mM sodium phosphate buffered saline at pH 7.4. The solid line represents the best non-linear fit of the data to a 1:1 binding model. (K_a = (4.39 ± 0.17) × 10^4 M^{-1}; ΔH = (–9.44 ± 0.14) kcal mol^{-1}).

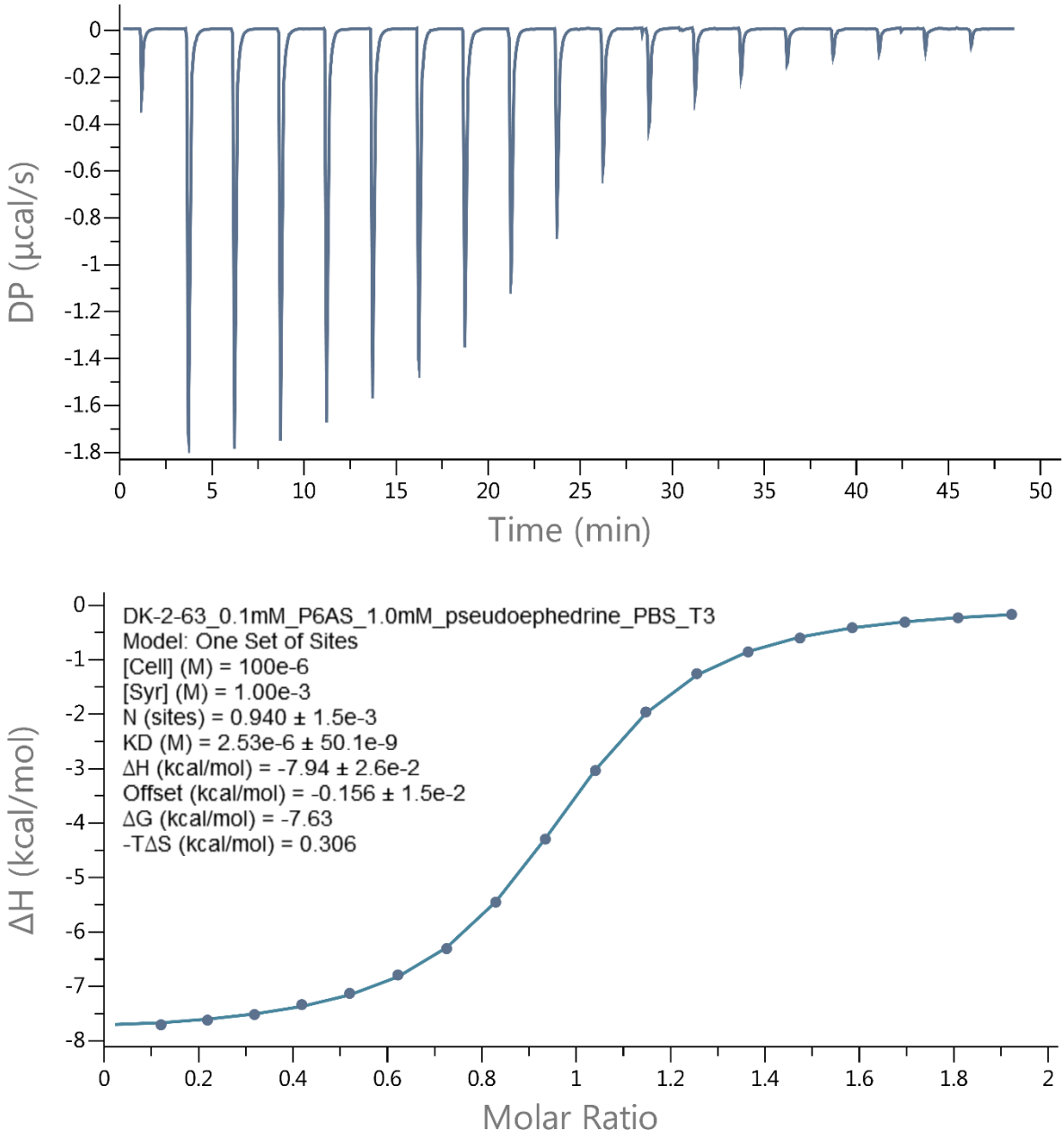

Figure SIV-15. Isothermal Titration Calorimetry (ITC) curve obtained through direct binding titration studies. A solution of P6AS (0.10 mM) in the cell was titrated with **Pseudo** (1.0 mM) in the syringe at 298.0 K in 10 mM sodium phosphate buffered saline at pH 7.4. The solid line represents the best non-linear fit of the data to a 1:1 binding model. (K_a = (3.76 ± 0.05) × 10^5 M^{-1}; ΔH = (–7.94 ± 0.02) kcal mol^{-1}).

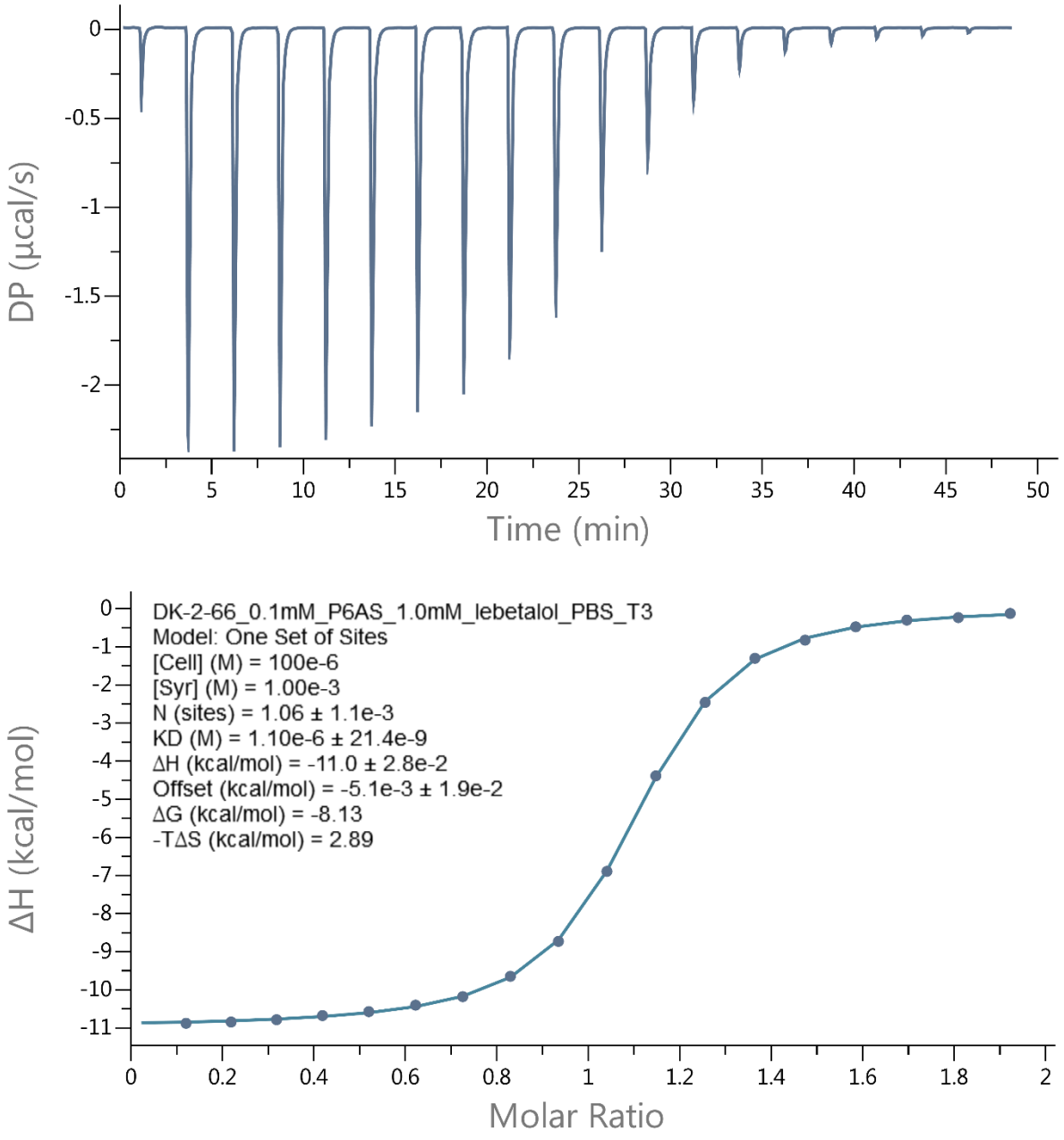

Figure SIV-16. Isothermal Titration Calorimetry (ITC) curve obtained through direct binding titration studies. A solution of P6AS (0.10 mM) in the cell was titrated with l**abetalol** (1.0 mM) in the syringe at 298.0 K in 10 mM sodium phosphate buffered saline at pH 7.4. The solid line represents the best non-linear fit of the data to a 1:1 binding model. (K_a = (9.26 ± 0.13) × 10^5 M^{-1}; ΔH = (–11.0 ± 0.02) kcal mol^{-1}).

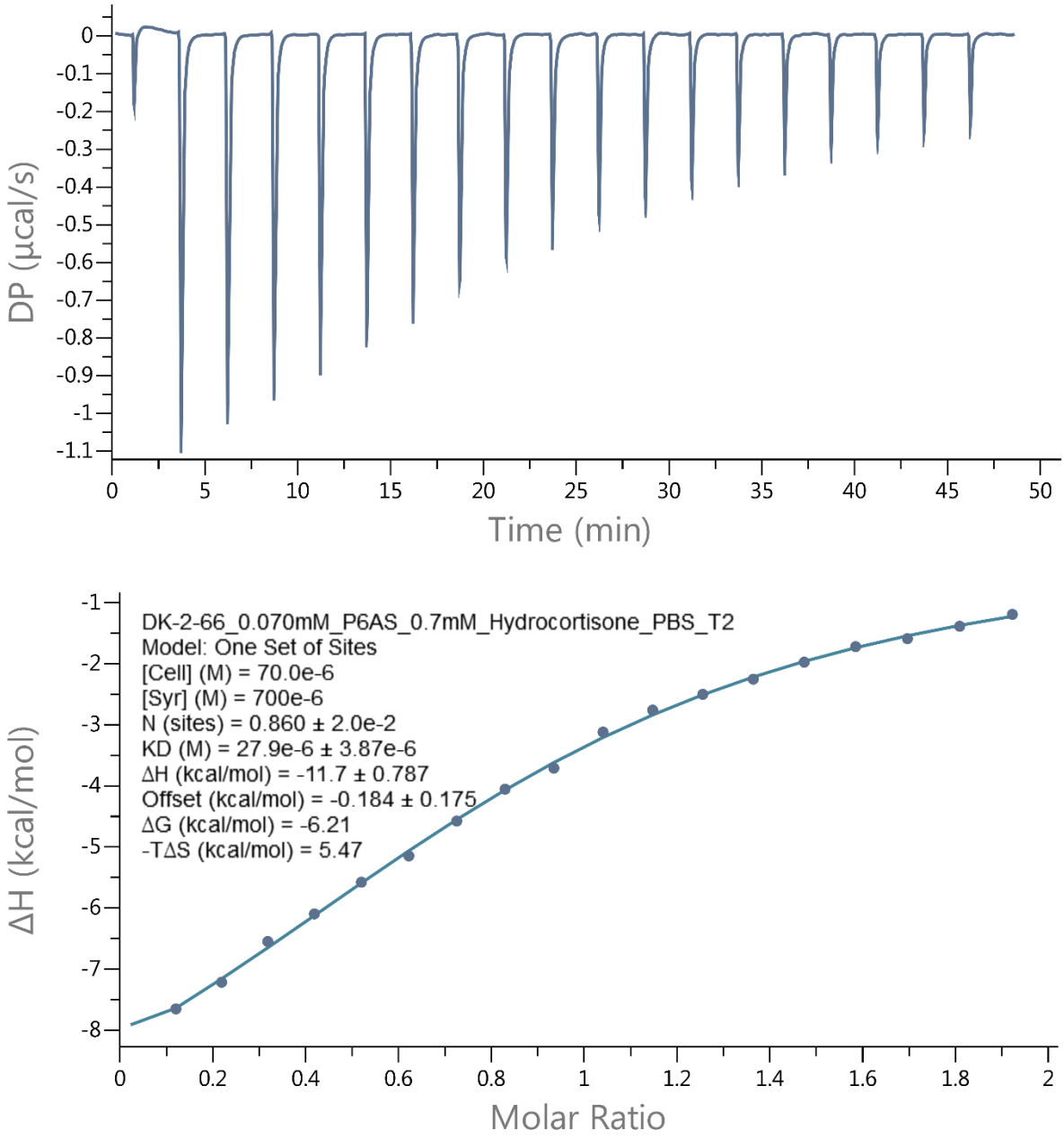

Figure SIV-17. Isothermal Titration Calorimetry (ITC) curve obtained through direct binding titration studies. A solution of P6AS (0.070 mM) in the cell was titrated with **Hcort** (0.70 mM) in the syringe at 298.0 K in 10 mM sodium phosphate buffered saline at pH 7.4. The solid line represents the best non-linear fit of the data to a 1:1 binding model. (K_a = (2.78 ± 0.18) × 10^4 M^{-1}; ΔH = (–12.7 ± 0.4) kcal mol^{-1}).

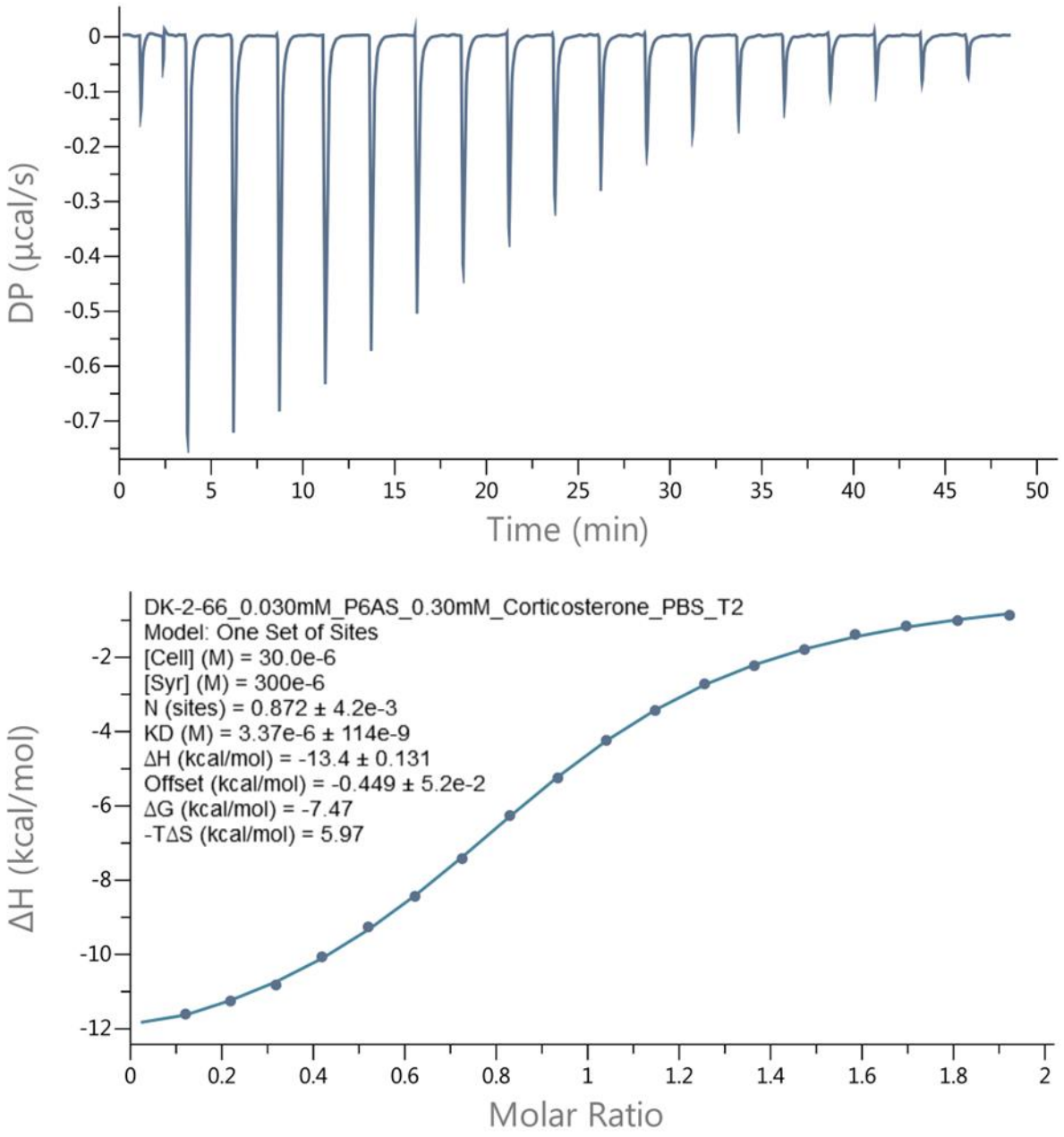

Figure SIV-18. Isothermal Titration Calorimetry (ITC) curve obtained through direct binding titration studies. A solution of P6AS (0.30 mM) in the cell was titrated with **Cort** (0.30 mM) in the syringe at 298.0 K in 10 mM sodium phosphate buffered saline at pH 7.4. The solid line represents the best non-linear fit of the data to a 1:1 binding model. (K_a = (1.84 ± 0.09) × 10^5 M^{-1}; ΔH = (–14.1 ± 0.2) kcal mol^{-1}).

Determination of K_a via Fluorescence Measurements.

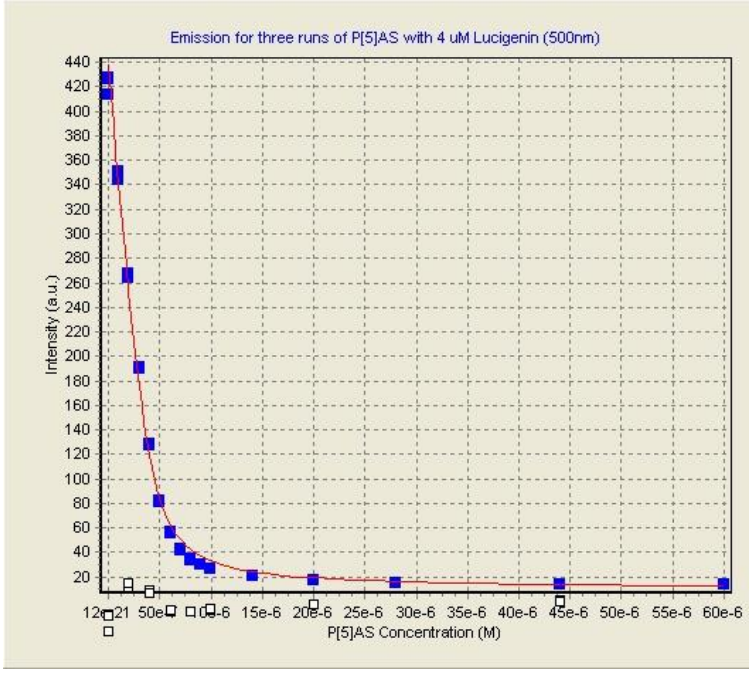

Figure SIV-19. Plot of emission intensity of **Lucigenin** (4.0 μM) at 500 nm (ex. 365 nm) versus [P5AS] (0-60.0 μM) for three replications. The solid curve represents the best non-linear fit of the data to a 1:1 binding model implemented in Scientist^{TM}. K_a was evaluated as (2.83 $\pm$ 0.14) x 10^6 M^{-1}.

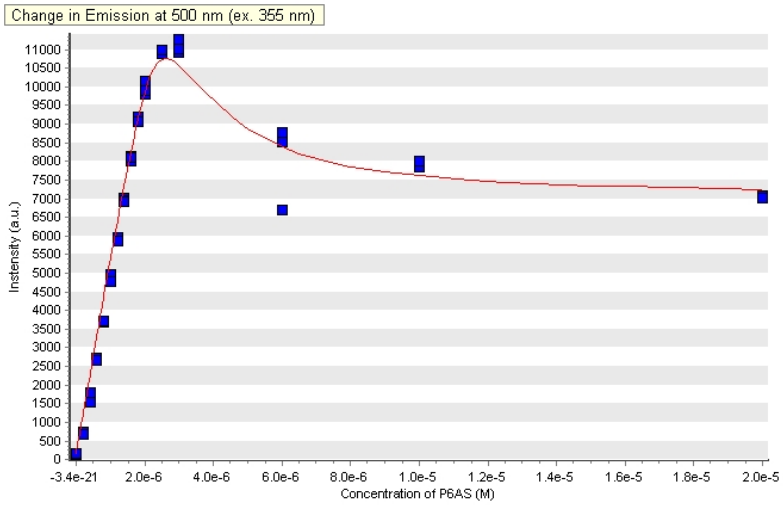

Figure SIV-20. Plot of emission intensity of **Hoechst** (2.0 μM) at 500 nm (ex. 355 nm) versus [P6AS] (0-20 **Lucigenin** (4 μM) for three replications. The solid curve represents the best non-linear fit of the data to a sequential 2:1 (H:G) binding model implemented in Scientist^{TM}. K_{a1} was evaluated as (1.05 $\pm$ 0.36) x 10^8 M^{-1}, and K_{a2} was evaluated as (1.27 $\pm$ 0.35) x 10^6 M^{-1}.

Binding Models Used to Determine Values of Ka with Micromath Scientist

1:1 Binding Model.

// Micromath Scientist Model File

// 1:1 Host:Guest binding model

//This model assumes the guest concentration is fixed and host concentration is varied

IndVars: ConcHostTot

DepVars: SpectroscopicSignal

Params: Ka, ConcGuestTot, SpectroscopicSignalMin, SpectroscopicSignalMax

Ka = ConcHostGuest/(ConcHostFree*ConcGuestFree)

ConcHostTot=ConcHostFree + ConcHostGuest

ConcGuestTot=ConcGuestFree + ConcHostGuest

SpectroscopicSignal = SpectroscopicSignalMin + (SpectroscopicSignalMax -

SpectroscopicSignalMin) * (ConcHostGuest/ConcGuestTot)

//Constraints

0 < ConcHostFree < ConcHostTot

0 < Ka

0 < ConcGuestFree < ConcGuestTot

0 < ConcHostGuest < ConcHostTot

2:1 (H:G) Binding Model.

// Micromath Scientist Model File

// 2:1 Host:Guest binding model

//This model assumes the guest concentration is fixed and host concentration is varied

IndVars: ConcHostTot

DepVars: SpectroscopicSignal

Params: Ka1, Ka2, ConcGuestTot, SpectroscopicSignalInit, SpectroscopicSignalFinal,

HG_Fixing

Ka1 = ConcHostGuest/(ConcHostFree*ConcGuestFree)

Ka2 = ConcHHG/(ConcHostFree*ConcHostGuest)

ConcHostTot = ConcHostFree + ConcHostGuest + 2*ConcHHG

ConcGuestTot = ConcGuestFree + ConcHostGuest + ConcHHG

SpectroscopicSignal = SpectroscopicSignalInit + (SpectroscopicSignalFinal -

SpectroscopicSignalInit) * (ConcHHG/ConcGuestTot) + HG_Fixing *

(ConcHostGuest/ConcGuestTot)

//Constraints

0 < ConcHostFree < ConcHostTot

0 < Ka1

0 < Ka2

0 < ConcGuestFree < ConcGuestTot

0 < ConcHostGuest < ConcHostTot

0 < ConcHHG < ConcHostFree/2

^{1}H NMR spectra of P5AS with selected guests.

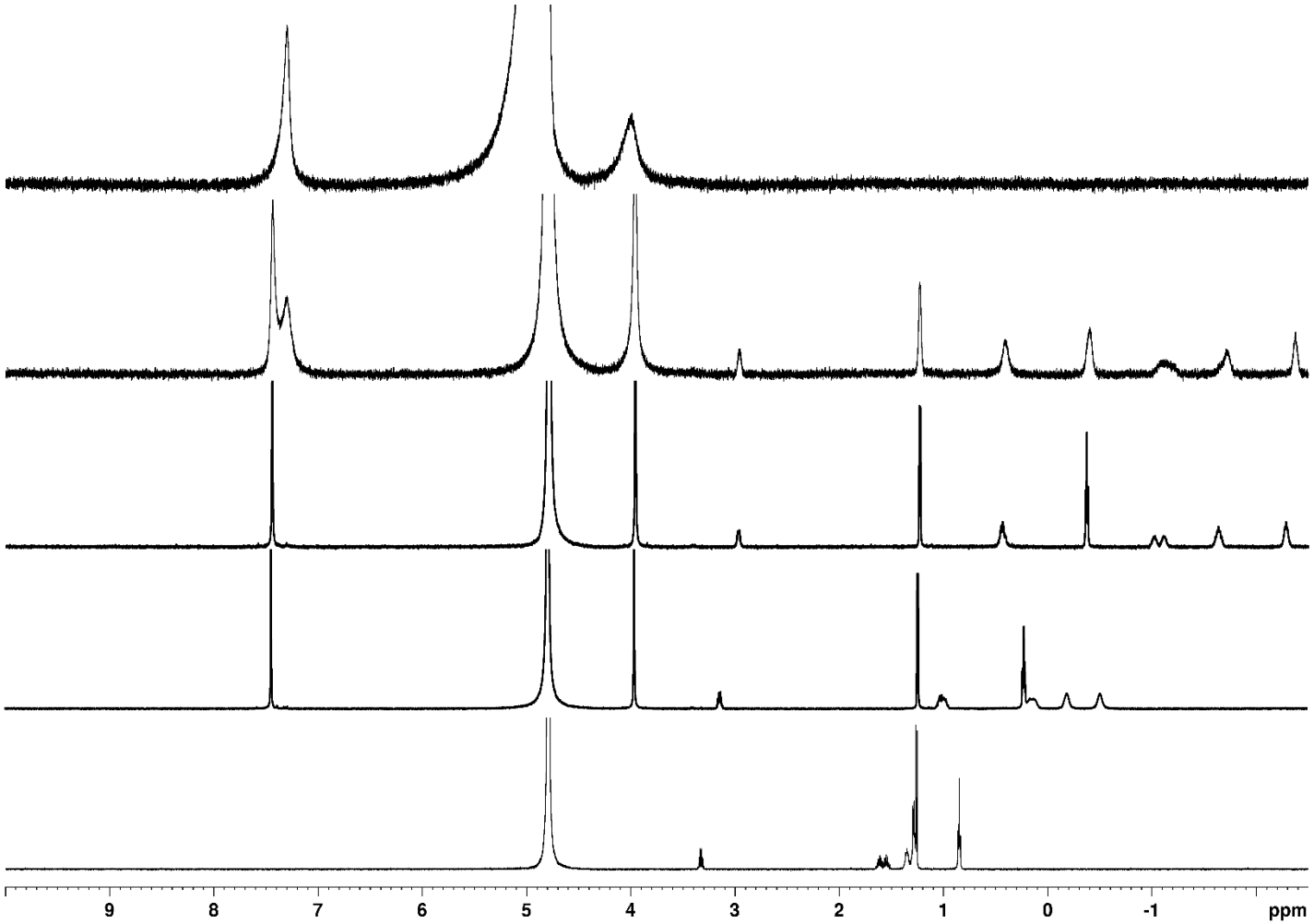

Figure SIV-21. ^{1}H NMR spectra recorded for (600 MHz, RT, PBS buffered D_2O, pD 7.4) for: a) **2HeptNH3** (1.0 mM), b) a mixture of **2HeptNH3** (2.0 mM) and P5AS (1.0 mM), c) an equimolar mixture of **2HeptNH3** and P5AS (1.0 mM), and d) a mixture of **2HeptNH3** (0.5 mM) and P5AS (1.0 mM), e) P5AS (1.0 mM).

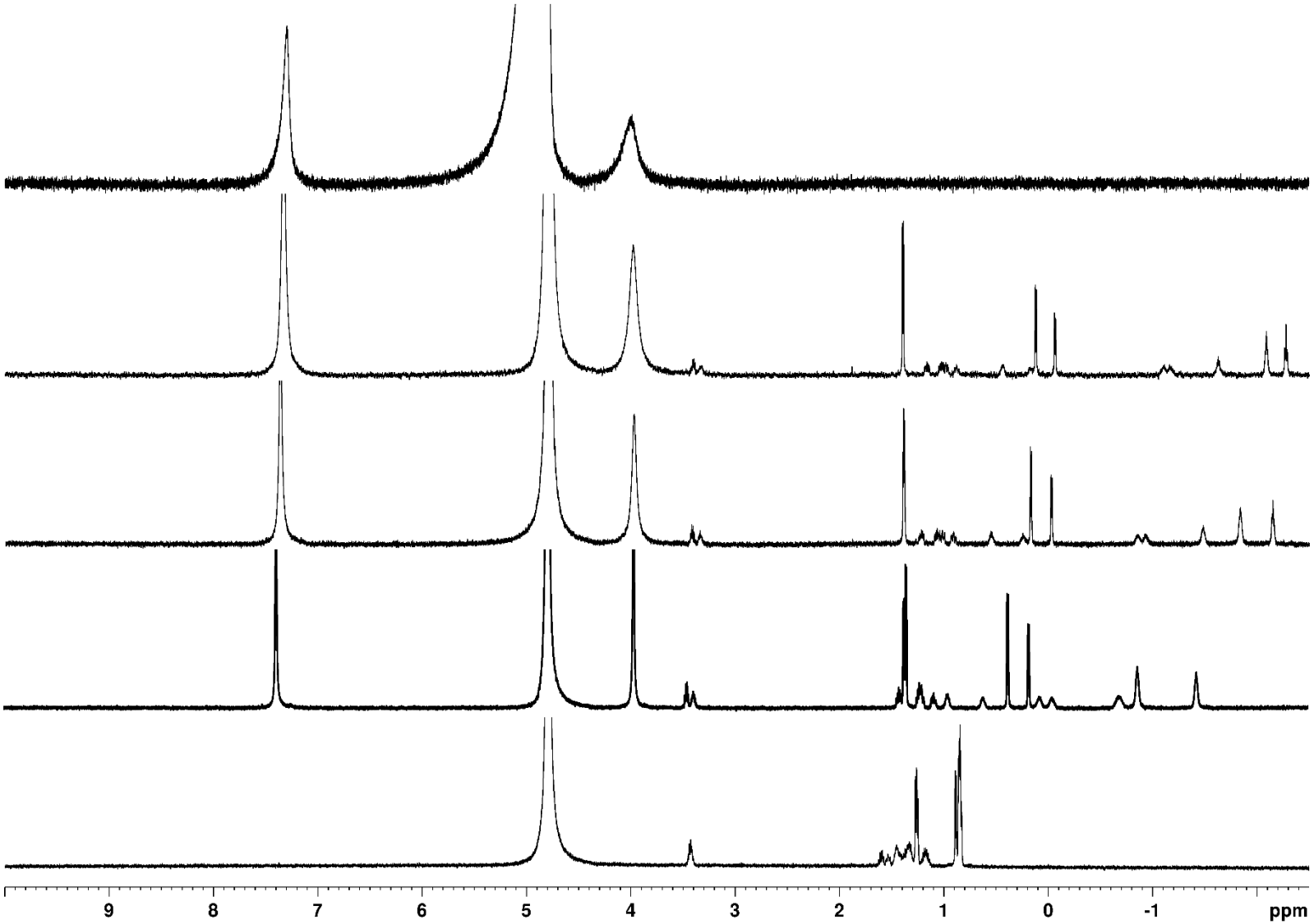

Figure SIV-22. ^{1}H NMR spectra recorded for (600 MHz, RT, PBS buffered D_2O, pD 7.4) for: a) **1,3dmPentNH3** (1.0 mM), b) a mixture of **1,3dmPentNH3** (2.0 mM) and P5AS (1.0 mM), c) an equimolar mixture of **1,3dmPentNH3** and P5AS (1.0 mM), and d) a mixture of **1,3dmPentNH3** (0.5 mM) and P5AS (1.0 mM), e) P5AS (1.0 mM).

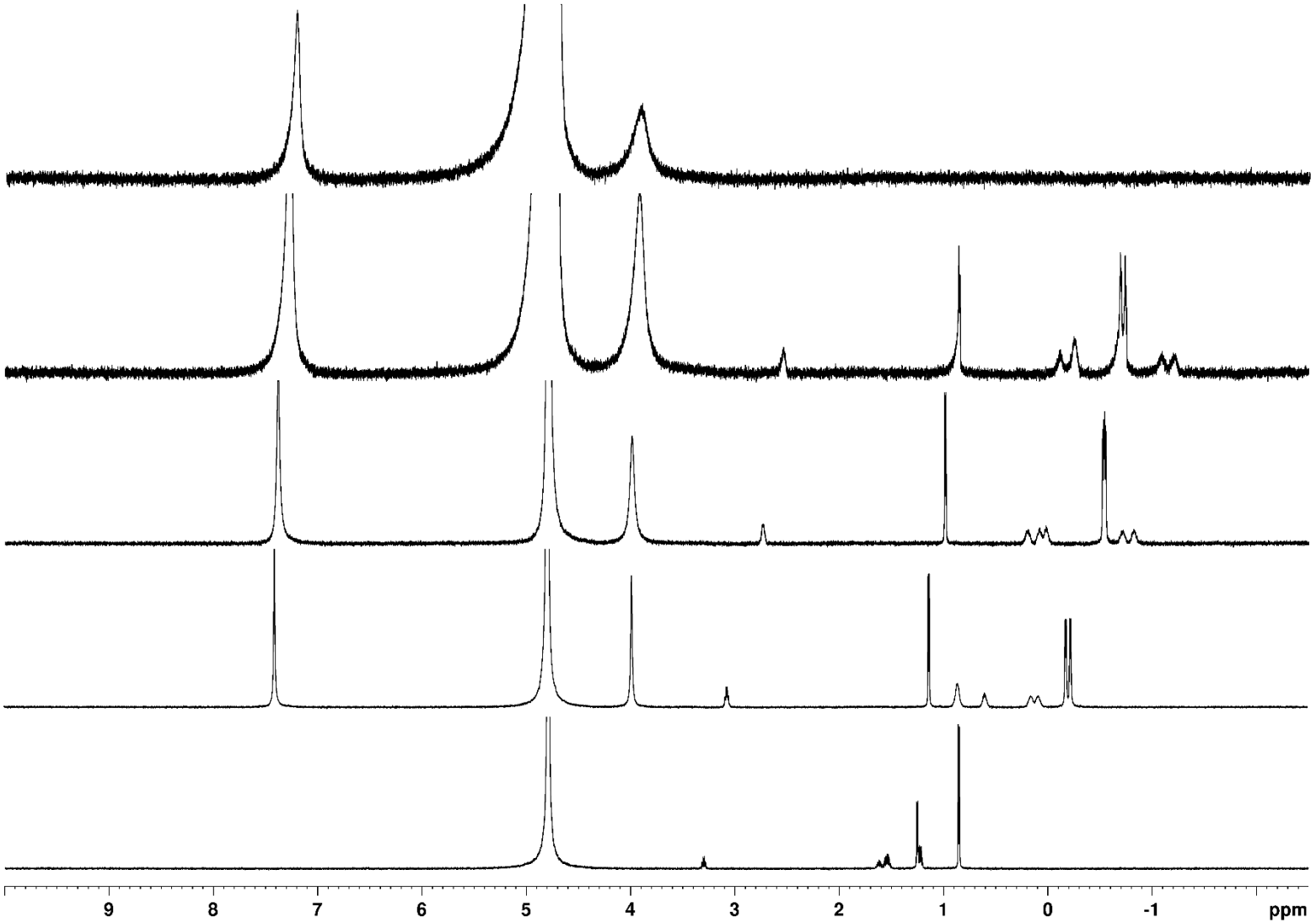

Figure SIV-23. ^{1}H NMR spectra recorded for (600 MHz, RT, PBS buffered D_2O, pD 7.4) for: a) **1,4dmPentNH3** (1.0 mM), b) a mixture of **1,4dmPentNH3** (2.0 mM) and P5AS (1.0 mM), c) an equimolar mixture of **1,4dmPentNH3** and P5AS (1.0 mM), and d) a mixture of **1,4dmPentNH3** (0.5 mM) and P5AS (1.0 mM), e) P5AS (1.0 mM),

^{1}H NMR spectra of P6AS with selected guests.

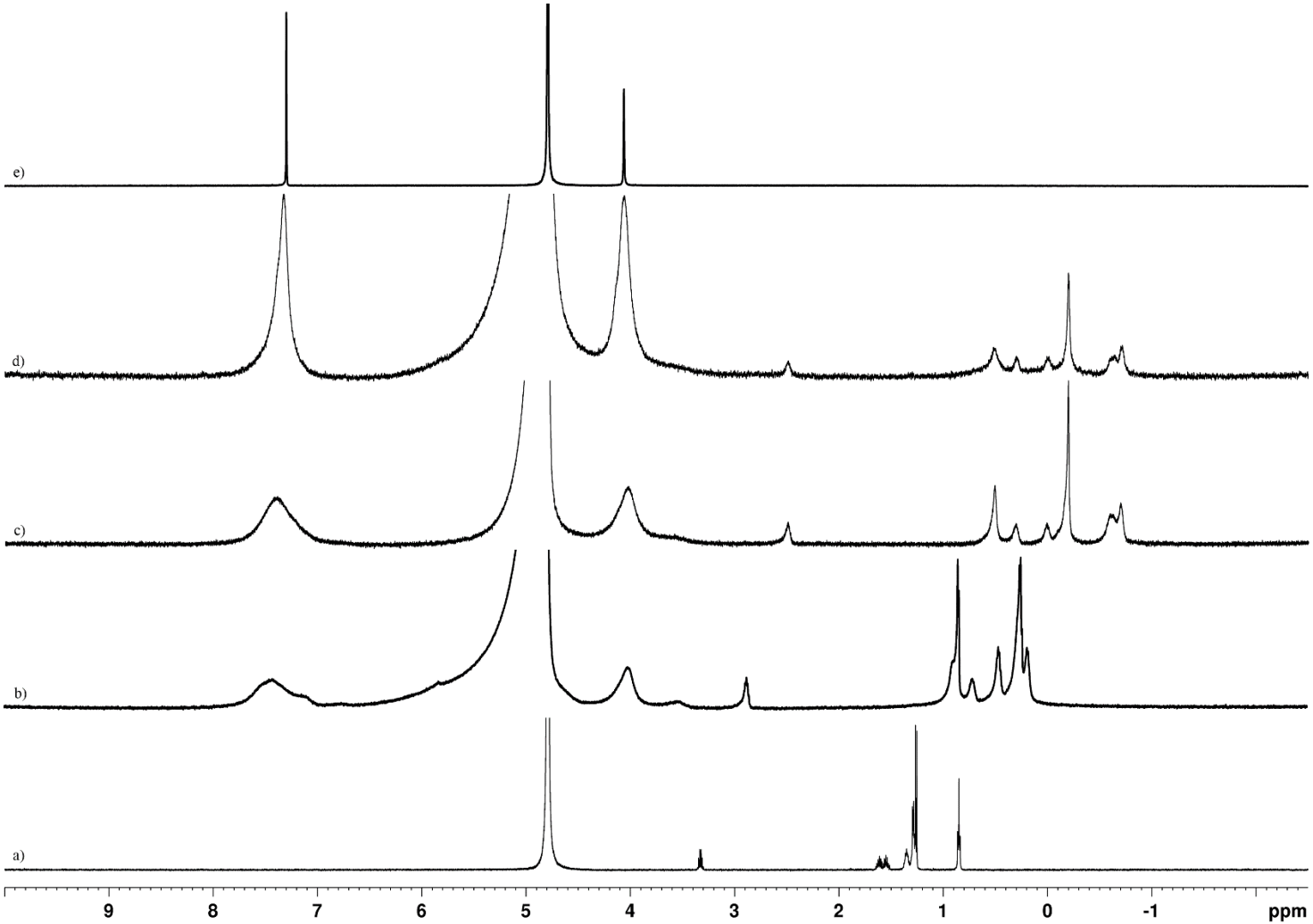

Figure SIV-24. ^{1}H NMR spectra recorded for (600 MHz, RT, PBS buffered D_2O, pD 7.4) for: a) **2HeptNH3** (1.0 mM), b) a mixture of **2HeptNH3** (2.0 mM) and P6AS (1.0 mM), c) an equimolar mixture of **2HeptNH3** and P6AS (1.0 mM), and d) a mixture of **2HeptNH3** (0.5 mM) and P6AS (1.0 mM), e) P6AS (1.0 mM).

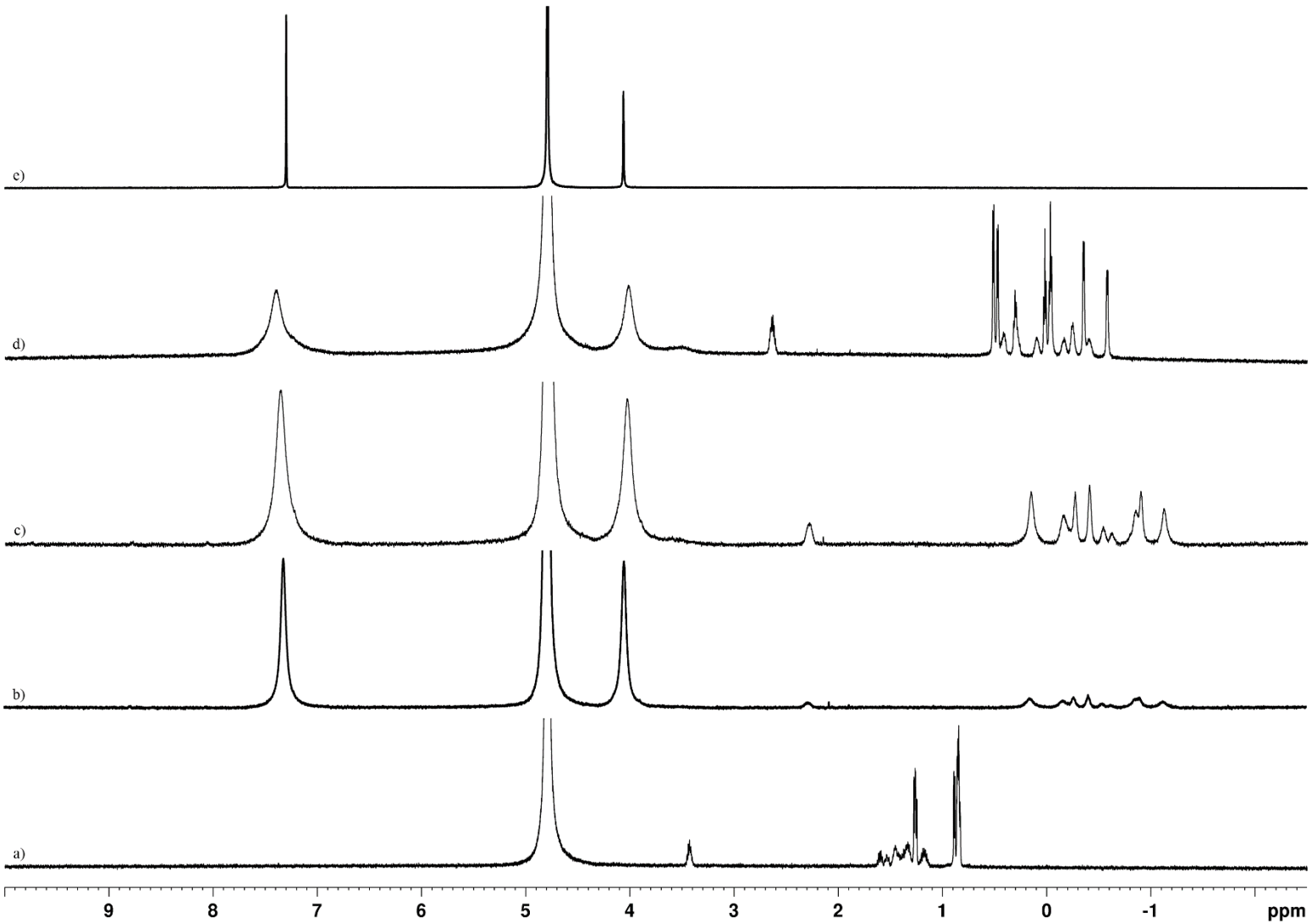

Figure SIV-25. ^{1}H NMR spectra recorded for (600 MHz, RT, PBS buffered D_2O, pD 7.4) for: a) **1,3dmPentNH3** (1.0 mM), b) a mixture of **1,3dmPentNH3** (2.0 mM) and P6AS (1.0 mM), c) an equimolar mixture of **1,3dmPentNH3** and P6AS (1.0 mM), d) a mixture of **1,3dmPentNH3** (0.5 mM) and P6AS (1.0 mM), and e) P6AS (1.0 mM).

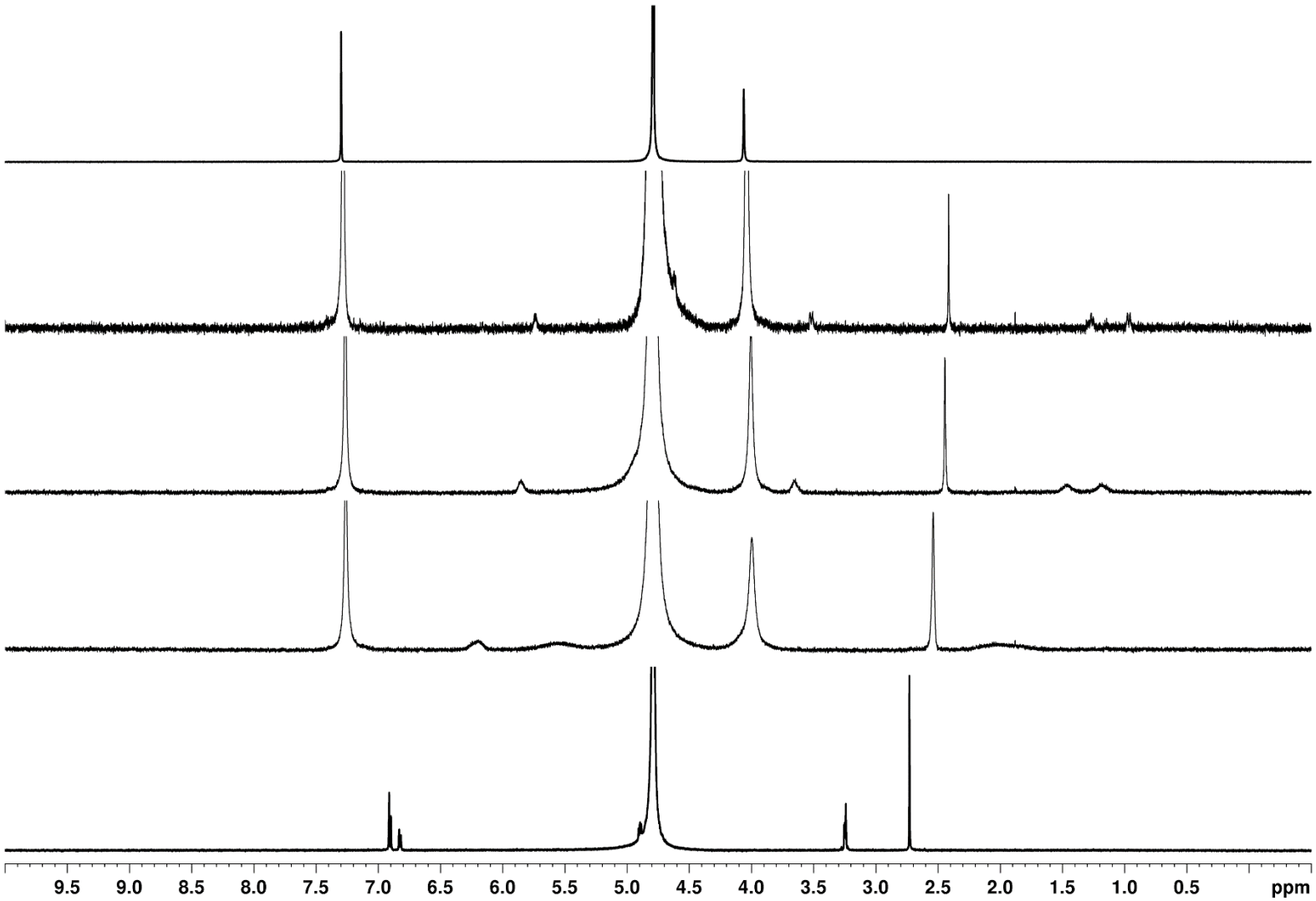

Figure SIV-26. ^{1}H NMR spectra recorded for (600 MHz, RT, PBS buffered D_2O, pD 7.4) for: a) **Epi** (1.0 mM), b) a mixture of **Epi** (2.0 mM) and P6AS (1.0 mM), c) an equimolar mixture of **Epi** and P6AS (1.0 mM), d) a mixture of **Epi** (0.5 mM) and P6AS (1.0 mM), and e) P6AS (1.0 mM).

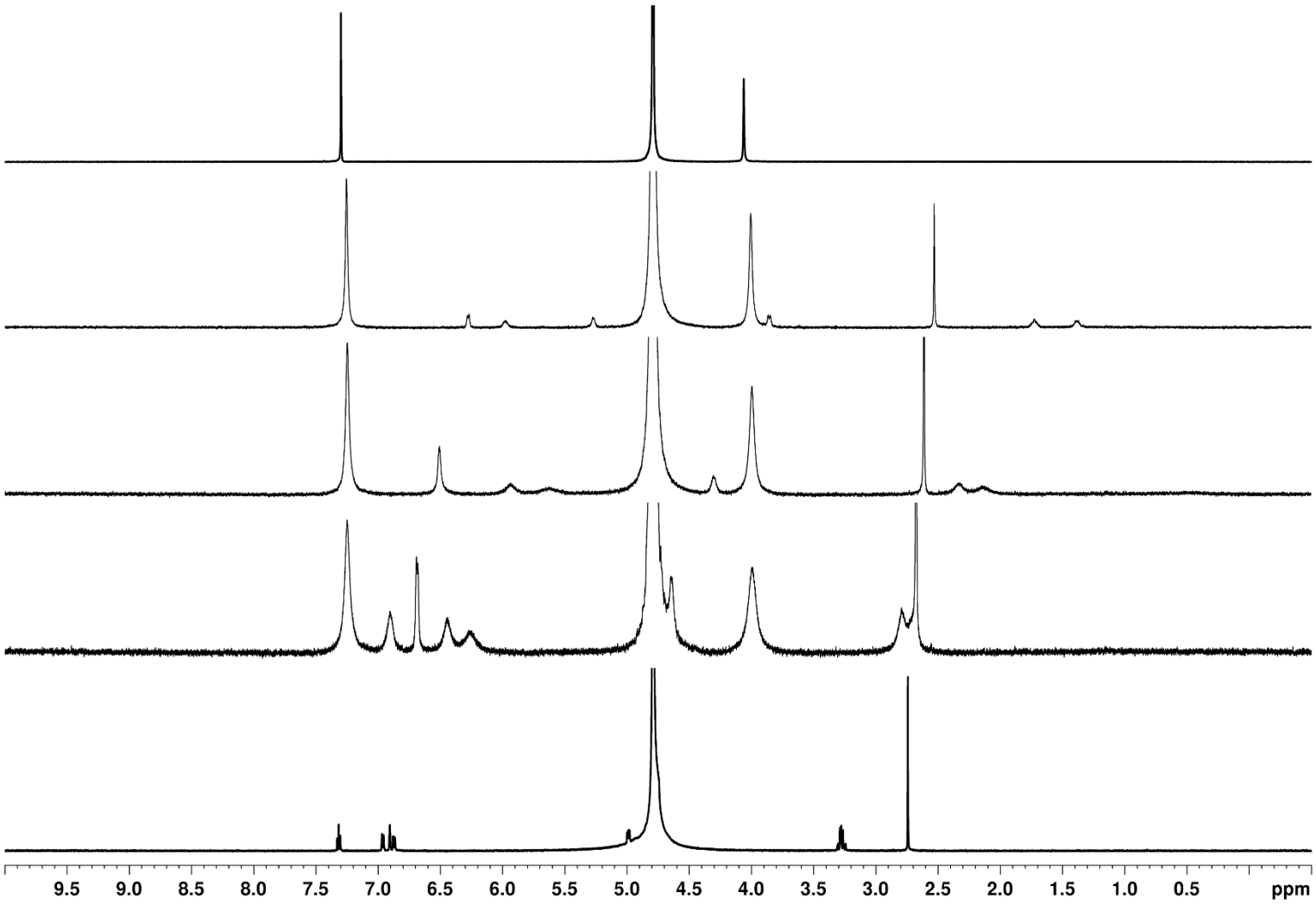

Figure SIV-27. ^{1}H NMR spectra recorded for (600 MHz, RT, PBS buffered D_2O, pD 7.4) for: a) **Pseudo** (1.0 mM), b) a mixture of **Pseudo** (2.0 mM) and P6AS (1.0 mM), c) an equimolar mixture of **Pseudo** and P6AS (1.0 mM), d) a mixture of **Pseudo** (0.5 mM) and P6AS (1.0 mM), and e) P6AS (1.0 mM).

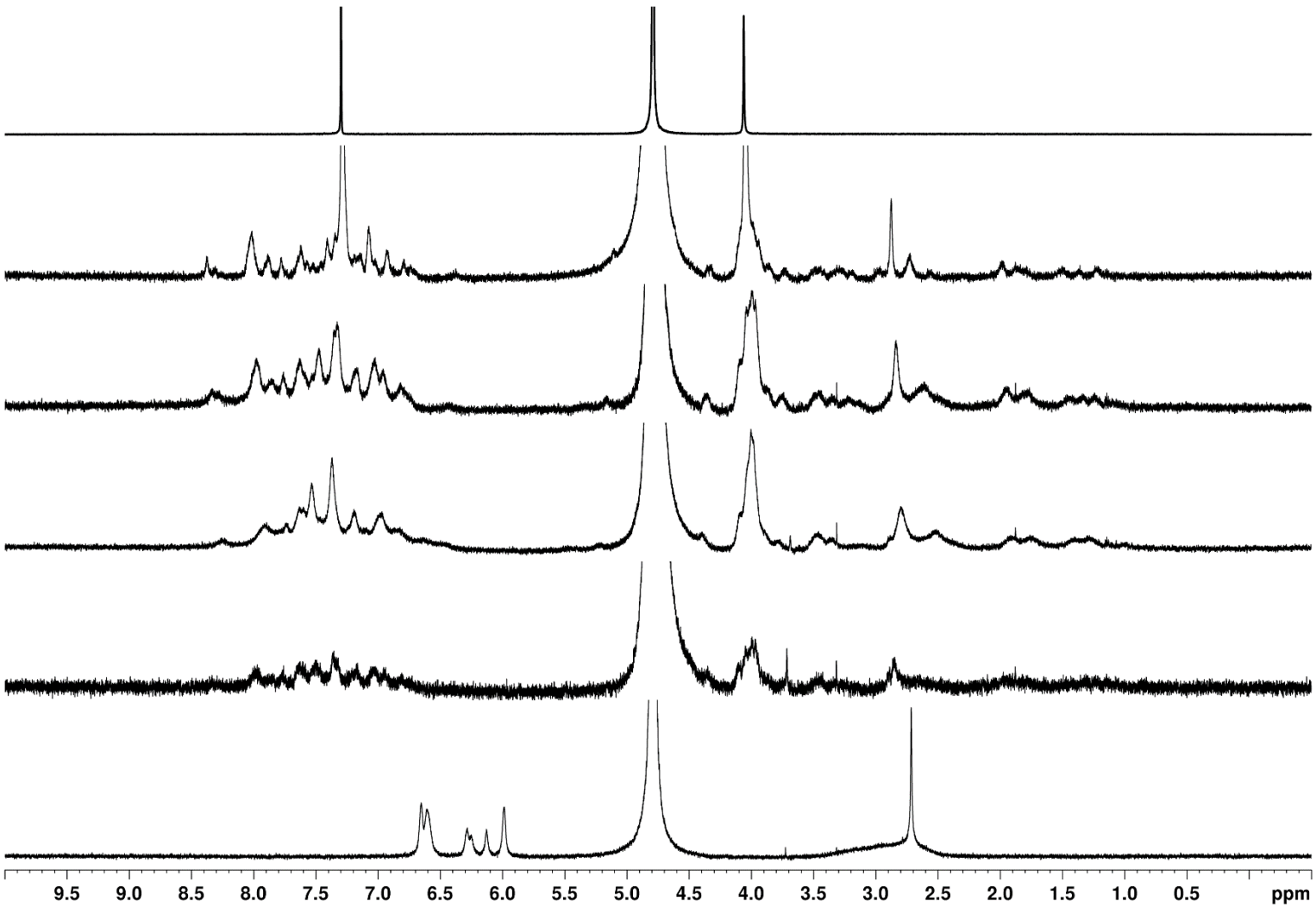

Figure SIV-28. ^{1}H NMR spectra recorded for (600 MHz, RT, PBS buffered D_2O, pD 7.4) for: a) **Hoechst 33258** (1.0 mM), b) a mixture of **Hoechst 33258** (2.0 mM) and P6AS (1.0 mM), c) an equimolar mixture of **Hoechst 33258** and P6AS (1.0 mM), d) a mixture of **Hoechst 33258** (0.5 mM) and P6AS (1.0 mM), e) a mixture of **Hoechst 33258** (0.25 mM) and P6AS (1.0 mM), and f) P6AS (1.0 mM).

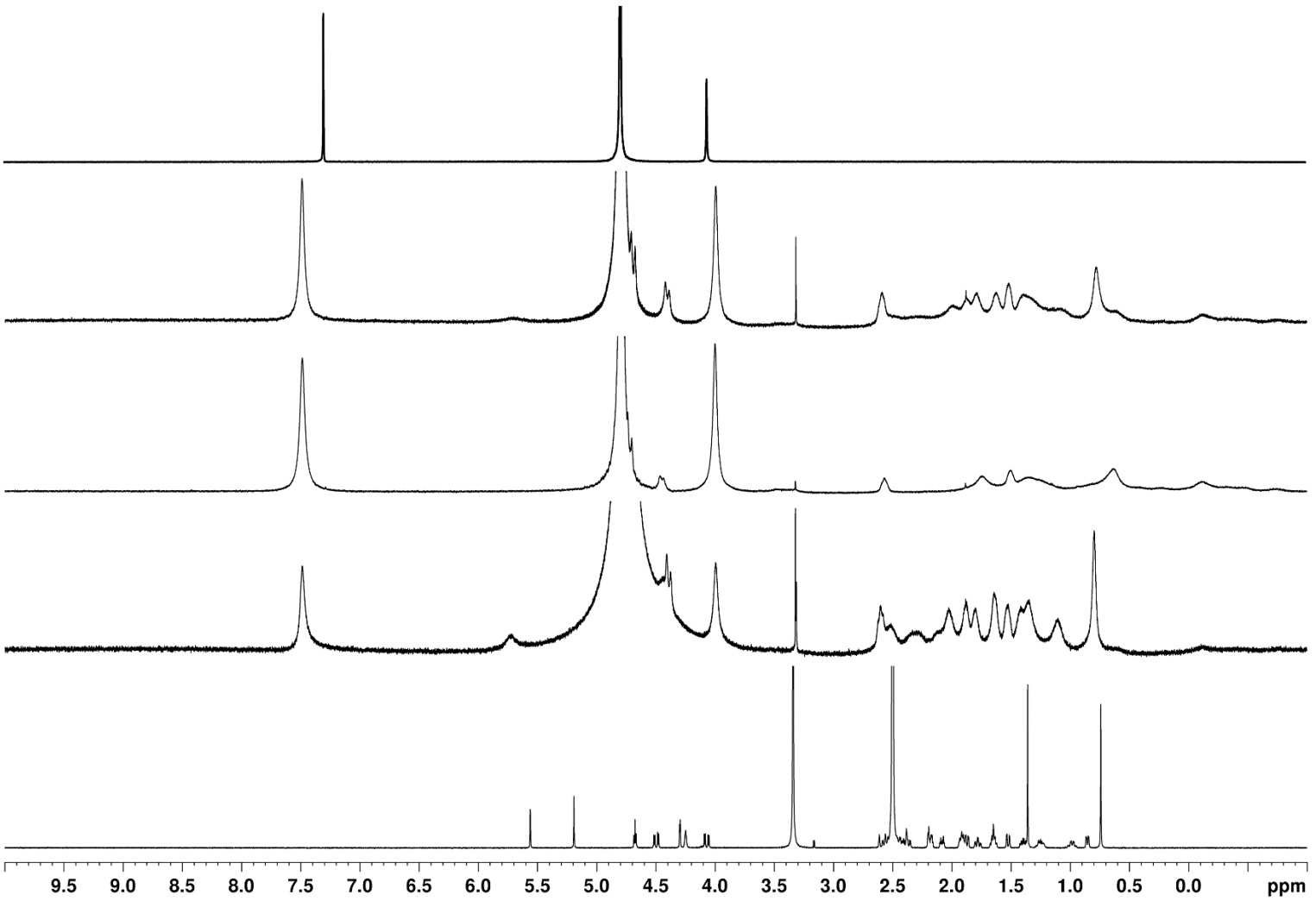

Figure SIV-29. ^{1}H NMR spectra recorded for (600 MHz, RT) for: a) **Hcort** (1.0 mM) (DMSO-d_6), b) a mixture of **Hcort** (1.0 mM) and P6AS (0.5 mM) (PBS buffered D_2O, pD 7.4), c) an equimolar mixture of **Hcort** and P6AS (1.0 mM) (PBS buffered D_2O, pD 7.4), d) a mixture of **Hcort** (1.0 mM) and P6AS (2.0 mM) (PBS buffered D_2O, pD 7.4), and e) P6AS (1.0 mM) (PBS buffered D_2O, pD 7.4).

Machine Learning Data

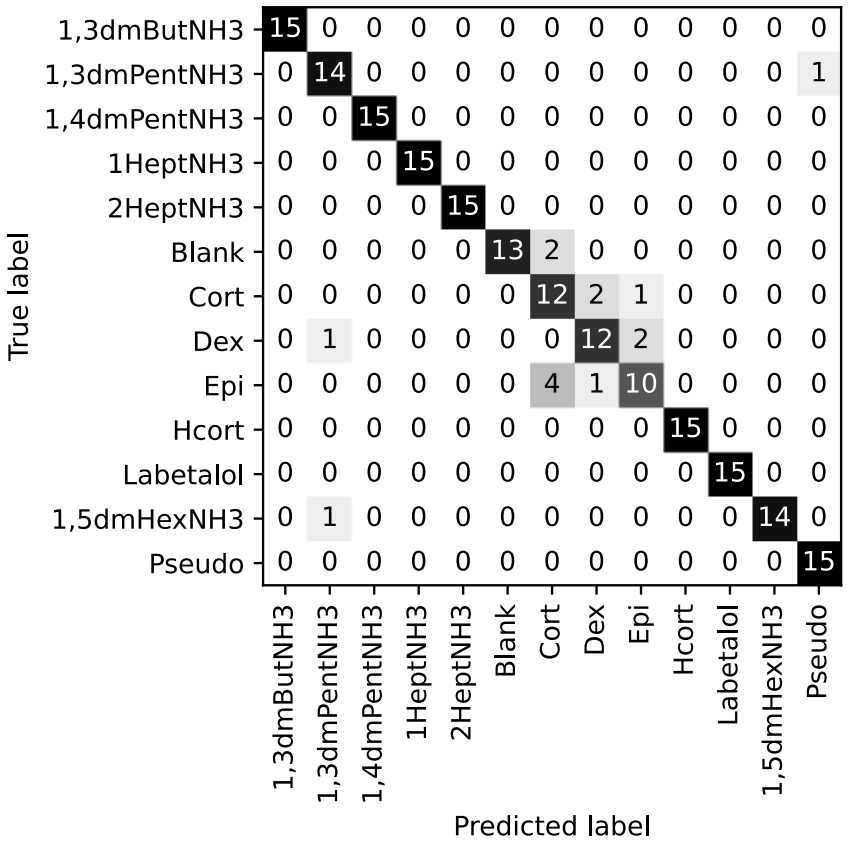

Figure SIV-30. Combined confusion matrix for the prediction of each compound for each iteration of the cross validation.

Table SIV-1. Explained Variance ratio for LDA

5.73838581e-01	3.53437210e-01	6.51012154e-02	4.14276278e-03
1.23408116e-03	7.59216632e-04	5.30418624e-04	4.19053531e-04
2.10302756e-04	1.62779079e-04	1.17815538e-04	4.65637430e-05

Table SIV-2. Predicted Compounds from **Estradiol** Measurements

Dex	Hcort	Blank	Dex	Hcort
Dex	Dex	Dex	Blank	Hcort
Dex	1,3dmPentNH3	Dex	Hcort	Dex

Table SIV-3. Predicted Accuracy of Cross Validation

0.92307692	0.76923077	0.92307692	0.84615385	0.92307692
1.	1.	0.92307692	0.92307692	1.
0.84615385	1.	0.84615385	0.92307692	1.

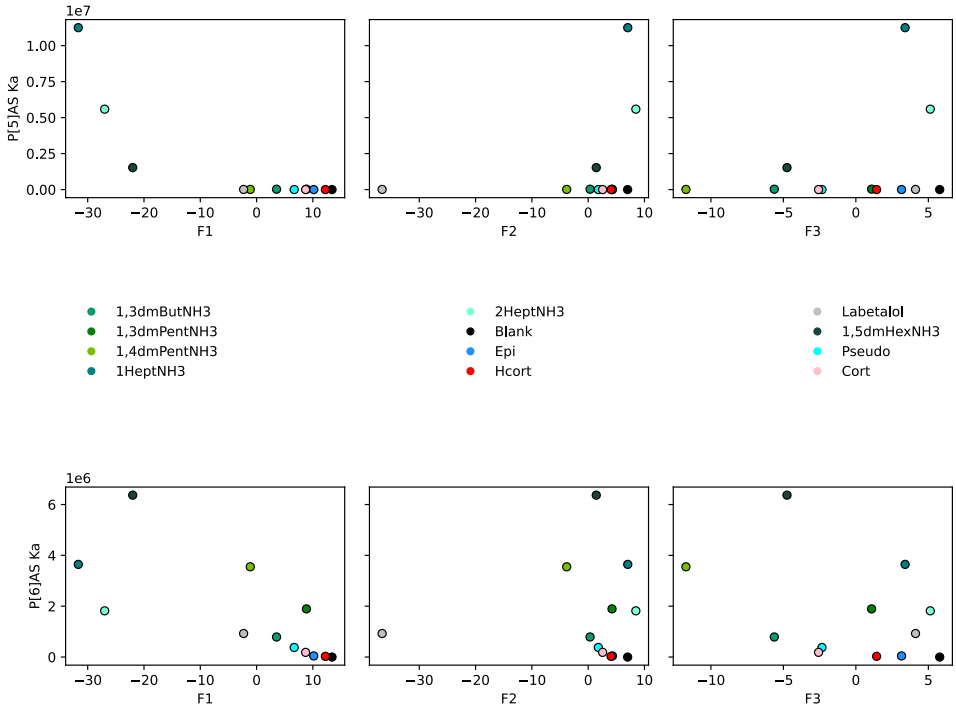

Figure SIV-31. Plots of the first three factors vs. K_a for P5AS (top) and P6AS (bottom).

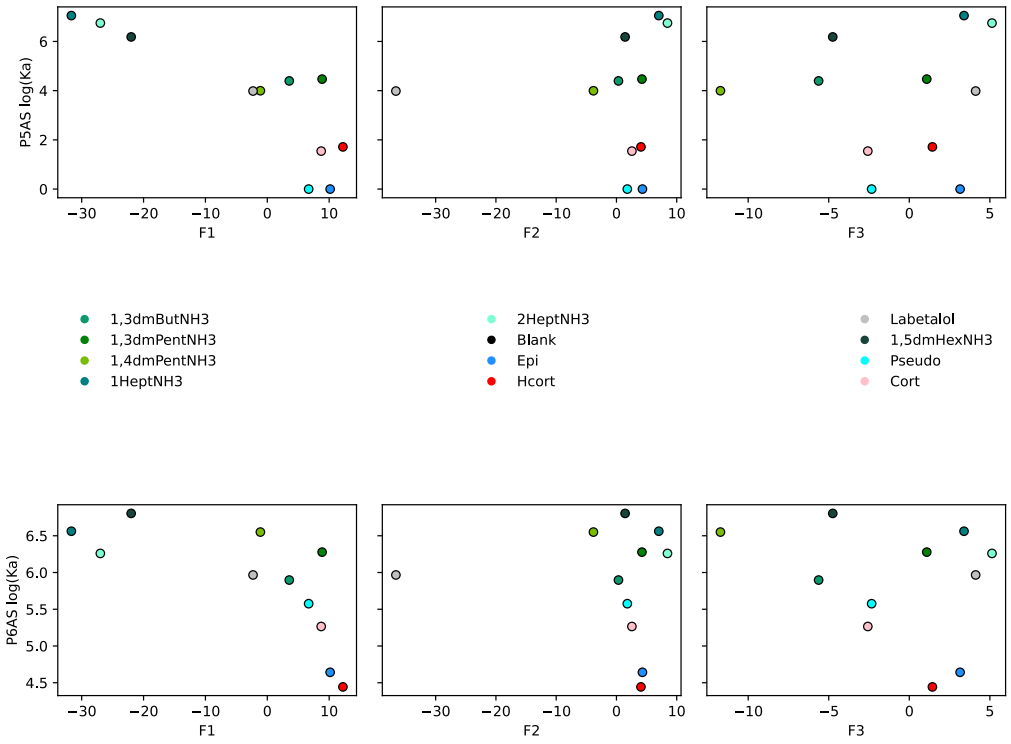

Figure SIV-32. Plots of the first three factors vs. log(K_a) for P5AS (top) and P6AS (bottom).

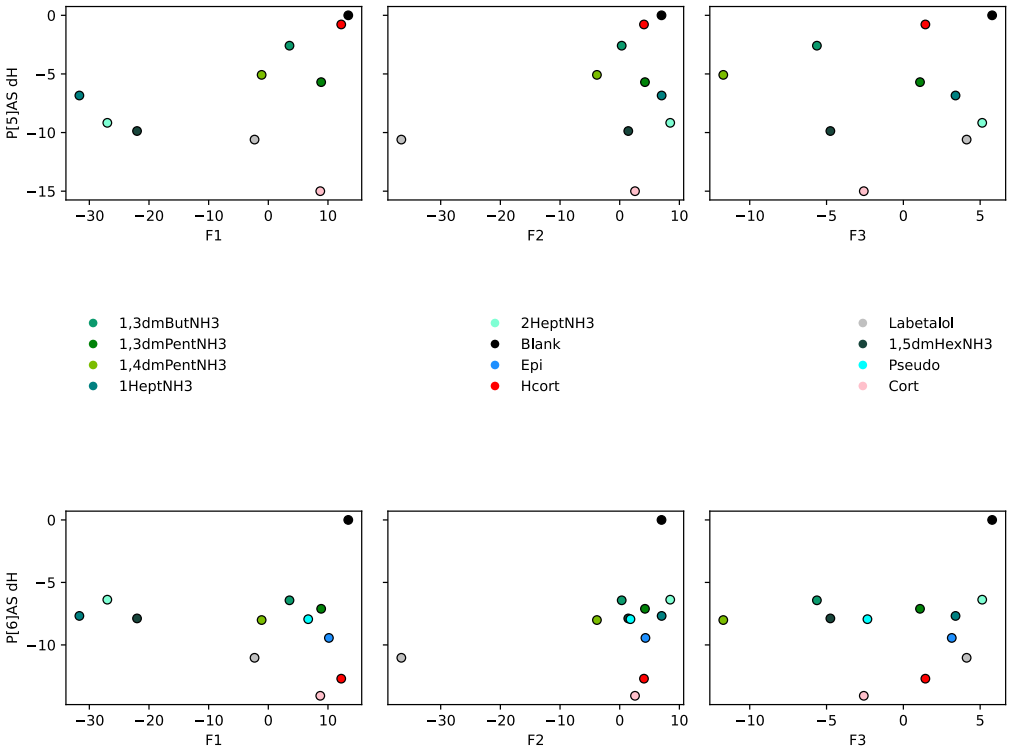

Figure SIV-33. Plots of the first three factors vs. ΔH for P5AS (top) and P6AS (bottom).

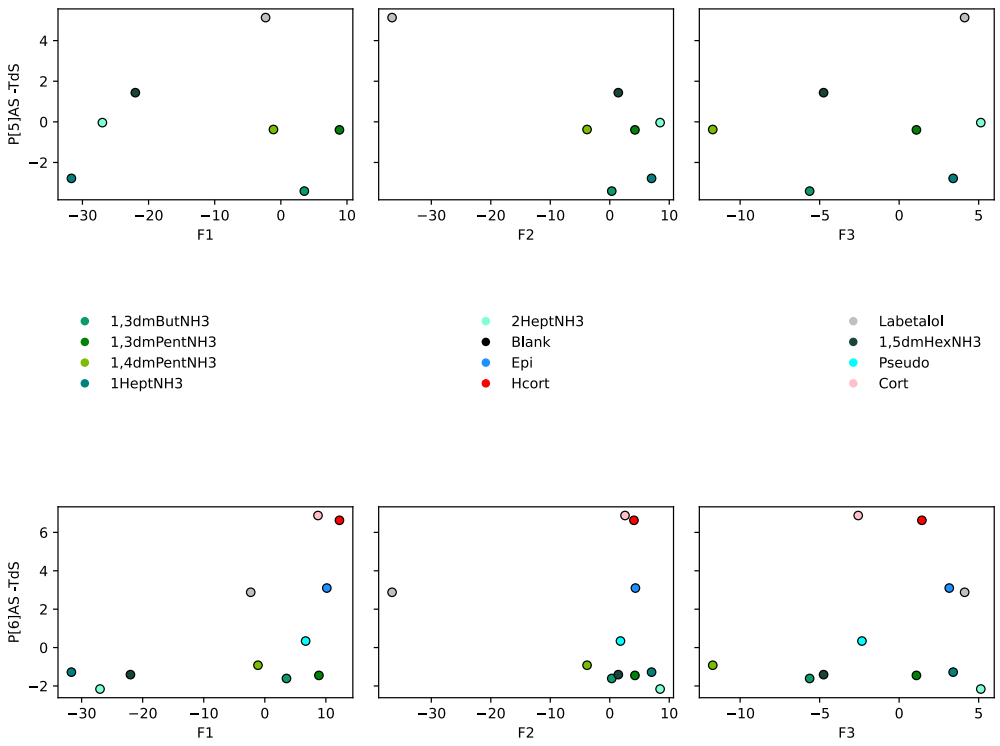

Figure SIV-34. Plots of the first three factors vs. -TΔS for P5AS (top) and P6AS (bottom).

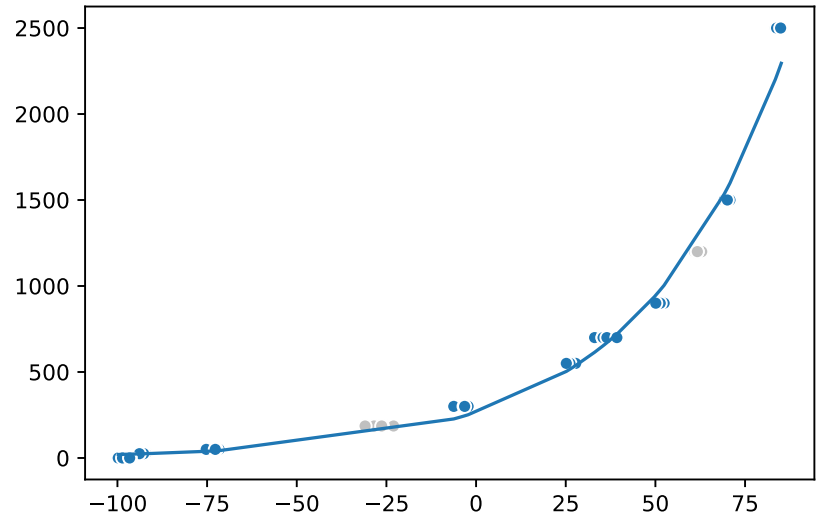

Figure SIV-35 Calibration curve of **Pseudo** from 0-2500 µM. Blue dots represent the data the curve was trained on, while silver dots represent the 'unknown' concentrations that were predicted.

Table SIV-4. Predicted Concentrations for **Pseudo** and **Epi**

Actual Concentration	Compound	Predicted Concentrations									
9.3	Epi	4.79	9.90	7.57	7.75	6.22	11.24	13.93	10.51	10.28	3.43
41.3	Epi	44.8	53.9	55.0	48.9	47.4	45.9	42.0	47.3	50.3	47.5
1200	Pseudo	1247	1268	1260	1267	1245	1301	1309	1267	1266	1270
186	Pseudo	138.5	134.0	134.0	139.4	148.1	136.8	135.6	129.0	121.0	136.2

Bibliography

(1) Pieters, B. J. G. E.; Van Eldijk, M. B.; Nolte, R. J. M.; Mecinović, J. *Chem Soc Rev* **2015**, *45*, 24–39.
(2) Frieden, E. *J Chem Educ* **1975**, *52*, 754.
(3) Cram, D. J. *Angewandte Chemie International Edition in English* **1988**, *27*, 1009–1020.
(4) Lehn, J. -M. *Angewandte Chemie International Edition in English* **1988**, *27*, 89–112.
(5) Pedersen, C. J. *Angewandte Chemie International Edition in English* **1988**, *27*, 1021–1027.
(6) *The Nobel Prize in Chemistry 1987 - NobelPrize.org*.
(7) Behrend, R.; Meyer, E.; Rusche, F. *Justus Liebigs Ann Chem* **1905**, *339*, 1–37.
(8) Freeman, W. A.; Mock, W. L.; Shih, N. Y. *J Am Chem Soc* **1981**, *103*, 7367–7368.
(9) Mock, W. L.; Shih, N. Y. *Journal of Organic Chemistry* **1983**, *48*, 3618–3619.
(10) Biedermann, F.; Uzunova, V. D.; Scherman, O. A.; Nau, W. M.; De Simone, A. *J Am Chem Soc* **2012**, *134*, 15318–15323.
(11) Biedermann, F.; Nau, W. M.; Schneider, H. J. *Angewandte Chemie - International Edition* **2014**, *53*, 11158–11171.
(12) Lazar, A. I.; Biedermann, F.; Mustafina, K. R.; Assaf, K. I.; Hennig, A.; Nau, W. M. *J Am Chem Soc* **2016**, *138*, 13022–13029.
(13) Shetty, D.; Khedkar, J. K.; Park, K. M.; Kim, K. *Chem Soc Rev* **2015**, *44*, 8747–8761.
(14) Kaizerman-Kane, D.; Hadar, M.; Joseph, R.; Logviniuk, D.; Zafrani, Y.; Fridman, M.; Cohen, Y. *ACS Infect Dis* **2021**, *7*, 579–585.
(15) Li, C.; Shu, X.; Li, J.; Fan, J.; Chen, Z.; Weng, L.; Jia, X. *Org Lett* **2012**, *14*, 4126–4129.
(16) Moghaddam, S.; Yang, C.; Rekharsky, M.; Ko, Y. H.; Kim, K.; Inoue, Y.; Gilson, M. K. *J Am Chem Soc* **2011**, *133*, 3570–3581.
(17) Rekharsky, M. V.; Mori, T.; Yang, C.; Young, H. K.; Selvapalam, N.; Kim, H.; Sobransingh, D.; Kaifer, A. E.; Liu, S.; Isaacs, L.; Chen, W.; Moghaddam, S.; Gilson, M. K.; Kim, O.; Inoue, Y. *Proc Natl Acad Sci U S A* **2007**, *104*, 20737–20742.
(18) Cao, L.; Šekutor, M.; Zavalij, P. Y.; Mlinarič-Majerski, K.; Glaser, R.; Isaacs, L. *Angewandte Chemie - International Edition* **2014**, *53*, 988–993.
(19) Cao, L.; Isaacs, L. *Supramol Chem* **2014**, *26*, 251–258.
(20) Sigwalt, D.; Šekutor, M.; Cao, L.; Zavalij, P. Y.; Hostaš, J.; Ajani, H.; Hobza, P.; Mlinarić-Majerski, K.; Glaser, R.; Isaacs, L. *J Am Chem Soc* **2017**, *139*, 3249–3258.
(21) Mukhopadhyay, P.; Wu, A.; Isaacs, L. *Journal of Organic Chemistry* **2004**, *69*, 6157–6164.
(22) Liu, S.; Ruspic, C.; Mukhopadhyay, P.; Chakrabarti, S.; Zavalij, P. Y.; Isaacs, L. *J Am Chem Soc* **2005**, *127*, 15959–15967.
(23) Jeon, W. S.; Moon, K.; Park, S. H.; Chun, H.; Ko, Y. H.; Lee, J. Y.; Lee, E. S.; Samal, S.; Selvapalam, N.; Rekharsky, M. V.; Sindelar, V.; Sobransingh, D.; Inoue, Y.; Kaifer, A. E.; Kim, K. *J Am Chem Soc* **2005**, *127*, 12984–12989.
(24) Connors, K. A. *Binding Constants*; John Wiley & Sons: New York, 1987.
(25) Hirose, K. *A Practical Guide for the Determination of Binding Constants* *; 2001; Vol. 39.
(26) Sinn, S.; Krämer, J.; Biedermann, F. *Chemical Communications* **2020**, *56*, 6620–6623.

(27) Malaspina, T.; Fileti, E.; Chaban, V. V. *Journal of Physical Chemistry B* **2016**, *120*, 7511–7516.
(28) Gutsche, C. D. *Acc Chem Res* **1983**, *16*, 161–170.
(29) Ma, D.; Glassenberg, R.; Ghosh, S.; Zavalij, P. Y.; Isaacs, L. *Supramol Chem* **2012**, *24*, 325–332.
(30) Xue, W.; Zavalij, P. Y.; Isaacs, L. *Angewandte Chemie - International Edition* **2020**, *59*, 13313–13319.
(31) Deng, C. L.; Murkli, S. L.; Isaacs, L. D. *Chem Soc Rev* **2020**, *49*, 7516–7532.
(32) Brockett, A. T.; Xue, W.; Deng, C.-L.; Zhai, C.; Shuster, M.; King, D.; Rastogi, S.; Briken, V.; Roesch, M. R.; Isaacs, L. **2022**.
(33) DiMaggio, D.; Brockett, A. T.; Shuster, M.; Murkli, S.; Zhai, C.; King, D.; O'Dowd, B.; Cheng, M.; Brady, K.; Briken, V.; Roesch, M. R.; Isaacs, L. *ChemMedChem* **2022**, *17*, e202200046.
(34) Murkli, S.; Klemm, J.; Brockett, A. T.; Shuster, M.; Briken, V.; Roesch, M. R.; Isaacs, L. *Chemistry – A European Journal* **2021**, *27*, 3098–3105.
(35) Nguyen, B. T.; Anslyn, E. V. *Coord Chem Rev* **2006**, *250*, 3118–3127.
(36) Anslyn, E. V. *Journal of Organic Chemistry* **2007**, *72*, 687–699.
(37) Beatty, M. A.; Borges-González, J.; Sinclair, N. J.; Pye, A. T.; Hof, F. *J Am Chem Soc* **2018**, *140*, 3500–3504.
(38) Beatty, M. A.; Selinger, A. J.; Li, Y.; Hof, F. *J Am Chem Soc* **2019**, *141*, 16763–16771.
(39) Minami, T.; Esipenko, N. A.; Akdeniz, A.; Zhang, B.; Isaacs, L.; Anzenbacher, P. *J Am Chem Soc* **2013**, *135*, 15238–15243.
(40) Shcherbakova, E. G.; Zhang, B.; Gozem, S.; Minami, T.; Zavalij, P. Y.; Pushina, M.; Isaacs, L. D.; Anzenbacher, P. *J Am Chem Soc* **2017**, *139*, 14954–14960.
(41) Murkli, S.; Klemm, J.; King, D.; Zavalij, P. Y.; Isaacs, L. *Chemistry - A European Journal* **2020**, *26*.
(42) Masson, E.; Ling, X.; Joseph, R.; Kyeremeh-Mensah, L.; Lu, X. *RSC Advanced* **2012**, *2*, 1213–1247.
(43) Barrow, S. J.; Kasera, S.; Rowland, M. J.; Del Barrio, J.; Scherman, O. A. *Chem Rev* **2015**, *115*, 12320–12406.
(44) Ganapati, S.; Isaacs, L. *Isr J Chem* **2018**, *58*, 250–263.
(45) Mock, W. L.; Shih, N. Y. *Journal of Organic Chemistry* **1986**, *51*, 4440–4446.
(46) Kim, Y.; Kim, H.; Ko, Y. H.; Selvapalam, N.; Rekharsky, M. V.; Inoue, Y.; Kim, K. *Chemistry – A European Journal* **2009**, *15*, 6143–6151.
(47) Nau, W. M.; Florea, M.; Assaf, K. I. *Isr J Chem* **2011**, *51*, 559–577.
(48) Biedermann, F.; Nau, W. M.; Schneider, H. J. *Angewandte Chemie - International Edition* **2014**, *53*, 11158–11171.
(49) Assaf, K. I.; Nau, W. M. *Chem Soc Rev* **2014**, *44*, 394–418.
(50) Muddana, H. S.; Varnado, C. D.; Bielawski, C. W.; Urbach, A. R.; Isaacs, L.; Geballe, M. T.; Gilson, M. K. *J Comput Aided Mol Des* **2012**, *26*, 475–487.
(51) Assaf, K. I.; Florea, M.; Antony, J.; Henriksen, N. M.; Yin, J.; Hansen, A.; Qu, Z. W.; Sure, R.; Klapstein, D.; Gilson, M. K.; Grimme, S.; Nau, W. M. *J Phys Chem B* **2017**, *121*, 11144–11162.
(52) Rizzi, A.; Murkli, S.; McNeill, J. N.; Yao, W.; Sullivan, M.; Gilson, M. K.; Chiu, M. W.; Isaacs, L.; Gibb, B. C.; Mobley, D. L.; Chodera, J. D. *J Comput Aided Mol Des* **2018**, *32*, 937–963.

(53) Šekutor, M.; Molčanov, K.; Cao, L.; Isaacs, L.; Glaser, R.; Mlinarič-Majerski, K. *European J Org Chem* **2014**, *2014*, 2533–2542.
(54) Masson, E.; Shaker, Y. M.; Masson, J. P.; Kordesch, M. E.; Yuwono, C. *Org Lett* **2011**, *13*, 3872–3875.
(55) Mock, W. L.; Pierpont, J. *J Chem Soc Chem Commun* **1990**, No. 21, 1509–1511.
(56) Ko, Y. H.; Kim, E.; Hwang, I.; Kim, K. *Chemical Communications* **2007**, No. 13, 1305–1315.
(57) Saleh, N.; Koner, A. L.; Nau, W. M. *Angewandte Chemie International Edition* **2008**, *47*, 5398–5401.
(58) Del Barrio, J.; Horton, P. N.; Lairez, D.; Lloyd, G. O.; Toprakcioglu, C.; Scherman, O. A. *J Am Chem Soc* **2013**, *135*, 11760–11763.
(59) Isaacs, L. *Acc Chem Res* **2014**, *47*, 2052–2062.
(60) Ghale, G.; Nau, W. M. *Acc Chem Res* **2014**, *47*, 2150–2159.
(61) Bockus, A. T.; Smith, L. C.; Grice, A. G.; Ali, O. A.; Young, C. C.; Mobley, W.; Leek, A.; Roberts, J. L.; Vinciguerra, B.; Isaacs, L.; Urbach, A. R. *J Am Chem Soc* **2016**, *138*, 16549–16552.
(62) Li, W.; Bockus, A. T.; Vinciguerra, B.; Isaacs, L.; Urbach, A. R. *Chemical Communications* **2016**, *52*, 8537–8540.
(63) Yin, H.; Wang, R. *Isr J Chem* **2018**, *58*, 188–198.
(64) Zhang, X.; Xu, X.; Li, S.; Li, L.; Zhang, J.; Wang, R. *Theranostics* **2019**, *9*, 633–645.
(65) Wang, H.; Tian, J.; Xu, Z. Y.; Zhang, D. W.; Wang, H.; Xie, S. H.; Xu, D. W.; Ren, Y. H.; Liu, Y.; Li, Z. T. *Nat Commun* **2016**, *7*.
(66) Grimm, L. M.; Spicher, S.; Tkachenko, B.; Schreiner, P. R.; Grimme, S.; Biedermann, F. *Chemistry* **2022**, *28*.
(67) Cao, L.; Škalamera, D.; Zavalij, P. Y.; Hostaš, J.; Hobza, P.; Mlinarić-Majerski, K.; Glaser, R.; Isaacs, L. *Org Biomol Chem* **2015**, *13*, 6249–6254.
(68) Hostaš, J.; Sigwalt, D.; Šekutor, M.; Ajani, H.; Dubecký, M.; Řezáč, J.; Zavalij, P. Y.; Cao, L.; Wohlschlager, C.; Mlinarić-Majerski, K.; Isaacs, L.; Glaser, R.; Hobza, P. *Chemistry - A European Journal* **2016**, *22*, 17226–17238.
(69) Fokin, A. A.; Merz, A.; Fokina, N. A.; Schwertfeger, H.; Liu, S. L.; Dahl, J. E. P.; Carlson, R. K. M.; Schreiner, P. R. *Synthesis (Stuttg)* **2009**, *2009*, 909–912.
(70) Schwertfeger, H.; Würtele, C.; Schreiner, P. R. *Synlett* **2010**, *2010*, 493–495.
(71) Grimme, S. *J Chem Theory Comput* **2019**, *15*, 2847–2862.
(72) Pracht, P.; Bohle, F.; Grimme, S. *Physical Chemistry Chemical Physics* **2020**, *22*, 7169–7192.
(73) Škalamera, D.; Cao, L.; Isaacs, L.; Glaser, R.; Mlinarić-Majerski, K. *Tetrahedron* **2016**, *72*, 1541–1546.
(74) Wiseman, T.; Williston, S.; Brandts, J. F.; Lin, L. N. *Anal Biochem* **1989**, *179*, 131–137.
(75) Velazquez-Campoy, A.; Freire, E. *Nat Protoc* **2006**, *1*, 186–191.
(76) Broecker, J.; Vargas, C.; Keller, S. *Anal Biochem* **2011**, *418*, 307–309.
(77) Sinn, S.; Spuling, E.; Bräse, S.; Biedermann, F. *Chem Sci* **2019**, *10*, 6584–6593.
(78) Montes-Navajas, P.; Corma, A.; Garcia, H. *ChemPhysChem* **2008**, *9*, 713–720.
(79) Rajewski, R. A.; Stella, V. J. *J Pharm Sci* **1996**, *85*, 1142–1169.
(80) Rowan, A. E.; Elemans, J. A. A. W.; Nolte, R. J. M. *Acc Chem Res* **1999**, *32*, 995–1006.
(81) Szente, L.; Szejtli, J. *Adv Drug Deliv Rev* **1999**, *36*, 17–28.

(82) Vial, L.; Ludlow, R. F.; Leclaire, J.; Pérez-Fernández, R.; Otto, S. *J Am Chem Soc* **2006**, *128*, 10253–10257.
(83) Rebek, J. *Acc Chem Res* **2009**, *42*, 1660–1668.
(84) Jordan, J. H.; Gibb, B. C. *Chem Soc Rev* **2014**, *44*, 547–585.
(85) Li, S. H.; Zhang, H. Y.; Xu, X.; Liu, Y. *Nat Commun* **2015**, *6*.
(86) Zarra, S.; Wood, D. M.; Roberts, D. A.; Nitschke, J. R. *Chem Soc Rev* **2014**, *44*, 419–432.
(87) Dale, E. J.; Vermeulen, N. A.; Juríček, M.; Barnes, J. C.; Young, R. M.; Wasielewski, M. R.; Stoddart, J. F. *Acc Chem Res* **2016**, *49*, 262–273.
(88) Murray, J.; Kim, K.; Ogoshi, T.; Yao, W.; Gibb, B. C. *Chem Soc Rev* **2017**, *46*, 2479–2496.
(89) Stoddart, J. F. *Angewandte Chemie - International Edition* **2017**, *56*, 11094–11125.
(90) Ueda, Y.; Ito, H.; Fujita, D.; Fujita, M. *J Am Chem Soc* **2017**, *139*, 6090–6093.
(91) Liu, W.; Johnson, A.; Smith, B. D. *J Am Chem Soc* **2018**, *140*, 3361–3370.
(92) Heilmann, M.; Tiefenbacher, K. *Chemistry - A European Journal* **2019**, *25*, 12900–12904.
(93) Zhang, Y. M.; Liu, Y. H.; Liu, Y. *Advanced Materials* **2020**, *32*.
(94) Beatty, M. A.; Hof, F. *Chem Soc Rev* **2021**, *50*, 4812–4832.
(95) Xue, M.; Yang, Y.; Chi, X.; Zhang, Z.; Huang, F. *Acc Chem Res* **2012**, *45*, 1294–1308.
(96) Zhang, H.; Ma, X.; Nguyen, K. T.; Zhao, Y. *ACS Nano* **2013**, *7*, 7853–7863.
(97) Ogoshi, T.; Yamagishi, T. A.; Nakamoto, Y. *Chem Rev* **2016**, *116*, 7937–8002.
(98) Sathiyajith, C. W.; Shaikh, R. R.; Han, Q.; Zhang, Y.; Meguellati, K.; Yang, Y. W. *Chemical Communications* **2017**, *53*, 677–696.
(99) Zhou, J.; Yu, G.; Huang, F. *Chem Soc Rev* **2017**, *46*, 7021–7053.
(100) Feng, W.; Jin, M.; Yang, K.; Pei, Y.; Pei, Z. *Chemical Communications* **2018**, *54*, 13626–13640.
(101) Jie, K.; Zhou, Y.; Li, E.; Huang, F. *Acc Chem Res* **2018**, *51*, 2064–2072.
(102) Shu, X.; Xu, K.; Hou, D.; Li, C. *Isr J Chem* **2018**, *58*, 1194–1204.
(103) Zhang, H.; Liu, Z.; Zhao, Y. *Chem Soc Rev* **2018**, *47*, 5491–5528.
(104) Chang, Y.; Chen, J. Y.; Yang, J.; Lin, T.; Zeng, L.; Xu, J. F.; Hou, J. L.; Zhang, X. *ACS Appl Mater Interfaces* **2019**, *11*, 38497–38502.
(105) Ogoshi, T.; Kakuta, T.; Yamagishi, T. aki. *Angewandte Chemie - International Edition* **2019**, *58*, 2197–2206.
(106) Song, N.; Lou, X. Y.; Ma, L.; Gao, H.; Yang, Y. W. *Theranostics* **2019**, *9*, 3075–3093.
(107) Li, M. H.; Lou, X. Y.; Yang, Y. W. *Chemical Communications* **2021**, *57*, 13429–13447.
(108) Wang, K.; Jordan, J. H.; Velmurugan, K.; Tian, X.; Zuo, M.; Hu, X. Y.; Wang, L. *Angewandte Chemie - International Edition* **2021**, *60*, 9205–9214.
(109) Yin, H.; Zhang, X.; Wei, J.; Lu, S.; Bardelang, D.; Wang, R. *Theranostics* **2021**, *11*, 1513–1526.
(110) Zhang, G.; Hua, B.; Dey, A.; Ghosh, M.; Moosa, B. A.; Khashab, N. M. *Acc Chem Res* **2021**, *54*, 155–168.
(111) Zhu, H.; Li, Q.; Zhu, W.; Huang, F. *Acc Mater Res* **2022**, *3*, 658–668.
(112) Li, C.; Ma, J.; Zhao, L.; Zhang, Y.; Yu, Y.; Shu, X.; Li, J.; Jia, X. *Chemical Communications* **2013**, *49*, 1924–1926.
(113) Bojtár, M.; Paudics, A.; Hessz, D.; Kubinyi, M.; Bitter, I. *RSC Adv* **2016**, *6*, 86269–86275.
(114) Yu, G.; Xue, M.; Zhang, Z.; Li, J.; Han, C.; Huang, F. *J Am Chem Soc* **2012**, *134*, 13248–13251.
(115) Li, Z.; Yang, J.; Yu, G.; He, J.; Abliz, Z.; Huang, F. *Org Lett* **2014**, *16*, 2066–2069.

(116) Lachner, M.; Jenuwein, T. *Curr Opin Cell Biol* **2002**, *14*, 286–298.
(117) Bannister, A. J.; Kouzarides, T. *Cell Res* **2011**, *21*, 381–395.
(118) Chervona, Y.; Costa, M. *Am J Cancer Res* **2012**, *2*, 589.
(119) McAnena, P.; Brown, J. A. L.; Kerin, M. J. *Cancers (Basel)* **2017**, *9*.
(120) He, C.; Xu, J.; Zhang, J.; Xie, D.; Ye, H.; Xiao, Z.; Cai, M.; Xu, K.; Zeng, Y.; Li, H.; Wang, J. *Hum Pathol* **2012**, *43*, 1425–1435.
(121) Sims, R. J.; Nishioka, K.; Reinberg, D. *Trends in Genetics* **2003**, *19*, 629–639.
(122) Martin, C.; Zhang, Y. *Nat Rev Mol Cell Biol* **2005**, *6*, 838–849.
(123) Black, J. C.; Van Rechem, C.; Whetstine, J. R. *Mol Cell* **2012**, *48*, 491–507.
(124) Ingerman, L. A.; Cuellar, M. E.; Waters, M. L. *Chemical Communications* **2010**, *46*, 1839–1841.
(125) Daze, K. D.; Hof, F. *Acc Chem Res* **2013**, *46*, 937–945.
(126) Gamal-Eldin, M. A.; MacArtney, D. H. *Org Biomol Chem* **2012**, *11*, 488–495.
(127) Beaver, J. E.; Waters, M. L. *ACS Chem Biol* **2016**, *11*, 643–653.
(128) Hof, F. *Chemical Communications* **2016**, *52*, 10093–10108.
(129) Liu, Y.; Perez, L.; Mettry, M.; Easley, C. J.; Hooley, R. J.; Zhong, W. *J Am Chem Soc* **2016**, *138*, 10746–10749.
(130) Peacock, H.; Thinnes, C. C.; Kawamura, A.; Hamilton, A. D. *Supramol Chem* **2016**, *28*, 575–581.
(131) Pinalli, R.; Brancatelli, G.; Pedrini, A.; Menozzi, D.; Hernández, D.; Ballester, P.; Geremia, S.; Dalcanale, E. *J Am Chem Soc* **2016**, *138*, 8569–8580.
(132) Liu, Y.; Perez, L.; Gill, A. D.; Mettry, M.; Li, L.; Wang, Y.; Hooley, R. J.; Zhong, W. *J Am Chem Soc* **2017**, *139*, 10964–10967.
(133) Gruber, T. *ChemBioChem* **2018**, *19*, 2324–2340.
(134) Mullins, A. G.; Pinkin, N. K.; Hardin, J. A.; Waters, M. L. *Angewandte Chemie - International Edition* **2019**, *58*, 5282–5285.
(135) Shaurya, A.; Garnett, G. A. E.; Starke, M. J.; Grasdal, M. C.; Dewar, C. C.; Kliuchynskyi, A. Y.; Hof, F. *Org Biomol Chem* **2021**, *19*, 4691–4696.
(136) Warmerdam, Z.; Kamba, B. E.; Le, M. H.; Schrader, T.; Isaacs, L.; Bayer, P.; Hof, F. *ChemBioChem* **2022**, *23*.
(137) Wang, J.; Wolf, R. M.; Caldwell, J. W.; Kollman, P. A.; Case, D. A. *J Comput Chem* **2004**, *25*, 1157–1174.
(138) Diederich, F. *Angewandte Chemie International Edition in English* **1988**, *27*, 362–386.
(139) Nau, W. M.; Florea, M.; Assaf, K. I. *Isr J Chem* **2011**, *51*, 559–577.
(140) Biedermann, F.; Uzunova, V. D.; Scherman, O. A.; Nau, W. M.; De Simone, A. *J Am Chem Soc* **2012**, *134*, 15318–15323.
(141) Persch, E.; Dumele, O.; Diederich, F. *Angewandte Chemie - International Edition* **2015**, *54*, 3290–3327.
(142) Barnett, J. W.; Sullivan, M. R.; Long, J. A.; Tang, D.; Nguyen, T.; Ben-Amotz, D.; Gibb, B. C.; Ashbaugh, H. S. *Nat Chem* **2020**, *12*, 589–594.
(143) Kapuscinski, J. *Biotechnic and Histochemistry* **1995**, *70*, 220–233.
(144) Biczók, L.; Wintgens, V.; Miskolczy, Z.; Megyesi, M. *Isr J Chem* **2011**, *51*, 625–633.
(145) Shao, Y.; Molnar, L. F.; Jung, Y.; Kussmann, J.; Ochsenfeld, C.; Brown, S. T.; Gilbert, A. T. B.; Slipchenko, L. V.; Levchenko, S. V.; O'Neill, D. P.; DiStasio, R. A.; Lochan, R. C.; Wang, T.; Beran, G. J. O.; Besley, N. A.; Herbert, J. M.; Yeh Lin, C.; Van Voorhis, T.; Hung Chien, S.; Sodt, A.; Steele, R. P.; Rassolov, V. A.; Maslen, P. E.; Korambath, P. P.;

Adamson, R. D.; Austin, B.; Baker, J.; Byrd, E. F. C.; Dachsel, H.; Doerksen, R. J.; Dreuw, A.; Dunietz, B. D.; Dutoi, A. D.; Furlani, T. R.; Gwaltney, S. R.; Heyden, A.; Hirata, S.; Hsu, C. P.; Kedziora, G.; Khalliulin, R. Z.; Klunzinger, P.; Lee, A. M.; Lee, M. S.; Liang, W.; Lotan, I.; Nair, N.; Peters, B.; Proynov, E. I.; Pieniazek, P. A.; Min Rhee, Y.; Ritchie, J.; Rosta, E.; David Sherrill, C.; Simmonett, A. C.; Subotnik, J. E.; Lee Woodcock, H.; Zhang, W.; Bell, A. T.; Chakraborty, A. K.; Chipman, D. M.; Keil, F. J.; Warshel, A.; Hehre, W. J.; Schaefer, H. F.; Kong, J.; Krylov, A. I.; Gill, P. M. W.; Head-Gordon, M. *Physical Chemistry Chemical Physics* **2006**, *8*, 3172–3191.

(146) MacKerell, A. D.; Bashford, D.; Bellott, M.; Dunbrack, R. L.; Evanseck, J. D.; Field, M. J.; Fischer, S.; Gao, J.; Guo, H.; Ha, S.; Joseph-McCarthy, D.; Kuchnir, L.; Kuczera, K.; Lau, F. T. K.; Mattos, C.; Michnick, S.; Ngo, T.; Nguyen, D. T.; Prodhom, B.; Reiher, W. E.; Roux, B.; Schlenkrich, M.; Smith, J. C.; Stote, R.; Straub, J.; Watanabe, M.; Wiórkiewicz-Kuczera, J.; Yin, D.; Karplus, M. *Journal of Physical Chemistry B* **1998**, *102*, 3586–3616.

(147) Hoover, W. G. *Phys Rev A (Coll Park)* **1985**, *31*, 1695–1697.

(148) Parrinello, M.; Rahman, A. *Phys Rev Lett* **1980**, *45*, 1196–1199.

(149) Van Der Spoel, D.; Lindahl, E.; Hess, B.; Groenhof, G.; Mark, A. E.; Berendsen, H. J. C. *J Comput Chem* **2005**, *26*, 1701–1718.

(150) Tribello, G. A.; Bonomi, M.; Branduardi, D.; Camilloni, C.; Bussi, G. *Comput Phys Commun* **2014**, *185*, 604–613.

(151) Chandler, D. *Introduction to Modern Statistical Mechanics*, 5th ed.; Oxford University Press: Oxford, 1987.

(152) Heitmann, L. M.; Taylor, A. B.; Hart, P. J.; Urbach, A. R. *J Am Chem Soc* **2006**, *128*, 12574–12581.

(153) Franjić, S. *J Phy Fit Treatment & Sports* **2020**, *8*.

(154) Thevis, M.; Krug, O.; Geyer, H.; Walpurgis, K.; Baume, N.; Thomas, A. *Anal Bioanal Chem* **2018**, *410*, 2275–2281.

(155) Raouf, M.; Bettinger, J. J.; Fudin, J. *Federal Practitioner* **2018**, *35*, 38.

(156) Hadland, S. E.; Levy, S. *Child Adolesc Psychiatr Clin N Am* **2016**, *25*, 549.

(157) Kale, N. *Am Fam Physician* **2019**, *99*, 33–39.

(158) DeIuliis, D.; DeIuliis, D. *Journal of Sport Administration and Supervision* **2012**, *4*.

(159) Pdxscholar, P.; Dowling, M.; Harris, S.; Washington, M. .

(160) *LA28 Initial Sports Programme to be put forward to the IOC Session - Olympic News*.

(161) Marchei, E.; Ferri, M. A.; Torrens, M.; Farré, M.; Pacifici, R.; Pichini, S.; Pellegrini, M. *Int J Mol Sci* **2021**, *22*, 4000.

(162) Minami, T.; Liu, Y.; Akdeniz, A.; Koutnik, P.; Esipenko, N. A.; Nishiyabu, R.; Kubo, Y.; Anzenbacher, P. *J Am Chem Soc* **2014**, *136*, 11396–11401.

(163) King, D.; Wilson, C. R.; Herron, L.; Deng, C. L.; Mehdi, S.; Tiwary, P.; Hof, F.; Isaacs, L. *Org Biomol Chem* **2022**, *20*, 7429–7438.

(164) World Anti-Doping Agency. *Prohibited List*; World Anti-Doping Agency: Canada, 2023.

(165) King, D.; Wilson, C. R.; Herron, L.; Deng, C. L.; Mehdi, S.; Tiwary, P.; Hof, F.; Isaacs, L. *Org Biomol Chem* **2022**, *20*, 7429–7438.

(166) Taylor, J. R. *An Introduction to Error Anaylsis*, 2nd ed.; McGuire, A., Ed.; University Science Books: Sausalito, 1997.

(167) Barooah, N.; Mohanty, J.; Bhasikuttan, A. C. *Journal of Physical Chemistry B* **2013**, *117*, 13595–13603.

(168) Barooah, N.; Mohanty, J.; Pal, H.; Bhasikuttan, A. C. *Physical Chemistry Chemical Physics* **2011**, *13*, 13117–13126.
(169) James, G.; Witten, D.; Hastie, T.; Tibshirani, R. *An Introduction to Statistical Learning*; Casella, G., Fienberg, S., Olkin, I., Eds.; Springer New York: New York, NY, 2013; Vol. 103.
(170) Miller, J. N.; Miller, J. C. *Statistics and Chemometrics for Analytical Chemistry*, 6th ed.; Pearson: Harlow, 2010.
(171) 2021 Anti-Doping Testing Figures. World Anti-Doping Agency January 2022.
(172) WADA Technical Document-TD2021DL. World Anti-Doping Agency April 1, 2020.
(173) WADA Technical Document – TD2022MRPL. World Anti-Doping Agency October 6, 2021.
(174) team, T. pandas development. **2023**.
(175) Harris, C. R.; Millman, K. J.; van der Walt, S. J.; Gommers, R.; Virtanen, P.; Cournapeau, D.; Wieser, E.; Taylor, J.; Berg, S.; Smith, N. J.; Kern, R.; Picus, M.; Hoyer, S.; van Kerkwijk, M. H.; Brett, M.; Haldane, A.; del Río, J. F.; Wiebe, M.; Peterson, P.; Gérard-Marchant, P.; Sheppard, K.; Reddy, T.; Weckesser, W.; Abbasi, H.; Gohlke, C.; Oliphant, T. E. *Nature 2020 585:7825* **2020**, *585*, 357–362.
(176) Pedregosa, F.; Varoquaux, G.; Gramfort, A.; Michel, V.; Thirion, B.; Grisel, O.; Blondel, M.; Prettenhofer, P.; Weiss, R.; Vanderplas, J.; Passos, A.; Cournapeau, D.; Brucher, M.; Perrot, M.; Duchesnay, É. *Journal of Machine Learning Research* **2011**, *12*, 2825–2830.